Lighting up cancer aggressiveness

Targeting the urokinase plasminogen activator receptor for intraoperative optical imaging

Victor M. Baart

Lighting Up Cancer Aggressiveness

Targeting the urokinase plasminogen activator receptor for intraoperative optical imaging

Victor M. Baart

© V.M. Baart 2023

ISBN: 978-94-6483-501-4

Cover: Tabitha Mosterdijk
Provided by thesis specialist Ridderprint, ridderprint.nl
Printing: Ridderprint
Layout and design: Tara Schollema, persoonlijkproefschrift.nl

All rights reserved. No parts of this thesis may be reproduced, distributed, stored in a retrieval system or transmitted in any form or by any means, without prior written permission of the author.

The research in this thesis was financially supported by the Center for Translational Molecular Medicine.

The printing of this thesis was financially supported by Centre for Human Drug Research.

Lighting Up Cancer Aggressiveness

Targeting the urokinase plasminogen activator receptor for intraoperative optical imaging

Proefschrift

ter verkrijging van
de graad van doctor aan de Universiteit Leiden,
op gezag van rector magnificus prof.dr.ir. H. Bijl,
volgens besluit van het college voor promoties
te verdedigen op donderdag 14 december 2023
klokke 12.30 uur

door
Victor Michiel Baart
geboren te Islamabad, Pakistan
in 1994

Promotiecommisie

Promotor:	Prof. Dr. J. Burggraaf
Copromotor:	Dr. A.L. Vahrmeijer
	Dr. C.F.M. Sier
Overige leden:	Prof.dr. P.H.A. Quax
	Prof.dr. S. Hernot – Vrije Universiteit Brussel
	Dr. S. Keereweer – Erasmus MC
	Dr. D. Cohen

Table of Contents

Part I: Introduction 7

Chapter 1 Introduction and thesis outline 9

Part II: uPAR as a tumor target in various tumor types 19

Chapter 2 Prognostic impact of urokinase plasminogen activator receptor expression in pancreatic cancer: malignant versus stromal cells. 21

Chapter 3 EGFR and αvβ6 as promising targets for molecular imaging of cutaneous and mucosal squamous cell carcinoma of the head-and-neck region 39

Part III. uPAR as target: beyond cancer imaging 57

Chapter 4 Molecular imaging of the urokinase plasminogen activator receptor: opportunities beyond cancer 59

Part IV: Development of uPAR targeted tracers 97

Chapter 5 uPAR directed-imaging of head-and-neck cancer 99

Chapter 6 A multimodal molecular imaging approach targeting uPAR for the diagnosis, resection, and surveillance of urothelial cell carcinoma 103

Chapter 7 Side-by-side comparison of uPAR targeting optical imaging agents for image-guided surgery of solid tumors 121

Part V. Summary and general discussion 141

Chapter 8 Summary 143

Chapter 9 General discussion and future perspectives 147

Appendices A. Dutch summary - Nederlandse samenvatting 173

B. List of publications 177

C. Curriculum vitae 181

D. Acknowledgements - Dankwoord 183

Part I
Introduction

Chapter 1

Introduction and thesis outline

Baart VM

Introduction

The radical mastectomy for breast cancer, described by William S. Halsted in 1891, represents a milestone in curative oncological surgery [1]. Believing that "cancer was a local disease, growing per continuum to lymph nodes and subsequent metastasis", he advocated grossly mutilating *en-bloc* resections of affected regions in order to achieve curation. Throughout the early 20th century the mindset that cancer can be cured if resected radically enough has laid the foundation of surgical care. However, with an increased understanding of cancer biology, the past century's technological advancements, and the wish to be less mutilating, cancer treatment has altered significantly from the aggressive dissections initially perpetuated for all patients [2].

Cancer treatment is now a multidisciplinary approach within which physicians have an increasing number of therapies at their disposal. Options include, but are not limited to, minimally-invasive/robotic excisions, ablation, irradiation, chemotherapy, targeted therapy and immunotherapy. Nonetheless, the cornerstone of curation for almost all solid tumors is still surgery, where attaining negative tumor margins is fundamental; positive surgical margins (R1/R2, irradical) repeatedly translate into worse overall survival [3]. Unlike what Halsted proclaimed though, organ-sparing surgeries have proven as effective for the majority of patients as extensive anatomical dissections. Another change, compared to Halsted's era, is that surgeons operate in, sometimes quite literally, different landscapes. First of all, due to neoadjuvant therapy, operating fields are full of fibrosis, inflammation and necrosis, challenging the discernment between malignant and reactive tissue. Secondly, with the advent of laparoscopic and robotic procedures, the visual field is digitalized and the discriminatory nature of tactile feedback is distorted, if not unfeasible.

The emergence of intraoperative imaging

In response to these challenges, intraoperative imaging modalities have entered the operating theatre to aid in navigation between malignant and non-malignant (i.e. normal, benign or reactive tissue) tissue. These modalities, each with their own strengths and weaknesses, can be categorized into conventional, optical, nuclear, and endogenous reflectance [4]. One of the most promising techniques is the optical imaging technique called fluorescence guided surgery (FGS) as it is relatively simple, gives real-time images, results in high contrast and sensitivity, and lacks ionizing radiation. FGS camera systems function by emitting a spectrally

resolved near-infrared (NIR[1]) light that subsequently excites the exogenous contrast agent (i.e. fluorophore) [4-8]. An excited fluorophore emits photons that are then captured by a detector and translated into a digital image and superimposed upon white-light images. As a result anatomical or pathophysiological structures 'light up' on screen, enabling clear identification of the desired tissue [9].

Identifying cancerous lesions revolves around creating a large enough contrast between malignant and benign tissue using fluorescent contrast agents [8]. Sole NIR fluorophores, such as indocyanine green (ICG) or IRDye800CW, generally do not sufficiently accumulate in tumours[2] [10]. Therefore a fluorophore needs to be conjugated to a targeting agent that recognizes a tumor and not surrounding healthy tissue. Furthest along in clinical development are the folate receptor targeting OTL38 (pafoliacianine; Cytalux) for ovarian cancer, the carcinoembryonic antigen targeting SGM-101 for colorectal cancer, and the cathepsin targeting LUM015 for breast cancer. Their strength, specific targeting, is also their weakness, either due to non-tumoral expression of the target[3] or heterogenous intra- and intertumoral expression of the target[4] [7, 11]. As a result, only a subset of oncological patients benefit from the current class of fluorescence agents. For the remaining cancer patients there is no suitable fluorescence contrast agent while there is a clinical need for tumor margin identification. The current challenge lies in expanding the library of available contrast agents and, with this expansion, a desire to identifying characteristics of the most optimal target-tracer combination for each patient.

1 Although almost all current FGS clinical trials currently use NIR (700 - 900 nm) light, the first clinical trials demonstrating the concept of fluorescence guided surgery used blue (380 - 500 nm) light to visualize brain tumors, colorectal carcinomas and ovarian cancer [5-7]. This change in light source is due to the favourable imaging characteristics of NIR light; absorption by biomolecules (i.e. deoxyhemoglobin, oxyhemoglobin, water, and lipids), scattering and tissue autofluorescence are all favorably low with NIR light compared to blue light. Consequently, background fluorescence is minimized, resulting in greater contrasts with which to discriminate structures. In addition, NIR light emitted by the camera system penetrate deeper into, and out of, tissue, resulting in improved imaging depths of up to several millimetres [8]. A more recent development has been the utilization of the second NIR window (NIR II; 900 - 1450 nm) with even better imaging characteristics, but translation to the clinic is currently limited by the availability of the appropriate camera systems [4].

2 One exception is using ICG for imaging of hepatobiliary tumors. Healthy hepatocytes rapidly excrete ICG into the biliary ducts. Hepatocytes located adjacent to the tumor cannot metabolize ICG in this manner and as a consequence ICG accumulates in these hepatocytes resulting in a fluorescent rim of hepatocytes incapable of metabolizing ICG around the tumor. This phenomon is subsequently utilized for intraoperative resection of hepatobiliary tumors [10].

3 Due to folate β expression in macrophages, pafolacianine signal also accumulates in lymph nodes with macrophages expressing folate β, resulting in false-positive fluorescence lymph nodes [11].

4 10% of ovarian cancer patients do not have folate receptor expression in their tumors and for solid tumors of other origins folate receptor expression is far more limited [7].

This thesis addresses this challenge by firstly confirming the urokinase plasminogen activator receptor (uPAR) as a potential target and secondly by evaluating the effect of tracer size on FGS using novel uPAR-targeted tracers. Thereafter, by combining the current literature and the studies described in this thesis the endgoal is to define a clinical framework for uPAR FGS.

The case for using the urokinase plasminogen activator receptor as target

The extracellular matrix (ECM) forms the scaffolding where cells are embedded in, guaranteeing the structural integrity of tissues and organs. Tissue maintenance, differentiation and proliferation, therefore requires a coordinated response between the disintegration and reassembling of the complex network of collagens, proteoglycans and glycoproteins that the ECM consists of. The uninhibited cell growth and eventual invasiveness that defines all solid cancers implicates that pathways involved in ECM remodelling are dysregulated [12]. As such proteins involved in tissue remodelling are a promising source of FGS targets that can be utilized in a universal nature (i.e. for all solid tumors).

An important regulator of ECM proteolysis and cell signalling, involving process like proliferation, differentiation and migration, is the urokinase plasminogen activator receptor (uPAR). Initially, its involvement was regarded as rather simple; as a receptor for urokinase plasminogen activator (uPA; urokinase), uPAR localized the proteolytic cascade initiated by uPA towards the leading edge of cells. The subsequent proteolysis creates room for cell migration into the direction where uPAR was expressed. Over 35 years later the story is much more complex. uPAR narrowly orchestrates cancer aggressiveness managing not only extracellular processes such as proteolysis, but also influencing intracellular pathways involved in tumor progression through its over 42 interacting proteins [13]. Not surprisingly, downregulating uPAR downregulates signaling pathways involved in eight of the ten Hallmarks of Cancer [14].

For molecular imaging applications, such as FGS, more important than the targets fundamental role in tumor progression is its expression pattern. The ideal target has no expression in non-malignant tissue while being overexpressed in malignant tissue as such an expression pattern allows for a high tumor-normal signal ratio. uPAR expression has been described on neoplastic cells and tumor-associated stromal cells, including neo-angiogenic endothelial cells, cancer-associated fibroblasts, and tumor-associated macrophages [15]. Furthermore, it is completely absent in surrounding non-malignant tissue. This pattern remains an overarching theme for virtually every solid malignancy [16]. With such an expression pattern, targeting uPAR is, not surprisingly, considered particularly suited for FGS [15]. However, up to now, no uPAR targeting tracer has made it to the clinic for FGS and only recently

uPAR-targeted positron emission tomography (PET) trials have reported results while the clinical potential is evident.

The case for considering structural variations of tracers

In 2019, Hernot et al. listed 19 different fluorescent tracers that had been or were being evaluated clinically for FGS [9]. Remarkebly, these contrast agents differed not only in their target but also in their structure; ranging from therapeutic monoclonal antibodies repurposed for imaging, to natural occurring ligands conjugated with a fluorophore, and from knotted peptides conjugated with a fluorophore to activatable tracers that only become fluorescent upon enzymatic cleavage. These differences in structure directly translate into differences in distribution, metabolism and excretion; characteristics surgeons will need to contemplate as they will influence uptake by target tissue and clearing organs, tissue penetration, time before image acquisition and imaging contrast [17, 18]. OTL38, for example, consists of a natural ligand (folate analogue) conjugated to a NIR fluorescence dye with a molecular weight of 1.414 Dalton (Da) while SGM-101 is a chimeric antibody conjugated to a NIR fluorescence dye with a molecular weight of approximately 150.000 Da (> 100 times larger). As a result, OTL38 has a relatively rapid clearance from the plasma with imaging windows 2 – 6 hours after administration while SGM-101 has a longer terminal half life and has to be administered 2 – 4 days before surgery [11, 19]. While a more rapid imaging window seems favorable, reducing molecular weight to increase pharmacokinetics can influence imaging outcomes. In a PET study using CD105 targeting antibodies and derivates, the smaller antibody fragments resulted in earlier but lower peak signal [20, 21]. This can potentially reduce contrast. Therefore, when designing a targeted agents, its structural characteristics should be carefully selected as structural variations can ultimaly make or break the subsequent clinical usability.

Practically, there exists a whole realm of deconstructed, rebuilt and fused molecules, where the possibilities are endless. However, generally speaking, they can be divided into one of the following categories: antibodies, antibody fragments, recombinant protein scaffolds, peptides or small molecules [9]. Antibodies are an appealing choice due to their naturally high specificity and affinity. In addition, there is extensive experience creating, optimizing and translating antibodies to the clinic [22]. The translation for FGS can be rather rapid by labelling already FDA-approved (therapeutic) antibodies with fluorescent dyes [9]. However, in addition to their extended half-life identified above, their large size limits intra-tumoral penetration and diffusion resulting in heterogenous intra-tumoral antibody concentrations and consequently effectiveness [23, 24]. As a result, other constructs are being considered. However, what the optimal characteristics of an adjusted construct are have not been clearly defined.

Thesis outline

This thesis aims to expand on the current knowledge of urokinase plasminogen activator receptor (uPAR) fluorescence guided surgery (FGS) with the endgoal of defining a clinical framework for uPAR molecular imaging. While the overarching focus is uPAR, this thesis also attempts to draw more general conclusions for the whole field of FGS. To achieve the before-mentioned goals this thesis is divided into five parts.

Part I. Introduction
The current chapter, **Chapter 1**, introduces important background concepts about FGS, uPAR, and tracer design so as to set the stage for the work in Parts II – V. The chapter ends with a thesis outline.

Part II. uPAR as a tumor target in various tumortypes
In **Chapter 2** the expression pattern in both malignant and stromal cells of is determined uPAR in pancreas adenocarcinoma and correlated with prognosis of patients. In **Chapter 3** the immunohistochemical expression of seven promising FGS targets, including uPAR, are compared in patients with high-risk cutaneous and mucosal squamous cell carcinoma of the head and neck. In addition, a novel scoring system is introduced for comparing the appropriateness of targets for FGS.

Part III. uPAR as target: Beyond cancer imaging
Not only does uPAR play a fundamental role in cancer, it also plays a central role in other pathologies. Therefore, in **Chapter 4**, a side step is made to discuss the potential of uPAR imaging in non-neoplastic diseases in order to identify possible novel aveneus for molecular imaging.

Part IV. Development of uPAR targeted tracers
Once uPAR has been identified as a potential target a fluorescent tracer needs to be designed that targets uPAR. The opportunities and pitfalls of fluorescence anti-uPAR tracer design are discussed in **Chapter 5**. Subsequently, **Chapter 6** presents the results of the preclinical development of a humanized anti-uPAR monoclonal antibody. Furthermore the tracers potential for multimodal optical and photoacoustic fluorescence imaging for urothelial cell carcinoma patients is demonstrated. In **Chapter 7**, this antibody is cleaved into $F(ab')_2$ and fab fragments and the fluorescent fragments are compared to the original humanized antibody in three orthotopic tumor models.

Part V. Summary and general discussion
After a summary in **chapter 8**, the stage is set for the discussion in **chapter 9**. This discussion includes uPAR as a next-generation target, the optimal structural characteristics of an uPAR FGS tracer, the translation of uPAR FGS to the clinic and the relevance of uPAR molecular imaging in other fields besides oncology. Where relevant, the discussion is generalized to the whole field.

References

1. Halsted WS. I. The Results of Operations for the Cure of Cancer of the Breast Performed at the Johns Hopkins Hospital from June, 1889, to January, 1894. Annals of surgery. 1894;20:497-555. doi:10.1097/00000658-189407000-00075.
2. Fisher B. Biological research in the evolution of cancer surgery: a personal perspective. Cancer Res. 2008;68:10007-20. doi:10.1158/0008-5472.Can-08-0186.
3. Orosco RK, Tapia VJ, Califano JA, Clary B, Cohen EEW, Kane C, et al. Positive Surgical Margins in the 10 Most Common Solid Cancers. Sci Rep. 2018;8:5686. doi:10.1038/s41598-018-23403-5.
4. Stammes MA, Bugby SL, Porta T, Pierzchalski K, Devling T, Otto C, et al. Modalities for image- and molecular-guided cancer surgery. The British journal of surgery. 2018;105:e69-e83. doi:10.1002/bjs.10789.
5. Moore GE, Peyton WT, et al. The clinical use of fluorescein in neurosurgery; the localization of brain tumors. J Neurosurg. 1948;5:392-8. doi:10.3171/jns.1948.5.4.0392.
6. Folli S, Wagnières G, Pèlegrin A, Calmes JM, Braichotte D, Buchegger F, et al. Immunophotodiagnosis of colon carcinomas in patients injected with fluoresceinated chimeric antibodies against carcinoembryonic antigen. Proceedings of the National Academy of Sciences of the United States of America. 1992;89:7973-7. doi:10.1073/pnas.89.17.7973.
7. van Dam GM, Themelis G, Crane LM, Harlaar NJ, Pleijhuis RG, Kelder W, et al. Intraoperative tumor-specific fluorescence imaging in ovarian cancer by folate receptor-α targeting: first in-human results. Nat Med. 2011;17:1315-9. doi:10.1038/nm.2472.
8. Gioux S, Choi HS, Frangioni JV. Image-guided surgery using invisible near-infrared light: fundamentals of clinical translation. Molecular imaging. 2010;9:237-55.
9. Hernot S, van Manen L, Debie P, Mieog JSD, Vahrmeijer AL. Latest developments in molecular tracers for fluorescence image-guided cancer surgery. The Lancet Oncology. 2019;20:e354-e67. doi:10.1016/s1470-2045(19)30317-1.
10. van Manen L, Handgraaf HJM, Diana M, Dijkstra J, Ishizawa T, Vahrmeijer AL, et al. A practical guide for the use of indocyanine green and methylene blue in fluorescence-guided abdominal surgery. Journal of surgical oncology. 2018;118:283-300. doi:10.1002/jso.25105.
11. Hoogstins CE, Tummers QR, Gaarenstroom KN, de Kroon CD, Trimbos JB, Bosse T, et al. A Novel Tumor-Specific Agent for Intraoperative Near-Infrared Fluorescence Imaging: A Translational Study in Healthy Volunteers and Patients with Ovarian Cancer. Clinical cancer research : an official journal of the American Association for Cancer Research. 2016;22:2929-38. doi:10.1158/1078-0432.Ccr-15-2640.
12. Winkler J, Abisoye-Ogunniyan A, Metcalf KJ, Werb Z. Concepts of extracellular matrix remodelling in tumour progression and metastasis. Nature communications. 2020;11:5120. doi:10.1038/s41467-020-18794-x.
13. Smith HW, Marshall CJ. Regulation of cell signalling by uPAR. Nature reviews Molecular cell biology. 2010;11:23-36. doi:10.1038/nrm2821.
14. Ahn SB, Mohamedali A, Pascovici D, Adhikari S, Sharma S, Nice EC, et al. Proteomics Reveals Cell-Surface Urokinase Plasminogen Activator Receptor Expression Impacts Most Hallmarks of Cancer. Proteomics. 2019;19:e1900026. doi:10.1002/pmic.201900026.
15. Baart VM, Houvast RD, de Geus-Oei LF, Quax PHA, Kuppen PJK, Vahrmeijer AL, et al. Molecular imaging of the urokinase plasminogen activator receptor: opportunities beyond cancer. EJNMMI Res. 2020;10:87. doi:10.1186/s13550-020-00673-7.
16. Boonstra MC, Verspaget HW, Ganesh S, Kubben FJ, Vahrmeijer AL, van de Velde CJ, et al. Clinical applications of the urokinase receptor (uPAR) for cancer patients. Current pharmaceutical design. 2011;17:1890-910. doi:10.2174/138161211796718233.

17. Holliger P, Hudson PJ. Engineered antibody fragments and the rise of single domains. Nat Biotechnol. 2005;23:1126-36. doi:10.1038/nbt1142.
18. De Vos J, Devoogdt N, Lahoutte T, Muyldermans S. Camelid single-domain antibody-fragment engineering for (pre)clinical in vivo molecular imaging applications: adjusting the bullet to its target. Expert Opin Biol Ther. 2013;13:1149-60. doi:10.1517/14712598.2013.800478.
19. Boogerd LSF, Hoogstins CES, Schaap DP, Kusters M, Handgraaf HJM, van der Valk MJM, et al. Safety and effectiveness of SGM-101, a fluorescent antibody targeting carcinoembryonic antigen, for intraoperative detection of colorectal cancer: a dose-escalation pilot study. The lancet Gastroenterology & hepatology. 2018;3:181-91. doi:10.1016/s2468-1253(17)30395-3.
20. Hong H, Zhang Y, Orbay H, Valdovinos HF, Nayak TR, Bean J, et al. Positron emission tomography imaging of tumor angiogenesis with a (61/64)Cu-labeled F(ab')(2) antibody fragment. Mol Pharm. 2013;10:709-16. doi:10.1021/mp300507r.
21. Zhang Y, Hong H, Orbay H, Valdovinos HF, Nayak TR, Theuer CP, et al. PET imaging of CD105/endoglin expression with a ^{61}/^{64}Cu-labeled Fab antibody fragment. Eur J Nucl Med Mol Imaging. 2013;40:759-67. doi:10.1007/s00259-012-2334-2.
22. Mullard A. FDA approves 100th monoclonal antibody product. Nature reviews Drug discovery. 2021;20:491-5. doi:10.1038/d41573-021-00079-7.
23. Bartelink IH, Jones EF, Shahidi-Latham SK, Lee PRE, Zheng Y, Vicini P, et al. Tumor Drug Penetration Measurements Could Be the Neglected Piece of the Personalized Cancer Treatment Puzzle. Clin Pharmacol Ther. 2019;106:148-63. doi:10.1002/cpt.1211.
24. Minchinton AI, Tannock IF. Drug penetration in solid tumours. Nat Rev Cancer. 2006;6:583-92. doi:10.1038/nrc1893.

Part II

uPAR as a tumor target in various tumor types

Chapter 2

Prognostic impact of urokinase plasminogen activator receptor expression in pancreatic cancer: malignant versus stromal cells

---

de Geus SWL, Baart VM, Boonstra MC, Kuppen PJK, Prevoo HAJM, Mazar AP, Bonsing BA, Morreau H, van de Velde CJH, Vahrmeijer AL, Sier CFM.

Biomark Insights 2017; 12:1177271917715443.

Abstract

The urokinase plasminogen activator receptor (uPAR) has been proposed as a potential prognostic factor for various malignancies. The aim of this study is to assess the prognostic value of uPAR expression in neoplastic and stromal cells of pancreatic adenocarcinoma patients.

Methods & Results: uPAR expression was determined by immunohistochemistry in 122 pancreatic ductal adenocarcinomas. Kaplan-Meier and Cox regression analyses were used to determine the association with survival. Respectively 66%, 82% and 62% of pancreatic cancer patients expressed uPAR in neoplastic cells, stromal, and in both combined. Multivariate analysis showed a significant inverse association between uPAR expression in both neoplastic and stromal cells and overall survival. The prognostic impact of uPAR in stromal cells is substantial, but not as pronounced as that of uPAR expression in neoplastic cells.

Conclusion: This study suggests a role for uPAR as a biomarker to single out higher risk subgroups of pancreatic cancer patients.

Introduction

Pancreatic cancer ranks the fourth leading cause of cancer-related death and is estimated to be the second leading cause of cancer death by 2020 [1, 2]. Complete surgical resection offers the only hope for cure; however, even after successful tumor removal, recurrence rates range from 46% to 89% [3-8]. Currently, anatomic resectability and carbohydrate antigen 19-9 (CA 19-9) serum levels are the most commonly used prognostic factors to select optimal treatment strategies for non-metastatic pancreatic cancer patients, but unfortunately with only modest impact [9, 10]. Consequently, there is a necessity for novel molecular markers that are able to predict biological behavior in order to identify patients requiring more aggressive systemic and/or surgical treatment.

Proteolysis via the plasminogen activation cascade is a crucial biological process involved in cancer cell invasion and metastasis. The urokinase plasminogen activator receptor (uPAR), a glycosyl-phosphatidylinositol-anchored membrane protein, plays a dominant role in this cascade by localizing the urokinase plasminogen activator (uPA) to the cell membrane [11]. After binding to uPAR, uPA converts the inactive zymogen plasminogen into plasmin. This active serine protease subsequently activates other proteinases, resulting in the proteolysis of basement membrane proteins and extracellular matrix [12]. Considerable evidence indicates that uPAR expression in neoplastic cells, as well as stromal cells, is correlated with shortened survival in various malignancies, including colorectal, breast, and renal carcinoma [13-21].

In pancreatic cancer, uPAR expression has been observed in both tumor and surrounding stromal cells. However, it remains unclear which cellular uPAR localization is more immediately involved with tumor behavior and therefore associated with patient prognosis [15, 22]. In the present immunohistochemistry study, performed in a large cohort of patients with pancreatic adenocarcinoma, the expression pattern of uPAR in both tumor and stromal cells, and its clinical implications were evaluated.

Materials and methods

Patient selection

Retrospectively collected, formalin-fixed and paraffin-embedded tissue blocks were obtained from the archives of the Pathology Department for 137 patients with pancreatic adenocarcinoma, who underwent resection with curative intent during the period from 2001 and 2012 at the Leiden University Medical Centre, Leiden,

The Netherlands. Only pancreatic adenocarcinoma were included in this study. None of the patients in this study received chemotherapy and/or radiation prior to surgery. Clinicopathological data were collected from electronic hospital records. Differentiation grade was determined according to the guideline of the World Health Organization and the TNM-stage was defined according to the American Joint Commission on Cancer criteria [23]. All samples were non-identifiable and used in accordance to the code for proper secondary use of human tissue as prescribed by the Dutch Federation of Medical Scientific Societies. The use of archived human tissue conformed to an informed protocol that had been reviewed and approved by the institutional review board of the Leiden University Medical Centre, Leiden, The Netherlands.

Immunohistochemistry

Tissue microarrays (TMAs) of pancreatic adenocarcinoma were constructed to perform uniform and simultaneous immunohistochemical staining's to limit intra-assay variation. A single representative block was selected for each patient based on hematoxylin-eosin stained sections. From each donor block, triplicate 2.0 mm cores were punched from areas with clear histopathological tumor representation and transferred to a recipient TMA block using the TMA Master (3DHISTECH, Budapest, Hungary). From each completed TMA block, 5-mm sections were sliced. The sections were deparaffinized in xylene and rehydrated in serially diluted alcohol solutions, followed by demineralized water according to standard protocols. Endogenous peroxidase was blocked by incubation in 0.3% hydrogen peroxide in phosphate buffered saline (PBS) for 20 min. Antigen retrieval was performed by heat induction at 95°C using PT Link (Dako, Glostrup, Denmark) with a low-pH Envision FLEX target retrieval solution (citrate buffer pH 6.0, Dako). Immunohistochemical staining was performed by incubating tissue microarrays overnight with antibodies against uPAR (ATN-615, provided by Prof A.P. Mazar) [24] alpha smooth muscle actin (a-SMA) for myofibroblasts (PA5-16697; Thermo Fisher Scientific), and vimentin for mesenchymal cells (clone V9, Santa Cruz, USA), all at room temperature. All antibodies were used at predetermined optimal dilutions using proper positive and negative control tissue: ATN-615 at 1 µg/ml; PA5-16697 at 0.25 µg/ml; V9 at 2 µg/ml. Control samples were incubated with PBS instead of the primary antibodies. The sections were washed with PBS, followed by incubation with Envision anti-mouse (K4001; Dako) or Envision anti-Rabbit (K4003; Dako), where applicable, for 30 minutes at room temperature. After additional washing, immunohistochemical staining was visualized using 3,3-diaminobenzidine tetrahydrochloride solution (Dako) for 5-10 min resulting in brown color, and counterstained with hematoxylin, dehydrated and finally mounted in pertex.

Immunohistochemistry evaluation

All stained sections were scanned and viewed at 200x magnification using the Philips Ultra Fast Scanner 1.6 EA (Philips, Eindhoven, The Netherlands). Evaluation of the immunohistochemical staining of all molecular targets was performed blinded and independently by two observers (SG and HP). In cases of discrepancy the two observers resolved the final score in accordance with a pathologist (HM). Immunostaining positivity was determined by a combination of staining intensity and percentage of tumor cells stained. Immunostaining intensity was scored as 0 = negative, 1 = weakly positive, 2 = moderately positive, and 3 = strongly positive. However, in this relatively small cohort the staining intensity did not contribute substantially to the survival analyses. Therefore, in the final analysis percentages of uPAR staining in neoplastic cells were dichotomized as low (< 50% moderate/strong expression) or high (≥ 50% moderate/strong expression) [21]. As described in a previous study, the staining results for a-SMA were scored, according to the extent of stromal positivity, as low/negative (<50% stroma positive) or high (diffuse expression throughout tumor, > 50% stroma positive) [25].

Statistical analysis

All statistical analyses were conducted using SPSS statistical software (version 23.0, IBM SPSS Inc, Chicago, USA). Baseline characteristics were reported as frequencies, and continuous data were presented as median with interquartile range [IQR] unless indicated otherwise. Comparison of the clinical and pathological characteristics of the two cohorts were made using the Chi-squared test. Fisher's exact test was used when one of the groups counted less than 5. Disease-free survival (DFS) was defined as the time from surgery to the first evidence of local or distant recurrence disease, death from any cause or lost to follow-up, whatever came first. Overall Survival (OS) was defined as the time from the date of surgery to the date of death or lost to follow-up. Kaplan-Meier estimates of the survival function, including *p*-values from the log-rank test were used to graphically compare the time-to-event outcomes based on uPAR expression and to estimate median OS and DFS. Furthermore, uni- and multivariate survival analyses were performed using the Cox proportional hazard regression model. Only variables that were significant on univariate analysis were included in multivariate analyses. Separate multivariate models were employed, one including uPAR expression in neoplastic and stromal cells as different covariates, and another incorporating uPAR expression in both neoplastic and stromal cells as one covariate. In case the proportional hazard assumption was violated the log-rank test was used and subsequently these covariates could not be included in the multivariate regression model [26]. Statistical significance was set at $p < 0.05$.

Results

Patient and tumor characteristics

Microscopic semi-quantification of uPAR expression in neoplastic and stromal cells was successful in 89% (n = 122) of pancreatic adenocarcinoma. Patient and tumor characteristics are listed in Table 1. The median age was 65 years (IQR, 60 – 72 years), 62 (51%) patients were female and 114 (93%) patients were diagnosed with pancreatic adenocarcinoma located in the head of the pancreas. Primary tumor stage was classified as pT1 in 17 (14%) patients, pT2 in 32 (26%), pT3 in 65 (53%) and pT4 in 8 (7%) patients. In addition, the majority of patients had positive nodes (n = 93; 76%) and moderately differentiated tumors (n = 41; 45%). Complete surgical resection (R0) was possible in 83 (68%) cases and 61 (50%) patients underwent adjuvant chemotherapy after surgical resection of the tumor.

Table 1. Characteristics of pancreatic adenocarcinoma patients subdivided by uPAR expression in neoplastic and/or stromal cells.

Characteristics	uPAR in neoplastic cells			uPAR in stromal cells			uPAR in neoplastic and stromal cells		
	Low (n = 41)	High (n = 81)	*p*-value	Low (n = 22)	High (n = 100)	*p*-value	Low (n = 47)	High (n = 75)	*p*-value
Age, n (%)									
<65 years	17 (42%)	45 (56%)	0.141	7 (32%)	55 (55%)	**0.049**	19 (40%)	43 (57%)	0.069
≥65 years	24 (58%)	36 (44%)		15 (68%)	45 (45%)		28 (60%)	43 (43%)	
Sex, n (%)									
Male	20 (49%)	40 (49%)	0.950	11 (50%)	49 (49%)	0.932	21(45%)	39 (52%)	0.431
Female	21 (51%)	41 (51%)		11 (50%)	51 (51%)		26 (55%)	36 (48%)	
Tumor location, n (%)									
Head of pancreas	38 (93%)	76 (94%)	0.549	21 (96%)	93 (93%)	0.662	44 (94%)	70 (93%)	0.585
Other	3 (7%)	5 (6%)		1 (4%)	7 (7%)		3 (6%)	5 (7%)	
pT-stage, n (%)									
pT1	9 (22%)	8 (10%)	0.074	5 (23%)	12 (12%)	0.163	11 (23%)	6 (8%)	**0.015**
pT2	14 (34%)	18 (22%)		8 (36%)	24 (24%)		15 (32%)	17 (23%)	
pT3	16 (39%)	49 (61%)		7 (32%)	58 (58%)		17 (36%)	48 (64%)	
pT4	2 (5%)	6 (7%)		2 (9%)	6 (6%)		4 (9%)	4 (5%)	
pN-stage, n (%)									
pN0	8 (20%)	21 (26%)	0.432	4 (18%)	25 (25%)	0.496	10 (21%)	19 (25%)	0.608
pN1	33 (80%)	60 (74%)		18 (82%)	75 (75%)		37 (79%)	56 (75%)	

Table 1. Continued.

Characteristics	uPAR in neoplastic cells			uPAR in stromal cells			uPAR in neoplastic and stromal cells		
	Low (n = 41)	High (n = 81)	*p*-value	Low (n = 22)	High (n = 100)	*p*-value	Low (n = 47)	High (n = 75)	*p*-value
Tumor differentiation, n (%)*									
Well differentiated	7 (22%)	4 (7%)	0.093	3 (18%)	8 (11%)	0.426	7 (20%)	4 (7%)	0.136
Moderately differentiated	14 (44%)	27 (46%)		9 (53%)	32 (43%)		17 (47%)	24 (44%)	
Poorly differentiated	11 (34%)	28 (47%)		5 (29%)	34 (46%)		12 (33%)	27 (49%)	
Adjuvant therapy, n (%)									
Yes	19 (46%)	42 (52%)	0.565	11 (50%)	50 (50%)	>0.999	22 (47%)	39 (52%)	0.577
No	22 (54%)	39 (48%)		11 (50%)	50 (50%)		25 (53%)	36 (48%)	

* Tumor differentiation was only available for 75% (n = 91) of the population; significant *p*-values are bold; n, number; uPAR, urokinase plasminogen activator receptor.

uPAR expression

In pancreatic adenocarcinoma, uPAR expression was detected in both neoplastic cells and tumor-associated stroma cells, including myofibroblasts and other mesenchymal cell, as identified by staining for α-SMA and vimentin (Figures 1 and 2). uPAR expression was elevated in neoplastic cells in 66% of the cases (n = 81) and in tumor-associated cells in 82% (n = 100). A significant correlation ($P < 0.001$) was found between uPAR expression in neoplastic and tumor-associated stromal cells. About 62% (n = 75) of the patients with pancreatic adenocarcinoma demonstrated uPAR overexpression in both neoplastic and tumor-associated tumor cells.

The uPAR expression in stromal cells was significantly associated ($p = 0.049$) with age < 65 years, whereas uPAR expression in both neoplastic and stromal cells correlated ($p = 0.015$) with more advanced pT-stage. No association was found between baseline clinicopathological characteristics and uPAR expression in either neoplastic and/or stromal cells (Table 1).

Overall survival

At time of analysis, 91% (n = 111) of the study population was deceased. The median overall survival in the overall cohort was 17 months (95% CI, 15 – 19 months). Using univariate analysis, age, sex, tumor location, pT-stage, tumor differentiation, and treatment with adjuvant therapy (log-rank $p = 0.382$) were not associated with overall survival. However, positive lymph nodes, uPAR expression in neoplastic cells (median OS, 14 vs. 23 months; Figure 2A), uPAR expression in stromal cells (median OS, 16 vs. 21 months; Figure 2C), and uPAR expression in both neoplastic and stromal cells (median OS, 13 vs. 24 months; $p < 0.001$; Figure 2E) were significantly predictive for OS (Table 2).

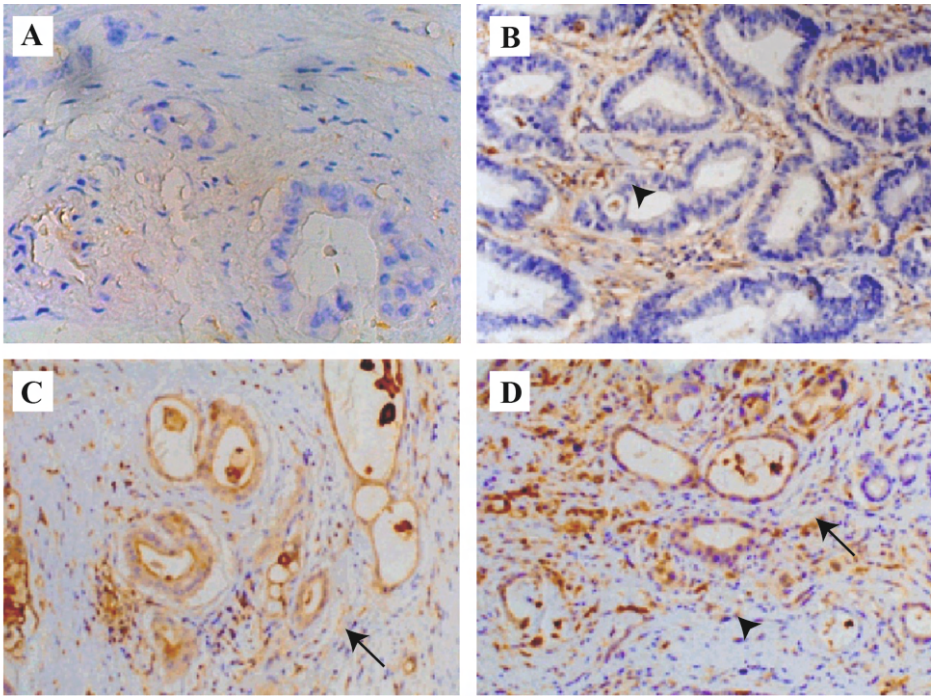

Figure 1. Representative images of pancreatic adenocarcinoma showing low uPAR expression in neoplastic epithelial (arrow) and stromal cells (arrow head). (A) Low uPAR expression; (B) uPAR expression only in stromal cells; uPAR expression in stromal and neoplastic cells (C, D) (200x magnification). uPAR; urokinase plasminogen activator receptor.

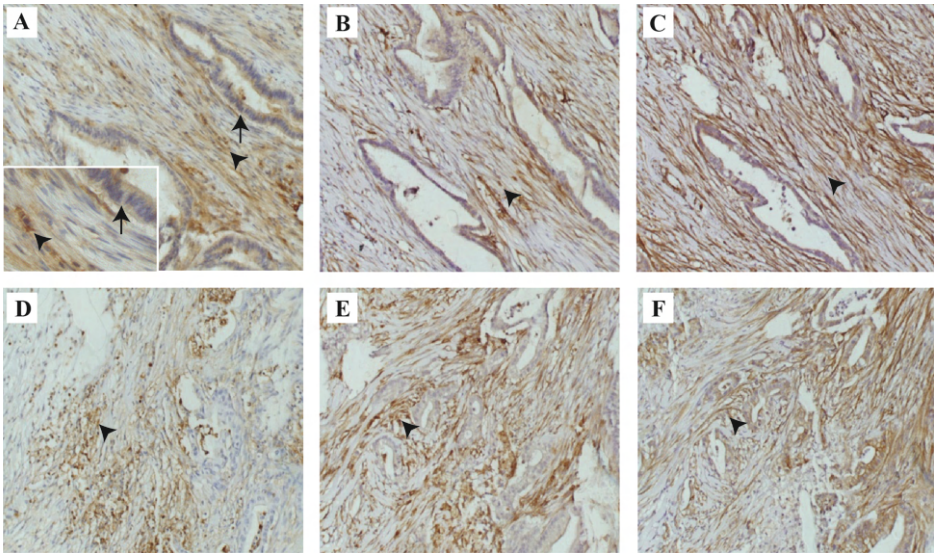

Figure 2. Representative images of immunohistochemical staining's on consecutive tissue sections demonstrating the presence of urokinase plasminogen activator receptor (A, D), vimentin (B, E) and alpha smooth muscle actin (C, F) in pancreatic adenocarcinoma (200x magnification). Arrows and arrow heads indicate respectively epithelial and stromal cells. The insert in A represents the 1000x magnification of the area with arrow and arrow head.

Table 2. Uni- and multivariate Cox proportional hazard regression analyses for the predictive value of uPAR expression on overall survival of pancreatic adenocarcinoma patients.

Covariates	Univariate analysis			Multivariate analysis (Model 1)			Multivariate analysis (Model 2)		
	HR	95% CI	*p*-value	HR	95% CI	*p*-value	HR	95% CI	*p*-value
Age (≥65 vs. 65 years)	1.11	0.76 – 1.60	0.598						
Sex (male vs. female)	1.38	0.95 – 2.00	0.096						
pT-stage (pT3-4 vs. pT1-2)	1.46	0.99 – 2.17	0.058						
pN-stage (pN1 vs. pN0)	1.86	1.16 – 3.00	**0.011**	1.96	1.21 – 3.15	**0.006**	1.92	1.19 – 3.08	**0.007**
Tumor differentiation* (well/moderately vs. poorly)	1.24	0.80 – 1.91	0.340						
uPAR in neoplastic cells (high vs. low)	1.93	1.28 – 2.91	**0.002**	1.83	1.17 – 2.85	**0.008**			
uPAR in stromal cells (high vs. low)	1.70	1.03 – 2.81	**0.036**	1.31	0.76 – 2.25	0.334			
uPAR in neoplastic and stromal cells (high vs. low)	2.27	1.52 – 3.40	**<0.001**				2.31	1.55 – 3.45	**<0.001**

*Tumor differentiation was available for 75% (n = 95) of the population; significant *p*-values are bold; CI, confidence interval; HR, hazard ratio; n, number; uPAR, urokinase plasminogen activator receptor.

In multivariate analysis, positive lymph nodes and uPAR expression in neoplastic cells were independent prognostic factors for OS, but uPAR expression in stromal cells did not keep its significance. On separate multivariate analysis, positive lymph nodes, and uPAR expression in both neoplastic and stromal cells were also significant prognostic factors for OS in pancreatic cancer (Table 2).

Disease-free survival

35% (n = 35) of all patients reported local recurrence, 63% (n = 64) distant recurrence, 42% (n = 42) liver metastasis, 22% (n = 22) lung metastasis, and 20% (n = 20) local and distant recurrence. uPAR expression in stromal cells ($p = 0.018$) was associated with the development of liver metastases. No correlations between uPAR expression and specific types of recurrence were found (Table 3).

Table 3. Recurrence by uPAR expression in pancreatic adenocarcinoma patients.

Characteristics	uPAR in neoplastic cells			uPAR in stromal cells			uPAR in neoplastic and stromal cells		
	Low (n = 34)	High (n = 67)	*p*-value	Low (n = 18)	High (n = 83)	*p*-value	Low (n = 40)	High (n = 61)	*p*-value
Local recurrence*	13 (38%)	22 (33%)	0.590	7 (39%)	28 (34%)	0.677	17 (43%)	18 (30%)	0.180
Distant recurrence*	18 (53%)	46 (69%)	0.121	10 (56%)	54 (65%)	0.448	21 (53%)	43 (71%)	0.066
Liver metastasis*	10 (29%)	32 (48%)	0.077	3 (17%)	39 (47%)	**0.018**	11 (28%)	31 (51%)	**0.020**
Lung metastasis*	7 (21%)	15 (22%)	0.836	5 (28%)	17 (21%)	0.497	9 (23%)	13 (21%)	0.887
Local and distant recurrence*	5 (15%)	15 (22%)	0.360	4 (22%)	16 (19%)	0.776	8 (20%)	12 (20%)	0.968

* Recurrence was documented for 83% (n = 101) of the cohort; significant *p*-values are bold; n, number; uPAR, urokinase plasminogen activator receptor.

In univariate analyses, age, sex, tumor location (log-rank $p = 0.727$), pT-stage, tumor differentiation, and receipt of adjuvant therapy (log-rank $p = 0.245$) did not demonstrate predictive value for DFS. However, positive lymph nodes, uPAR expression in neoplastic cells (median DFS, 11 vs. 16 months; Figure 2B), and uPAR expression in both neoplastic and stromal cells (median DFS, 10 vs. 16 months; Figure 3F) were significantly associated with poor survival (Table 4). The association of uPAR expression in stromal cells with OS did not reach statistical significance (median DFS, 11 vs. 15 months; HR, Figure 2D).

Multivariate analysis showed that positive lymph nodes, uPAR expression in neoplastic cells and uPAR expression in both neoplastic and stromal cells were independently associated with poor DFS (Table 4).

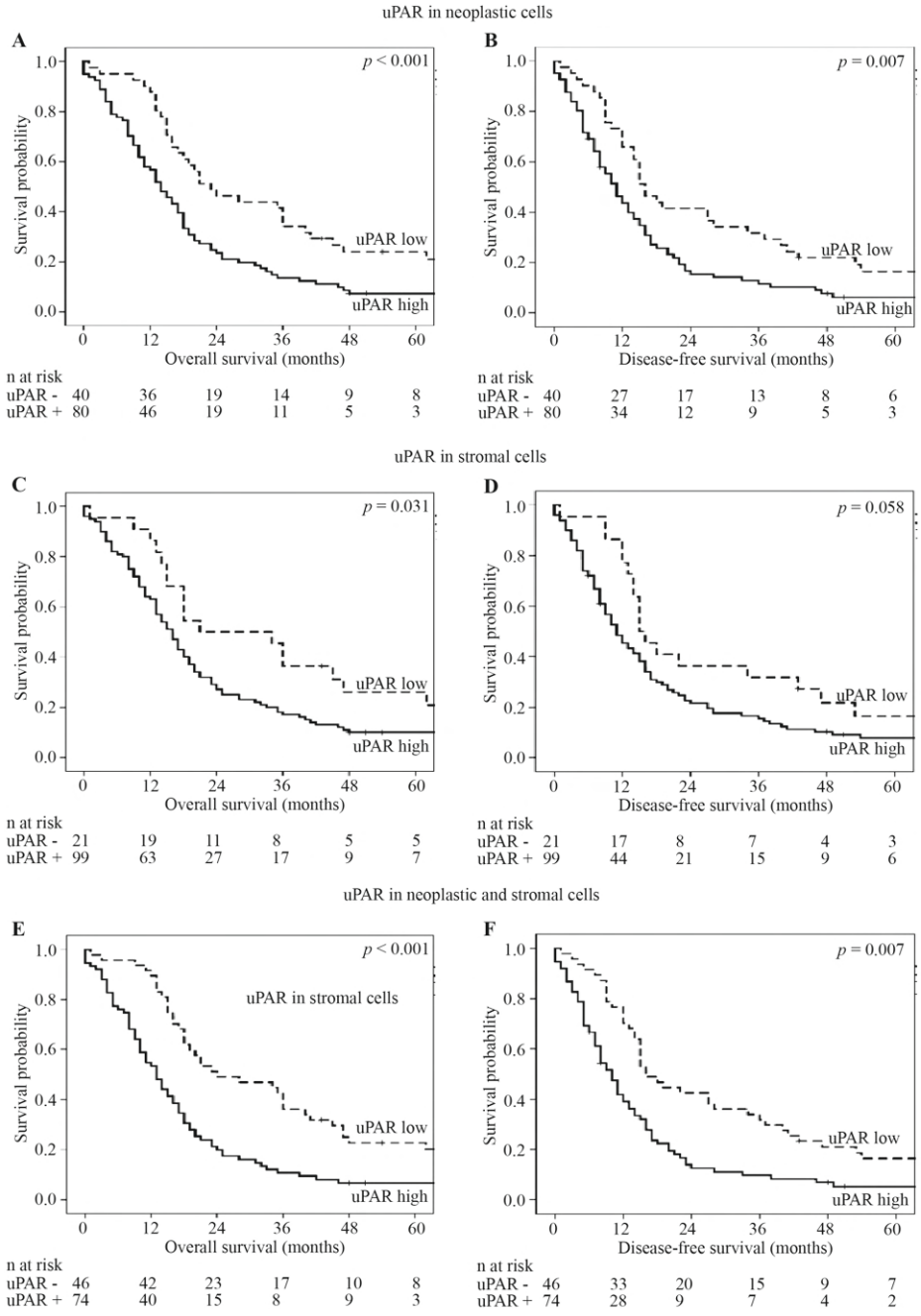

Figure 3. Kaplan-Meier curves for overall and disease-free survival for pancreatic adenocarcinoma patients after surgical treatment, stratified by the status of uPAR expression in neoplastic cells (A, B), uPAR expression in stromal cells (C, D), and in both neoplastic and stromal cells (E, F). n, number; uPAR; urokinase plasminogen activator receptor.

Table 4. Uni- and multivariate Cox proportional hazard regression analyses for the predictive value of uPAR expression on disease-free survival in pancreatic adenocarcinoma patients.

Covariates	Univariate analysis			Multivariate analysis (Model 1)			Multivariate analysis (Model 2)		
	HR	95% CI	*p*-value	HR	95% CI	*p*-value	HR	95% CI	*p*-value
Age (≥65 vs. 65 years)	1.03	0.71 – 1.49	0.892						
Sex (female vs. male)	1.21	0.83 – 1.76	0.319						
pT-stage (pT3-4 vs. pT1-2)	1.01	1.00 – 1.03	0.153						
pN-stage (pN1 vs. pN0)	1.86	1.15 – 2.99	**0.011**	1.95	1.21 – 3.14	**0.006**	1.91	1.19 – 3.08	**0.007**
Tumor differentiation* (well/moderately vs. poorly)	1.16	0.75 – 1.80	0.511						
uPAR in neoplastic cells (high vs. low)	1.72	1.15 – 2.58	**0.009**	1.66	1.06 – 2.58	**0.025**			
uPAR in stromal cells (high vs. low)	1.58	0.97 – 2.58	0.065	1.26	0.74 – 2.15	0.394			
uPAR in neoplastic and stromal cells (high vs. low)	2.00	1.34 – 2.98	**0.001**				2.05	1.37 – 3.04	**<0.001**

* Tumor differentiation was available for 75% (n = 95) of the population; significant *p*-values are bold; CI, confidence interval; HR, hazard ratio; n, number; uPAR, urokinase plasminogen activator receptor

Discussion

Outcomes after resection for pancreatic adenocarcinoma are variable and contingent on both the biology of the disease and the efficacy of the treatment. Determination of proteins or pathways that increase risk of recurrence and impair survival might be helpful to assist with the selection of pancreatic cancer patients who could benefit from (neo)adjuvant and targeted therapies. The results of this immunohistochemical study reveal a significant inverse correlation between uPAR expression and OS and DFS of pancreatic cancer patients. The prognostic impact of uPAR in stromal cells is striking, but it is not an independent parameter, like uPAR expression in neoplastic cells.

Relatively few studies have analyzed tissue expression of uPAR and its association with prognosis in pancreatic cancer [27]. In 1997 Cantero and co-workers were the first to report worse survival for patients with high uPAR positive pancreas tumors in a small cohort of 30 patients [15]. Although they noticed uPAR staining in malignant epithelial cells and stroma cells, they did not correlate these separately with survival. More than 10 years later the level of uPAR mRNA was shown not to be correlated with prognosis in a small cohort of 25 patients, whereas in another

study with 46 patients uPAR mRNA appeared to be the strongest biological prognostic marker [28, 29]. The prognostic association of uPAR with pancreatic cancer was further confirmed by the measurement of high levels of soluble uPAR in urine of these patients [30]. Our data, in a relatively large cohort of pancreatic cancer patients, confirm the association between uPAR and survival. This suggests a role for uPAR as a potential independent indicator for the identification of higher risk patient subgroups, like has been found for other tumor types, including colorectal, breast, and lung cancer [20, 31, 32].

uPAR enhancement on malignant cells can partly be explained by oncogenic amplification of the PLAUR gene, as has been identified by Ströbel and co-workers in 52% of the cases in a cohort of 50 pancreatic cancer patients [22]. However, uPAR up-regulation in neoplastic cells is not dependent solely on gene amplification, as uPAR expression is also up-regulated by several oncologic pathways in which transcription factors like AP1 and PEA3/ETS are involved [11]. Furthermore, environmental factors like TNF-α and interleukins can enhance uPAR expression, which could partly explain the up-regulation in tumor stromal cells, like myofibroblasts, macrophages and endothelial cells [33]. Up-regulation of uPAR in these cells has no genetic background and is primarily a response to signals from the cancer cells. The association of uPAR up-regulation in stromal cells with survival, as found in this study, turned out not to be independent in multivariate analyses, like has been found in other tumor types [21, 34-36]. However, in these other tumors the uPAR positive stromal cells were often located at the invasive front, which seems not specifically the case for uPAR expressing stromal cells in pancreatic cancer.

Just the presence of uPAR on certain cell types does not contribute to the malignancy of a tumor and could not explain a prognostic relevance. As a receptor, uPAR is strongly dependent on its interaction with other proteins for its functions [11]. The most obvious function of uPAR is the stimulation of proteolysis, which does not exist without the presence of plasminogen and uPA, and is otherwise tightly regulated by the presence of inhibitors PAI-1 and PAI-2. The chemotactic function of uPAR depends on cleavage by uPA, where again the inhibitors play a regulatory role. Also, uPAR-mediated intracellular signaling relies on the binding of uPA, vimentin, and several integrins as ligands. Because uPAR itself does not contain an intracellular domain, these signals are transduced by other, 'professional' signaling proteins with transmembrane and intracellular domains like tyrosine kinase receptors, g-protein coupled receptors, and integrins [37]. All these interactions between uPAR and other proteins, plus the shedding of one of the 3 domains by uPA influence the 3-dimensional structure of uPAR. Therefore, it is well established that different anti-uPAR antibodies with varying epitope specificity result in different immunohistochemical staining patterns [38]. Obviously, part of the discrepancies regarding the prognostic

value of uPAR in pancreatic cancer described in the literature may be explained by the use of antibodies targeting different domains within the uPAR protein. In the present study the extensively validated antibody ATN-615 was used, which detects almost all forms of uPAR, probably explaining the abundant presence of uPAR in multiple cell types in comparison with some other studies [24].

Another difference with previous studies is the use of a TMA, which might also be the biggest limitation of this study. Although the tumor areas were carefully selected to represent a complete overview of the tumor, the possibility of discrepant patterns of uPAR in comparison with conventional tissue sections is not ruled out. However, previous studies in breast cancer demonstrated that analysis of at least two cores on the tissue micro array is comparable to the analysis of whole tissue sections in >95% of cases [39]. Another restriction of this study is that patients with metastatic unresectable disease at time of diagnosis could not be included, since these patients rarely have adequate tissue for detailed immunohistochemical evaluation. Considering the uPAR distribution in stage and grade, it seems not likely that including these patients with expected bad prognosis would have influenced the analysis dramatically.

Next to a possible application as prognostic marker, uPAR may also hold promise as a selective target for either tumor-specific image-guided surgery or targeted-therapy, because of its absence in normal pancreatic tissue and chronic pancreatitis [40, 41]. A pre-clinical study has indeed demonstrated the ability of uPAR-targeted NIR-dye-labelled theranostic nanoparticles, to visualize residual disease in pancreatic xenografts [42]. Furthermore, uPAR-targeted magnetic iron oxide nanoparticles carrying gemcitabine were able to overcome the tumor stromal barrier and subsequently were able to enhance the efficiency of the drug. This is particularly relevant, as high resistance to therapy is a major challenge in pancreatic cancer care [43, 44].

Conclusion

In summary, this study demonstrates in a relatively large cohort of pancreatic adenocarcinoma patients, that uPAR expression, in particular determined in stromal cells as well as in cancerous cells, is predictive for unfavorable OS and DFS. Evaluation of uPAR expression, alone or in combination with other predictive factors, may improve the identification of patients who could benefit from more aggressive treatment. Although the combination of uPAR determination in neoplastic cells and stromal cells seemed to have the highest prognostic impact, further studies for better understanding of the mechanisms involved are still necessary.

References

1. Rahib L, Smith BD, Aizenberg R, Rosenzweig AB, Fleshman JM, Matrisian LM. Projecting cancer incidence and deaths to 2030: the unexpected burden of thyroid, liver, and pancreas cancers in the United States. Cancer Res. 2014;74:2913-21. doi:10.1158/0008-5472.CAN-14-0155.
2. Siegel R, Ma J, Zou Z, Jemal A. Cancer statistics, 2014. CA Cancer J Clin. 2014;64:9-29. doi:10.3322/caac.21208.
3. Griffin JF, Smalley SR, Jewell W, Paradelo JC, Reymond RD, Hassanein RE, et al. Patterns of failure after curative resection of pancreatic carcinoma. Cancer. 1990;66:56-61.
4. Westerdahl J, Andren-Sandberg A, Ihse I. Recurrence of exocrine pancreatic cancer--local or hepatic? Hepatogastroenterology. 1993;40:384-7.
5. Yeo CJ, Cameron JL, Lillemoe KD, Sitzmann JV, Hruban RH, Goodman SN, et al. Pancreaticoduodenectomy for cancer of the head of the pancreas. 201 patients. Ann Surg. 1995;221:721-31.
6. Sperti C, Pasquali C, Piccoli A, Pedrazzoli S. Recurrence after resection for ductal adenocarcinoma of the pancreas. World J Surg. 1997;21:195-200.
7. Fischer R, Breidert M, Keck T, Makowiec F, Lohrmann C, Harder J. Early recurrence of pancreatic cancer after resection and during adjuvant chemotherapy. Saudi J Gastroenterol. 2012;18:118-21. doi:10.4103/1319-3767.93815.
8. Aoyama T, Murakawa M, Katayama Y, Yamaoku K, Kanazawa A, Higuchi A, et al. Impact of postoperative complications on survival and recurrence in pancreatic cancer. Anticancer Res. 2015;35:2401-9.
9. Sho M, Akahori T, Tanaka T, Kinoshita S, Nagai M, Nishiwada S, et al. Optimal indication of neoadjuvant chemoradiotherapy for pancreatic cancer. Langenbecks Arch Surg. 2015;400:477-85. doi:10.1007/s00423-015-1304-0.
10. Bergquist JR, Puig CA, Shubert CR, Groeschl RT, Habermann EB, Kendrick ML, et al. Carbohydrate Antigen 19-9 Elevation in Anatomically Resectable, Early Stage Pancreatic Cancer Is Independently Associated with Decreased Overall Survival and an Indication for Neoadjuvant Therapy: A National Cancer Database Study. J Am Coll Surg. 2016;223:52-65. doi:10.1016/j.jamcollsurg.2016.02.009.
11. Blasi F, Sidenius N. The urokinase receptor: focused cell surface proteolysis, cell adhesion and signaling. FEBS Lett. 2010;584:1923-30. doi:S0014-5793(09)01085-0 [pii];10.1016/j.febslet.2009.12.039 [doi].
12. Mazar AP. Urokinase plasminogen activator receptor choreographs multiple ligand interactions: implications for tumor progression and therapy. Clin Cancer Res. 2008;14:5649-55. doi:10.1158/1078-0432.CCR-07-4863.
13. Grøndahl-Hansen J, Peters HA, van Putten WL, Look MP, Pappot H, Rønne E, et al. Prognostic significance of the receptor for urokinase plasminogen activator in breast cancer. Clin Cancer Res. 1995;1:1079-87.
14. Duggan C, Maguire T, McDermott E, O'Higgins N, Fennelly JJ, Duffy MJ. Urokinase plasminogen activator and urokinase plasminogen activator receptor in breast cancer. Int J Cancer. 1995;61:597-600.
15. Cantero D, Friess H, Deflorin J, Zimmermann A, Brundler MA, Riesle E, et al. Enhanced expression of urokinase plasminogen activator and its receptor in pancreatic carcinoma. Br J Cancer. 1997;75:388-95.
16. de Bock CE, Wang Y. Clinical significance of urokinase-type plasminogen activator receptor (uPAR) expression in cancer. Med Res Rev. 2004;24:13-39. doi:10.1002/med.10054.

17. Bhuvarahamurthy V, Schroeder J, Denkert C, Kristiansen G, Schnorr D, Loening SA, et al. In situ gene expression of urokinase-type plasminogen activator and its receptor in transitional cell carcinoma of the human bladder. Oncol Rep. 2004;12:909-13.
18. Bhuvarahamurthy V, Schroeder J, Kristiansen G, Roigas J, Denkert C, Johannsen M, et al. Differential gene expression of urokinase-type plasminogen activator and its receptor in human renal cell carcinoma. Oncol Rep. 2005;14:777-82.
19. Cozzi PJ, Wang J, Delprado W, Madigan MC, Fairy S, Russell PJ, et al. Evaluation of urokinase plasminogen activator and its receptor in different grades of human prostate cancer. Hum Pathol. 2006;37:1442-51. doi:10.1016/j.humpath.2006.05.002.
20. Hildenbrand R, Schaaf A, Dorn-Beineke A, Allgayer H, Sutterlin M, Marx A, et al. Tumor stroma is the predominant uPA-, uPAR-, PAI-1-expressing tissue in human breast cancer: prognostic impact. Histol Histopathol. 2009;24:869-77.
21. Boonstra MC, Verbeek FP, Mazar AP, Prevoo HA, Kuppen PJ, Van de Velde CJ, et al. Expression of uPAR in tumor-associated stromal cells is associated with colorectal cancer patient prognosis: a TMA study. BMC Cancer. 2014;14:269. doi:1471-2407-14-269 [pii];10.1186/1471-2407-14-269 [doi].
22. Hildenbrand R, Niedergethmann M, Marx A, Belharazem D, Allgayer H, Schleger C, et al. Amplification of the urokinase-type plasminogen activator receptor (uPAR) gene in ductal pancreatic carcinomas identifies a clinically high-risk group. Am J Pathol. 2009;174:2246-53. doi:S0002-9440(10)61083-8 [pii];10.2353/ajpath.2009.080785 [doi].
23. Greene FL. The American Joint Committee on Cancer: updating the strategies in cancer staging. Bull Am Coll Surg. 2002;87:13-5.
24. Li Y, Parry G, Chen L, Callahan JA, Shaw DE, Meehan EJ, et al. An anti-urokinase plasminogen activator receptor (uPAR) antibody: crystal structure and binding epitope. J Mol Biol. 2007;365:1117-29. doi:S0022-2836(06)01439-2 [pii];10.1016/j.jmb.2006.10.059 [doi].
25. Horn LC, Schreiter C, Canzler A, Leonhardt K, Einenkel J, Hentschel B. CD34(low) and SMA(high) represent stromal signature in uterine cervical cancer and are markers for peritumoral stromal remodeling. Ann Diagn Pathol. 2013;17:531-5. doi:10.1016/j.anndiagpath.2013.05.009.
26. Putter H, Sasako M, Hartgrink HH, van de Velde CJ, van Houwelingen JC. Long-term survival with non-proportional hazards: results from the Dutch Gastric Cancer Trial. Stat Med. 2005;24:2807-21. doi:10.1002/sim.2143.
27. Boonstra MC, Verspaget HW, Ganesh S, Kubben FJ, Vahrmeijer AL, Van de Velde CJ, et al. Clinical Applications of the Urokinase Receptor (uPAR) for Cancer Patients. Curr Pharm Des. 2011;17:1890-910. doi:BSP/CPD/E-Pub/000490 [pii].
28. Warnecke-Eberz U, Prenzel KL, Baldus SE, Metzger R, Dienes HP, Bollschweiler E, et al. Significant down-regulation of the plasminogen activator inhibitor 1 mRNA in pancreatic cancer. Pancreas. 2008;36:173-7. doi:10.1097/MPA.0b013e31815ac538.
29. Xue A, Scarlett CJ, Jackson CJ, Allen BJ, Smith RC. Prognostic significance of growth factors and the urokinase-type plasminogen activator system in pancreatic ductal adenocarcinoma. Pancreas. 2008;36:160-7. doi:10.1097/MPA.0b013e31815750f0 [doi];00006676-200803000-00009 [pii].
30. Sorio C, Mafficini A, Furlan F, Barbi S, Bonora A, Brocco G, et al. Elevated urinary levels of urokinase-type plasminogen activator receptor (uPAR) in pancreatic ductal adenocarcinoma identify a clinically high-risk group. BMC Cancer. 2011;11:448. doi:1471-2407-11-448 [pii];10.1186/1471-2407-11-448 [doi].
31. Pedersen H, Brünner N, Francis D, Osterlind K, Rønne E, Hansen HH, et al. Prognostic impact of urokinase, urokinase receptor, and type 1 plasminogen activator inhibitor in squamous and large cell lung cancer tissue. Cancer Res. 1994;54:4671-5.

32. Boonstra MC, Verbeek FP, Mazar AP, Prevoo HA, Kuppen PJ, van de Velde CJ, et al. Expression of uPAR in tumor-associated stromal cells is associated with colorectal cancer patient prognosis: a TMA study. BMC Cancer. 2014;14:269. doi:10.1186/1471-2407-14-269.
33. Tran-Thang C, Kruithof E, Lahm H, Schuster WA, Tada M, Sordat B. Modulation of the plasminogen activation system by inflammatory cytokines in human colon carcinoma cells. Br J Cancer. 1996;74:846-52.
34. Laerum OD, Ovrebo K, Skarstein A, Christensen IJ, Alpizar-Alpizar W, Helgeland L, et al. Prognosis in adenocarcinomas of lower oesophagus, gastro-oesophageal junction and cardia evaluated by uPAR-immunohistochemistry. Int J Cancer. 2012;131:558-96. doi:10.1002/ijc.26382 [doi].
35. Illemann M, Laerum OD, Hasselby JP, Thurison T, Hoyer-Hansen G, Nielsen HJ, et al. Urokinase-type plasminogen activator receptor (uPAR) on tumor-associated macrophages is a marker of poor prognosis in colorectal cancer. Cancer Med. 2014;3:855-64. doi:10.1002/cam4.242 [doi].
36. Dohn LH, Illemann M, Hoyer-Hansen G, Christensen IJ, Hostmark J, Litlekalsoy J, et al. Urokinase-type plasminogen activator receptor (uPAR) expression is associated with T-stage and survival in urothelial carcinoma of the bladder. Urol Oncol. 2015;33:165 e15-24. doi:10.1016/j.urolonc.2014.12.001.
37. Ferraris GM, Sidenius N. Urokinase plasminogen activator receptor: a functional integrator of extracellular proteolysis, cell adhesion, and signal transduction. Semin Thromb Hemost. 2013;39:347-55. doi:10.1055/s-0033-1334485 [doi].
38. Ahn SB, Chan C, Dent OF, Mohamedali A, Kwun SY, Clarke C, et al. Epithelial and stromal cell urokinase plasminogen activator receptor expression differentially correlates with survival in rectal cancer stages B and C patients. PLoS ONE. 2015;10:e0117786. doi:10.1371/journal.pone.0117786 [doi];PONE-D-14-41445 [pii].
39. Kyndi M, Sorensen FB, Knudsen H, Overgaard M, Nielsen HM, Andersen J, et al. Tissue microarrays compared with whole sections and biochemical analyses. A subgroup analysis of DBCG 82 b&c. Acta Oncol. 2008;47:591-9. doi:10.1080/02841860701851871.
40. Chen Y, Zheng B, Robbins DH, Lewin DN, Mikhitarian K, Graham A, et al. Accurate discrimination of pancreatic ductal adenocarcinoma and chronic pancreatitis using multimarker expression data and samples obtained by minimally invasive fine needle aspiration. Int J Cancer. 2007;120:1511-7. doi:10.1002/ijc.22487.
41. de Geus SW, Boogerd LS, Swijnenburg RJ, Mieog JS, Tummers WS, Prevoo HA, et al. Selecting Tumor-Specific Molecular Targets in Pancreatic Adenocarcinoma: Paving the Way for Image-Guided Pancreatic Surgery. Mol Imaging Biol. 2016. doi:10.1007/s11307-016-0959-4.
42. Yang L, Sajja HK, Cao Z, Qian W, Bender L, Marcus AI, et al. uPAR-targeted optical imaging contrasts as theranostic agents for tumor margin detection. Theranostics. 2013;4:106-18. doi:10.7150/thno.7409.
43. Warshaw AL, Fernandez-del Castillo C. Pancreatic carcinoma. N Engl J Med. 1992;326:455-65. doi:10.1056/NEJM199202133260706.
44. Lee GY, Qian WP, Wang L, Wang YA, Staley CA, Satpathy M, et al. Theranostic nanoparticles with controlled release of gemcitabine for targeted therapy and MRI of pancreatic cancer. ACS nano. 2013;7:2078-89. doi:10.1021/nn3043463.

Chapter 3

EGFR and $\alpha_v\beta_6$ as promising targets for molecular imaging of cutaneous and mucosal squamous cell carcinoma of the head-and-neck region

---

Baart VM, van Duijn C, van Egmond SL, Dijckmeester WA, Jansen JC, Vahrmeijer AL, Sier CFM, Cohen D.

Cancers 2020; 12(6):1474.

Abstract

R0 resection is paramount in cutaneous squamous cell carcinoma (CSCC) and head-and-neck squamous cell carcinoma (HNSCC). However, in the setting of recurrence, immunocompromised patients or non-keratinizing squamous cell carcinoma (SCC) with spindled growth pattern, tumor borders are difficult if not impossible to determine. Fluorescence-guided surgery (FGS) aids in this differentiation.

Methods & Results: Potential targets for FGS of CSCC and HNSCC were evaluated. Most sections stained intensely for $\alpha_v\beta_6$ and epidermal growth factor receptor (EGFR) on tumor cells. However, normal epithelium stained less for $\alpha_v\beta_6$ than EGFR. Soft tissue and stroma stained negative for both, allowing for clear discrimination of the soft tissue margin. Tumor cells weakly expressed urokinase plasminogen activator receptor (uPAR) while expression on stromal cells was moderate. Normal epithelium rarely expressed uPAR resulting in clear discrimination of superficial margins. Tumors did not consistently express integrin β_3, carcinoembryonic antigen, epithelial cell adhesion molecule and vascular endothelial growth factor A.

Conclusion: In conclusion, $\alpha_v\beta_6$ and EGFR allowed for precise discrimination of SSC at the, for surgeons, problematic soft-tissue margins. Superficial margins are ideally distinguished with uPAR. In the future, FGS in the surgically challenging setting of cutaneous and mucosal SCC could benefit from a tailor-made approach, with EGFR and $\alpha_v\beta_6$ as targets.

Introduction

Cutaneous squamous cell carcinoma (CSCC) accounts for roughly 20% of all skin malignancies and unlike the most common skin cancer, basal cell carcinoma, has a substantial risk of metastasizing [1]. Furthermore, recurrence rates can exceed 50% in patients with high risk factors such as head-and-neck localization, perineural involvement, or immunosuppression [2-5]. In all these cases, local control by achieving tumor free margins is paramount in decreasing the risk for metastasis and recurrence [6].

Head-and-neck squamous cell carcinoma (HNSCC) arises from the mucosal epithelium of the oral cavity, nasal cavity, paranasal sinuses and pharynx [7]. By incidence, these tumors are the eight most common cancer types worldwide and account for more than 400,000 deaths annually [8]. Although the last decades have led to significant insights into the risk factors, carcinogenesis, and therapeutic possibilities of HNSCC, the 5-year mortality rate is still around a devastating 50% [9]. Considering that incomplete resection rates are currently at 15-30% and are directly associated with poor patient outcomes, a significant gain can be achieved by decreasing positive margin rates [10-12].

Margins are tumor-positive in 6.3-12.8% of tumor resections of cutaneous and mucosal squamous cell carcinomas (SCC) of the head-and-neck region [13, 14]. Especially in the setting of recurrence after previous R1 resection or irradiation, immunocompromised patients or non-keratinizing SCC with spindled growth pattern, tumor borders are difficult if not impossible to determine. In these high-risk cases, irradical resection rates can be up to 60% and local recurrence rates as high as 50% [2, 14]. To reduce the number of positive resection margins, fluorescence-guided imaging (FGS) has been introduced into the operating theaters. FGS grants a unique opportunity to visualize tumors and possible (nodal) metastasis using an advanced camera system and fluorescently labeled tracers targeting specific membrane-associated proteins on cancer cells [15]. Proper identification of tumor-specific targets for molecular imaging is key to the success of FGS [16, 17]. For HNSCC the epidermal growth factor receptor (EGFR) has been identified as a suitable candidate and various exploratory preclinical and clinical trials have indicated the potential of this concept in aiding surgeons during head-and-neck tumor removal [18, 19]. However, an appropriate study comparing the expression of molecular targets suitable for rapid translation towards the clinic in HNSCC and CSSC for the goal of FGS has not yet been undertaken.

Therefore, this study aims to compare the immunohistochemical expression of EGFR versus $\alpha_v\beta_6$, integrin β_3, carcinoembryonic antigen (CEA), epithelial cell adhesion molecule (EpCAM), urokinase plasminogen activator receptor (uPAR) and vascular endothelial growth factor A (VEGF-A) as targets for FGS of high-risk CSCC and HNSCC.

Materials and methods

Patient and tissue selection

Medical records of patients who underwent surgical resection for confirmed squamous cell carcinoma at the department of Otorhinolaryngology and Head & Neck Surgery of the Leiden University Medical Center between January 2014 and February 2019 were retrospectively reviewed. Patients were sub-grouped based on tumor localization (CSCC n = 37, HNSCC n = 19). Clinicopathological data were collected to assess the immune status of the patients. Patients with a positive history for an organ transplant at least one year before tumor occurrence and subsequent use of immune-suppressive medication were considered immune-compromised. Patients who did not have a transplant history but used immune-suppressive medication in the year before their tumor-associated surgery were regarded as possibly immune-compromised. Immune-competent patients had no history of transplant or immune-suppressive drug use.

Tissue samples were selected based on the simultaneous presence of tumor tissue, surrounding unaffected tissue, and pre-existent normal squamous epithelium. A specialized, experienced pathologist (DC) reviewed the tissue samples before inclusion in the study. The local ethics review board (Medische-Ethische Toetsingscommissie Leiden Den Haag Delft (METC-LDD)) approved the study protocol and research was conducted according to Code Goed Gebruik (Human Tissue and Medical Research: Code of conduct for responsible use (2011)) and Code Goed Gedrag (Code of Conduct for Medical Research (2004)). Both codes are prescribed by the Dutch Federation of Medical Scientific Societies. Informed consent was not needed for this study. Samples and data were non-identifiable and used in accordance with the 1964 Helsinki declaration.

Antibodies and reagents

The molecular target selection was based on both the potential of a quick clinical translation (EGFR, CEA, EpCAM, VEGF-A) and the potential specificity for squamous cell carcinoma ($\alpha_v\beta_6$, integrin β_3 and uPAR). The antibodies and reagents used for the immunohistochemical stainings can be found in supplementary table 1.

Immunohistochemistry

Formalin-fixed, paraffin-embedded tissue blocks from the department of Pathology of the Leiden University Medical Center were collected and sliced into tissue sections of 4 µm. Sections were deparaffinized in xylene and rehydrated via serially diluted ethanol solutions. Endogenous peroxide was blocked for 20 minutes with 0.3% hydrogen peroxide diluted in demi-water. When appropriate, antigen retrieval

was performed as described in supplementary table 1. Subsequently, sections were incubated overnight at room temperature with the primary antibody. Optimal dilution for each of the primary antibodies was determined beforehand on squamous cell tissue (see supplementary table 1). Slides were washed three times with phosphate-buffered saline (pH 7.5) before incubating the slides for 30 minutes at room temperature with the secondary antibody, followed by another washing step. Staining was visualized with 3,3-diaminobenzidine tetrahydrochloride solution (Dako, K3468) for 5 minutes at room temperature and counterstained for 20 seconds with hematoxylin (Klinipath 4085.9002). After dehydration of the slides, they were mounted in Pertex (Histolab, 0081EX).

Immunohistochemistry analysis

Stained sections were digitized with the Panoramic Digital Slide Scanner and viewed with CaseViewer 2.3 (both from 3D Histech). Evaluation of immunohistochemical staining of all tissues occurred independently by two observers after a training period by an experienced pathologist. Upon disagreement, observers discussed together to reach a consensus. If no agreement could be reached, the pathologist determined the final score. Expression of each molecular biomarker was assessed for presence on tumor, stromal, and normal squamous epithelial cells based on an intensity and percentage score. The intensity was subdivided in four groups (0 = none, 1 = weak, 2 = moderate, 3 = intense) and the percentage of cells in five groups (0 = 0-5 %, 1 = 6-25%, 2 = 26-50%, 3 = 51-75%, 4 >75%). The final intensity and percentage scores were multiplied together to get a total score, resulting in a 9-point ordinal scale (0, 1, 2, 3, 4, 6, 8, 9, 12).

Whether the biomarker was suitable as a molecular tumor-imaging target was assessed by the newly introduced tumor-border score (TBS). Relevant for tumor imaging is the difference in expression of the biomarker between cancerous and non-cancerous tissue, whether that be normal epithelium, subcutaneous tissue or other soft tissue [20]. For the TBS an imaginary line was drawn on the H&E stained slide along the tumor border by the pathologist and the difference in intensity between the tumor area and non-cancerous tissue (0 = no difference, 1 = slight difference, 2 = moderate difference, 3 = large difference) and the percentage of border that contained this difference (0 = 0-5 %, 1 = 6-25%, 2 = 26-50%, 3 = 51-75%, 4 >75%) was scored. These scores were multiplied, resulting in a 9-point ordinal scale (0, 1, 2, 3, 4, 6, 8, 9, 12) indicating the usefulness of the molecular target for tumor-imaging. Supplementary Figure 1 contains examples.

Statistical analysis

Statistical analysis was performed using IBM SPSS Statistics 23.0 (SPSS, IBM Corporation). Results were reported as medians followed by the 1st and 3rd quartile in brackets. The Kruskal-Wallis one-way ANOVA test with Dunn's post hoc test and Bonferroni correction determined the difference of staining between patients with various immune-status. Results of $p < 0.05$ were considered statistically significant.

Results

Patient characteristics

Tumor tissue from 56 patients, 37 with CSCC and 19 with HNSCC, treated at the Department of Otorhinolaryngology and Head & Neck Surgery in the Leiden University Medical Center were included in the study and stained for the biomarkers. Clinical characteristics of this cohort are included in table 1. Importantly, 25.0% (14/56) of patients had involved margins, and 21.5% (12/56) had narrow margins (<3 mm). Furthermore 37.8% (14/37) of CSCC patients were immune-compromised, 18.9% (7/37) potentially immune-compromised, and 43.2% (16/37) not immune-compromised. As the compromised patients represent an important group of high-risk cases, a sub-group analysis was performed with the three most promising biomarkers to determine whether immunosuppression altered biomarker expression.

Table 1. Characteristics of high-risk SCC patients subdivided by origin: CSCC vs HNSCC.

Characteristics	Total Population (n = 56)	CSCC (n = 37)	HNSCC (n = 19)
Age, mean (SD)	70 (11)	72 (10)	67 (11)
Male gender, n (%)	49 (87.5%)	34 (91.9%)	15 (78.9%)
Tumor differentiation, n (%)			
Well differentiated	4 (7.1%)	3 (8.1%)	1 (5.3%)
Moderately differentiated	18 (32.1%)	8 (21.6%)	10 (52.6%)
Poorly differentiated	10 (17.9%)	8 (21.6%)	2 (10.5%)
Missing	24 (42.9%)	18 (48.6%)	6 (31.6%)
Primary tumor, n (%)			
pT1	31 (55.3%)	22 (59.5%)	9 (47.4)
pT2	11 (19.6%)	10 (27.0%)	1 (5.3%)
pT3	4 (7.1%)	2 (5.4%)	2 (10.5%)
pT4	10 (17.9%)	3 (8.1%)	7 (36.8%)
Regional lymph nodes, n (%)			
cN0, pN not assessed	41 (73.2%)	32 (86.5%)	9 (47.4%)

Table 1. Continued.

Characteristics	Total Population (n = 56)	CSCC (n = 37)	HNSCC (n = 19)
pN0	8 (14.3%)	1 (2.7%)	7 (36.8%)
pN1	2 (3.6%)	1 (2.7%)	1 (5.3%)
pN2	5 (9.0%)	3 (8.1%)	2 (10.5%)
Surgical margin status, n (%)			
R0	30 (53.6%)	19 (51.4%)	11 (57.9%)
Narrow	12 (21.4%)	7 (18.9%)	5 (26.3%)
R1	14 (25.0%)	11 (29.7%)	3 (15.8%)
Immune Status, n (%)			
Compromised	n.a.	14 (37.8%)	n.a.
Potentially Compromised	n.a.	7 (18.9%)	n.a.
Not compromised	n.a.	16 (43.2%)	n.a.

CSCC, cutaneous squamous cell carcinoma; HNSCC, head-and-neck squamous cell carcinoma; n, number; n.a., not applicable; SD, standard deviation; SCC, squamous cell carcinoma.

EGFR immunohistochemical staining

For EGFR, there was intense membranous staining of tumor cells, whereas a rare tumor also stained weakly in the tumor stroma cell population and subcutaneous tissue. Besides staining within the tumor, normal squamous epithelium and skin adnexa also expressed EGFR in similar intensity as found in the tumor (Figure 1A). This resulted in the following staining scores for tumor cells, stromal cells and normal epithelium: 12 (12, 12), 0 (0, 1), 12 (9, 12) respectively (Figure 1B).

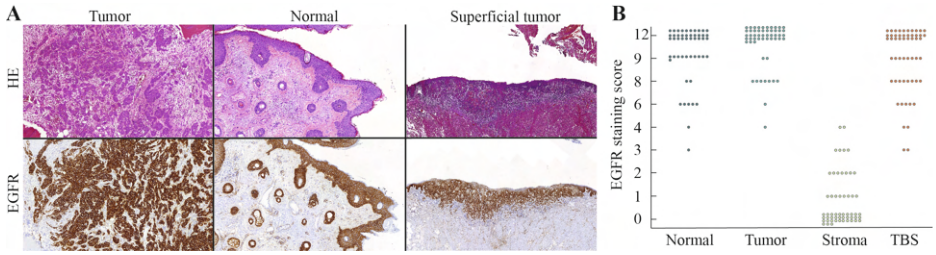

Figure 1. EGFR expression of SCC of the head-and-neck. (A) HE and EGFR immunohistochemical staining showing the results of a typical tumor (left), normal squamous epithelium and skin adnexa (middle), and a superficial tumor (right). (B) Graph demonstrating the distribution of the immunohistochemical staining scores for tumor cells, stromal cells, normal epithelium and TBS. EGFR, epidermal growth factor receptor; HE, hematoxylin & eosin; SCC, squamous cell carcinoma; TBS, tumor-border score.

$\alpha_v\beta_6$ immunohistochemical staining

$\alpha_v\beta_6$ showed a clear membranous presence and tumor cells were intensely positive with no expression in the tumor stroma. There was varied expression in normal

squamous tissue that was mostly restricted to the basal membrane. In well-differentiated tumor areas, only tumor cells of the 'pearl-like structures' in contact with the stroma stained positive, leaving the core unstained.

Interestingly, an 'on/off' phenomenon was seen in CSCC patients, with 13% (n = 5) of patients showing no or minimal staining of tumor cells (Figure 2A). Occasionally muscle tissue showed a weak membranous and cytoplasmic staining. The resulting staining scores for $\alpha_v\beta_6$ were 12 (9, 12), 0 (0, 0) and 3 (2, 6) for tumor cells, stromal cells and normal epithelium, respectively (Figure 2B).

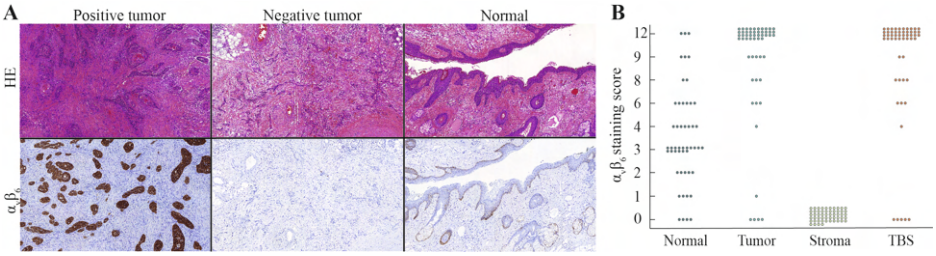

Figure 2. $\alpha_v\beta_6$ expression of SCC of the head-and-neck. (A) HE and the corresponding $\alpha_v\beta_6$ immunohistochemical staining showing the results of a positive tumor (left), negative tumor (middle) and normal squamous epithelium. (B) Graph demonstrating the distribution of the immunohistochemical staining scores for tumor cells, stromal cells, normal epithelium and TBS. HE, hematoxylin & eosin; SCC, squamous cell carcinoma; TBS, tumor-border score.

uPAR immunohistochemical staining

uPAR expression was seen in most tumors but with different staining patterns. In 34% (n = 18) of tumors more than half of the tumor cells stained with the uPAR antibody and in 64% (n = 34) of cases more than half of the stromal cells stained positive (Figure 3A). Stromal cells expressing uPAR were tumor-associated macrophages, fibroblasts, and neo-angiogenic endothelium found at the invasive margin. Except for two cases, the normal epithelium was consistently negative as was the surrounding subcutaneous tissue. One (1/53) case with a diffuse immune-infiltrate also stained intensely. Median scores were 2 (1, 4), 6 (2, 8) and 0 (0, 0) for tumor, stromal and normal tissue, respectively (Figure 3B).

VEGF-A immunohistochemical staining

Tumors weakly expressed VEGF-A with antibody staining in both the tumor as well as the stromal compartment. Abundant VEGF-A expression was also seen regularly in normal squamous epithelium, blood vessels and muscle tissue, with both a membranous and intracellular presence (Figure 4A). The tumor median staining score was 3 (2, 4), while that of the stromal and healthy tissue was 1 (0, 2) and 2 (1, 3), respectively.

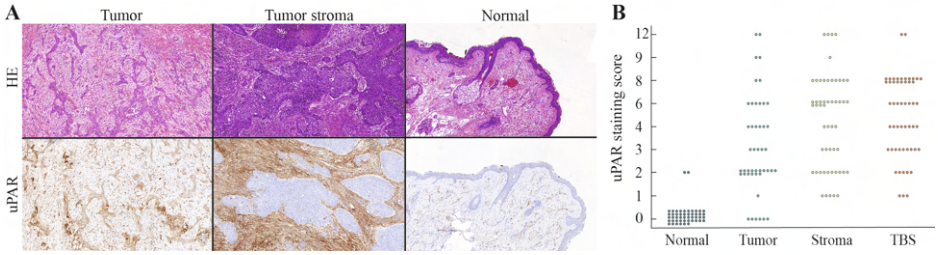

Figure 3. uPAR expression of SCC of the head-and-neck. (A) HE and uPAR immunohistochemical staining showing the results of uPAR expression on tumor cells (left), stromal cells (middle) and normal squamous epithelium. (B) Graph demonstrating the distribution of the immunohistochemical staining scores for tumor cells, stromal cells, normal epithelium and TBS. HE, hematoxylin & eosin; SCC, squamous cell carcinoma; TBS, tumor-border score; uPAR, urokinase plasminogen activator receptor.

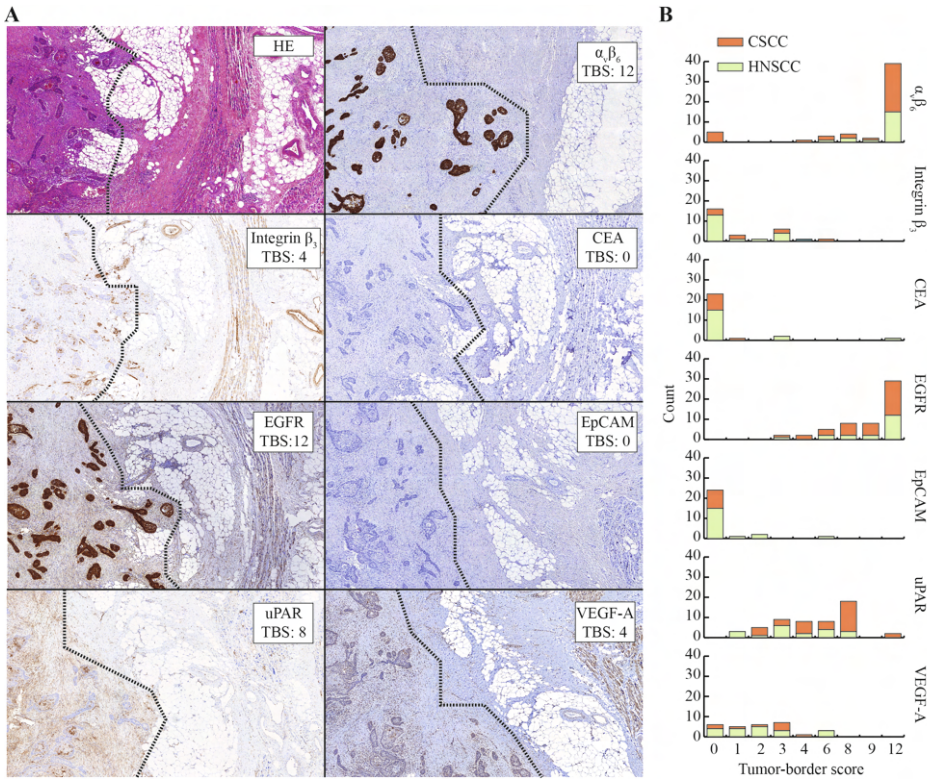

Figure 4. Assessing target expression at the border of SCC using the TBS. (A) Representative HE and immunohistochemical stainings at 5x magnification from one single case of the border of a SCC with a branching growth pattern. Left of the dotted line is tumor tissue and right is surrounding tissue. (B) TBS categorized by location of the tumor (CSCC vs HNSCC) for all evaluated targets. CEA, carcinoembryonic antigen; CSSC, cutaneous squamous cell carcinoma; EGFR, epidermal growth factor receptor; EpCAM, epithelial cell adhesion molecule; HE, hematoxylin & eosin; HNSCC, head-and-neck squamous cell carcinoma; TBS, tumor-border score; uPAR, urokinase plasminogen activator receptor; VEGF-A, vascular endothelial growth factor-A.

Integrin β_3 immunohistochemical staining

Integrin β_3 expression was mostly absent on tumor cells except for occasional well-differentiated tumors, where it stained the outer cells weakly. As expected, most of the tumor staining was seen on the endothelium, both in and outside of the tumor compartment (Figure 4A). This resulted in median staining scores of 0 (0, 2), 3 (2, 3) and 0 (0, 0) for tumor, stromal and healthy squamous epithelium tissue, respectively.

EpCAM and CEA immunohistochemical staining

EpCAM and CEA were not consistently expressed on tumor, stromal or normal tissue compartments. The median staining scores for CEA were 0 (0, 2), 0 (0, 0) and 0 (0, 0) for tumor, stromal and normal cells, respectively.

Introducing the tumor-border score (TBS) for evaluation of EGFR as target for FGS

The appropriateness of a molecular marker for FGS could be semi-quantitatively evaluated by the novel tumor-border score (TBS). By drawing an imaginary line between the tumor and surrounding normal tissue and comparing the percentage and intensity of cells staining the TBS compares tumor and surrounding tissue expression across all margins, whether these are mucosal or soft-tissue (Supplementary Figure 1). The TBS method was assessed using EGFR because its utility has already been demonstrated in clinical trials. The median TBS was 12 (8, 12) for all tumors (n = 54) and did not differ, particularly between CSCC and HNSCC (Figure 4B). As both tumor cells and healthy squamous epithelium tissue scored high for EGFR, superficial tumors with mostly superficial margins resulted in a relatively low TBS.

TBS of the other molecular targets

Figure 4A shows images of a representative case of SCC from the head-and-neck region stained for all seven evaluated targets and with their respective TBS. Integrin β_3, CEA and EpCAM were not suitable targets for FGS with TBS of respectively 0 (0, 3), 0 (0, 0) and 0 (0, 0), as indicated in Figure 4B. VEGF-A presented a low TBS with a median score of 2 (1, 3), as expression was also seen in normal epithelium, endothelium and muscle tissue. A moderate TBS was achieved with the uPAR staining resulting in a median score of 6 (3, 8), mostly because, although uPAR expression was present, it rarely stained intensely. Lastly, αvβ6 integrin resulted in the highest median TBS of 12 (8, 12), even though 11% (n = 6) of cases did not stain positive in the tumor cells resulting in a TBS of 0 for these cases (Figure 4B).

Target expression in immune-compromised patients

Patients with an immune-compromised status inherently have a higher risk of developing cutaneous squamous cell carcinomas [21, 22]. On top of the increased incidence these tumors have a more insidious course of disease justifying the need for fluorescence-guided resections [23]. Whether the same molecular targets could be used for this subset of CSCC patients was assessed by using the results of the candidates that proved usable by the TBS scores, i.e. EGFR, $\alpha_v\beta_6$ and uPAR. There was a significant difference in tumor $\alpha_v\beta_6$ expression between immune status, $X^2 = 6.362$, $p = 0.042$, with a mean rank score of 14.11 for immune-compromised, 22.46 for competent and 16.86 for possibly compromised patients. Post hoc testing provided evidence that there was a significant difference between the immune-compromised and competent patients ($p = 0.038$, adjusted using the Bonferroni correction). The other pairs revealed no significant difference. uPAR and EGFR showed no differences across immune status.

Discussion

Considering that incomplete resection rates of high-risk CSCC and HNSCC are currently as high as 60%, and are directly associated with poor patient outcomes, finding methods to decrease positive margins is of vital importance. FGS with targeted fluorescent tracers offers a unique opportunity to provide real-time visual feedback on the location of the resection margins and possible presence of metastasis without altering the view of the operative field [15]. However, crucial for the successful application of fluorescence imaging is the selection of appropriate tracers [20]. Ideal tracers will target cell membrane-associated proteins that are overexpressed in cancerous and absent in non-cancerous tissue.

With these characteristics in mind, we evaluated seven molecular imaging tracers that are currently in various stages of clinical translation for their potential as suitable molecular targets for FGS of SSC of the head-and-neck region. Our results show that EGFR, $\alpha_v\beta_6$ and uPAR are promising targets. Importantly, our data, including a wide variety of patients and settings, underline that a one-size-fits-all approach is not feasible: EGFR allowed clear delineation between CSCC or HNSCC and surrounding tissue, except in areas where normal squamous epithelium, glands and adnexa where in proximity to the tumor, and $\alpha_v\beta_6$ showed intense tumor expression with minimal staining in the basal layer of the dermis but also exhibited an 'on/off' phenomenon [24-30]. Lastly, uPAR showed tumor-specific heterogeneous staining patterns in both tumor and stromal cells [20, 30-32].

Considering these results, in the future, a three-tiered approach can be visualized to determine whether FGS is indicated and what tracer should be ideally used (Figure 5A). Initially, HNSCC and CSCC should be differentiated. For HNSCC $\alpha_v\beta_6$ is preferred over EGFR due to its lower expression in normal squamous epithelium. For cutaneous lesions, a further distinction should be made between cases of high and low metastatic risk. With low-risk tumors, FGS is not mandatory while the biopsies of high-risk patients should be stained immunohistochemically for $\alpha_v\beta_6$ after which the most appropriate tracer can be used. As expression was homogeneously positive in the whole tumor for both markers, false-positives or false-negatives in tumor biopsies due to tumor heterogeneity should not be a problem. In $\alpha_v\beta_6$ negative cases where superficial margins are possibly tumor-positive, surgeons can opt for uPAR-targeting tracers (Figure 5B).

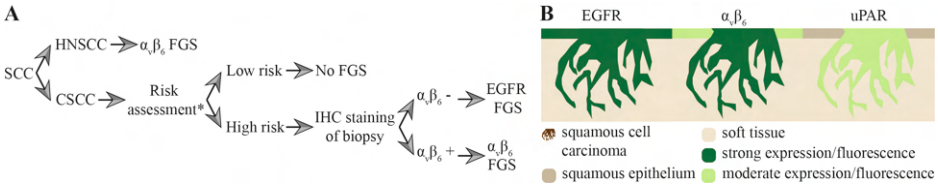

Figure 5. (A) Proposed algorithm to decide what target to use during FGS of squamous cell carcinoma of the head-and-neck region. (B) Illustrations depicting, based on the immunohistochemical results, where fluorescence would be expected during FGS using EGFR-, αvβ6- or uPAR-based probes. Dark green represents more fluorescence than light green. CSCC, cutaneous squamous cell carcinoma; EGFR, epidermal growth factor receptor; FGS, fluorescence-guided surgery; HNSCC, head-and-neck squamous cell carcinoma; IHC, immunohistochemistry; SCC, squamous cell carcinoma; uPAR, urokinase plasminogen activator receptor. * as determined by the NCCN or AJCC criteria for high-risk CSCC.

Expression of EGFR in normal squamous epithelium could lead to aggregation of tracer and subsequent fluorescence in the mucosa or skin. To circumvent this effect, preloading with unlabeled tracer has been performed in oral cancer clinical trials evaluating cetuximab and panitumumab based FGS [18, 33, 34]. However, recent studies have shown that off-target fluorescence still occurred after preloading and no difference in tumor-to-background ratios and mean fluorescent intensities between no loading and preloading cohorts exist [35, 36]. Consequently, the expression of EGFR in the normal squamous epithelium is a limiting factor, especially in superficial growing tumors.

Our data showed a puzzling disadvantage of $\alpha_v\beta_6$ as a target for FGS of CSCC, because of an 'on/off' phenomenon in the immunohistochemical staining. In 13% of cases, immunohistochemical staining was completely negative. A compromised immune status seemed to be associated with lower $\alpha_v\beta_6$ tumor expression. This is important as immune-suppressed patients represent a high-risk group for aggres-

sive tumors and consequently challenging resections [21-23]. An explanation for the 'on/off' phenomenon remains to be elucidated. Mechanistically $\alpha_v\beta_6$ has been implicated in tumor genesis as direct upstream regulators of matrix metalloproteinases and transforming growth factor-β (TGF-β), where the latter plays a vital role in the immune evasion of cancer cells [37, 38]. Theoretically, one could speculate that immune evasion is not an essential hallmark of cancer in immune-compromised patients and consequently $\alpha_v\beta_6$ regulating TGF-β loses its significance in tumor genesis. Nonetheless, whether our observations in a small cohort of patients and the pathway-related mechanisms are essential for specific subgroups of patients should be tested and confirmed in larger groups. While fluorescence-based clinical studies are currently being set up, an early PET/CT study demonstrated that the $\alpha_v\beta_6$ targeting tracer ^{68}Ga-DOTA-SFITGv6 was more specific than ^{18}F-FDG for the detection of cancerous lesions [39].

A disadvantage of uPAR encountered in this study appears to be the intensity of the immunohistochemical staining for uPAR, which was considerably less than for EGFR and $\alpha_v\beta_6$. This can probably be explained by the relatively low copy numbers of uPAR per cell even if more cells than the malignant tumor cells are targeted [40]. Furthermore, the low intensity might be a drawback of using the immunohistochemical staining technique and might not be an issue for *in vivo* imaging. In fact, first in-human clinical trials with the uPAR AE-105 PET tracer have demonstrated the capability to identify primary and metastatic lesions of various tumor types, and currently 7 clinical trials, including one with HNSCC, are running to further assess the potential of uPAR-imaging [41, 42]. Regarding fluorescence molecular imaging, various groups have published advanced preclinical studies and clinical trials should be following soon [31, 43]. Ultimately, the advantage of performing fluorescent guided surgery with a uPAR targeting tracer, as opposed to EGFR or $\alpha_v\beta_6$ is the non-existent expression in normal tissue and the uPAR expression in stromal cells. Therefore, performing FGS with a uPAR targeting tracer will automatically also result in fluorescent stromal cells and consequently removal of stroma by the surgeon.

Limitations of this study include the semi-quantitative evaluation of targets and comparison of them. However, these are inherent to immunohistochemical methods [44]. Pivotal is the choice of primary antibodies. In this study, only antibodies were used that interacted with extracellular epitopes close to the binding-domain of the clinical tracers. Although clinical trials will need to confirm the binding characteristics of the appropriate tracers, these antibodies give a fair indication of whether the extracellular domain of the target is present. Interpretation is further limited by the small sample size, especially for subgroup analyses. But even with large cohorts and validated antibodies, staining results can vary depending on the representative tumor specimen and scoring method chosen [45].

For this study, the novel scoring method TBS was introduced, adapted to the purpose of evaluating targets for FGS. The TBS, using specimens that contain both tumor and surrounding tissue, evaluates the staining difference between the tumor border and surrounding tissue, allowing precise evaluation of whether a target is suitable for FGS. Often the expression between tumor and healthy cells is compared by comparing the tumor staining with its healthy counterpart and not the normal tissue surrounding the tumor. However, this does not account for the expression of the markers in the surgical, more troublesome, soft-tissue margins [46]. Another scoring method to evaluate markers for molecular imaging that has been used in the literature is the Target Selection Criteria (TASC) scoring system. In this score, targets are scored based on seven characteristics. However, the importance of certain criteria of the TASC score, for example, internalization of the probe, are questionable while other criteria, such as T/N of greater than 10, are challenging to measure [47]. All-in-all the TBS allows an alternative assessment for the suitability of a marker for FGS.

Conclusion

In conclusion, $\alpha_v\beta_6$ and EGFR allowed for precise discrimination of SSC at the often more problematic soft-tissue margins in CSCC and HNSCC. When superficial margins are at risk for irradical resection due to difficult clinical tumor delineation, uPAR is a promising target. In the future, FGS in the surgically challenging setting of high-risk CSCC and HNSCC could benefit from a tailor-made approach, with EGFR and αvβ6 as promising targets.

References

1. Alam M, Ratner D. Cutaneous squamous-cell carcinoma. N Engl J Med. 2001;344:975-83. doi:10.1056/nejm200103293441306.
2. Rowe DE, Carroll RJ, Day CL, Jr. Prognostic factors for local recurrence, metastasis, and survival rates in squamous cell carcinoma of the skin, ear, and lip. Implications for treatment modality selection. Journal of the American Academy of Dermatology. 1992;26:976-90.
3. Brantsch KD, Meisner C, Schonfisch B, Trilling B, Wehner-Caroli J, Rocken M, et al. Analysis of risk factors determining prognosis of cutaneous squamous-cell carcinoma: a prospective study. The Lancet Oncology. 2008;9:713-20. doi:10.1016/s1470-2045(08)70178-5.
4. Lansbury L, Bath-Hextall F, Perkins W, Stanton W, Leonardi-Bee J. Interventions for non-metastatic squamous cell carcinoma of the skin: systematic review and pooled analysis of observational studies. BMJ (Clinical research ed). 2013;347:f6153. doi:10.1136/bmj.f6153.
5. O'Reilly Zwald F, Brown M. Skin cancer in solid organ transplant recipients: advances in therapy and management: part I. Epidemiology of skin cancer in solid organ transplant recipients. Journal of the American Academy of Dermatology. 2011;65:253-61. doi:10.1016/j.jaad.2010.11.062.
6. Weinberg AS, Ogle CA, Shim EK. Metastatic cutaneous squamous cell carcinoma: an update. Dermatologic surgery : official publication for American Society for Dermatologic Surgery [et al]. 2007;33:885-99. doi:10.1111/j.1524-4725.2007.33190.x.
7. Kang H, Kiess A, Chung CH. Emerging biomarkers in head and neck cancer in the era of genomics. Nat Rev Clin Oncol. 2015;12:11-26. doi:10.1038/nrclinonc.2014.192.
8. Bray F, Ferlay J, Soerjomataram I, Siegel RL, Torre LA, Jemal A. Global cancer statistics 2018: GLOBOCAN estimates of incidence and mortality worldwide for 36 cancers in 185 countries. CA: a cancer journal for clinicians. 2018;68:394-424. doi:10.3322/caac.21492.
9. Svahn MF, Munk C, Nielsen TS, von Buchwald C, Frederiksen K, Kjaer SK. Trends in all-cause five-year mortality after head and neck cancers diagnosed over a period of 33 years. Focus on estimated degree of association with human papillomavirus. Acta oncologica (Stockholm, Sweden). 2016;55:1084-90. doi:10.1080/0284186x.2016.1185148.
10. Eldeeb H, Macmillan C, Elwell C, Hammod A. The effect of the surgical margins on the outcome of patients with head and neck squamous cell carcinoma: single institution experience. Cancer biology & medicine. 2012;9:29-33. doi:10.3969/j.issn.2095-3941.2012.01.005.
11. Ettl T, El-Gindi A, Hautmann M, Gosau M, Weber F, Rohrmeier C, et al. Positive frozen section margins predict local recurrence in R0-resected squamous cell carcinoma of the head and neck. Oral Oncol. 2016;55:17-23. doi:10.1016/j.oraloncology.2016.02.012.
12. McMahon J, O'Brien CJ, Pathak I, Hamill R, McNeil E, Hammersley N, et al. Influence of condition of surgical margins on local recurrence and disease-specific survival in oral and oropharyngeal cancer. The British journal of oral & maxillofacial surgery. 2003;41:224-31.
13. Orosco RK, Tapia VJ, Califano JA, Clary B, Cohen EEW, Kane C, et al. Positive Surgical Margins in the 10 Most Common Solid Cancers. Sci Rep. 2018;8:5686. doi:10.1038/s41598-018-23403-5.
14. Tan PY, Ek E, Su S, Giorlando F, Dieu T. Incomplete excision of squamous cell carcinoma of the skin: a prospective observational study. Plastic and reconstructive surgery. 2007;120:910-6. doi:10.1097/01.prs.0000277655.89728.9f.
15. Vahrmeijer AL, Hutteman M, van der Vorst JR, van de Velde CJ, Frangioni JV. Image-guided cancer surgery using near-infrared fluorescence. Nature reviews Clinical oncology. 2013;10:507-18. doi:10.1038/nrclinonc.2013.123.

16. Tummers WS, Miller SE, Teraphongphom NT, van den Berg NS, Hasan A, Longacre TA, et al. Detection of visually occult metastatic lymph nodes using molecularly targeted fluorescent imaging during surgical resection of pancreatic cancer. HPB : the official journal of the International Hepato Pancreato Biliary Association. 2019. doi:10.1016/j.hpb.2018.11.008.
17. van Dam GM, Themelis G, Crane LM, Harlaar NJ, Pleijhuis RG, Kelder W, et al. Intraoperative tumor-specific fluorescence imaging in ovarian cancer by folate receptor-alpha targeting: first in-human results. Nat Med. 2011;17:1315-9. doi:10.1038/nm.2472.
18. Gao RW, Teraphongphom N, de Boer E, van den Berg NS, Divi V, Kaplan MJ, et al. Safety of panitumumab-IRDye800CW and cetuximab-IRDye800CW for fluorescence-guided surgical navigation in head and neck cancers. Theranostics. 2018;8:2488-95. doi:10.7150/thno.24487.
19. Pola R, Böhmová E, Filipová M, Pechar M, Pankrác J, Větvička D, et al. Targeted Polymer-Based Probes for Fluorescence Guided Visualization and Potential Surgery of EGFR-Positive Head-and-Neck Tumors. Pharmaceutics. 2020;12. doi:10.3390/pharmaceutics12010031.
20. Boonstra MC, Verspaget HW, Ganesh S, Kubben FJ, Vahrmeijer AL, van de Velde CJ, et al. Clinical applications of the urokinase receptor (uPAR) for cancer patients. Current pharmaceutical design. 2011;17:1890-910. doi:10.2174/138161211796718233.
21. Jensen P, Hansen S, Moller B, Leivestad T, Pfeffer P, Geiran O, et al. Skin cancer in kidney and heart transplant recipients and different long-term immunosuppressive therapy regimens. Journal of the American Academy of Dermatology. 1999;40:177-86.
22. Hartevelt MM, Bavinck JN, Kootte AM, Vermeer BJ, Vandenbroucke JP. Incidence of skin cancer after renal transplantation in The Netherlands. Transplantation. 1990;49:506-9.
23. Manyam BV, Gastman B, Zhang AY, Reddy CA, Burkey BB, Scharpf J, et al. Inferior outcomes in immunosuppressed patients with high-risk cutaneous squamous cell carcinoma of the head and neck treated with surgery and radiation therapy. Journal of the American Academy of Dermatology. 2015;73:221-7. doi:10.1016/j.jaad.2015.04.037.
24. Gaffney DC, Soyer HP, Simpson F. The epidermal growth factor receptor in squamous cell carcinoma: An emerging drug target. Australas J Dermatol. 2014;55:24-34. doi:10.1111/ajd.12025.
25. Canueto J, Cardenoso E, Garcia JL, Santos-Briz A, Castellanos-Martin A, Fernandez-Lopez E, et al. Epidermal growth factor receptor expression is associated with poor outcome in cutaneous squamous cell carcinoma. The British journal of dermatology. 2017;176:1279-87. doi:10.1111/bjd.14936.
26. Jones J, Watt FM, Speight PM. Changes in the expression of alpha v integrins in oral squamous cell carcinomas. Journal of oral pathology & medicine : official publication of the International Association of Oral Pathologists and the American Academy of Oral Pathology. 1997;26:63-8.
27. Hamidi S, Salo T, Kainulainen T, Epstein J, Lerner K, Larjava H. Expression of alpha(v)beta6 integrin in oral leukoplakia. Br J Cancer. 2000;82:1433-40. doi:10.1054/bjoc.1999.1130.
28. Impola U, Uitto VJ, Hietanen J, Hakkinen L, Zhang L, Larjava H, et al. Differential expression of matrilysin-1 (MMP-7), 92 kD gelatinase (MMP-9), and metalloelastase (MMP-12) in oral verrucous and squamous cell cancer. The Journal of pathology. 2004;202:14-22. doi:10.1002/path.1479.
29. Van Aarsen LA, Leone DR, Ho S, Dolinski BM, McCoon PE, LePage DJ, et al. Antibody-mediated blockade of integrin alpha v beta 6 inhibits tumor progression in vivo by a transforming growth factor-beta-regulated mechanism. Cancer Res. 2008;68:561-70. doi:10.1158/0008-5472.can-07-2307.

30. Christensen A, Kiss K, Lelkaitis G, Juhl K, Persson M, Charabi BW, et al. Urokinase-type plasminogen activator receptor (uPAR), tissue factor (TF) and epidermal growth factor receptor (EGFR): tumor expression patterns and prognostic value in oral cancer. BMC Cancer. 2017;17:572. doi:10.1186/s12885-017-3563-3.
31. Boonstra MC, Van Driel PB, Keereweer S, Prevoo HA, Stammes MA, Baart VM, et al. Preclinical uPAR-targeted multimodal imaging of locoregional oral cancer. Oral Oncol. 2017;66:1-8. doi:10.1016/j.oraloncology.2016.12.026.
32. Magnussen S, Rikardsen OG, Hadler-Olsen E, Uhlin-Hansen L, Steigen SE, Svineng G. Urokinase plasminogen activator receptor (uPAR) and plasminogen activator inhibitor-1 (PAI-1) are potential predictive biomarkers in early stage oral squamous cell carcinomas (OSCC). PLoS One. 2014;9:e101895. doi:10.1371/journal.pone.0101895.
33. Rosenthal EL, Warram JM, de Boer E, Chung TK, Korb ML, Brandwein-Gensler M, et al. Safety and Tumor Specificity of Cetuximab-IRDye800 for Surgical Navigation in Head and Neck Cancer. Clin Cancer Res. 2015;21:3658-66. doi:10.1158/1078-0432.ccr-14-3284.
34. Moore LS, Rosenthal EL, de Boer E, Prince AC, Patel N, Richman JM, et al. Effects of an Unlabeled Loading Dose on Tumor-Specific Uptake of a Fluorescently Labeled Antibody for Optical Surgical Navigation. Molecular imaging and biology : MIB : the official publication of the Academy of Molecular Imaging. 2017;19:610-6. doi:10.1007/s11307-016-1022-1.
35. Nishio N, van den Berg NS, van Keulen S, Martin BA, Fakurnejad S, Zhou Q, et al. Optimal Dosing Strategy for Fluorescence-Guided Surgery with Panitumumab-IRDye800CW in Head and Neck Cancer. Molecular imaging and biology : MIB : the official publication of the Academy of Molecular Imaging. 2019. doi:10.1007/s11307-019-01358-x.
36. de Boer E, Warram JM, Tucker MD, Hartman YE, Moore LS, de Jong JS, et al. In Vivo Fluorescence Immunohistochemistry: Localization of Fluorescently Labeled Cetuximab in Squamous Cell Carcinomas. Sci Rep. 2015;5:10169. doi:10.1038/srep10169.
37. Bandyopadhyay A, Raghavan S. Defining the role of integrin alphavbeta6 in cancer. Current drug targets. 2009;10:645-52.
38. Yang SB, Du Y, Wu BY, Xu SP, Wen JB, Zhu M, et al. Integrin alphavbeta6 promotes tumor tolerance in colorectal cancer. Cancer immunology, immunotherapy : CII. 2012;61:335-42. doi:10.1007/s00262-011-1108-1.
39. Hausner SH, Bold RJ, Cheuy LY, Chew HK, Daly ME, Davis RA, et al. Preclinical Development and First-in-Human Imaging of the Integrin alphavbeta6 with [(18)F]alphavbeta6-Binding Peptide in Metastatic Carcinoma. Clin Cancer Res. 2019;25:1206-15. doi:10.1158/1078-0432.ccr-18-2665.
40. Boonstra MC, van Driel PB, van Willigen DM, Stammes MA, Prevoo HA, Tummers QR, et al. uPAR-targeted multimodal tracer for pre- and intraoperative imaging in cancer surgery. Oncotarget. 2015;6:14260-73. doi:10.18632/oncotarget.3680.
41. Skovgaard D, Persson M, Brandt-Larsen M, Christensen C, Madsen J, Klausen TL, et al. Safety, Dosimetry, and Tumor Detection Ability of 68Ga-NOTA-AE105: First-in-Human Study of a Novel Radioligand for uPAR PET Imaging. J Nucl Med. 2017;58:379-86. doi:10.2967/jnumed.116.178970.
42. Persson M, Skovgaard D, Brandt-Larsen M, Christensen C, Madsen J, Nielsen CH, et al. First-in-human uPAR PET: Imaging of Cancer Aggressiveness. Theranostics. 2015;5:1303-16. doi:10.7150/thno.12956.
43. Christensen A, Juhl K, Persson M, Charabi BW, Mortensen J, Kiss K, et al. uPAR-targeted optical near-infrared (NIR) fluorescence imaging and PET for image-guided surgery in head and neck cancer: proof-of-concept in orthotopic xenograft model. Oncotarget. 2017;8:15407-19. doi:10.18632/oncotarget.14282.

44. True LD. Methodological requirements for valid tissue-based biomarker studies that can be used in clinical practice. Virchows Arch. 2014;464:257-63. doi:10.1007/s00428-013-1531-0.
45. Serpa MS, Mafra RP, Queiroz S, Silva LPD, Souza LB, Pinto LP. Expression of urokinase-type plasminogen activator and its receptor in squamous cell carcinoma of the oral tongue. Brazilian oral research. 2018;32:e93. doi:10.1590/1807-3107bor-2018.vol32.0093.
46. Shah AK. Postoperative pathologic assessment of surgical margins in oral cancer: A contemporary review. Journal of oral and maxillofacial pathology : JOMFP. 2018;22:78-85. doi:10.4103/jomfp.JOMFP_185_16.
47. van Oosten M, Crane LM, Bart J, van Leeuwen FW, van Dam GM. Selecting Potential Targetable Biomarkers for Imaging Purposes in Colorectal Cancer Using TArget Selection Criteria (TASC): A Novel Target Identification Tool. Translational oncology. 2011;4:71-82.

Part III

uPAR as a target: beyond cancer imaging

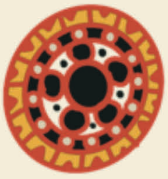

Chapter 4

Molecular imaging of the urokinase plasminogen activator receptor: opportunities beyond cancer

Baart VM, Houvast RD, de Geus-Oei LF, Quax PHA, Kuppen PJK, Vahrmeijer AL, Sier CFM.

EJNMMI Res. 2020; 10(1):87.

Abstract

The urokinase plasminogen activator receptor (uPAR) plays a multifaceted role in almost any process where migration of cells and tissue-remodeling is involved such as inflammation, but also in diseases as arthritis and cancer. Normally, uPAR, is absent in healthy tissues. By its carefully orchestrated interaction with the protease urokinase-plasminogen activator and its inhibitor (plasminogen activator inhibitor-1), uPAR localizes a cascade of proteolytic activities, enabling (patho-)physiologic cell migration. Moreover, via the interaction with a broad range of cell membrane proteins, like vitronectin and various integrins, uPAR plays a significant, but not yet completely understood, role in differentiation and proliferation of cells, affecting also disease progression. The implications of these processes, either for diagnostics or therapeutics, have received much attention in oncology, but only limited beyond. Nonetheless, the role of uPAR in different diseases provides ample opportunity to exploit new applications for targeting. Especially in the fields of oncology, cardiology, rheumatology, neurology and infectious diseases, uPAR-targeted molecular imaging could offer insights for new directions in diagnosis, surveillance or treatment options.

Introduction

Tissue remodeling is pivotal in embryonic development, tissue repair, and numerous pathologies. Temporary degradation of the extracellular matrix (ECM) is a delicate process requiring the careful coordination of proteases, receptors and cell-signaling molecules where over-degradation can result in osteoarthritis, osteolysis, cardiomyopathy and invasion/metastasis of tumor cells, and where over-production of the ECM often leads to fibrosis [1]. It seems conceivable that monitoring of the process of matrix remodeling offers possibilities for diagnosis, surveillance, and possibly even treatment of the associated diseases. For clinical applications, such as biomedical imaging or therapy, a cell-associated target protein with a central role within the ECM remodeling process, but with limited expression in healthy tissue, would be helpful in identifying patient groups requiring more intensive monitoring or therapy. Furthermore, molecular imaging enables real-time imaging of pathophysiology, providing novel insights into disease processes that cannot be gathered with current techniques such as *post-mortem* tissue analysis or with animal models [2, 3].

Inherent to its nature, molecular imaging is fundamentally dependent on identifying appropriate targets that are informative about the underlying pathophysiology of the process studied [4]. As targeting different epitopes on the same protein may influence the ability to image specific processes, formal description of the epitope is crucial. Important to realize is that differing epitopes on the same protein can alter the results and consequently, describing the epitope of interest is just as crucial [5, 6]. Therefore, a key competence of targeted imaging is designing the best performing probe for the imaging modality of choice. The choices to be made are extensive and have already been covered in reviews elsewhere [7-9].

The urokinase plasminogen activator receptor (uPAR) holds a central position in ECM proteolysis, but, next to the proteolytic role, uPAR is also involved in cell-cell and cell-ECM interactions, regulating cell signaling and hereby controlling cell proliferation, differentiation and migration [10]. uPAR is normally hardly found in healthy tissue, but it is present in virtually all human malignancies, associated with disease aggressiveness, allowing tumors to escape their original boundaries [11, 12]. As a result, the field of uPAR-based oncological imaging is progressing rapidly and, not surprisingly, various positron-emission tomography (PET)-based molecular imaging clinical trials are currently being conducted for diagnosing aggressive cancers and determining cancer aggressiveness (NCT02755675, NCT02945826, and NCT03307460) [13, 14].

The last two decades have revealed that uPAR is not only a central orchestrator in oncology but also in processes ranging from neurology to auto-immune diseases

[15, 16]. Likewise, by unravelling the various (patho-)physiological processes uPAR contributes to, novel opportunities to diagnose, treat or monitor diseases have been revealed. The current review aims to identify non-neoplastic diseases where uPAR is of pathophysiological relevance and elaborate on the molecular imaging opportunities this provides.

The urokinase plasminogen activator receptor: a central player in an extensive interactome

In 1985 uPAR was first identified on monocytes as the cell membrane-receptor of the urokinase plasminogen activator (uPA) [17, 18]. In the following 35 years uPAR has been identified, although often only expressed transiently, on, amongst others, fibroblasts, endothelial cells, epithelial cells, and neurons [11, 19]. Rather than being cell-specific, uPAR expression should be considered as process-specific with all cells being able to express uPAR, but only doing this at very specific events, such as the cell extravasation and migration observed during wound healing (Figure 1A). Consequently, most cells at rest have no uPAR on their cell membrane [11]. A closer look at uPAR-expressing cells reveals that uPAR is implicated in multiple processes where the balance of this determines the end result (Figure 1B).

To understand how uPAR can play such a diverse and central role, a careful examination of its structure needs to be made. uPAR is a 283 amino acid glycosylphosphatidylinositol (GPI)-anchored membrane protein consisting of three domains (D1-D3) linked by two flexible hinges (Figure 1C) [20]. These three domains form a concave surface where uPA can bind [21]. Subsequently, uPAR mediates its other, non-proteolytic related effects via protein interactions on the outer surface. D1 and the hinge region between D1-D2 are vital for uPAR-vitronectin interactions, whereas various epitopes on D2-D3 interact with integrins, G protein-coupled receptors (GPCRs) and receptor tyrosine kinases like epidermal growth factor receptor, platelet-derived growth factor receptor, and insulin-like growth factor 1 receptor [22, 23]. With over 42 interacting proteins described, uPAR forms a central orchestrator of cell proliferation, differentiation, migration and survival [10, 22].

Classically, the function of uPAR is fairly straightforward. Without intracellular or transmembrane domains, uPAR primarily functions as a receptor for (pro-)uPA (Figure 1D) [24]. uPA is a serine protease that catalyzes the activation of the ubiquitously present plasminogen into plasmin. Active plasmin degrades ECM-proteins by itself or via activation of latent matrix metalloproteases (MMPs) [25]. Localization of both the inactive form, pro-uPA, and active uPA to the cell surface, allows cells to focus extracellular matrix degradation towards the leading edge of the cell [26, 27].

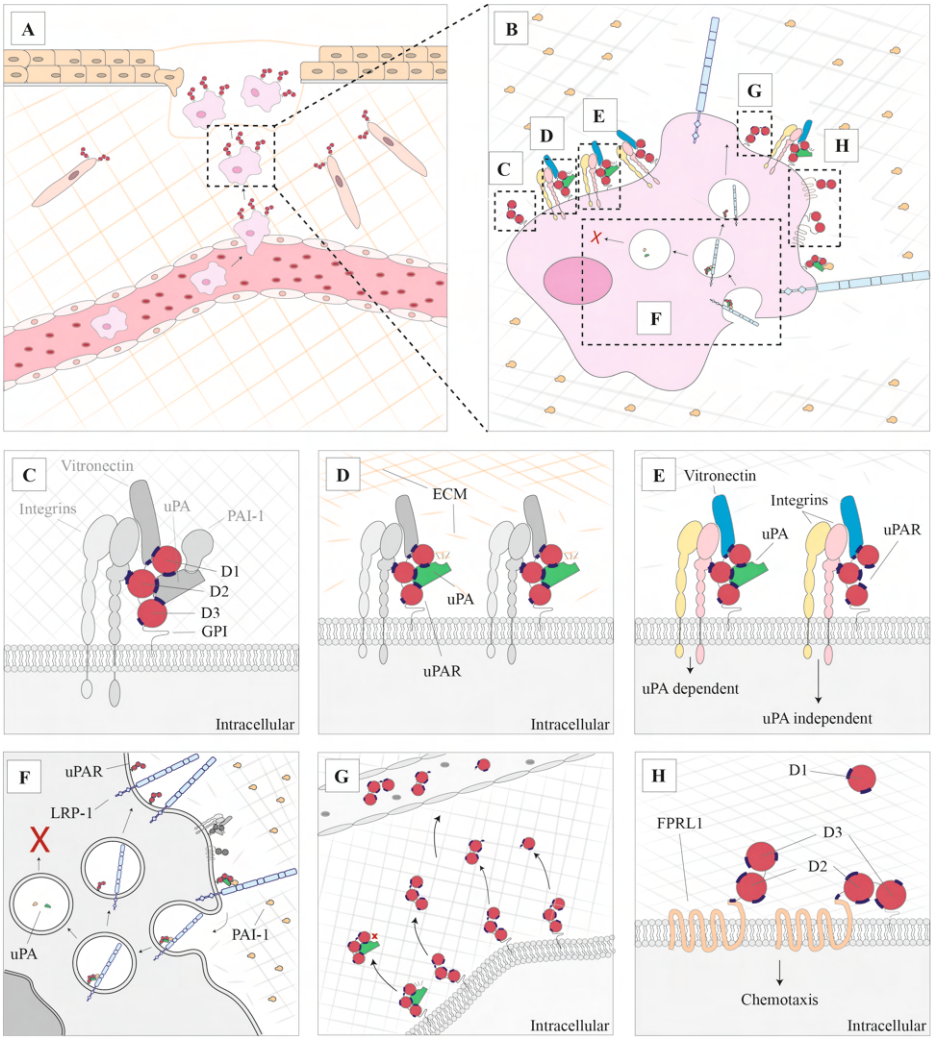

Figure 1. Overview of uPAR. (A) While usually quiescent in normal tissue, uPAR expression is observed transiently and locally during specific cellular processes such as extravasation and migration by wound healing. (B) At a cellular level, uPAR interacts in a multitude of pathways where the balance of each dictates the end result. (C) uPAR itself is a three domain extracellular structure linked to the plasma membrane by a GPI anchor. (D) Classically uPAR functions as receptor for urokinase plasminogen activator (uPA) which subsequently breaks down the ECM via plasminogen activation. (E) Intracellular signaling occurs via other receptors including vitronectin and integrins and can be uPA dependent and independent. (F) Internalization and recycling of uPAR occurs after a uPAR/uPA/PAI-1/LRP-1 complex has formed, which results in the degradation of uPA and PAI-1 and the recycling of uPAR and LRP-1. (G) uPAR can be cleaved at the GPI-anchor and between D1 and D2 resulting in various isoforms of soluble uPAR which can be quantified in the blood. (H) After cleavage of D1, uPAR D2-D3 induces chemotaxis by interacting with FPRL1. D, domain; ECM, extracellular matrix; FPRL1, formyl peptide receptor-like 1; GPI, glycosylphosphatidylinositol; LRP-1, LDL receptor-related protein 1; PAI-1, plasminogen activator inhibitor 1; uPA, urokinase plasminogen activator; uPAR, urokinase plasminogen activator receptor.

However, this classic view of uPAR does not justify the many subtleties present in the uPAR interactome. For instance, the distinct central binding cavity of uPAR and the flexible hinges result in a conformational change after uPA binding that alters the vitronectin binding site, enhancing uPAR-vitronectin interaction on the outer surface of uPAR [23, 28-30]. Vice versa, vitronectin binding to uPAR influences the affinity for uPA [31]. Another subtlety of uPAR characteristics lies in the GPI-anchoring to the cell, which influences distribution of uPAR towards lipid rafts and subsequently promotes specific protein-protein interactions [32-34]. Furthermore, GPI-anchorage allows a rapid removal from the cell membrane, allowing a quick turnover and response time.

The intracellular signaling pathway initiated by uPAR, either enabled by uPA, with or without vitronectin, is still not entirely understood (Figure 1E) [35-39]. On neutrophils and macrophages, CD11b/CD18 (MAC1, complement receptor 3 or αMβ2) colocalizes with uPAR and is essential for adhesion, migration and phagocytosis [40-47]. In combination with the β1 integrin subunit, uPAR promotes differentiation, proliferation, adhesion, of epithelial and other cells and stimulates expression of uPA, uPAR and MMPs, promoting extracellular proteolysis [38, 48-54]. Furthermore, β3-uPAR-mediated signaling enhances cell motility and invasion, while β6-uPAR interaction stimulates proliferation and cell differentiation [55-58].

Finally, recycling and cleavage of uPAR play an important role in cell functioning (Figure 1F). Plasminogen activator inhibitor-1 (PAI-1) and uPA are internalized for degradation via uPAR and lipoprotein receptor-related protein 1 interaction (LRP1) [59-61]. uPAR and LRP1 are recycled to the cell membrane ready for new interactions [62]. Cleavage of uPAR can occur at two sites: (I) within the GPI-anchor by lipases, resulting in soluble uPAR (suPAR) and (II) between D1 and D2 resulting in cleaved uPAR (soluble D1 and soluble or membrane-bound D2-D3) (Figure 1G) [63]. The exact function of full length suPAR is unclear but suPAR might function as a scavenger protein for uPA, consequently competitively inhibiting cell surface proteolysis [64, 65]. Cleavage of D1 unveils an amino acid sequence (amino acids: 88-92) on D2-D3 that is unable to interact with integrins but interacts with GPCR formyl peptide receptor-like 1 (FPRL1), prompting migration (Figure 1H) [66]. When cleaved, the same D2-D3 epitope induces chemotaxis in FPRL1-expressing cells [67, 68].

uPAR in cardiovascular disease: determining plaque instability in atherosclerosis

Although significant improvements have been made in the management of cardiovascular disease it is still a leading cause of death worldwide [69]. The current state-of-art diagnostic techniques, such as angiography or perfusion imaging, can accurately identify stenosis location and luminal occlusion in order to guide revascularization, however, fail to determine risk of rupture [70, 71]. Identifying these patients is the next challenging frontier in cardiovascular disease research: more than 50% of patients who die suddenly have no evident clinical symptoms and autopsy studies indicate that the majority of myocardial infarctions are caused by non-flow limiting lesions [72-74]. Based on its mechanistic role, molecular imaging of uPAR expression status might be an alternative and more targeted tool to improve the recognition of atherosclerotic plaques and the risk of rupture.

Atherosclerosis is the formation of intimal plaques consisting of two interacting regions: a central core covered by a fibrous cap. Cholesterol filled monocyte-derived macrophage-foam cells form the core whereas the cap consists of vascular smooth muscle cells (VSMCs), that have been recruited from the media [75-77]. In both regions of the plaques the urokinase plasminogen activation axis (uPA/uPAR/PAI-1 axis) has been shown pivotal for development and progression of the disease. Monocyte adherence and recruitment towards lesion sites are dependent on uPAR expression, and upon arrival in the lesion, uPA interaction with uPAR has been implicated in the differentiation of monocytes to macrophages, and cholesterol biosynthesis and subsequent lipid uptake (Figure 2A-B) [78-83]. In response to vascular injury, VSMCs undergo a change from a physiological contractile phenotype to the pathological synthetic phenotype, allowing them to migrate, proliferate and produce extracellular matrix, as found in the caps of atherosclerotic plaques. This process is stimulated by intimal macrophages-derived uPA binding to the uPAR present on VSMCs (Figure 2C) [84-93]. Furthermore, uPAR expression up-regulates the calcification of these lesions, although the consequences for plaque stability remain to be clarified [94, 95]. Overall, many *in vitro* mechanistic studies demonstrate the enhanced presence and pivotal role of uPAR in atherogenesis and , negative (inward) remodeling [78, 92, 96]. These data are supported by various immunohistochemical studies on patients, which have clearly localized uPAR overexpression to atherosclerosis: while normal arterial tissue is negative for uPAR, intensely positive stained lymphocytes, macrophages, and intimal smooth muscle cells are found in atherosclerotic lesions and atheroma's [93, 97-101]. Likewise, the overexpression of uPAR is confirmed in gene analysis with a 1.5 fold higher uPAR expression in endarterectomies [99]. The level of uPAR overexpression has been associated with disease

severity and localized uPAR expression is indicative for areas at risk for rupture (Figure 2D) [98, 99, 102].

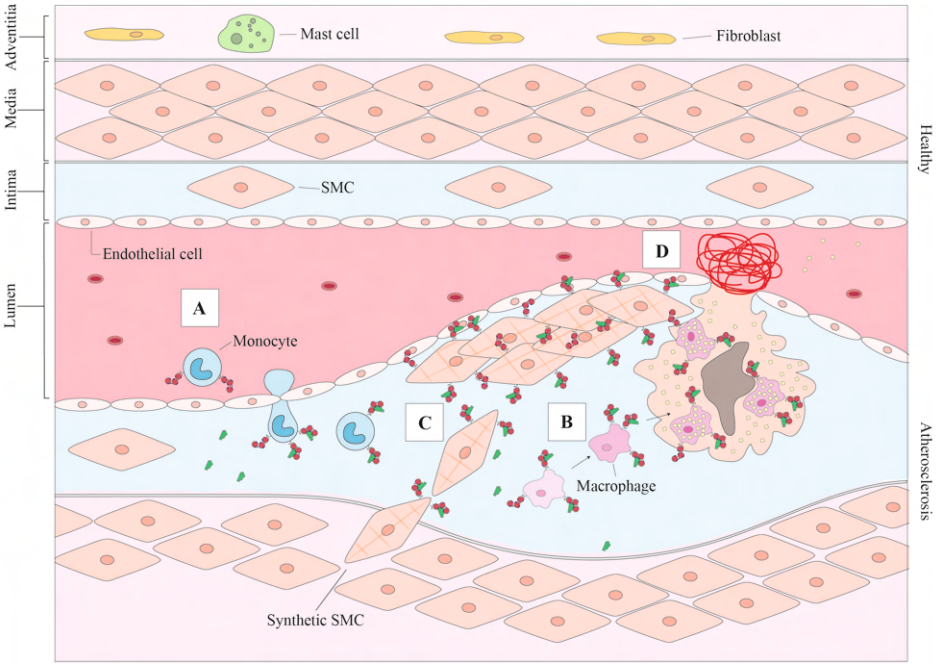

Figure 2. uPAR in atherosclerosis. (A) Monocyte extravasation across the endothelium lesions is dependent on uPAR. (B) Upon interaction with uPA these monocytes differentiate into macrophages, eventually resulting in cholesterol filled monocyte-derived macrophages. (C) uPA released from macrophages interacts with uPAR on synthetic smooth muscle cells stimulating their migration. (D) Localized uPAR overexpression in an atherosclerotic plaque increases the risk of rupture. uPAR is represented by the red 3-domain structure as described in figure 1 on the cell membrane of uPAR expressing cells and uPA by the green structure in the extracellular matrix and bound to uPAR. SMC, smooth muscle cell; uPA, urokinase plasminogen activator; uPAR, urokinase plasminogen activator receptor.

As uPAR has been implicated in the pathophysiology of atherosclerosis, various studies have attempted to improve disease outcomes by targeting of uPAR to block its function. Viral and non-viral expression vectors, encoding constructs consisting of ATF (the amino-terminal fragment of urokinase with high affinity for uPAR) in combination with inhibitors of the plasminogen pathway like BPTI (bovine pancreas trypsin inhibitor) or of matrix metalloproteinases like TIMP1 (tissue inhibitor of matrix metalloproteinases 1), successfully inhibited neointimal formation, VSMC migration, and vein graft thickening in rodent models and human saphenous vein cultures [103-106]. Eventually, a construct consisting of all three of these proteins has been shown to lead to the strongest reduction in vein graft

thickening in hypercholesterolemic mice [107]. While these preclinical studies show evident potential of uPAR as target for atherosclerosis targeting, the concept has not yet been progressed towards a clinical application for therapy nor for diagnostic monitoring via molecular targeted imaging.

uPAR in auto-immune disease: imaging disease activity in rheumatoid arthritis

Rheumatoid arthritis (RA) is a chronic inflammatory disease with a lifetime risk of 3.6% for women and 1.7% for men [108]. Anatomical imaging techniques, such as conventional radiology, ultrasound and magnetic resonance imaging, along with clinical criteria, are the standard to diagnose and monitor RA [109]. These modalities are able to identify RA as soon as 6-8 weeks after arthritis onset and sometimes even before the first clinical symptoms [110, 111]. Current research efforts lie in patient stratification according to disease severity and identifying responders to expensive novel biologicals [111]. Targeted molecular imaging might offer a solution for the current goals of identifying aggressive disease and treatment potential, providing a more reliable prognosis, evaluating/comparing new therapies and provide new insights in the pathophysiology of RA [110, 112].

As RA progresses, the initially sparsely populated articular region becomes infiltrated with immune cells, neutrophils and monocytes/macrophages, fibroblast-like synoviocytes (FLS), and osteoclasts [113, 114]. The interaction of these cells directly with each other and via cytokines has many similarities with locally-invasive malignancies, leading to chronic inflammation, and tissue invasion, remodeling and destruction [113, 115]. In the RA microenvironment, FLS acquire the tumor-like characteristic of being able to escape growth limits, enhance migration and invasion and to prompt angiogenesis [16]. The similarities between RA and cancer has led to the identification of commonly activated pathways with one being centered around uPAR.

RA manifestation in joints is defined by persistent synovial inflammation, where leukocytes from the innate and adaptive immune system infiltrate the synovial compartment and interact with present synoviocytes [116]. To support the influx, adhesion, and migration of cells into the synovial compartment, endothelial cells overexpress uPAR (Figure 3A) [45, 117, 118]. However, uPAR expression is limited to endothelial cells. Neutrophils stimulate the inflammatory process through secretion of uPA and domain 2-3 of uPAR, whereby the latter probably functions as a chemoattractant for other formyl peptide receptor expressing leukocytes (Figure 3B) [114, 118, 119]. The secreted uPA interacts in autocrine and paracrine fashion

with uPAR on neutrophils, FLS, macrophages, and chondrocytes, enhancing the invasive and proliferative properties of these cells (Figure 3C-D) [16, 115, 120-131]. The importance of uPAR has been confirmed by studies where knockdown of uPAR in FLS inhibited proliferation, migration and invasion *in vitro* [16]. Furthermore, compared to their wildtype littermates, PLAUR -/- mice show significant reduction of arthritis incidence and severity in a collagen-induced arthritis model [132]. However, an earlier study suggested that uPAR is not essential for RA development [133]. Induction of arthritis by intra-articular uPA injection is not dependent on the uPAR-binding fragment of uPA. Furthermore, the arthritis incidence is similar in PLAUR -/- mice and their genetic counterparts after uPA injection [133]. While this model results in joints with morphological features of arthritis, the question can be beckoned if intra-articular injection of uPA accurately reflects the etiology and progression of RA in humans.

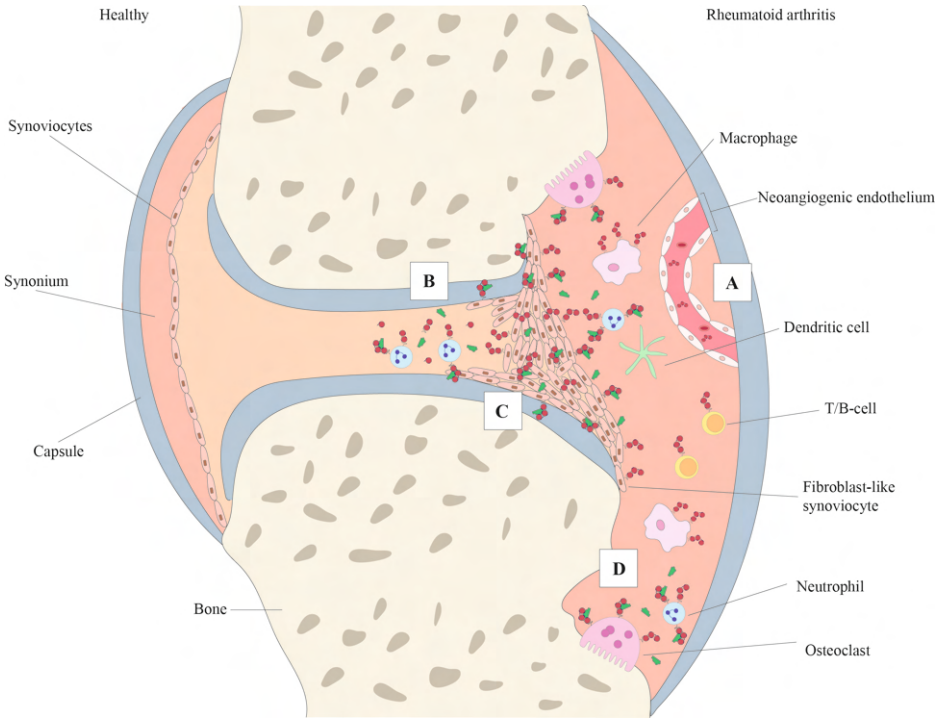

Figure 3. uPAR in rheumatoid arthritis. (A) uPAR on neo-angiogenic endothelium support the influx of inflammatory cells. (B) Neutrophils secrete uPA and uPAR-D2/3 further escalating the inflammation. (C) The uPA interacts via autocrine and paracrine methods with neutrophils, fibroblast-like synoviocytes, macrophages and chondrocytes, activating invasive and proliferative pathways in these cells. (D) uPAR on osteoclasts promotes bone destruction. uPAR is represented by the red 3-domain structure as described in figure 1 on the cell membrane of uPAR expressing cells and uPA by the green structure in the extracellular matrix and bound to uPAR. D, domain; uPA, urokinase plasminogen activator; uPAR, urokinase plasminogen activator receptor.

Besides influencing the inflammatory stage of RA, uPAR also attenuates the bone destruction occurring in late stage RA disease. Osteoclast differentiation, the subsequent bone destruction and bone mineral density (BMD), is significantly decreased in uPAR knockout mice and stimulated by uPAR overexpression [134]. With this knowledge in mind, loss of BMD has been successfully inhibited in a lipopolysaccharide-induced bone destruction mouse model using the uPAR targeting peptide (Å6) [135].

The therapeutic possibilities by targeting uPAR *in vivo* have been investigated using uPAR antisense treatment and adenovirus-mediated gene transfer of the amino terminal fragment of uPA fused to human serum albumin. Both inhibit cartilage invasion while the latter also decreases both the incidence and severity of the disease [115, 136, 137]. However, blocking uPAR using the anti-uPAR monoclonal antibody mR1 in collagen-induced and delayed-type hypersensitivity arthritis models has no effect on RA progression [118]. This discrepancy can partly be explained by difference in methods (antisense vs. adenovirus vs. monoclonal antibody administration), targeting uPA vs. uPAR, and by the differences in models used.

While preclinical *in vivo* research is still inconclusive, several studies with clinically used agents have demonstrated that various treatment options for RA reach their effect by targeting the urokinase plasminogen activation pathway. Tenoxicam, a non-steroidal anti-inflammatory drug, has been shown to downregulate monocyte uPAR expression and hyaluronic acid treatment decreases the immunostaining for uPAR expression on FLS [122, 123]. Furthermore, the widely used corticosteroid deflazacort also modulates the urokinase pathway by inducing PAI-1 and inhibiting uPA and uPAR expression in RA FLS but not in healthy cells [138]. Physiologically, proliferation and invasion of RA FLS are inhibited by deflazacort. In addition, soluble uPAR levels correlate with response to biologicals such as the tumor necrosis factor (TNF)-inhibitor adalimumab [139].

All-in-all there is substantial evidence for the role of uPA/uPAR/PAI-1 axis in RA development and progression. Although future studies will need to confirm this, targeting uPAR for imaging purposes has the potential of providing relevant information on disease activity, prognosis and treatment effect [140].

Central nervous system pathology: Unravelling pathophysiology of degenerative disease

The nervous system, with the brain as its helm, is the most complex and pivotal system of the human body. Therefore, neurodegenerative disorders, such as Alzheimer's disease (AD) and Creutzfeld-Jakob disease (CJD), auto-immune diseases,

such as multiple sclerosis (MS), and infectious diseases, such as cerebral malaria (CM) and acquired immunodeficiency syndrome dementia complex (ADC), have disastrous consequences for patients. The emergence of molecular imaging has enabled more in-depth research into these pathologies as well as possibilities for diagnosis and monitoring of disease before clinical features occur [141-144].

While uPAR expression is very low, if not absent, in the adult brain, it plays a pivotal role in the developing brain (Figure 4A) [15, 145]. In the early brain binding of uPA to uPAR stimulated neuritogenesis, neuronal migration, and differentiation via both proteolytic and nonproteolytic pathways resulting in axonal growth and branching of both the central and peripheral nerves [146-150]. The uPA/uPAR axis is of such importance that dysregulation has been implicated with epilepsy, schizophrenia and autism. *PLAUR*, the gene encoding uPAR, and its promotor have been found to be upregulated in autistic patients [151, 152]. Furthermore, in rats uPAR expression was increased in interneurons after spontaneous seizures [153]. On the other hand, uPAR -/- mice were more susceptible to seizures, increased anxiety and altered social behavior; all characteristics of epilepsy, schizophrenia and autism [154, 155]. The discovery that uPAR functions as a receptor for SRPX2, an important regulator of synapse formation, and that both are co-located both spatially and temporally in the developing brain, further implicates uPAR's role in the (patho) physiology of the nervous system. Although the actual function of SRPX2 remains to be elucidated, the Y72S mutation in SRPX2 leads to an almost six-fold increased affinity for uPAR, and clinically manifests in seizures, speech deficit, and mental retardation [156, 157].

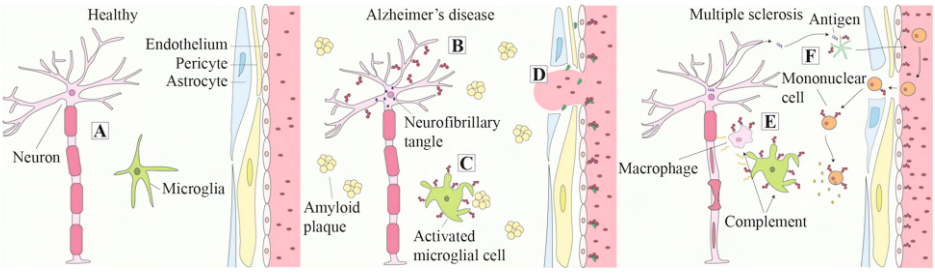

Figure 4. uPAR in degenerative nervous system disorders. (A) uPAR expression is practically absent in the healthy human brain. In Alzheimer's disease uPAR expression is found on (B) cortical neurons, (C) activated microglial cells after exposure to the amyloid plaques and (D) in the vascular wall promoting uPA activation, subsequent extracellular matrix breakdown and corresponding spontaneous hemorrhages. In multiple sclerosis uPAR (E) is expressed on inflammatory cells and activated microglial cells promoting local damage. (F) Furthermore, uPAR expression on dendritic cells influences subsequent T-cell differentiation. uPAR is represented by the red 3-domain structure as described in figure 1 on the cell membrane of uPAR expressing cells and uPA by the green structure in the extracellular matrix and bound to uPAR. uPA, urokinase plasminogen activator; uPAR, urokinase plasminogen activator receptor.

Various neurodegenerative diseases present with enhanced uPAR expression. AD is the leading cause of dementia and can be characterized pathologically as intracellular tangles and extracellular deposition of amyloid β creating senile plaques [158, 159]. uPAR expression has been found in both the cortical neurons and the vascular wall of AD patients (Figure 4B) [19, 160-162]. Interestingly, the cerebellum, a region of the brain that is usually not affected by AD, is negative for uPAR in these patients [162]. Corresponding *in vitro* studies demonstrate that microglia upregulate uPAR mRNA and protein after exposure to aggregated amyloid β (Figure 4C) [161, 162]. Furthermore, uPA and plasminogen activity is increased, which could lead to the vulnerability of the cerebral vessel wall due to extracellular matrix breakdown and corresponding spontaneous hemorrhages observed in AD (Figure 4D) [161]. In CJD, another fatal degenerative disease with a mean survival of 7.3+/-0.2 months after clinical onset, significantly more neurons, primarily focused in cortical layer 3-5, express uPAR, where the expression has been associated with damaged neurons as seen by chromatin condensation, hypertrophic swelling and degeneration [160, 163]. Microglial cells, but not astrocytes, also express uPAR [160].

MS is an autoimmune disease where an immune response is mounted against the central nervous system by autoreactive lymphocytes resulting in lesions that are characterized by inflammation, demyelination, and degeneration of neurons [164]. While autopsy material from healthy brains exhibits almost no uPAR expression, uPAR gene and protein expression is significantly elevated on MS microvessels, mononuclear cells, macrophages, pericytes and smooth muscle cells [165-169]. Microglial cells, cultured from an MS patient, show an activated morphology in combination with high levels of uPAR, whereas control microglial cells from normal brain tissue express little to no uPAR mRNA and protein. After *in vitro* activation these normal microglia present a spindle-shape morphology and express uPAR [170]. In an animal model of experimental autoimmune encephalomyelitis (EAE), elevated uPAR expression is detected in the inflammatory lesions by both immune and microglial cells (Figure 4E) and increased uPA activity at the dorsal horn and central spinal cord [171, 172]. EAE in uPAR -/- mice is characterized by a delayed onset, chronicity, persisting inflammatory cuffs with increased levels of uPA and more extensive demyelination. The dysregulated adhesion and migration of inflammatory cells in uPAR -/- mice explains the delayed onset while the inability to recycle uPA via uPAR reflects the increased neuronal damage [173]. In a later study uPAR -/- mice with EAE are shown to exhibit more severe disease with a two-fold increase in microglial activation and increased infiltration of mononuclear cells but reduced immune response, rendering the mouse incapable of recovery [174]. The recently revealed crosstalk between the coagulation pathway (coagulation factor XII, FXII) and immunity in MS underlines the role of uPAR in this disease. uPAR on dendritic

cells (Figure 4F) is responsible for the immune modulatory function of FXII, tipping the balance of T-cell differentiation towards the TH17 phenotype, as a signal receiver and relaying the message, via CD11b integrin, intracellularly [175]. All-in-all, there is initial evidence that uPAR plays a fundamental role in MS, but whether uPAR expression is protective or destructive remains to be elucidated and, considering uPAR's multifaceted aspects, could actually be both.

Various infectious diseases can have drastic neurological manifestations. ADC is one of the most severe consequences of human immunodeficiency virus 1 (HIV-1) infection [176]. The lesions showed membranous uPAR expression in immunohistochemical staining's that colocalized with HIV-1 p24 antigen in both macrophages, microglial and multinucleated giant cells [177, 178]. Not coincidentally, soluble uPAR levels are a strong independent predictor for HIV-1 infection survival [179]. While combination antiretroviral therapy has successfully dropped the incidence of ADC from 20% to 5%, milder forms of HIV-associated neurocognitive disorder still occur with an incidence of 20-50% [176]. No study has evaluated uPAR in these cases. Plasmodium falciparum is another infectious agent that can lead to severe neurologic impairment with persistent neurocognitive deficits characterized as CM [180]. In *post-mortem* specimens of patients with CM uPAR expression, detected by immunohistochemical staining, of microglia, reactive astrocytes and endothelial cells is limited to areas with microvasculature containing parasitized erythrocytes, petechial bleedings and Dürck's granulomas [181]. In the mouse model of CM, known as severe malaria (SM) as the syndrome in mice is not limited to the brain, uPAR deficiency has profound effect on thrombocytopenia. Platelet trapping, which is a reliable predictor of forthcoming death, does not occur in uPAR -/- mice [182]. The current theory holds that platelets form an adhesive surface in microvascular beds for parasitized erythrocytes in the cerebrum and consequently play a pivotal role in the development of CM [183].

While in most neurological disease processes there is no clear indication whether uPAR expression is protective or destructive, the evidence currently accumulated suggests a critical role for uPAR in the pathophysiology of AD, MS, ADC and MC. Grossly, aberrant uPAR expression is linked to an altered immune-phenotype, consequently altering the progressing of the disease. In addition to the *post-mortem* pathology and animal models we are dependent on for research, an uPAR targeting tracer may enable *in vivo* imaging of the various pathophysiological processes going on in real-time and consequently enrich our understanding of these disease. This knowledge can potentially be used to dictate treatment and monitor disease based on uPAR signaling.

Inflammatory bowel disease: imaging macrophage polarization

Inflammatory bowel disease (IBD) is an umbrella term consisting of chronic relapsing inflammatory disorders of the intestinal tract. Ulcerative colitis (UC) characterizes itself as inflammation of the mucosal layer of the colon while Crohn's disease (CD) displays transmural inflammation of any part of the gastrointestinal tract ranging from the mouth to the anus [184]. The current gold standard for diagnosis and surveillance of IBD is endoscopy and x-ray exams, but these techniques are limited by their invasiveness and patient tolerance. Molecular imaging might provide an opportunity for accurate non-invasive or endoscopic specification of IBD presence, transmural and extra-intestinal tissue involvement, and specific inflammatory profile [185-188]. While the etiology of IBD has not been fully elucidated yet, genetic, environmental and immune factors have all been implicated.

The impaired immune response leads to extensive tissue remodeling and degradation in which the plasminogen activation cascade, including various MMPs and localized by uPAR, plays a major role [189-192]. Patients with active IBD have increased uPAR specific for macrophages at active lesions. Interestingly, uPAR D1-D3 is downregulated while uPAR D2-D3 is increased. In, two different IBD mice models, uPAR expression has shown specific for $CX_3CR_1^+$ macrophages and mirrored disease onset [193]. This subset of macrophages has an anti-inflammatory phenotype [194]. Therefore, knocking out uPAR exaggerates disease by amplifying the release of pro-inflammatory cytokines and altering polarization of macrophages. Low expression of uPAR D1-D3 and high expression of uPAR D2-3 by IBD patients can consequently lead to increased inflammation and disrupted bacterial removal (Figure 5A-B) [193].

The therapeutic potential that targeting macrophages, and in extension uPAR, brings has not been unnoticed [195]. A cyclic peptide based of amino acids 88-92 of uPAR, [SRSRY], competed with uPAR for binding to FPRL1 but exerted an opposite effect: inhibiting migration as opposed to promoting it [196]. *In vivo*, [SRSRY] altered macrophage polarization and migration in colitis mice models and as such attenuated disease severity [197]. By competing with the migration sensitive epitope that becomes available after uPAR cleavage, [SRSRY] diminishes the destructive potential of uPAR D2-D3. While the research is still in its infancy, there is potential to determine macrophage polarization and disease progression by molecular imaging of uPAR. Determining the right epitope to direct the uPAR targeting moiety to, will be crucial for correct implementation and interpretation of uPAR-targeted molecular imaging in IBD as well as for other applications. If addressed well, uPAR imaging has the potential to non-invasively diagnose IBD by identifying aberrant macrophage polarization and subsequently be used to monitor disease activity.

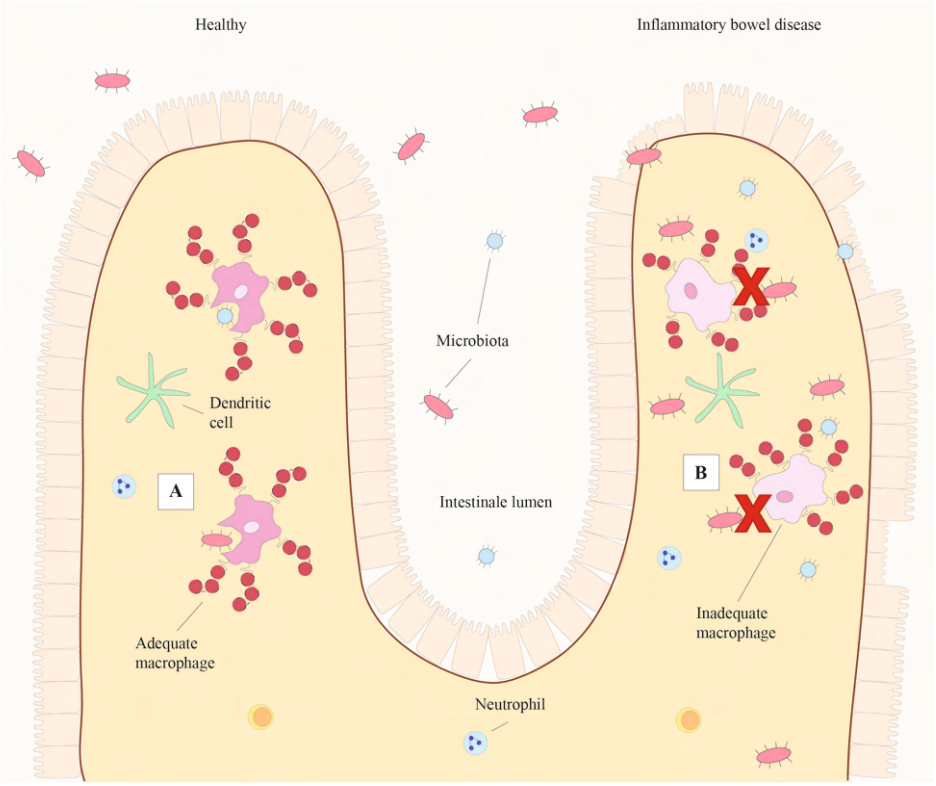

Figure 5. uPAR in inflammatory bowel disease. (A) Macrophage uPAR D1-D3 expression plays a significant role in bacterial removal while (B) in inflammatory bowel disease macrophage differentiation is altered with as consequence an increase in uPAR D2-D3 expression and inadequate microbial maintenance. uPAR is represented by the red 3-domain structure as described in figure 1 on the cell membrane of uPAR expressing cells. D, domain; uPAR, urokinase plasminogen activator receptor.

uPAR imaging

uPAR has been targeted for molecular imaging according by various approaches, each with its own advantages and disadvantages (Table 1, Figure 6A). The first peptides targeting uPAR were ligand-based, utilizing the growth-factor domain of urokinase [198]. Targeting this natural interaction between uPA and uPAR with ATF or ATF-like constructs has been employed for magnetic-resonance imaging, near-infrared imaging, photo-acoustic imaging and nuclear-imaging [199-205]. With a molecular weight of 18.5 kilodalton, ATF is cleared rapidly by the kidneys resulting in quick imaging times (30 minutes to 2 hours) but also minimizing the time available to get sufficient contrast [206]. Conjugating ATF to nanoparticles (NPs) enhances blood circulation times resulting in optimal imaging times around 24-48

hours after injection *in vivo* [199, 200, 203, 205]. Another advantage of ATF-NPs is their internalization, potentially increasing contrast [200, 201, 205]. Nonetheless, whether conjugated to a NP or not, uPAR targeting efficiency with ATF is dependent on the absence of endogenous urokinase on the majority of uPAR copies present and markedly reduced in models with high uPA expression [5, 202].

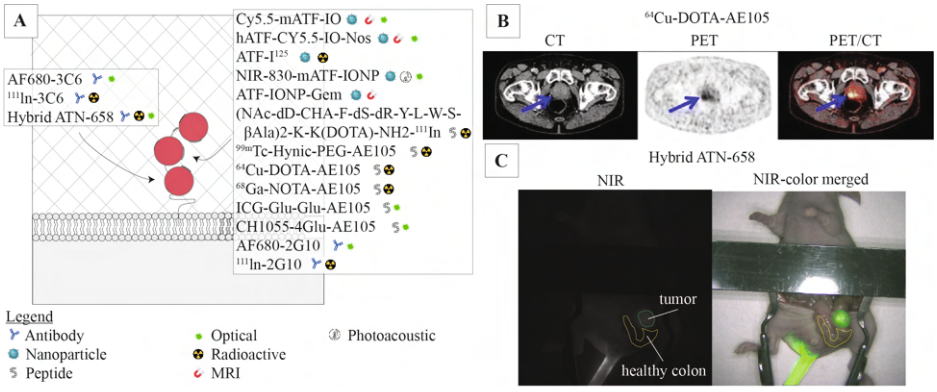

Figure 6. Targeting uPAR for molecular imaging. (A) Representation of binding domains of the uPAR imaging agents currently under development, their classification and suitable imaging modality. (B) Positive primary lesion with uPAR PET in human prostate cancer after injection of 64Cu-DOTA-AE105. Images adapted from Skovgaard et al. (218) and used under the terms of the Creative Commons CC BY license. (C) NIR optical imaging of orthotopic colon cancer with hybrid ATN-658. CT, computed tomography; MRI, magnetic resonance imaging; NIR, near-infrared; PET, positron-emission tomography; uPAR, urokinase plasminogen activator receptor.

An alternative uses a 9-mer peptide which has led to the first uPAR PET clinical trials. This peptide, AE105, is the refined version of a 15-mer peptide identified by a phage display with uPAR-transfected cell lines and binds uPAR at the uPA-binding site in a species specific manner, like ATF [207, 208]. While AE105 has also been conjugated with (radio)-labels for single-photon emission computed tomography (SPECT) and near-infrared fluorescence (NIRF) in preclinical oncology studies, this section will focus on positron-emission tomography as AE105 PET is further along the clinical pipeline [209-216]. Initially, AE105 has been conjugated with the metal chelator DOTA and subsequently labelled with ^{64}Cu. ^{64}Cu-DOTA-AE105 specifically targets uPAR positive lesions in preclinical studies with signal corresponding to uPAR expression levels and epitope availability, but also resulted in high non-specific liver-uptake [217, 218]. Alternative ^{64}Cu, ^{68}Ga and ^{18}F tracer-chelator combinations decrease non-specific uptake but at the cost of lower tumor specific signal [219]. Phase I clinical trials with ^{64}Cu-DOTA-AE105 have shown no adverse events or detectable pharmacological effects related to the tracer. Furthermore all primary tumors (bladder, breast and prostate) and the majority of metastasis are identifiable between 1 and 24 hours after administration (Figure 6B). In this study, two liver

Table 1. uPAR targeting imaging agents currently in development.

Agent	Classification	Targeting Epitope	Imaging Modality	Imaging window	Notes	Translation Stage	Ref
Cy5.5-mATF-IO	ATF-based NP	uPA-binding region	MRI, optical	24 - 48 hrs	mouse ATF	*In vivo* preclinical	199, 200
hATF-Cy5.5-IO-Nos	ATF-based NP	uPA-binding region	MRI, optical	n.a.	human ATF	*In vitro* preclinical	201
ATF-I^{125}	ATF-based	uPA-binding region	n.a.	n.a.	-	*In vitro* preclinical	202
NIR-830-mATF-IONP	ATF-based NP	uPA-binding region	PA, Optical	24 hrs	mouse ATF	*In vivo* preclinical	203
ATF-IONP-Gem	ATF-based NP	uPA-binding region	MRI	48 hrs	mouse and human ATF	*In vivo* preclinical	204
NIR-830-hATF-IONP	ATF-based NP	uPA-binding region	Optical	24 hrs	human ATF	*In vivo* preclinical	205
NAc-dD-CHA-F-dS-dR-Y-L-W-S-βAla)$_2$-K-K(DOTA)-NH_2-^{111}In	Peptide	uPA-binding region	n.a.	n.a.	-	*In vitro* preclinical	202
^{99m}Tc-Hynic-PEG-AE105	Peptide	uPA-binding region	SPECT	4 - 6 hrs	-	*In vivo* preclinical	209
^{64}Cu-DOTA-AE105	Peptide	uPA-binding region	PET	24 hrs	-	phase I clinical	13, 214, 215 217, 218, 220
^{68}Ga-NOTA-AE105	Peptide	uPA-binding region	PET	10 min – 1 hr	-	phase I clinical	14, 216
ICG-Glu-Glu-AE105	Peptide	uPA-binding region	Optical	6 - 24 hrs	-	*In vivo* preclinical	210, 211, 213
CH1055-4Glu-AE105	Peptide	uPA-binding region	Optical	72 - 96 hrs	-	*In vivo* preclinical	212

Table 1. Continued.

Agent	Classification	Targeting Epitope	Imaging Modality	Imaging window	Notes	Translation Stage	Ref
AF680-2G10	Antibody	uPA-binding region	Optical	48 - 96 hrs	recombinant antibody with trastuzumab Fc region	*In vivo* preclinical	223, 224
^{111}In-2G10	Antibody	uPA-binding region	SPECT	48 – 120 hrs	recombinant antibody with trastuzumab Fc region	*In vivo* preclinical	223, 224
AF680-3C6	Antibody	β1-binding region	Optical	48 - 96 hrs	recombinant antibody with trastuzumab Fc region	*In vivo* preclinical	223
^{111}In-3C6	Antibody	β1-binding region	SPECT	48 – 96 hrs	recombinant antibody with trastuzumab Fc region	*In vivo* preclinical	223
^{111}In-ZW800-1-ATN-658 (Hybrid ATN-658)	Antibody	domain 3, amino acids 268-275	Optical, SPECT	24-72 hrs	mouse antibody	*In vivo* preclinical	228, 229

ATF, amino-terminal fragment; hrs, hours; min, minutes; MRI, magnetic resonance imaging; n.a., not applicable; NP, nanoparticle; PET, positron emission tomography; Ref, reference(s); SPECT, single photon emission computed tomography; uPA, urokinase plasminogen activator; uPAR, urokinase plasminogen activator receptor.

metastasis have not been visualized due to high background signal [13]. In addition, the feasibility of measuring mean ^{64}Cu-DOTA-AE105 uptake in the arterial beds of these patients in order to non-invasively identify atherogenic lesions have been retrospectively evaluated [220]. While activated macrophages have higher uPAR expression clear imaging capability of atherosclerosis has yet to be demonstrated with this tracer. The possibility to scan at early time points and the independence of ^{68}Ga on an on-site cyclotron prompted to phase I trials of ^{68}Ga-NOTA-AE105 [13, 14, 219]. ^{68}Ga-Nota-AE105 resulted in decreased liver signal and specifically identified both primary tumors and one metastasis missed in the standard work-up [14]. While initial clinical trials results are promising, allowing for rapid identification of cancerous lesions, endogenous uPA expression could present the biggest limiting factor of AE105 molecular imaging, especially in diseases where the expression of uPA is likely to be increased and paramount for outcomes [5, 221].

Another approach utilizes monoclonal antibodies to target uPAR. Both antibodies 2G10 and 3C6 are identified from a human fragment of the antigen binding (Fab) phage display library to have high affinities for uPAR. Consequently these are expressed as recombinant IgG's using the trastuzumab Fc domain [222]. 2G10 competes with uPA for uPAR binding while 3C6 prevents β1 integrin association with uPAR [223]. In human xenograft breast cancer models, 2G10 shows higher tumor uptake with NIRF and SPECT/CT than 3C6, probably due to higher epitope availability for 2G10 [222, 224].

Another thoroughly and extensively studied anti-uPAR antibody is ATN658. ATN658 was raised against a soluble D2-D3 uPAR fragment and recognizes domain 3 of uPAR, close to the C-terminus at amino acids 268-275 [47, 225]. ATN658 enables and anti-tumor effect by impairing α5β1 integrin adhesion to the ECM and is not effected by uPA or vitronectin interaction with uPAR [47, 226, 227]. In colorectal and oral xenograft cancer models NIRF and SPECT hybrid-labelled ATN658, accurately localized lesions as small as 1-2 mm in size in a range from 24 to 72 hours post-injection (Figure 6C) [228, 229]. ATN658 has been humanized and is awaiting clinical translation for NIRF-imaging [227].

A thorough assessment of the uPAR targeting agents reveals crucial differences in modalities, biodistributions, imaging windows, epitopes targeted and production methods. Therefore, a one-size-fits-all solution to target all types of diseases where uPAR is involved is probably not feasible, like for most, if not all, molecular targets [5]. For instance, peptides may find their utility in more acute situations such as atherosclerosis imaging. Antibodies seem more ideal for abdominal imaging where the high non-specific background of kidneys can be a hindrance or in more elective settings where a large imaging window is desired. Not only will selecting an optimal agent be challenging, also designing and selecting preclinical animal models that

take the species specificity of the imaging agents into account, since most tracers designed for clinical applications have high affinities for human uPAR but no or reduced affinities for mouse uPAR [202, 208, 222, 225].

Conclusion

uPAR is a central unit in regulating ECM proteolysis, migration, differentiation and proliferation and hereby implicated in a range of inflammatory-related diseases, often holding pivotal roles and tipping the balance towards disease aggravation. Even though uPAR is almost completely absent in normal tissue, it will likely not be an appropriate target for the diagnosis of diseases, due to the common pathophysiological role. However, when it comes to visualization of diagnosed disease lesions, whether it be plaques that are about to rupture or aggravation of RA or IBD, uPAR plays a central pathophysiological role prompting its usefulness as a molecular imaging target. Furthermore, molecular imaging of uPAR can unravel the complex pathophysiological processes occurring, increasing our understanding of the disease and consequently allowing the development of novel therapies; ultimately improving patient outcomes.

References

1. Bonnans C, Chou J, Werb Z. Remodelling the extracellular matrix in development and disease. Nature reviews Molecular cell biology. 2014;15:786-801. doi:10.1038/nrm3904.
2. Hamburg MA, Collins FS. The path to personalized medicine. The New England journal of medicine. 2010;363:301-4. doi:10.1056/NEJMp1006304.
3. Jung KH, Lee KH. Molecular imaging in the era of personalized medicine. Journal of pathology and translational medicine. 2015;49:5-12. doi:10.4132/jptm.2014.10.24.
4. Herschman HR. Molecular imaging: looking at problems, seeing solutions. Science (New York, NY). 2003;302:605-8. doi:10.1126/science.1090585.
5. Baart VM, Boonstra MC, Sier CFM. uPAR directed-imaging of head-and-neck cancer. Oncotarget. 2017;8:20519-20. doi:10.18632/oncotarget.16240.
6. Ahn SB, Chan C, Dent OF, Mohamedali A, Kwun SY, Clarke C, et al. Epithelial and stromal cell urokinase plasminogen activator receptor expression differentially correlates with survival in rectal cancer stages B and C patients. PloS one. 2015;10:e0117786. doi:10.1371/journal.pone.0117786.
7. Willmann JK, van Bruggen N, Dinkelborg LM, Gambhir SS. Molecular imaging in drug development. Nature reviews Drug discovery. 2008;7:591-607. doi:10.1038/nrd2290.
8. Chen K, Chen X. Design and development of molecular imaging probes. Current topics in medicinal chemistry. 2010;10:1227-36. doi:10.2174/156802610791384225.
9. Boonstra MC, de Geus SW, Prevoo HA, Hawinkels LJ, van de Velde CJ, Kuppen PJ, et al. Selecting Targets for Tumor Imaging: An Overview of Cancer-Associated Membrane Proteins. Biomarkers in cancer. 2016;8:119-33. doi:10.4137/bic.S38542.
10. Smith HW, Marshall CJ. Regulation of cell signalling by uPAR. Nature reviews Molecular cell biology. 2010;11:23-36. doi:10.1038/nrm2821.
11. Boonstra MC, Verspaget HW, Ganesh S, Kubben FJ, Vahrmeijer AL, van de Velde CJ, et al. Clinical applications of the urokinase receptor (uPAR) for cancer patients. Current pharmaceutical design. 2011;17:1890-910. doi:10.2174/138161211796718233.
12. Mahmood N, Mihalcioiu C, Rabbani SA. Multifaceted Role of the Urokinase-Type Plasminogen Activator (uPA) and Its Receptor (uPAR): Diagnostic, Prognostic, and Therapeutic Applications. Frontiers in oncology. 2018;8:24. doi:10.3389/fonc.2018.00024.
13. Persson M, Skovgaard D, Brandt-Larsen M, Christensen C, Madsen J, Nielsen CH, et al. First-in-human uPAR PET: Imaging of Cancer Aggressiveness. Theranostics. 2015;5:1303-16. doi:10.7150/thno.12956.
14. Skovgaard D, Persson M, Brandt-Larsen M, Christensen C, Madsen J, Klausen TL, et al. Safety, Dosimetry, and Tumor Detection Ability of (68)Ga-NOTA-AE105: First-in-Human Study of a Novel Radioligand for uPAR PET Imaging. Journal of nuclear medicine : official publication, Society of Nuclear Medicine. 2017;58:379-86. doi:10.2967/jnumed.116.178970.
15. Bruneau N, Szepetowski P. The role of the urokinase receptor in epilepsy, in disorders of language, cognition, communication and behavior, and in the central nervous system. Curr Pharm Des. 2011;17:1914-23. doi:10.2174/138161211796718198.
16. Liu Y, Pan YF, Xue YQ, Fang LK, Guo XH, Guo X, et al. uPAR promotes tumor-like biologic behaviors of fibroblast-like synoviocytes through PI3K/Akt signaling pathway in patients with rheumatoid arthritis. Cell Mol Immunol. 2018;15:171-81. doi:10.1038/cmi.2016.60.
17. Stoppelli MP, Corti A, Soffientini A, Cassani G, Blasi F, Assoian RK. Differentiation-enhanced binding of the amino-terminal fragment of human urokinase plasminogen activator to a specific receptor on U937 monocytes. Proceedings of the National Academy of Sciences of the United States of America. 1985;82:4939-43. doi:10.1073/pnas.82.15.4939.

18. Vassalli JD, Baccino D, Belin D. A cellular binding site for the Mr 55,000 form of the human plasminogen activator, urokinase. The Journal of cell biology. 1985;100:86-92. doi:10.1083/jcb.100.1.86.
19. Asahina M, Yoshiyama Y, Hattori T. Expression of matrix metalloproteinase-9 and urinary-type plasminogen activator in Alzheimer's disease brain. Clinical neuropathology. 2001;20:60-3.
20. Ploug M, Ellis V. Structure-function relationships in the receptor for urokinase-type plasminogen activator. Comparison to other members of the Ly-6 family and snake venom alpha-neurotoxins. FEBS letters. 1994;349:163-8. doi:10.1016/0014-5793(94)00674-1.
21. Huai Q, Mazar AP, Kuo A, Parry GC, Shaw DE, Callahan J, et al. Structure of human urokinase plasminogen activator in complex with its receptor. Science (New York, NY). 2006;311:656-9. doi:10.1126/science.1121143.
22. Eden G, Archinti M, Furlan F, Murphy R, Degryse B. The urokinase receptor interactome. Current pharmaceutical design. 2011;17:1874-89. doi:10.2174/138161211796718215.
23. Huai Q, Zhou A, Lin L, Mazar AP, Parry GC, Callahan J, et al. Crystal structures of two human vitronectin, urokinase and urokinase receptor complexes. Nature structural & molecular biology. 2008;15:422-3. doi:10.1038/nsmb.1404.
24. Ploug M, Ronne E, Behrendt N, Jensen AL, Blasi F, Dano K. Cellular receptor for urokinase plasminogen activator. Carboxyl-terminal processing and membrane anchoring by glycosyl-phosphatidylinositol. The Journal of biological chemistry. 1991;266:1926-33.
25. Mondino A, Blasi F. uPA and uPAR in fibrinolysis, immunity and pathology. Trends in immunology. 2004;25:450-5. doi:10.1016/j.it.2004.06.004.
26. Ellis V, Behrendt N, Dano K. Plasminogen activation by receptor-bound urokinase. A kinetic study with both cell-associated and isolated receptor. The Journal of biological chemistry. 1991;266:12752-8.
27. Vassalli JD, Wohlwend A, Belin D. Urokinase-catalyzed plasminogen activation at the monocyte/macrophage cell surface: a localized and regulated proteolytic system. Current topics in microbiology and immunology. 1992;181:65-86. doi:10.1007/978-3-642-77377-8_3.
28. Wei Y, Waltz DA, Rao N, Drummond RJ, Rosenberg S, Chapman HA. Identification of the urokinase receptor as an adhesion receptor for vitronectin. The Journal of biological chemistry. 1994;269:32380-8.
29. Barinka C, Parry G, Callahan J, Shaw DE, Kuo A, Bdeir K, et al. Structural basis of interaction between urokinase-type plasminogen activator and its receptor. Journal of molecular biology. 2006;363:482-95. doi:10.1016/j.jmb.2006.08.063.
30. Gardsvoll H, Jacobsen B, Kriegbaum MC, Behrendt N, Engelholm L, Ostergaard S, et al. Conformational regulation of urokinase receptor function: impact of receptor occupancy and epitope-mapped monoclonal antibodies on lamellipodia induction. The Journal of biological chemistry. 2011;286:33544-56. doi:10.1074/jbc.M111.220087.
31. Zhao B, Gandhi S, Yuan C, Luo Z, Li R, Gardsvoll H, et al. Stabilizing a flexible interdomain hinge region harboring the SMB binding site drives uPAR into its closed conformation. Journal of molecular biology. 2015;427:1389-403. doi:10.1016/j.jmb.2015.01.022.
32. Cunningham O, Andolfo A, Santovito ML, Iuzzolino L, Blasi F, Sidenius N. Dimerization controls the lipid raft partitioning of uPAR/CD87 and regulates its biological functions. The EMBO journal. 2003;22:5994-6003. doi:10.1093/emboj/cdg588.
33. Caiolfa VR, Zamai M, Malengo G, Andolfo A, Madsen CD, Sutin J, et al. Monomer dimer dynamics and distribution of GPI-anchored uPAR are determined by cell surface protein assemblies. The Journal of cell biology. 2007;179:1067-82. doi:10.1083/jcb.200702151.
34. Gaus K, Le Lay S, Balasubramanian N, Schwartz MA. Integrin-mediated adhesion regulates membrane order. The Journal of cell biology. 2006;174:725-34. doi:10.1083/jcb.200603034.

35. Madsen CD, Ferraris GM, Andolfo A, Cunningham O, Sidenius N. uPAR-induced cell adhesion and migration: vitronectin provides the key. The Journal of cell biology. 2007;177:927-39. doi:10.1083/jcb.200612058.
36. Degryse B, Resnati M, Czekay RP, Loskutoff DJ, Blasi F. Domain 2 of the urokinase receptor contains an integrin-interacting epitope with intrinsic signaling activity: generation of a new integrin inhibitor. The Journal of biological chemistry. 2005;280:24792-803. doi:10.1074/jbc.M413954200.
37. Chaurasia P, Aguirre-Ghiso JA, Liang OD, Gardsvoll H, Ploug M, Ossowski L. A region in urokinase plasminogen receptor domain III controlling a functional association with alpha5beta1 integrin and tumor growth. The Journal of biological chemistry. 2006;281:14852-63. doi:10.1074/jbc.M512311200.
38. Tang CH, Hill ML, Brumwell AN, Chapman HA, Wei Y. Signaling through urokinase and urokinase receptor in lung cancer cells requires interactions with beta1 integrins. Journal of cell science. 2008;121:3747-56. doi:10.1242/jcs.029769.
39. Grove LM, Southern BD, Jin TH, White KE, Paruchuri S, Harel E, et al. Urokinase-type plasminogen activator receptor (uPAR) ligation induces a raft-localized integrin signaling switch that mediates the hypermotile phenotype of fibrotic fibroblasts. The Journal of biological chemistry. 2014;289:12791-804. doi:10.1074/jbc.M113.498576.
40. May AE, Kanse SM, Lund LR, Gisler RH, Imhof BA, Preissner KT. Urokinase receptor (CD87) regulates leukocyte recruitment via beta 2 integrins in vivo. The Journal of experimental medicine. 1998;188:1029-37. doi:10.1084/jem.188.6.1029.
41. Simon DI, Rao NK, Xu H, Wei Y, Majdic O, Ronne E, et al. Mac-1 (CD11b/CD18) and the urokinase receptor (CD87) form a functional unit on monocytic cells. Blood. 1996;88:3185-94.
42. Sitrin RG, Todd RF, 3rd, Albrecht E, Gyetko MR. The urokinase receptor (CD87) facilitates CD11b/CD18-mediated adhesion of human monocytes. The Journal of clinical investigation. 1996;97:1942-51. doi:10.1172/jci118626.
43. Ross GD. Role of the lectin domain of Mac-1/CR3 (CD11b/CD18) in regulating intercellular adhesion. Immunologic research. 2002;25:219-27. doi:10.1385/ir:25:3:219.
44. Simon DI, Wei Y, Zhang L, Rao NK, Xu H, Chen Z, et al. Identification of a urokinase receptor-integrin interaction site. Promiscuous regulator of integrin function. The Journal of biological chemistry. 2000;275:10228-34. doi:10.1074/jbc.275.14.10228.
45. Pliyev BK, Antonova OA, Menshikov M. Participation of the urokinase-type plasminogen activator receptor (uPAR) in neutrophil transendothelial migration. Molecular immunology. 2011;48:1168-77. doi:10.1016/j.molimm.2011.02.011.
46. Pliyev BK, Arefieva TI, Menshikov MY. Urokinase receptor (uPAR) regulates complement receptor 3 (CR3)-mediated neutrophil phagocytosis. Biochemical and biophysical research communications. 2010;397:277-82. doi:10.1016/j.bbrc.2010.05.100.
47. Xu X, Cai Y, Wei Y, Donate F, Juarez J, Parry G, et al. Identification of a new epitope in uPAR as a target for the cancer therapeutic monoclonal antibody ATN-658, a structural homolog of the uPAR binding integrin CD11b (alphaM). PloS one. 2014;9:e85349. doi:10.1371/journal.pone.0085349.
48. Aguirre-Ghiso JA, Liu D, Mignatti A, Kovalski K, Ossowski L. Urokinase receptor and fibronectin regulate the ERK(MAPK) to p38(MAPK) activity ratios that determine carcinoma cell proliferation or dormancy in vivo. Molecular biology of the cell. 2001;12:863-79. doi:10.1091/mbc.12.4.863.
49. Aguirre Ghiso JA, Kovalski K, Ossowski L. Tumor dormancy induced by downregulation of urokinase receptor in human carcinoma involves integrin and MAPK signaling. The Journal of cell biology. 1999;147:89-104. doi:10.1083/jcb.147.1.89.

50. Ghosh S, Johnson JJ, Sen R, Mukhopadhyay S, Liu Y, Zhang F, et al. Functional relevance of urinary-type plasminogen activator receptor-alpha3beta1 integrin association in proteinase regulatory pathways. The Journal of biological chemistry. 2006;281:13021-9. doi:10.1074/jbc.M508526200.
51. Wei Y, Tang CH, Kim Y, Robillard L, Zhang F, Kugler MC, et al. Urokinase receptors are required for alpha 5 beta 1 integrin-mediated signaling in tumor cells. The Journal of biological chemistry. 2007;282:3929-39. doi:10.1074/jbc.M607989200.
52. Wei Y, Czekay RP, Robillard L, Kugler MC, Zhang F, Kim KK, et al. Regulation of alpha5beta1 integrin conformation and function by urokinase receptor binding. The Journal of cell biology. 2005;168:501-11. doi:10.1083/jcb.200404112.
53. Ferraris GM, Schulte C, Buttiglione V, De Lorenzi V, Piontini A, Galluzzi M, et al. The interaction between uPAR and vitronectin triggers ligand-independent adhesion signalling by integrins. The EMBO journal. 2014;33:2458-72. doi:10.15252/embj.201387611.
54. Margheri F, Luciani C, Taddei ML, Giannoni E, Laurenzana A, Biagioni A, et al. The receptor for urokinase-plasminogen activator (uPAR) controls plasticity of cancer cell movement in mesenchymal and amoeboid migration style. Oncotarget. 2014;5:1538-53. doi:10.18632/oncotarget.1754.
55. Smith HW, Marra P, Marshall CJ. uPAR promotes formation of the p130Cas-Crk complex to activate Rac through DOCK180. The Journal of cell biology. 2008;182:777-90. doi:10.1083/jcb.200712050.
56. Adachi Y, Lakka SS, Chandrasekar N, Yanamandra N, Gondi CS, Mohanam S, et al. Down-regulation of integrin alpha(v)beta(3) expression and integrin-mediated signaling in glioma cells by adenovirus-mediated transfer of antisense urokinase-type plasminogen activator receptor (uPAR) and sense p16 genes. The Journal of biological chemistry. 2001;276:47171-7. doi:10.1074/jbc.M104334200.
57. Xiong JP, Mahalingham B, Alonso JL, Borrelli LA, Rui X, Anand S, et al. Crystal structure of the complete integrin alphaVbeta3 ectodomain plus an alpha/beta transmembrane fragment. The Journal of cell biology. 2009;186:589-600. doi:10.1083/jcb.200905085.
58. Ahn SB, Mohamedali A, Anand S, Cheruku HR, Birch D, Sowmya G, et al. Characterization of the interaction between heterodimeric alphavbeta6 integrin and urokinase plasminogen activator receptor (uPAR) using functional proteomics. Journal of proteome research. 2014;13:5956-64. doi:10.1021/pr500849x.
59. Conese M, Nykjaer A, Petersen CM, Cremona O, Pardi R, Andreasen PA, et al. alpha-2 Macroglobulin receptor/Ldl receptor-related protein(Lrp)-dependent internalization of the urokinase receptor. The Journal of cell biology. 1995;131:1609-22. doi:10.1083/jcb.131.6.1609.
60. Czekay RP, Kuemmel TA, Orlando RA, Farquhar MG. Direct binding of occupied urokinase receptor (uPAR) to LDL receptor-related protein is required for endocytosis of uPAR and regulation of cell surface urokinase activity. Molecular biology of the cell. 2001;12:1467-79. doi:10.1091/mbc.12.5.1467.
61. Degryse B, Sier CF, Resnati M, Conese M, Blasi F. PAI-1 inhibits urokinase-induced chemotaxis by internalizing the urokinase receptor. FEBS letters. 2001;505:249-54. doi:10.1016/s0014-5793(01)02797-1.
62. Nykjaer A, Conese M, Christensen EI, Olson D, Cremona O, Gliemann J, et al. Recycling of the urokinase receptor upon internalization of the uPA:serpin complexes. The EMBO journal. 1997;16:2610-20. doi:10.1093/emboj/16.10.2610.
63. Sidenius N, Sier CF, Blasi F. Shedding and cleavage of the urokinase receptor (uPAR): identification and characterisation of uPAR fragments in vitro and in vivo. FEBS letters. 2000;475:52-6. doi:10.1016/s0014-5793(00)01624-0.

64. Wilhelm O, Weidle U, Hohl S, Rettenberger P, Schmitt M, Graeff H. Recombinant soluble urokinase receptor as a scavenger for urokinase-type plasminogen activator (uPA). Inhibition of proliferation and invasion of human ovarian cancer cells. FEBS letters. 1994;337:131-4. doi:10.1016/0014-5793(94)80259-9.
65. Thuno M, Macho B, Eugen-Olsen J. suPAR: the molecular crystal ball. Disease markers. 2009;27:157-72. doi:10.3233/dma-2009-0657.
66. Montuori N, Carriero MV, Salzano S, Rossi G, Ragno P. The cleavage of the urokinase receptor regulates its multiple functions. The Journal of biological chemistry. 2002;277:46932-9. doi:10.1074/jbc.M207494200.
67. Resnati M, Pallavicini I, Wang JM, Oppenheim J, Serhan CN, Romano M, et al. The fibrinolytic receptor for urokinase activates the G protein-coupled chemotactic receptor FPRL1/LXA4R. Proceedings of the National Academy of Sciences of the United States of America. 2002;99:1359-64. doi:10.1073/pnas.022652999.
68. de Paulis A, Montuori N, Prevete N, Fiorentino I, Rossi FW, Visconte V, et al. Urokinase induces basophil chemotaxis through a urokinase receptor epitope that is an endogenous ligand for formyl peptide receptor-like 1 and -like 2. Journal of immunology (Baltimore, Md : 1950). 2004;173:5739-48. doi:10.4049/jimmunol.173.9.5739.
69. Benjamin EJ, Muntner P, Alonso A, Bittencourt MS, Callaway CW, Carson AP, et al. Heart Disease and Stroke Statistics-2019 Update: A Report From the American Heart Association. Circulation. 2019;139:e56-e528. doi:10.1161/cir.0000000000000659.
70. Tavakoli S, Vashist A, Sadeghi MM. Molecular imaging of plaque vulnerability. Journal of nuclear cardiology : official publication of the American Society of Nuclear Cardiology. 2014;21:1112-28; quiz 29. doi:10.1007/s12350-014-9959-4.
71. Anwaier G, Chen C, Cao Y, Qi R. A review of molecular imaging of atherosclerosis and the potential application of dendrimer in imaging of plaque. Int J Nanomedicine. 2017;12:7681-93. doi:10.2147/ijn.s142385.
72. Virmani R, Burke AP, Farb A, Kolodgie FD. Pathology of the vulnerable plaque. J Am Coll Cardiol. 2006;47:C13-8. doi:10.1016/j.jacc.2005.10.065.
73. Tarkin JM, Dweck MR, Evans NR, Takx RA, Brown AJ, Tawakol A, et al. Imaging Atherosclerosis. Circulation research. 2016;118:750-69. doi:10.1161/circresaha.115.306247.
74. Bala G, Broisat A, Lahoutte T, Hernot S. Translating Molecular Imaging of the Vulnerable Plaque-a Vulnerable Project? Molecular imaging and biology : MIB : the official publication of the Academy of Molecular Imaging. 2018;20:337-9. doi:10.1007/s11307-017-1147-x.
75. Rafieian-Kopaei M, Setorki M, Doudi M, Baradaran A, Nasri H. Atherosclerosis: process, indicators, risk factors and new hopes. International journal of preventive medicine. 2014;5:927-46.
76. Weber C, Noels H. Atherosclerosis: current pathogenesis and therapeutic options. Nat Med. 2011;17:1410-22. doi:10.1038/nm.2538.
77. Fuhrman B. The urokinase system in the pathogenesis of atherosclerosis. Atherosclerosis. 2012;222:8-14. doi:10.1016/j.atherosclerosis.2011.10.044.
78. Larmann J, Jurk K, Janssen H, Muller M, Herzog C, Lorenz A, et al. Hepatic Overexpression of Soluble Urokinase Receptor (uPAR) Suppresses Diet-Induced Atherosclerosis in Low-Density Lipoprotein Receptor-Deficient (LDLR-/-) Mice. PLoS One. 2015;10:e0131854. doi:10.1371/journal.pone.0131854.
79. May AE, Schmidt R, Kanse SM, Chavakis T, Stephens RW, Schomig A, et al. Urokinase receptor surface expression regulates monocyte adhesion in acute myocardial infarction. Blood. 2002;100:3611-7. doi:10.1182/blood-2002-03-0778.

80. Gu JM, Johns A, Morser J, Dole WP, Greaves DR, Deng GG. Urokinase plasminogen activator receptor promotes macrophage infiltration into the vascular wall of ApoE deficient mice. J Cell Physiol. 2005;204:73-82. doi:10.1002/jcp.20262.
81. Fuhrman B, Nitzan O, Karry R, Volkova N, Dumler I, Aviram M. Urokinase plasminogen activator (uPA) stimulates cholesterol biosynthesis in macrophages through activation of SREBP-1 in a PI3-kinase and MEK-dependent manner. Atherosclerosis. 2007;195:e108-16. doi:10.1016/j.atherosclerosis.2007.06.025.
82. Ohwaki K, Bujo H, Jiang M, Yamazaki H, Schneider WJ, Saito Y. A secreted soluble form of LR11, specifically expressed in intimal smooth muscle cells, accelerates formation of lipid-laden macrophages. Arteriosclerosis, thrombosis, and vascular biology. 2007;27:1050-6. doi:10.1161/atvbaha.106.137091.
83. Yu H, Maurer F, Medcalf RL. Plasminogen activator inhibitor type 2: a regulator of monocyte proliferation and differentiation. Blood. 2002;99:2810-8. doi:10.1182/blood.v99.8.2810.
84. Mukhina S, Stepanova V, Traktouev D, Poliakov A, Beabealashvilly R, Gursky Y, et al. The chemotactic action of urokinase on smooth muscle cells is dependent on its kringle domain. Characterization of interactions and contribution to chemotaxis. J Biol Chem. 2000;275:16450-8. doi:10.1074/jbc.M909080199.
85. Stepanova V, Jerke U, Sagach V, Lindschau C, Dietz R, Haller H, et al. Urokinase-dependent human vascular smooth muscle cell adhesion requires selective vitronectin phosphorylation by ectoprotein kinase CK2. J Biol Chem. 2002;277:10265-72. doi:10.1074/jbc.M109057200.
86. Kunigal S, Kusch A, Tkachuk N, Tkachuk S, Jerke U, Haller H, et al. Monocyte-expressed urokinase inhibits vascular smooth muscle cell growth by activating Stat1. Blood. 2003;102:4377-83. doi:10.1182/blood-2002-12-3872.
87. Kusch A, Tkachuk S, Lutter S, Haller H, Dietz R, Lipp M, et al. Monocyte-expressed urokinase regulates human vascular smooth muscle cell migration in a coculture model. Biol Chem. 2002;383:217-21. doi:10.1515/bc.2002.022.
88. Kiyan Y, Tkachuk S, Hilfiker-Kleiner D, Haller H, Fuhrman B, Dumler I. oxLDL induces inflammatory responses in vascular smooth muscle cells via urokinase receptor association with CD36 and TLR4. J Mol Cell Cardiol. 2014;66:72-82. doi:10.1016/j.yjmcc.2013.11.005.
89. Kiyan Y, Limbourg A, Kiyan R, Tkachuk S, Limbourg FP, Ovsianikov A, et al. Urokinase receptor associates with myocardin to control vascular smooth muscle cells phenotype in vascular disease. Arteriosclerosis, thrombosis, and vascular biology. 2012;32:110-22. doi:10.1161/atvbaha.111.234369.
90. Vallabhaneni KC, Tkachuk S, Kiyan Y, Shushakova N, Haller H, Dumler I, et al. Urokinase receptor mediates mobilization, migration, and differentiation of mesenchymal stem cells. Cardiovascular research. 2011;90:113-21. doi:10.1093/cvr/cvq362.
91. Kiyan J, Smith G, Haller H, Dumler I. Urokinase-receptor-mediated phenotypic changes in vascular smooth muscle cells require the involvement of membrane rafts. Biochem J. 2009;423:343-51. doi:10.1042/bj20090447.
92. Kiyan J, Kusch A, Tkachuk S, Kramer J, Haller H, Dietz R, et al. Rosuvastatin regulates vascular smooth muscle cell phenotypic modulation in vascular remodeling: role for the urokinase receptor. Atherosclerosis. 2007;195:254-61. doi:10.1016/j.atherosclerosis.2006.12.030.
93. Noda-Heiny H, Daugherty A, Sobel BE. Augmented urokinase receptor expression in atheroma. Arteriosclerosis, thrombosis, and vascular biology. 1995;15:37-43.
94. Kalbasi Anaraki P, Patecki M, Tkachuk S, Kiyan Y, Haller H, Dumler I. Urokinase receptor mediates osteoclastogenesis via M-CSF release from osteoblasts and the c-Fms/PI3K/Akt/NF-kappaB pathway in osteoclasts. Journal of bone and mineral research : the official journal of the American Society for Bone and Mineral Research. 2015;30:379-88. doi:10.1002/jbmr.2350.

95. Kalbasi Anaraki P, Patecki M, Larmann J, Tkachuk S, Jurk K, Haller H, et al. Urokinase receptor mediates osteogenic differentiation of mesenchymal stem cells and vascular calcification via the complement C5a receptor. Stem cells and development. 2014;23:352-62. doi:10.1089/scd.2013.0318.
96. Farris SD, Hu JH, Krishnan R, Emery I, Chu T, Du L, et al. Mechanisms of urokinase plasminogen activator (uPA)-mediated atherosclerosis: role of the uPA receptor and S100A8/A9 proteins. J Biol Chem. 2011;286:22665-77. doi:10.1074/jbc.M110.202135.
97. Salame MY, Samani NJ, Masood I, deBono DP. Expression of the plasminogen activator system in the human vascular wall. Atherosclerosis. 2000;152:19-28. doi:10.1016/s0021-9150(99)00441-4.
98. Svensson PA, Olson FJ, Hagg DA, Ryndel M, Wiklund O, Karlstrom L, et al. Urokinase-type plasminogen activator receptor is associated with macrophages and plaque rupture in symptomatic carotid atherosclerosis. Int J Mol Med. 2008;22:459-64.
99. Chen W, Jin WQ, Chen LF, Williams T, Zhu WL, Fang Q. Urokinase receptor surface expression regulates monocyte migration and is associated with accelerated atherosclerosis. Int J Cardiol. 2012;161:103-10. doi:10.1016/j.ijcard.2011.12.094.
100. Raghunath PN, Tomaszewski JE, Brady ST, Caron RJ, Okada SS, Barnathan ES. Plasminogen activator system in human coronary atherosclerosis. Arteriosclerosis, thrombosis, and vascular biology. 1995;15:1432-43.
101. Okada SS, Golden MA, Raghunath PN, Tomaszewski JE, David ML, Kuo A, et al. Native atherosclerosis and vein graft arterialization: association with increased urokinase receptor expression in vitro and in vivo. Thrombosis and haemostasis. 1998;80:140-7.
102. Steins MB, Padro T, Schwaenen C, Ruiz S, Mesters RM, Berdel WE, et al. Overexpression of urokinase receptor and cell surface urokinase-type plasminogen activator in the human vessel wall with different types of atherosclerotic lesions. Blood Coagul Fibrinolysis. 2004;15:383-91.
103. Quax PH, Lamfers ML, Lardenoye JH, Grimbergen JM, de Vries MR, Slomp J, et al. Adenoviral expression of a urokinase receptor-targeted protease inhibitor inhibits neointima formation in murine and human blood vessels. Circulation. 2001;103:562-9. doi:10.1161/01.cir.103.4.562.
104. Lamfers ML, Grimbergen JM, Aalders MC, Havenga MJ, de Vries MR, Huisman LG, et al. Gene transfer of the urokinase-type plasminogen activator receptor-targeted matrix metalloproteinase inhibitor TIMP-1.ATF suppresses neointima formation more efficiently than tissue inhibitor of metalloproteinase-1. Circulation research. 2002;91:945-52. doi:10.1161/01.res.0000041418.51906.57.
105. Eefting D, de Vries MR, Grimbergen JM, Karper JC, van Bockel JH, Quax PH. In vivo suppression of vein graft disease by nonviral, electroporation-mediated, gene transfer of tissue inhibitor of metalloproteinase-1 linked to the amino terminal fragment of urokinase (TIMP-1.ATF), a cell-surface directed matrix metalloproteinase inhibitor. Journal of vascular surgery. 2010;51:429-37. doi:10.1016/j.jvs.2009.09.026.
106. Lamfers ML, Lardenoye JH, de Vries MR, Aalders MC, Engelse MA, Grimbergen JM, et al. In vivo suppression of restenosis in balloon-injured rat carotid artery by adenovirus-mediated gene transfer of the cell surface-directed plasmin inhibitor ATF.BPTI. Gene Ther. 2001;8:534-41. doi:10.1038/sj.gt.3301437.
107. Eefting D, Seghers L, Grimbergen JM, de Vries MR, de Boer HC, Lardenoye JW, et al. A novel urokinase receptor-targeted inhibitor for plasmin and matrix metalloproteinases suppresses vein graft disease. Cardiovascular research. 2010;88:367-75. doi:10.1093/cvr/cvq203.

108. Crowson CS, Matteson EL, Myasoedova E, Michet CJ, Ernste FC, Warrington KJ, et al. The lifetime risk of adult-onset rheumatoid arthritis and other inflammatory autoimmune rheumatic diseases. Arthritis Rheum. 2011;63:633-9. doi:10.1002/art.30155.
109. Colebatch AN, Edwards CJ, Ostergaard M, van der Heijde D, Balint PV, D'Agostino MA, et al. EULAR recommendations for the use of imaging of the joints in the clinical management of rheumatoid arthritis. Ann Rheum Dis. 2013;72:804-14. doi:10.1136/annrheumdis-2012-203158.
110. Wunder A, Straub RH, Gay S, Funk J, Muller-Ladner U. Molecular imaging: novel tools in visualizing rheumatoid arthritis. Rheumatology (Oxford). 2005;44:1341-9. doi:10.1093/rheumatology/keh709.
111. Put S, Westhovens R, Lahoutte T, Matthys P. Molecular imaging of rheumatoid arthritis: emerging markers, tools, and techniques. Arthritis Res Ther. 2014;16:208. doi:10.1186/ar4542.
112. Malviya G, Conti F, Chianelli M, Scopinaro F, Dierckx RA, Signore A. Molecular imaging of rheumatoid arthritis by radiolabelled monoclonal antibodies: new imaging strategies to guide molecular therapies. European journal of nuclear medicine and molecular imaging. 2010;37:386-98. doi:10.1007/s00259-009-1272-0.
113. McInnes IB, Schett G. Pathogenetic insights from the treatment of rheumatoid arthritis. Lancet. 2017;389:2328-37. doi:10.1016/s0140-6736(17)31472-1.
114. Dinesh P, Rasool M. uPA/uPAR signaling in rheumatoid arthritis: Shedding light on its mechanism of action. Pharmacol Res. 2018;134:31-9. doi:10.1016/j.phrs.2018.05.016.
115. Serrati S, Margheri F, Chilla A, Neumann E, Muller-Ladner U, Benucci M, et al. Reduction of in vitro invasion and in vivo cartilage degradation in a SCID mouse model by loss of function of the fibrinolytic system of rheumatoid arthritis synovial fibroblasts. Arthritis Rheum. 2011;63:2584-94. doi:10.1002/art.30439.
116. Guo Q, Wang Y, Xu D, Nossent J, Pavlos NJ, Xu J. Rheumatoid arthritis: pathological mechanisms and modern pharmacologic therapies. Bone research. 2018;6:15. doi:10.1038/s41413-018-0016-9.
117. Szekanecz Z, Haines GK, Koch AE. Differential expression of the urokinase receptor (CD87) in arthritic and normal synovial tissues. Journal of clinical pathology. 1997;50:314-9. doi:10.1136/jcp.50.4.314.
118. Almholt K, Hebsgaard JB, Nansen A, Andersson C, Pass J, Rono B, et al. Antibody-Mediated Neutralization of uPA Proteolytic Function Reduces Disease Progression in Mouse Arthritis Models. J Immunol. 2018;200:957-65. doi:10.4049/jimmunol.1701317.
119. Pliyev BK, Menshikov MY. Release of the soluble urokinase-type plasminogen activator receptor (suPAR) by activated neutrophils in rheumatoid arthritis. Inflammation. 2010;33:1-9. doi:10.1007/s10753-009-9152-0.
120. Fibbi G, Pucci M, Serni U, Cerinic MM, Del Rosso M. Antisense targeting of the urokinase receptor blocks urokinase-dependent proliferation, chemoinvasion, and chemotaxis of human synovial cells and chondrocytes in vitro. Proceedings of the Association of American Physicians. 1998;110:340-50.
121. Baran M, Mollers LN, Andersson S, Jonsson IM, Ekwall AK, Bjersing J, et al. Survivin is an essential mediator of arthritis interacting with urokinase signalling. Journal of cellular and molecular medicine. 2009;13:3797-808. doi:10.1111/j.1582-4934.2009.00721.x.
122. Kirchheimer JC. Modulation of receptor bound urokinase-type plasminogen activator on human monocytes by non-steroidal antiinflammatory drugs. Scand J Rheumatol. 1993;22:53-7.
123. Nonaka T, Kikuchi H, Ikeda T, Okamoto Y, Hamanishi C, Tanaka S. Hyaluronic acid inhibits the expression of u-PA, PAI-1, and u-PAR in human synovial fibroblasts of osteoarthritis and rheumatoid arthritis. J Rheumatol. 2000;27:997-1004.

124. Nonaka T, Kikuchi H, Sohen S, Fukuda K, Hamanishi C, Tanaka S. Comparison of the inhibitory effects of two types (90 kDa and 190 kDa) of hyaluronic acid on the expression of fibrinolytic factors in human synovial fibroblasts. Modern rheumatology. 2002;12:160-6. doi:10.3109/s101650200027.
125. Guiducci S, Del Rosso A, Cinelli M, Margheri F, D'Alessio S, Fibbi G, et al. Rheumatoid synovial fibroblasts constitutively express the fibrinolytic pattern of invasive tumor-like cells. Clinical and experimental rheumatology. 2005;23:364-72.
126. Del Rosso M, Fibbi G, Magnelli L, Pucci M, Dini G, Grappone C, et al. Modulation of urokinase receptors on human synovial cells and osteoarthritic chondrocytes by diacetylrhein. Int J Tissue React. 1990;12:91-100.
127. Kirchheimer JC, Remold HG, Wanivenhaus A, Binder BR. Increased proteolytic activity on the surface of monocytes from patients with rheumatoid arthritis. Arthritis Rheum. 1991;34:1430-3.
128. Belcher C, Fawthrop F, Bunning R, Doherty M. Plasminogen activators and their inhibitors in synovial fluids from normal, osteoarthritis, and rheumatoid arthritis knees. Ann Rheum Dis. 1996;55:230-6. doi:10.1136/ard.55.4.230.
129. Ronday HK, Smits HH, Van Muijen GN, Pruszczynski MS, Dolhain RJ, Van Langelaan EJ, et al. Difference in expression of the plasminogen activation system in synovial tissue of patients with rheumatoid arthritis and osteoarthritis. British journal of rheumatology. 1996;35:416-23.
130. Busso N, Peclat V, So A, Sappino AP. Plasminogen activation in synovial tissues: differences between normal, osteoarthritis, and rheumatoid arthritis joints. Ann Rheum Dis. 1997;56:550-7. doi:10.1136/ard.56.9.550.
131. Cerinic MM, Generini S, Partsch G, Pignone A, Dini G, Konttinen YT, et al. Synoviocytes from osteoarthritis and rheumatoid arthritis produce plasminogen activators and plasminogen activator inhibitor-1 and display u-PA receptors on their surface. Life Sci. 1998;63:441-53. doi:10.1016/s0024-3205(98)00293-8.
132. Thornton S, Raghu H, Cruz C, Frederick MD, Palumbo JS, Mullins ES, et al. Urokinase plasminogen activator and receptor promote collagen-induced arthritis through expression in hematopoietic cells. Blood advances. 2017;1:545-56. doi:10.1182/bloodadvances.2016004002.
133. Jin T, Tarkowski A, Carmeliet P, Bokarewa M. Urokinase, a constitutive component of the inflamed synovial fluid, induces arthritis. Arthritis Res Ther. 2003;5:R9-r17.
134. Kanno Y, Ishisaki A, Miyashita M, Matsuo O. The blocking of uPAR suppresses lipopolysaccharide-induced inflammatory osteoclastogenesis and the resultant bone loss through attenuation of integrin beta3/Akt pathway. Immunity, inflammation and disease. 2016;4:338-49. doi:10.1002/iid3.116.
135. Kanno Y, Maruyama C, Matsuda A, Ishisaki A. uPA-derived peptide, A6 is involved in the suppression of lipopolysaccaride-promoted inflammatory osteoclastogenesis and the resultant bone loss. Immunity, inflammation and disease. 2017;5:289-99. doi:10.1002/iid3.169.
136. Apparailly F, Bouquet C, Millet V, Noel D, Jacquet C, Opolon P, et al. Adenovirus-mediated gene transfer of urokinase plasminogen inhibitor inhibits angiogenesis in experimental arthritis. Gene Ther. 2002;9:192-200. doi:10.1038/sj.gt.3301628.
137. van der Laan WH, Pap T, Ronday HK, Grimbergen JM, Huisman LG, TeKoppele JM, et al. Cartilage degradation and invasion by rheumatoid synovial fibroblasts is inhibited by gene transfer of a cell surface-targeted plasmin inhibitor. Arthritis Rheum. 2000;43:1710-8. doi:10.1002/1529-0131(200008)43:8<1710::AID-ANR6>3.0.CO;2-Y.

138. Del Rosso A, Cinelli M, Guiducci S, Pignone A, Fibbi G, Margheri F, et al. Deflazacort modulates the fibrinolytic pattern and reduces uPA-dependent chemioinvasion and proliferation in rheumatoid arthritis synoviocytes. Rheumatology (Oxford). 2005;44:1255-62. doi:10.1093/rheumatology/kei006.
139. Koga T, Okada A, Kawashiri S, Kita J, Suzuki T, Nakashima Y, et al. Soluble urokinase plasminogen activator receptor as a useful biomarker to predict the response to adalimumab in patients with rheumatoid arthritis in a Japanese population. Clinical and experimental rheumatology. 2011;29:811-5.
140. Buckley BJ, Ali U, Kelso MJ, Ranson M. The Urokinase Plasminogen Activation System in Rheumatoid Arthritis: Pathophysiological Roles and Prospective Therapeutic Targets. Current drug targets. 2019;20:970-81. doi:10.2174/1389450120666181204164140.
141. Kim E, Howes OD, Kapur S. Molecular imaging as a guide for the treatment of central nervous system disorders. Dialogues in clinical neuroscience. 2013;15:315-28.
142. Lu FM, Yuan Z. PET/SPECT molecular imaging in clinical neuroscience: recent advances in the investigation of CNS diseases. Quant Imaging Med Surg. 2015;5:433-47. doi:10.3978/j.issn.2223-4292.2015.03.16.
143. Hargreaves RJ, Hoppin J, Sevigny J, Patel S, Chiao P, Klimas M, et al. Optimizing Central Nervous System Drug Development Using Molecular Imaging. Clin Pharmacol Ther. 2015;98:47-60. doi:10.1002/cpt.132.
144. Bohnen NI, Kanel P, Muller M. Molecular Imaging of the Cholinergic System in Parkinson's Disease. International review of neurobiology. 2018;141:211-50. doi:10.1016/bs.irn.2018.07.027.
145. Merino P, Diaz A, Jeanneret V, Wu F, Torre E, Cheng L, et al. Urokinase-type Plasminogen Activator (uPA) Binding to the uPA Receptor (uPAR) Promotes Axonal Regeneration in the Central Nervous System. J Biol Chem. 2017;292:2741-53. doi:10.1074/jbc.M116.761650.
146. Lino N, Fiore L, Rapacioli M, Teruel L, Flores V, Scicolone G, et al. uPA-uPAR molecular complex is involved in cell signaling during neuronal migration and neuritogenesis. Developmental dynamics : an official publication of the American Association of Anatomists. 2014;243:676-89. doi:10.1002/dvdy.24114.
147. Farias-Eisner R, Vician L, Silver A, Reddy S, Rabbani SA, Herschman HR. The urokinase plasminogen activator receptor (UPAR) is preferentially induced by nerve growth factor in PC12 pheochromocytoma cells and is required for NGF-driven differentiation. J Neurosci. 2000;20:230-9.
148. Semina E, Rubina K, Sysoeva V, Rysenkova K, Klimovich P, Plekhanova O, et al. Urokinase and urokinase receptor participate in regulation of neuronal migration, axon growth and branching. Eur J Cell Biol. 2016;95:295-310. doi:10.1016/j.ejcb.2016.05.003.
149. Del Bigio MR, Hosain S, Altumbabic M. Localization of urokinase-type plasminogen activator, its receptor, and inhibitors in mouse forebrain during postnatal development. International journal of developmental neuroscience : the official journal of the International Society for Developmental Neuroscience. 1999;17:387-99.
150. Hayden SM, Seeds NW. Modulated expression of plasminogen activator system components in cultured cells from dissociated mouse dorsal root ganglia. J Neurosci. 1996;16:2307-17.
151. Campbell DB, D'Oronzio R, Garbett K, Ebert PJ, Mirnics K, Levitt P, et al. Disruption of cerebral cortex MET signaling in autism spectrum disorder. Annals of neurology. 2007;62:243-50. doi:10.1002/ana.21180.
152. Campbell DB, Li C, Sutcliffe JS, Persico AM, Levitt P. Genetic evidence implicating multiple genes in the MET receptor tyrosine kinase pathway in autism spectrum disorder. Autism research : official journal of the International Society for Autism Research. 2008;1:159-68. doi:10.1002/aur.27.

153. Lahtinen L, Huusko N, Myohanen H, Lehtivarjo AK, Pellinen R, Turunen MP, et al. Expression of urokinase-type plasminogen activator receptor is increased during epileptogenesis in the rat hippocampus. Neuroscience. 2009;163:316-28. doi:10.1016/j.neuroscience.2009.06.019.
154. Powell EM, Campbell DB, Stanwood GD, Davis C, Noebels JL, Levitt P. Genetic disruption of cortical interneuron development causes region- and GABA cell type-specific deficits, epilepsy, and behavioral dysfunction. J Neurosci. 2003;23:622-31.
155. Levitt P. Disruption of interneuron development. Epilepsia. 2005;46 Suppl 7:22-8. doi:10.1111/j.1528-1167.2005.00305.x.
156. Roll P, Rudolf G, Pereira S, Royer B, Scheffer IE, Massacrier A, et al. SRPX2 mutations in disorders of language cortex and cognition. Human molecular genetics. 2006;15:1195-207. doi:10.1093/hmg/ddl035.
157. Royer-Zemmour B, Ponsole-Lenfant M, Gara H, Roll P, Leveque C, Massacrier A, et al. Epileptic and developmental disorders of the speech cortex: ligand/receptor interaction of wild-type and mutant SRPX2 with the plasminogen activator receptor uPAR. Human molecular genetics. 2008;17:3617-30. doi:10.1093/hmg/ddn256.
158. Anand R, Gill KD, Mahdi AA. Therapeutics of Alzheimer's disease: Past, present and future. Neuropharmacology. 2014;76 Pt A:27-50. doi:10.1016/j.neuropharm.2013.07.004.
159. Kumar A, Singh A, Ekavali. A review on Alzheimer's disease pathophysiology and its management: an update. Pharmacol Rep. 2015;67:195-203. doi:10.1016/j.pharep.2014.09.004.
160. Deininger MH, Trautmann K, Magdolen V, Luther T, Schluesener HJ, Meyermann R. Cortical neurons of Creutzfeldt-Jakob disease patients express the urokinase-type plasminogen activator receptor. Neurosci Lett. 2002;324:80-2. doi:10.1016/s0304-3940(02)00168-4.
161. Davis J, Wagner MR, Zhang W, Xu F, Van Nostrand WE. Amyloid beta-protein stimulates the expression of urokinase-type plasminogen activator (uPA) and its receptor (uPAR) in human cerebrovascular smooth muscle cells. J Biol Chem. 2003;278:19054-61. doi:10.1074/jbc.M301398200.
162. Walker DG, Lue LF, Beach TG. Increased expression of the urokinase plasminogen-activator receptor in amyloid beta peptide-treated human brain microglia and in AD brains. Brain Res. 2002;926:69-79. doi:10.1016/s0006-8993(01)03298-x.
163. Pocchiari M, Puopolo M, Croes EA, Budka H, Gelpi E, Collins S, et al. Predictors of survival in sporadic Creutzfeldt-Jakob disease and other human transmissible spongiform encephalopathies. Brain : a journal of neurology. 2004;127:2348-59. doi:10.1093/brain/awh249.
164. Dendrou CA, Fugger L, Friese MA. Immunopathology of multiple sclerosis. Nature reviews Immunology. 2015;15:545-58. doi:10.1038/nri3871.
165. Washington R, Burton J, Todd RF, 3rd, Newman W, Dragovic L, Dore-Duffy P. Expression of immunologically relevant endothelial cell activation antigens on isolated central nervous system microvessels from patients with multiple sclerosis. Annals of neurology. 1994;35:89-97. doi:10.1002/ana.410350114.
166. Dore-Duffy P, Washington R, Dragovic L. Expression of endothelial cell activation antigens in microvessels from patients with multiple sclerosis. Advances in experimental medicine and biology. 1993;331:243-8. doi:10.1007/978-1-4615-2920-0_38.
167. Gveric D, Hanemaaijer R, Newcombe J, van Lent NA, Sier CF, Cuzner ML. Plasminogen activators in multiple sclerosis lesions: implications for the inflammatory response and axonal damage. Brain : a journal of neurology. 2001;124:1978-88. doi:10.1093/brain/124.10.1978.

168. Archinti M, Britto M, Eden G, Furlan F, Murphy R, Degryse B. The urokinase receptor in the central nervous system. CNS & neurological disorders drug targets. 2011;10:271-94.
169. Cox MB, Bowden NA, Scott RJ, Lechner-Scott J. Altered expression of the plasminogen activation pathway in peripheral blood mononuclear cells in multiple sclerosis: possible pathomechanism of matrix metalloproteinase activation. Multiple sclerosis (Houndmills, Basingstoke, England). 2013;19:1268-74. doi:10.1177/1352458513475493.
170. Washington RA, Becher B, Balabanov R, Antel J, Dore-Duffy P. Expression of the activation marker urokinase plasminogen-activator receptor in cultured human central nervous system microglia. Journal of neuroscience research. 1996;45:392-9. doi:10.1002/(sici)1097-4547(19960815)45:4<392::Aid-jnr8>3.0.Co;2-4.
171. Teesalu T, Hinkkanen AE, Vaheri A. Coordinated induction of extracellular proteolysis systems during experimental autoimmune encephalomyelitis in mice. Am J Pathol. 2001;159:2227-37. doi:10.1016/s0002-9440(10)63073-8.
172. Cunningham O, Campion S, Perry VH, Murray C, Sidenius N, Docagne F, et al. Microglia and the urokinase plasminogen activator receptor/uPA system in innate brain inflammation. Glia. 2009;57:1802-14. doi:10.1002/glia.20892.
173. East E, Baker D, Pryce G, Lijnen HR, Cuzner ML, Gveric D. A role for the plasminogen activator system in inflammation and neurodegeneration in the central nervous system during experimental allergic encephalomyelitis. Am J Pathol. 2005;167:545-54. doi:10.1016/s0002-9440(10)62996-3.
174. Gur-Wahnon D, Mizrachi T, Maaravi-Pinto FY, Lourbopoulos A, Grigoriadis N, Higazi AA, et al. The plasminogen activator system: involvement in central nervous system inflammation and a potential site for therapeutic intervention. Journal of neuroinflammation. 2013;10:124. doi:10.1186/1742-2094-10-124.
175. Gobel K, Pankratz S, Asaridou CM, Herrmann AM, Bittner S, Merker M, et al. Blood coagulation factor XII drives adaptive immunity during neuroinflammation via CD87-mediated modulation of dendritic cells. Nat Commun. 2016;7:11626. doi:10.1038/ncomms11626.
176. Brew BJ, Chan P. Update on HIV dementia and HIV-associated neurocognitive disorders. Current neurology and neuroscience reports. 2014;14:468. doi:10.1007/s11910-014-0468-2.
177. Cinque P, Nebuloni M, Santovito ML, Price RW, Gisslen M, Hagberg L, et al. The urokinase receptor is overexpressed in the AIDS dementia complex and other neurological manifestations. Annals of neurology. 2004;55:687-94. doi:10.1002/ana.20076.
178. Sidenius N, Nebuloni M, Sala S, Zerbi P, Price RW, Gisslen M, et al. Expression of the urokinase plasminogen activator and its receptor in HIV-1-associated central nervous system disease. Journal of neuroimmunology. 2004;157:133-9. doi:10.1016/j.jneuroim.2004.08.038.
179. Sidenius N, Sier CF, Ullum H, Pedersen BK, Lepri AC, Blasi F, et al. Serum level of soluble urokinase-type plasminogen activator receptor is a strong and independent predictor of survival in human immunodeficiency virus infection. Blood. 2000;96:4091-5.
180. Idro R, Jenkins NE, Newton CR. Pathogenesis, clinical features, and neurological outcome of cerebral malaria. The Lancet Neurology. 2005;4:827-40. doi:10.1016/s1474-4422(05)70247-7.
181. Fauser S, Deininger MH, Kremsner PG, Magdolen V, Luther T, Meyermann R, et al. Lesion associated expression of urokinase-type plasminogen activator receptor (uPAR, CD87) in human cerebral malaria. Journal of neuroimmunology. 2000;111:234-40. doi:10.1016/s0165-5728(00)00368-4.

182. Piguet PF, Da Laperrousaz C, Vesin C, Tacchini-Cottier F, Senaldi G, Grau GE. Delayed mortality and attenuated thrombocytopenia associated with severe malaria in urokinase- and urokinase receptor-deficient mice. Infect Immun. 2000;68:3822-9. doi:10.1128/iai.68.7.3822-3829.2000.
183. Wassmer SC, Combes V, Grau GE. Pathophysiology of cerebral malaria: role of host cells in the modulation of cytoadhesion. Annals of the New York Academy of Sciences. 2003;992:30-8. doi:10.1111/j.1749-6632.2003.tb03135.x.
184. Khor B, Gardet A, Xavier RJ. Genetics and pathogenesis of inflammatory bowel disease. Nature. 2011;474:307-17. doi:10.1038/nature10209.
185. Caobelli F, Evangelista L, Quartuccio N, Familiari D, Altini C, Castello A, et al. Role of molecular imaging in the management of patients affected by inflammatory bowel disease: State-of-the-art. World journal of radiology. 2016;8:829-45. doi:10.4329/wjr.v8.i10.829.
186. Catalano O, Maccioni F, Lauri C, Auletta S, Dierckx R, Signore A. Hybrid imaging in Crohn's disease: from SPECT/CT to PET/MR and new image interpretation criteria. The quarterly journal of nuclear medicine and molecular imaging : official publication of the Italian Association of Nuclear Medicine (AIMN) [and] the International Association of Radiopharmacology (IAR), [and] Section of the So. 2018;62:40-55. doi:10.23736/s1824-4785.17.03053-9.
187. Meijer MJ, Mieremet-Ooms MA, Sier CF, van Hogezand RA, Lamers CB, Hommes DW, et al. Matrix metalloproteinases and their tissue inhibitors as prognostic indicators for diagnostic and surgical recurrence in Crohn's disease. Inflammatory bowel diseases. 2009;15:84-92. doi:10.1002/ibd.20581.
188. Birch GP, Campbell T, Bradley M, Dhaliwal K. Optical Molecular Imaging of Inflammatory Cells in Interventional Medicine-An Emerging Strategy. Frontiers in oncology. 2019;9:882-. doi:10.3389/fonc.2019.00882.
189. de Bruin PA, Crama-Bohbouth G, Verspaget HW, Verheijen JH, Dooijewaard G, Weterman IT, et al. Plasminogen activators in the intestine of patients with inflammatory bowel disease. Thrombosis and haemostasis. 1988;60:262-6.
190. de Jong E, Porte RJ, Knot EA, Verheijen JH, Dees J. Disturbed fibrinolysis in patients with inflammatory bowel disease. A study in blood plasma, colon mucosa, and faeces. Gut. 1989;30:188-94. doi:10.1136/gut.30.2.188.
191. Ravi A, Garg P, Sitaraman SV. Matrix metalloproteinases in inflammatory bowel disease: boon or a bane? Inflammatory bowel diseases. 2007;13:97-107. doi:10.1002/ibd.20011.
192. Laerum OD, Illemann M, Skarstein A, Helgeland L, Ovrebo K, Dano K, et al. Crohn's disease but not chronic ulcerative colitis induces the expression of PAI-1 in enteric neurons. The American journal of gastroenterology. 2008;103:2350-8. doi:10.1111/j.1572-0241.2008.01930.x.
193. Genua M, D'Alessio S, Cibella J, Gandelli A, Sala E, Correale C, et al. The urokinase plasminogen activator receptor (uPAR) controls macrophage phagocytosis in intestinal inflammation. Gut. 2015;64:589-600. doi:10.1136/gutjnl-2013-305933.
194. Weber B, Saurer L, Schenk M, Dickgreber N, Mueller C. CX3CR1 defines functionally distinct intestinal mononuclear phagocyte subsets which maintain their respective functions during homeostatic and inflammatory conditions. European journal of immunology. 2011;41:773-9. doi:10.1002/eji.201040965.
195. Na YR, Stakenborg M, Seok SH, Matteoli G. Macrophages in intestinal inflammation and resolution: a potential therapeutic target in IBD. Nature reviews Gastroenterology & hepatology. 2019;16:531-43. doi:10.1038/s41575-019-0172-4.

196. Yousif AM, Minopoli M, Bifulco K, Ingangi V, Di Carluccio G, Merlino F, et al. Cyclization of the urokinase receptor-derived ser-arg-ser-arg-tyr Peptide generates a potent inhibitor of trans-endothelial migration of monocytes. PloS one. 2015;10:e0126172. doi:10.1371/journal.pone.0126172.
197. Genua M, Ingangi V, Fonteyne P, Piontini A, Yousif AM, Merlino F, et al. Treatment with a Urokinase Receptor-derived Cyclized Peptide Improves Experimental Colitis by Preventing Monocyte Recruitment and Macrophage Polarization. Inflammatory bowel diseases. 2016;22:2390-401. doi:10.1097/mib.0000000000000896.
198. Appella E, Blasi F. The growth factor module of urokinase is the binding sequence for its receptor. Annals of the New York Academy of Sciences. 1987;511:192-5. doi:10.1111/j.1749-6632.1987.tb36247.x.
199. Yang L, Peng XH, Wang YA, Wang X, Cao Z, Ni C, et al. Receptor-targeted nanoparticles for in vivo imaging of breast cancer. Clinical cancer research : an official journal of the American Association for Cancer Research. 2009;15:4722-32. doi:10.1158/1078-0432.Ccr-08-3289.
200. Yang L, Mao H, Cao Z, Wang YA, Peng X, Wang X, et al. Molecular imaging of pancreatic cancer in an animal model using targeted multifunctional nanoparticles. Gastroenterology. 2009;136:1514-25.e2. doi:10.1053/j.gastro.2009.01.006.
201. Abdalla MO, Karna P, Sajja HK, Mao H, Yates C, Turner T, et al. Enhanced noscapine delivery using uPAR-targeted optical-MR imaging trackable nanoparticles for prostate cancer therapy. Journal of controlled release : official journal of the Controlled Release Society. 2011;149:314-22. doi:10.1016/j.jconrel.2010.10.030.
202. Liu D, Overbey D, Watkinson L, Giblin MF. Synthesis and characterization of an (111) In-labeled peptide for the in vivo localization of human cancers expressing the urokinase-type plasminogen activator receptor (uPAR). Bioconjugate chemistry. 2009;20:888-94. doi:10.1021/bc800433y.
203. Xi L, Zhou G, Gao N, Yang L, Gonzalo DA, Hughes SJ, et al. Photoacoustic and fluorescence image-guided surgery using a multifunctional targeted nanoprobe. Annals of surgical oncology. 2014;21:1602-9. doi:10.1245/s10434-014-3541-9.
204. Lee GY, Qian WP, Wang L, Wang YA, Staley CA, Satpathy M, et al. Theranostic nanoparticles with controlled release of gemcitabine for targeted therapy and MRI of pancreatic cancer. ACS nano. 2013;7:2078-89. doi:10.1021/nn3043463.
205. Yang L, Sajja HK, Cao Z, Qian W, Bender L, Marcus AI, et al. uPAR-targeted optical imaging contrasts as theranostic agents for tumor margin detection. Theranostics. 2013;4:106-18. doi:10.7150/thno.7409.
206. Lwin TM, Hoffman RM, Bouvet M. The development of fluorescence guided surgery for pancreatic cancer: from bench to clinic. Expert review of anticancer therapy. 2018;18:651-62. doi:10.1080/14737140.2018.1477593.
207. Goodson RJ, Doyle MV, Kaufman SE, Rosenberg S. High-affinity urokinase receptor antagonists identified with bacteriophage peptide display. Proceedings of the National Academy of Sciences of the United States of America. 1994;91:7129-33. doi:10.1073/pnas.91.15.7129.
208. Ploug M, Østergaard S, Gårdsvoll H, Kovalski K, Holst-Hansen C, Holm A, et al. Peptide-derived antagonists of the urokinase receptor. affinity maturation by combinatorial chemistry, identification of functional epitopes, and inhibitory effect on cancer cell intravasation. Biochemistry. 2001;40:12157-68. doi:10.1021/bi010662g.
209. Zhang X, Tian YE, Sun F, Feng H, Yang C, Gong X, et al. Imaging of human pancreatic cancer xenografts by single-photon emission computed tomography with (99m)Tc-Hynic-PEG-AE105. Oncol Lett. 2015;10:2253-8. doi:10.3892/ol.2015.3504.

210. Juhl K, Christensen A, Persson M, Ploug M, Kjaer A. Peptide-Based Optical uPAR Imaging for Surgery: In Vivo Testing of ICG-Glu-Glu-AE105. PloS one. 2016;11:e0147428. doi:10.1371/journal.pone.0147428.
211. Christensen A, Juhl K, Persson M, Charabi BW, Mortensen J, Kiss K, et al. uPAR-targeted optical near-infrared (NIR) fluorescence imaging and PET for image-guided surgery in head and neck cancer: proof-of-concept in orthotopic xenograft model. Oncotarget. 2017;8:15407-19. doi:10.18632/oncotarget.14282.
212. Kurbegovic S, Juhl K, Chen H, Qu C, Ding B, Leth JM, et al. Molecular Targeted NIR-II Probe for Image-Guided Brain Tumor Surgery. Bioconjugate chemistry. 2018;29:3833-40. doi:10.1021/acs.bioconjchem.8b00669.
213. Juhl K, Christensen A, Rubek N, Karnov KKS, von Buchwald C, Kjaer A. Improved surgical resection of metastatic pancreatic cancer using uPAR targeted in vivo fluorescent guidance: comparison with traditional white light surgery. Oncotarget. 2019;10:6308-16. doi:10.18632/oncotarget.27220.
214. Persson M, El Ali HH, Binderup T, Pfeifer A, Madsen J, Rasmussen P, et al. Dosimetry of 64Cu-DOTA-AE105, a PET tracer for uPAR imaging. Nuclear medicine and biology. 2014;41:290-5. doi:10.1016/j.nucmedbio.2013.12.007.
215. Persson M, Hosseini M, Madsen J, Jørgensen TJ, Jensen KJ, Kjaer A, et al. Improved PET imaging of uPAR expression using new (64)Cu-labeled cross-bridged peptide ligands: comparative in vitro and in vivo studies. Theranostics. 2013;3:618-32. doi:10.7150/thno.6810.
216. Persson M, Nedergaard MK, Brandt-Larsen M, Skovgaard D, Jørgensen JT, Michaelsen SR, et al. Urokinase-Type Plasminogen Activator Receptor as a Potential PET Biomarker in Glioblastoma. Journal of nuclear medicine : official publication, Society of Nuclear Medicine. 2016;57:272-8. doi:10.2967/jnumed.115.161703.
217. Li ZB, Niu G, Wang H, He L, Yang L, Ploug M, et al. Imaging of urokinase-type plasminogen activator receptor expression using a 64Cu-labeled linear peptide antagonist by microPET. Clinical cancer research : an official journal of the American Association for Cancer Research. 2008;14:4758-66. doi:10.1158/1078-0432.Ccr-07-4434.
218. Persson M, Madsen J, Østergaard S, Jensen MM, Jørgensen JT, Juhl K, et al. Quantitative PET of human urokinase-type plasminogen activator receptor with 64Cu-DOTA-AE105: implications for visualizing cancer invasion. Journal of nuclear medicine : official publication, Society of Nuclear Medicine. 2012;53:138-45. doi:10.2967/jnumed.110.083386.
219. Skovgaard D, Persson M, Kjaer A. Imaging of Prostate Cancer Using Urokinase-Type Plasminogen Activator Receptor PET. PET Clin. 2017;12:243-55. doi:10.1016/j.cpet.2016.12.005.
220. Pedersen SF, Petersen LR, Skovgaard DC, Persson M, Johannesen HH, Brandt-Larsen M, et al. Feasibility of 64Cu-DOTA-AE105 for arterial wall in vivo PET of the urokinase-plasminogen-activator-receptor (uPAR). 2016;57:1632.
221. Schmitt M, Mengele K, Napieralski R, Magdolen V, Reuning U, Gkazepis A, et al. Clinical utility of level-of-evidence-1 disease forecast cancer biomarkers uPA and its inhibitor PAI-1. Expert Rev Mol Diagn. 2010;10:1051-67. doi:10.1586/erm.10.71.
222. Duriseti S, Goetz DH, Hostetter DR, LeBeau AM, Wei Y, Craik CS. Antagonistic anti-urokinase plasminogen activator receptor (uPAR) antibodies significantly inhibit uPAR-mediated cellular signaling and migration. The Journal of biological chemistry. 2010;285:26878-88. doi:10.1074/jbc.M109.077677.
223. LeBeau AM, Duriseti S, Murphy ST, Pepin F, Hann B, Gray JW, et al. Targeting uPAR with antagonistic recombinant human antibodies in aggressive breast cancer. Cancer Res. 2013;73:2070-81. doi:10.1158/0008-5472.Can-12-3526.

224. LeBeau AM, Sevillano N, King ML, Duriseti S, Murphy ST, Craik CS, et al. Imaging the urokinase plasminongen activator receptor in preclinical breast cancer models of acquired drug resistance. Theranostics. 2014;4:267-79. doi:10.7150/thno.7323.
225. Bauer TW, Liu W, Fan F, Camp ER, Yang A, Somcio RJ, et al. Targeting of urokinase plasminogen activator receptor in human pancreatic carcinoma cells inhibits c-Met- and insulin-like growth factor-I receptor-mediated migration and invasion and orthotopic tumor growth in mice. Cancer Res. 2005;65:7775-81. doi:10.1158/0008-5472.Can-05-0946.
226. Rabbani SA, Ateeq B, Arakelian A, Valentino ML, Shaw DE, Dauffenbach LM, et al. An anti-urokinase plasminogen activator receptor antibody (ATN-658) blocks prostate cancer invasion, migration, growth, and experimental skeletal metastasis in vitro and in vivo. Neoplasia. 2010;12:778-88. doi:10.1593/neo.10296.
227. Mahmood N, Arakelian A, Khan HA, Tanvir I, Mazar AP, Rabbani SA. uPAR antibody (huATN-658) and Zometa reduce breast cancer growth and skeletal lesions. Bone Res. 2020;8:18. doi:10.1038/s41413-020-0094-3.
228. Boonstra MC, Van Driel P, Keereweer S, Prevoo H, Stammes MA, Baart VM, et al. Preclinical uPAR-targeted multimodal imaging of locoregional oral cancer. Oral oncology. 2017;66:1-8. doi:10.1016/j.oraloncology.2016.12.026.
229. Boonstra MC, van Driel PB, van Willigen DM, Stammes MA, Prevoo HA, Tummers QR, et al. uPAR-targeted multimodal tracer for pre- and intraoperative imaging in cancer surgery. Oncotarget. 2015;6:14260-73. doi:10.18632/oncotarget.3680.

Part IV
Development of uPAR targeted tracers

Chapter 5

uPAR directed-imaging of head-and-neck cancer

Baart VM, Boonstra MC, Sier CFM.

Oncotarget 2017; 8(13):20519-20520.

According to two recently published preclinical studies, targeted multimodal imaging via uPAR (urokinase plasminogen activator receptor) could be the next step in achieving more balanced radical resections in head-and-neck cancer surgery [1, 2]. Multimodal imaging, using a single targeting agent conjugated with a radionuclide as well as a near infrared (NIR) fluorescent dye, is able to provide essential information before (radionuclide, PET/SPECT) and during (NIR fluorescence imaging) surgery, allowing sharp delineation between tumor and surrounding tissue. Sharp assessment is especially crucial in head-and-neck cancer surgery, where sparing of healthy tissue can prevent functional loss and improve cosmetic outcome [3]. The expression of uPAR, a key player in tumor cell adhesion, proliferation and migration, in tumor tissue and its absence in normal tissue allows for sub-millimeter delineation of tumor edges and casts it as a robust target for imaging.

Both studies use uPAR recognizing agents with comparable multimodal labels in similar models but differ in the targeting vehicle: a smart peptide (AE105, 1 kDa) versus a monoclonal antibody (ATN-658, 150 kDa) (Figure 1). The nonamer peptide AE105 has been optimized from a 15-mer variant, identified from a random-phage display library. It has a high affinity for the third domain (D3) of uPAR in the uPA-binding cavity [4]. Due to its small size, the imaging timeframes of AE105 are relatively short, generally within several hours [5, 6]. The monoclonal antibody ATN-658 is a mouse IgG antibody (humanized version: huATN-658), exhibiting relatively long serum half-lives (15-20 hours) and showing imaging timeframes up to days [7, 8]. The longer time frame of antibodies are caused by the larger size rendering them well-suited for multimodal clinical applications, where preoperative PET or SPECT imaging and intraoperative NIR fluorescent imaging presumably take place over a couple of days. In the presented study, AE105 was conjugated separately with each label and administered consecutively. ATN-658 was conjugated with a hybrid label and administered once. For hybrid conjugation the compromise has to be made that none of the labels can be fully optimized, whereas administering multiple labels consecutively can result in *in vivo* competition and allergic reactions. The generally observed and size related hepatic clearance of antibodies is disadvantageous for the detection of liver metastasis, but is not relevant for head and neck cancer liver [8]. Next to size, the *in vivo* behavior of imaging agents dependents on other physical characteristics like affinity, lipo- or hydrophilicity and net charge, which are influenced by the conjugated dyes and chelators used for radiolabeling, especially with small peptides.

Both AE105 and ATN-658 have been designed for anti-tumor activity but achieve this differently (Figure 1). AE105 is a competitive inhibitor of uPA binding to uPAR [4]. On the other hand, ATN-658's anti-tumor activity is independent of the uPA-uPAR interaction and is attributed to its antagonistic effects on integrin-uPAR interactions

possibly leading to disruption of the uPAR signalosome [7]. Since AE105 is incapable of displacing formed uPA-uPAR complexes, it is unable to target occupied uPAR [4]. Consequently, for imaging applications the signal intensity of tumors targeted with AE105 constructs will additionally depend on the degree of uPAR saturation by uPA. ATN-658 binding is not affected by uPAR-occupancy with uPA, possibly leading to a stronger signal and perhaps more relevant signal.

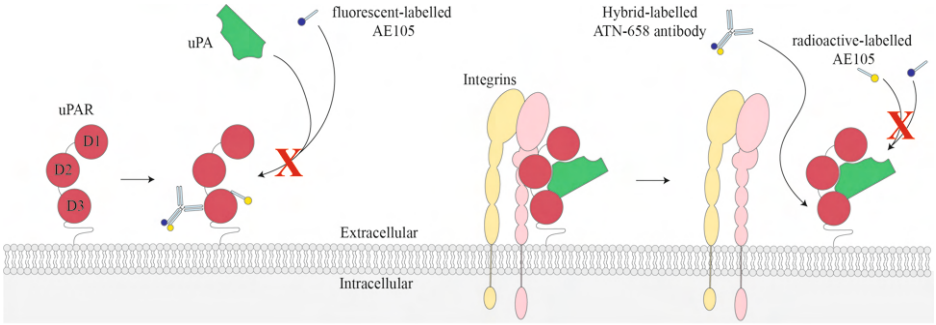

Figure 1. Differences between ATN-658 and AE105 uPAR-targeting strategies. D1, domain one; D2, domain two; D3, domain three; uPA, urokinase plasminogen activator; uPAR urokinase plasminogen activator receptor.

Given that AE105 and ATN-658 are different targeting agents, their production and clinical translation diverge significantly. Antibodies are generally produced in mammalian cells, while peptides are synthesized using non-biological systems, leading to favorable safety profiles and lower costs. However, antibodies are known to possess superior binding characteristics as they exhibit high specificity and long half-life times, are stable and show sufficient tumor penetration. Comparison of both concepts is difficult in animal models. Although ATN658 and AE105 both show encouraging results, the real value of uPAR targeted multimodal imaging will come from the first clinical trials and associated follow-up studies, that are expected to be performed within the next few years. The first phase 1 trials have recently been published for AE105 [4,5] and therapeutic trials are expected to begin for the humanized version of ATN-658 in early 2018. Only then will we know whether patients really benefit from enhanced imaging techniques, either by improved quality of life or increased survival. Until then, basic science and preclinical research should further widen our understanding of uPAR targeting and explore the possibilities for clinical applications. Possibly, targeting agents with different characteristics might be needed in the clinic: peptides may be more amenable as single labelled agents in acute situations for direct imaging, whereas antibodies may be useful for more elective applications like oncologic surgery, where both pre-operative imaging as well as intraoperative guidance is desired.

References

1. Christensen A, Juhl K, Persson M, Charabi BW, Mortensen J, Kiss K, et al. uPAR-targeted optical near-infrared (NIR) fluorescence imaging and PET for image-guided surgery in head and neck cancer: proof-of-concept in orthotopic xenograft model. Oncotarget. 2016. doi:10.18632/oncotarget.14282.
2. Boonstra MC, van Driel PB, Keereweer S, Prevoo HA, Stammes MA, Baart VM, et al. Preclinical uPAR-targeted multimodal imaging of locoregional oral cancer. Oral Oncology. 2017;66.
3. Tschiesner U, Sabariego C, Linseisen E, Becker S, Stier-Jarmer M, Cieza A, et al. Priorities of head and neck cancer patients: a patient survey based on the brief ICF core set for HNC. Eur Arch Otorhinolaryngol. 2013;270:3133-42. doi:10.1007/s00405-013-2446-8.
4. Ploug M, Ostergaard S, Gardsvoll H, Kovalski K, Holst-Hansen C, Holm A, et al. Peptide-derived antagonists of the urokinase receptor. affinity maturation by combinatorial chemistry, identification of functional epitopes, and inhibitory effect on cancer cell intravasation. Biochemistry. 2001;40:12157-68.
5. Persson M, Skovgaard D, Brandt-Larsen M, Christensen C, Madsen J, Nielsen CH, et al. First-in-human uPAR PET: Imaging of Cancer Aggressiveness. Theranostics. 2015;5:1303-16. doi:10.7150/thno.12956 [doi];thnov05p1303 [pii].
6. Skovgaard D, Persson M, Brandt-Larsen M, Christensen C, Madsen J, Klausen TL, et al. Safety, dosimetry and tumor detection ability of 68Ga-NOTA-AE105 - a novel radioligand for uPAR PET imaging: first-in-humans study. J Nucl Med. 2016. doi:10.2967/jnumed.116.178970.
7. Xu X, Cai Y, Wei Y, Donate F, Juarez J, Parry G, et al. Identification of a new epitope in uPAR as a target for the cancer therapeutic monoclonal antibody ATN-658, a structural homolog of the uPAR binding integrin CD11b (alphaM). PloS one. 2014;9:e85349. doi:10.1371/journal.pone.0085349.
8. Boonstra MC, Van Driel PB, Van Willigen DM, Stammes MA, Prevoo HA, Tummers QR, et al. uPAR-targeted multimodal tracer for pre- and intraoperative imaging in cancer surgery. Oncotarget. 2015;6:14260-73. doi:3680 [pii];10.18632/oncotarget.3680 [doi].

Chapter 6

A multimodal molecular imaging approach targeting uPAR for the diagnosis, resection, and surveillance of urothelial cell carcinoma

---

Baart VM, van der Horst G, Deken MM, Bhairosingh SS, Schomann T, Sier VQ, van der Mark M, Iamele L, de Jonge H, Resnati M, Mazar AP, Pelger RCM, van der Pluijm G, Kuppen PJK, Vahrmeijer AL, Sier CFM.

Eur J Cancer 2021; 146:11-20.

Abstract

With a 5-year recurrence rate of 30-78%, urothelial cell carcinoma (UCC) rates amongst the highest of all solid malignancies. Consequently, after transurethral resection patients are subjugated to life-long endoscopic surveillance. A multimodal near-infrared (NIR) fluorescence based imaging strategy can improve diagnosis, resection, and surveillance, hence increasing quality of life.

Methods & Results: Per immunohistochemistry, UCCs show prominent uPAR expression at the tumor-stroma interface and EpCAM on epithelial cells. uPAR and EpCAM are expressed by 6/7 and 4/7 UCC cell lines, respectively. *In vitro,* MNPR-101-IRDye800CW has a picomolar affinity for domain 2-3 of uPAR. *In vivo* fluorescence imaging with MNPR-101-IRDye800CW, specifically delineates both subcutaneous and orthotopic human UM-UC-3luc2 tumors with TBRs reaching as high as 6.8, differing significantly from the isotype controls Infliximab-IRDye800CW and Rituximab-IRDye800CW ($p < 0.0001$). Photoacoustic 3D in depth imaging confirms the homogenous distribution of MNPR-101-IRDye800CW through the tumor.

Conclusion: MNPR-101-IRDye800CW is suitable for multimodal imaging of UCC, awaiting clinical translation.

Introduction

Despite advances in detection, treatment, and surveillance of urothelial cell carcinoma (UCC) there has been no major improvement in overall prognosis over the past 30 years, with nearly 200,000 patients still succumbing annually [1, 2]. Clinically, UCC represents two sequential entities: non-muscle invasive bladder cancer (NMIBC), where malignant cells are constrained to the epithelial layer, and muscle-invasive bladder cancer (MIBC) wherein the tumor invades surrounding subepithelial tissue [3]. The majority of UCC cases (75-85%) are NMIBC and are marked by a high 5-year recurrence rate of 30-78% and 7-40% chance of progression to MIBC disease after transurethral resection (TUR). Therefore, NMIBC requires intensive surveillance via cystoscopy [4, 5]. Once UCC progresses, definitive therapy, defined as radical cystectomy with or without (neo) adjuvant therapy, is indicated [3]. Hereof, 6.3% show involved margins with significantly reduced recurrence-free and cancer specific survival [6]. Consequentially, UCC causes a high burden of disease, where patients could benefit from improved TUR and tumor free resection margins.

Real-time intraoperative guidance with near-infrared (NIR) fluorescence tracers has the potential to function as an extra sense, not only informing surgeons about tumor localization during resection, but also about the degree of disease-aggressiveness [7]. Fundamental for successful imaging is the identification of appropriate cancer-specific targets [8]. Ideally, a single target overexpressed in all patients (across multiple tumor types) is identified. Currently no such target exists. Epithelial cell adhesion molecule (EpCAM) is one of the most promising pan-tumor targets, found to be over-expressed in most solid tumor types and is clinically being evaluated in NIR imaging studies (NL7363). UCC's, however, do not universally express EpCAM; 56% of UCCs are EpCAM negative and the overexpression rate compared to healthy tissue is 27% [9]. Hence, EpCAM-based tracers will not be applicable for all UCC patients, requiring the search for alternative targets with complementary expression patterns.

An alternative candidate for UCC targeting is the urokinase plasminogen activator receptor (uPAR). uPAR narrowly orchestrates various tumor specific processes, including cell differentiation, proliferation, and migration, but is barely present in healthy tissues. Immunohistochemical localization of uPAR on 186 human UCC specimen revealed expression of this receptor in 96% of the tumors, particularly at the invasive front, irrespective of grade and stage, while being completely absent in normal bladder [10]. Such a pattern is ideal for molecular imaging [11]. Recent preclinical studies confirmed the applicability of mouse anti-uPAR antibodies conjugated to the fluorophore ZW800-1 for optical imaging of oral and colorectal

cancer [12, 13]. However, the use of an alternative fluorophore, IRDye800CW (800F), offers the possibility of imaging via NIR light, as well as via photoacoustic (PA) imaging [8, 14]. PA imaging utilizes the contrast of optical imaging with the spatial resolution of ultrasound, enabling a tissue penetration depth of several centimeters [14, 15]. In the clinic, a bimodal tracer, capable of both optical NIR- and PA-imaging, can be utilized during non-invasive (trans-abdominal) surveillance, TURs and radical cystectomies.

In this study we developed a humanized NIR molecular imaging tracer for simultaneous fluorescence and PA-imaging to facilitate resection of human UCC in a clinically relevant mouse model.

Materials and methods

Human samples and immunohistochemistry

Formalin-fixed, paraffin-embedded tissue blocks of fourteen patients who underwent cystectomy or TUR for UCC were collected from the Department of Pathology of the Leiden University Medical Centre (LUMC). Sections of 4 μm were stained according to standard immunohistochemical methods as described in Appendix A. Sections were digitalized using the Panoramic Digital Slide Scanner, viewed with Caseviewer 2.3 (both 3D Histech, Hungary) and scored for percentage of positive cells and staining intensity with the total-immunostaining score (TIS). TIS > 4 was defined as overexpression [16]. The LUMC ethics review board approved the study protocol (B20.030). Samples and data were non-identifiable and used in accordance with the 1964 Helsinki declaration.

In silico analysis of gene expression in a TCGA dataset

The freely available raw TCGA (The Cancer Genome Atlas) transcriptome database, consisting of bladder urothelial carcinoma samples (http://www.cbioportal.org/study?id=blca_tcga) was used to determine the correlation between the gene expression of EpCAM and uPAR/PLAUR in a mostly non-chemo treated MIBC cohort of 408 patients.

Cells

Suppliers and culture conditions of the UCC cell lines UM-UC-3, J82, T24, RT112, RT4, HT-1197 and HT-1376, and the transfected cell lines HEK EV (empty vector), HEK uPAR wildtype (WT) and the cleaved isoform HEK uPAR D2-3 are described in Appendix B. Further characterization of the UCC cells according to patient

characteristics and molecular profile can be found in Appendix C.1-2. Cell lines were routinely tested for mycoplasma.

Antibodies

ATN658 is an extensively validated mouse monoclonal antibody of the IgG1 κ isotype targeting domain 3 of uPAR [12, 13]. MNPR-101 (formerly known as huATN658) is the humanized variant. Both antibodies are not cross-reactive with mouse uPAR [17]. Rituximab and Infliximab (Remicade®) are clinical grade chimeric human-mouse antibodies, consisting of the glycosylated human IgG1 κ isotype constant domain, targeting CD20 and tumor necrosis factor-α (TNFα), respectively.

Surface Plasmon Resonance

Binding of ATN658 and MNPR-101(-800F) to recombinant human uPAR (10925-H08H, Sinobiological, China) was measured by surface plasmon resonance on a Biacore T200 instrument (GE Healthcare, USA) at 25°C. uPAR was immobilized on a NiHC 1500M chip (Xantec, Germany) and the interaction was measured at 2.5, 5, 10, 20, and 40 nM with four separate single-cycle kinetic experiments.

Cell-based assays

Quantitative flow cytometry using Qifi-kit (Agilent Technologies, USA) was performed according to suppliers instructions. Confluent chamber slides were incubated with primary antibodies, stained with FITC-labelled secondary antibodies and DAPI, and imaged with a DM500 B microscope (Leica Microsystems, Germany). Binding of serially diluted fluorescence antibodies to cell-based plate assays were determined using the Odyssey CLx Imaging System (LI-COR Biosciences, USA). For detailed descriptions of these assays see the Appendix D.

Animal Models

The Dutch Central Commission for Animal Experimentation approved all animal experiments (AVD1160020172925). Experiments were performed in accordance with the code of practice 'Dierproeven In Het Kankeronderzoek". Each experimental group consisted of three-to-four 6 - 10-week-old female BALB/c-Nude mice (CAnN. Cg-*Foxn1*^{nu}/Crl, Charles River laboratories, France). Subcutaneous tumor models were induced by subcutaneous injection of 0.5 x 10^6 UM-UC-3luc2 cells (Appendix D). For the preclinical orthotopic xenograft model, luciferase-expressing UM-U3-luc2 cells were inoculated into the bladder as previously described [18].

In vivo NIRF imaging
Anesthetized (1.5 – 4% isoflurane; Teva Pharmachemie BV, The Netherlands) mice were imaged with The Pearl Trilogy Small Animal Imaging System (LI-COR Biosciences, USA) and Artemis (Quest Medical Imaging, The Netherlands) 1 – 7 days after intravenous tracer injection. After sacrifice, tumors were resected, stained and scanned for 800 nm fluorescence using the Odyssey CLx Imaging System (LI-COR Biosciences, USA).

Photoacoustic imaging
Anesthetized mice were immobilized on the preheated imaging table of the Vevo 3100 Imaging System (FUJIFILM VisualSonics, Canada) and covered with ultrasound gel. The Vevo 3100 Imaging System was equipped with a Vevo LAZR-X cart, a Vevo LAZRTight Enclosure, and a Vevo Imaging Station. For ultrasound and PA imaging, the MX550D transducer (25-55 MHz; Axial Resolution: 40 μm; excitation 780 nm) was used.

Image analyses and statistics
Tumor-to-background ratios (TBRs) were measured by drawing regions of interest around the tumor and the surrounding tissue, and dividing the mean fluorescence intensities (MFIs). In the orthotopic model, either fat or the cecum were used as background to determine tumor-to-organ ratios (TOR). For respective software see Appendix D. Means, reported with standard deviations, were compared by two-way repeated measurement ANOVA with GraphPad Prism 8 (GraphPad Software, USA). Correlations are calculated according to Pearson and indicated by R^2. Significance levels are < 0.05.

Results

EpCAM and uPAR are complementary targets for UCC
The IHC expression profiles of EpCAM and uPAR in UCC specimens were compared, as shown in Figure 1A. Staining for EpCAM, when present, was homogenous throughout the tumor, resulting in a moderate to intense membrane staining of malignant cells. However, one-third of cases had no EpCAM expression. uPAR staining was most prominent at the tumor-stroma interface localizing towards cancer cells and tumor-associated stromal cells, including macrophages (CD68 positive) and cancer associated fibroblasts (αSMA positive) (Figure 1B). Staining was moderate to strong in intensity at the cell membranes. Approximately two-thirds of tumor over-expressed uPAR. EpCAM expression did not correlate with either epithelial uPAR

(R^2 = 0.20, p = 0.30) or stromal uPAR (R^2 = 0.21, p = 0.30), see also Appendix E. All in all, 79% of patients overexpressed one or both targets. Expression patterns matched those seen in literature (Appendix F). In addition, mRNA expression levels of PLAUR and EpCAM on UCC tumor cells was independent of each other and confirmed their complementary nature (p = 0.0059, Appendix G).

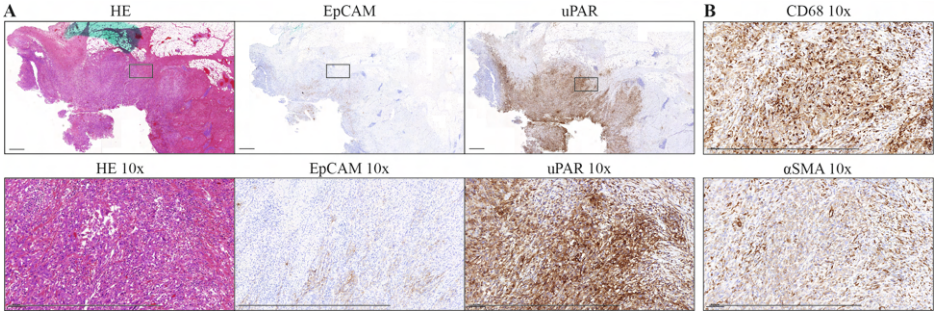

Figure 1. UCC expression of uPAR and EpCAM. (A) Consecutive sections of a UCC case showing absent to weak EpCAM immunohistochemistry staining at the tumor borders and intense staining for uPAR in both tumor cells and tumor-associated stroma. (B) uPAR positive stroma cells are, amongst others, CD68 positive macrophages and αSMA positive cancer-associated fibroblasts. Black line = 1000 µm. Black box = insert. EpCAM, epithelial cell adhesion molecule; HE, hematoxylin & eosin; UCC, urothelial cell carcinoma; uPAR, urokinase plasminogen activator receptor; αSMA, α-smooth muscle actin.

Using a panel of UCC cell lines, spanning the clinical range from NMIBC to MIBC, we assessed the number of copies for uPAR and EpCAM per cell. Six out of seven cell lines expressed uPAR, ranging from 7,000 – 84,000 copies per cell (Table 1). For EpCAM 4/7 cell lines were positive, ranging from 60,000 - 226,000. In summary, each cell line expressed either uPAR, EpCAM or both, with T24 as possibly problematic cell line, depending on only 7,000 uPAR copies and none for EpCAM.

Table 1. Number of uPAR and EpCAM receptors per cell on UCC cell lines.

Cell line	uPAR	EpCAM
UM-UC-3luc2	20,000	n.d.
J82	84,000	n.d.
T24	7,000	n.d.
RT112	25,000	139,000
RT4	n.d.	226,000
HT-1197	17,000	194,000
HT-1376	7,000	64,000

EpCAM, epithelial cell adhesion molecular; n.d., not detectable, below detection limit; UCC, urothelial cell carcinoma; uPAR, urokinase plasminogen activator receptor.

MNPR-101 targets domain 2-3 of uPAR with nanomolar affinities

Ideally, tracers for molecular imaging have a high affinity for all tumor-associated isoforms of the target. Humanization of ATN658 into MNPR-101 did not alter the affinity for recombinant uPAR with a K_D for ATN658 of 0.5 x 10^{-9} M (K_a 1.6 x 10^5 M^{-s} s^{-1}; K_d 7.0 x 10^{-5} s^{-1}) and MNPR-101 having a K_D of 0.2 x 10^{-9} M (K_a 3.6 x 10^5 M^{-1} s^{-1}; K_d 7.8 x 10^{-5} s^{-1}). MNPR-101 binding was specific for the cell membranes of uPAR WT and D2-3 HEK cells but not HEK EV cells (Figure 2A-B).

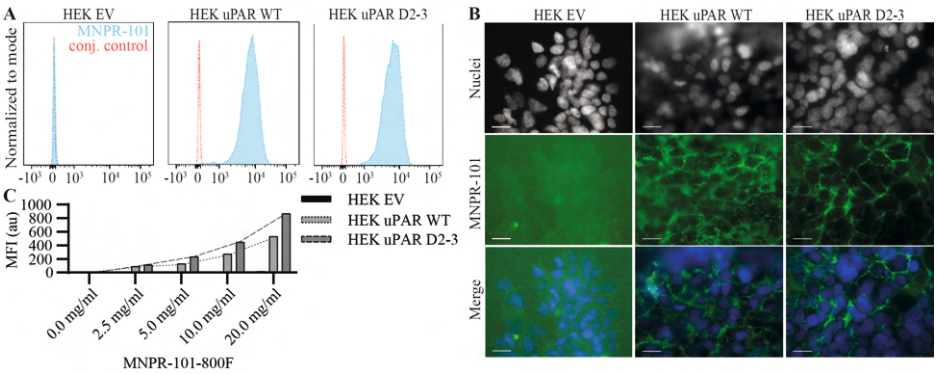

Figure 2. In vitro validation of MNPR-101. (A) MNPR-101 binding per flow cytometry to EV, WT and cleaved D2-3 transfected HEK cell lines. (B) Upon immunofluorescence microscopy binding could be seen to localize towards the cell membranes of WT and cleaved D2-3 transfected HEK cells but not EV transfected HEK cells. Green is MNPR-101 signal and grey/blue is a nuclear staining. Bar = 50 µm. (C) After conjugation to a near-infrared fluorescence dye, MNPR-101-800F demonstrated a concentration-dependent 800 nm signal increase on uPAR transfected HEK cells as measured using the Odyssey CLx. Au, arbitrary unit; Conj, conjugate; D2-3, domain 2-3; EV, empty vector; HEK, human embryonic kidney; MFI, mean fluorescence intensity; uPAR, urokinase plasminogen activator receptor; WT, wildtype.

MNPR-101 was conjugated with 800F at a 1.1-1.5 labelling-ratio, and was checked for unconjugated dye, as confirmed by respectively MALDI-TOF analysis and SDS-PAGE scanning. Conjugation did not substantially affect the affinity of MNPR-101-800F for uPAR (K_D 0.3 x 10^{-9} M; K_a 6.1 x 10^5 M^{-1} s^{-1}; K_d 1.5 x 10^{-5} s^{-1}). A dose-dependent increase of 800 nm signal on cell-based plated assays with HEK uPAR WT and uPAR D2-3 cells, and constant low signal with HEK EV cells confirmed binding capacity (Figure 2C).

NIR Image-guided surgery of UCC with MNPR-101-800F

Fluorescence tracers can accumulate in tumors due to nonspecific effects such as the enhanced-permeability and retention effect or blood pooling. In order to account for this effect, two non-cancer related humanized monoclonal antibodies were

used as non-specific controls. *In vitro,* MNPR-101 but not Infliximab (anti-TNFα) or Rituximab (anti-CD20) bound UM-UC-3luc2 cells (Figure 3A).

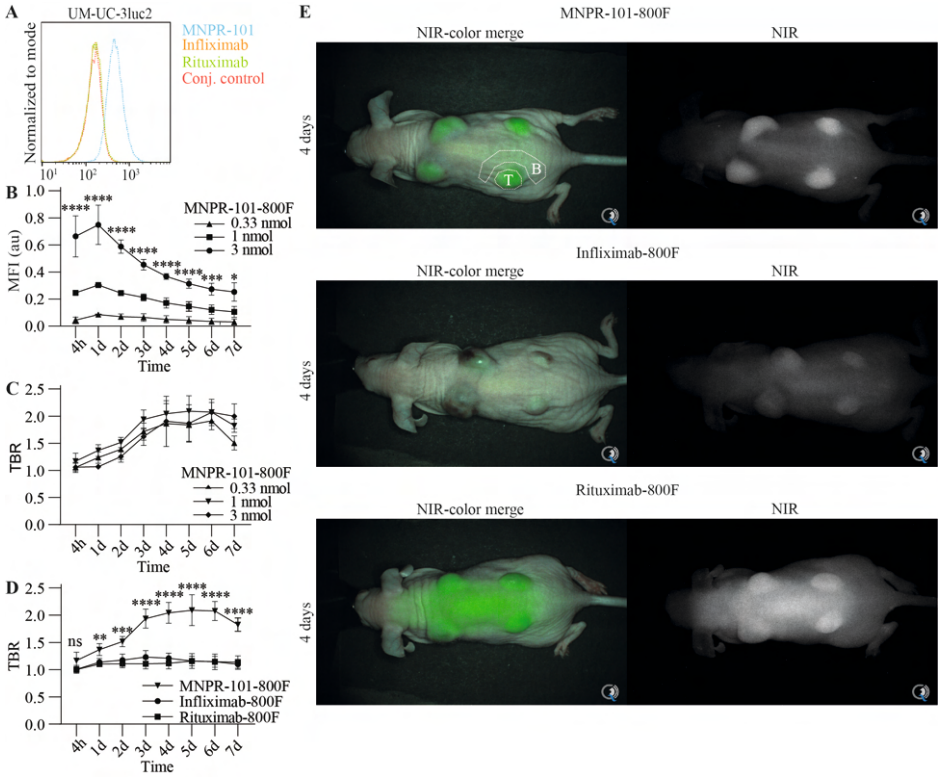

Figure 3. NIR fluorescence imaging with MNPR-101-800F. (A) Flow cytometry of MNPR-101, Infliximab and Rituximab of UCC UM-UC-3luc2 cells. (B) In vivo tumor MFIs determined using the Pearl imaging system and (C) TBRs determined by the Artemis imaging system after intravenous injection of 0.33, 1 and 3 nmol MNPR-101-800F in subcutaneous UM-UC-3luc2 tumor-bearing mice. D) In vivo TBRs determined by the Artemis imaging system after intravenous injection of 1 nmol MNPR-101-800F, Infliximab-800F or Rituximab-800F. (E) NIR-images of subcutaneous UM-UC-3luc2-bearing mice four days after administration of MNPR-101-800F, Infliximab-800F and Rituximab-800F. NIR images were taken with the clinical Artemis NIR-camera. A representative tumor (T) and background (B) ROI is shown. Au, arbitrary unit; Conj, conjugate; d, day; h, hour; MFI, mean fluorescence intensity; NIR, near-infrared; nmol, nanomole; TBR, tumor-to-background ratio.

The *in vivo* tumor recognition potential was subsequently assessed in mice bearing UM-UC-3luc2 subcutaneous tumors. Total mouse tumor burden did not differ significantly between experimental groups ($p = 0.6581$). After intravenous injection of 0.33 nmol, 1 nmol and 3 nmol MNPR-101-800F, mice were imaged daily with the preclinical Pearl and clinical Artemis imaging systems. Tumor MFI corresponded

with the injected dose ($p < 0.0001$, Figure 3B). TBRs did not differ significantly between dose groups with sufficient TBRs 3-7 days after imaging (Figure 3C) and a TBR max of 2.9 five days after injection of 1 nmol MNPR-101-800F.

As specificity controls, subcutaneous UM-UC-3luc2-bearing mice were injected intravenously with 1 nmol Infliximab-800F or Rituximab-800F. TBRs differed significantly between MNPR-101-800F and the controls across all time points except for 4 hours post injection ($p < 0.0001$, Figure 3D). In contrast to Infliximab-800F or Rituximab-800F, tumors were readily visualized with the clinical Artemis system starting 3 days after MNPR-101-800F injection (Figure 3D-E).

Intravesical injection of bioluminescent UM-UC-3luc2 cells into the murine bladder represents a preclinical orthotopic UCC model that allows optical imaging of cancer growth in real time [18]. Three weeks post tumor inoculation 1 nmol

MNPR-101-800F and Rituximab-800F were injected intravenously and imaged three days later. Tumors where highly fluorescent after MNPR-101-800F injection matching bioluminescence signal and allowing image-guided resection (Figure 4A, Appendix H). Importantly, *post-mortem* histology, fluorescence scanning and immunohistochemistry confirmed tumor cell specificity of MNPR-101-800F and only non-specific signal with Rituximab-800F (Figure 4B). MNPR-101-800F exhibited an average tumor-to-fat ratio of 2.6 (range: 2.3 – 3.2) and tumor-to-caecum ratios of 5.8 (range: 5.3 – 6.8) (Figure 4C). The tumor-to-fat ratio and tumor-to-caecum ratio for Rituximab-800F were 1.3 and 3.2, respectively. On *post-mortem* biodistribution analysis of MNPR-101-800F, the majority of the fluorescence was seen in the tumor followed by the metabolizing organs (Figure 4D). The CD20 targeting Rituximab-800F preferentially localized towards the liver and kidneys.

Photoacoustic imaging of UCC with MNPR-101-800F

The multi-modal imaging potential of MNPR-101-800F was investigated by PA-imaging. Subcutaneous UM-UC-3luc2 tumor-bearing mice were injected intravenously with 3 nmol MNPR-101-800F and imaged three days post-injection. High intensity signal was evident throughout the tumor and the skin while signal in surrounding structures remained minimal (Figure 5A). Nonspecific signal was noticed in the skin of PBS-injected negative control mice (Figure 5B).

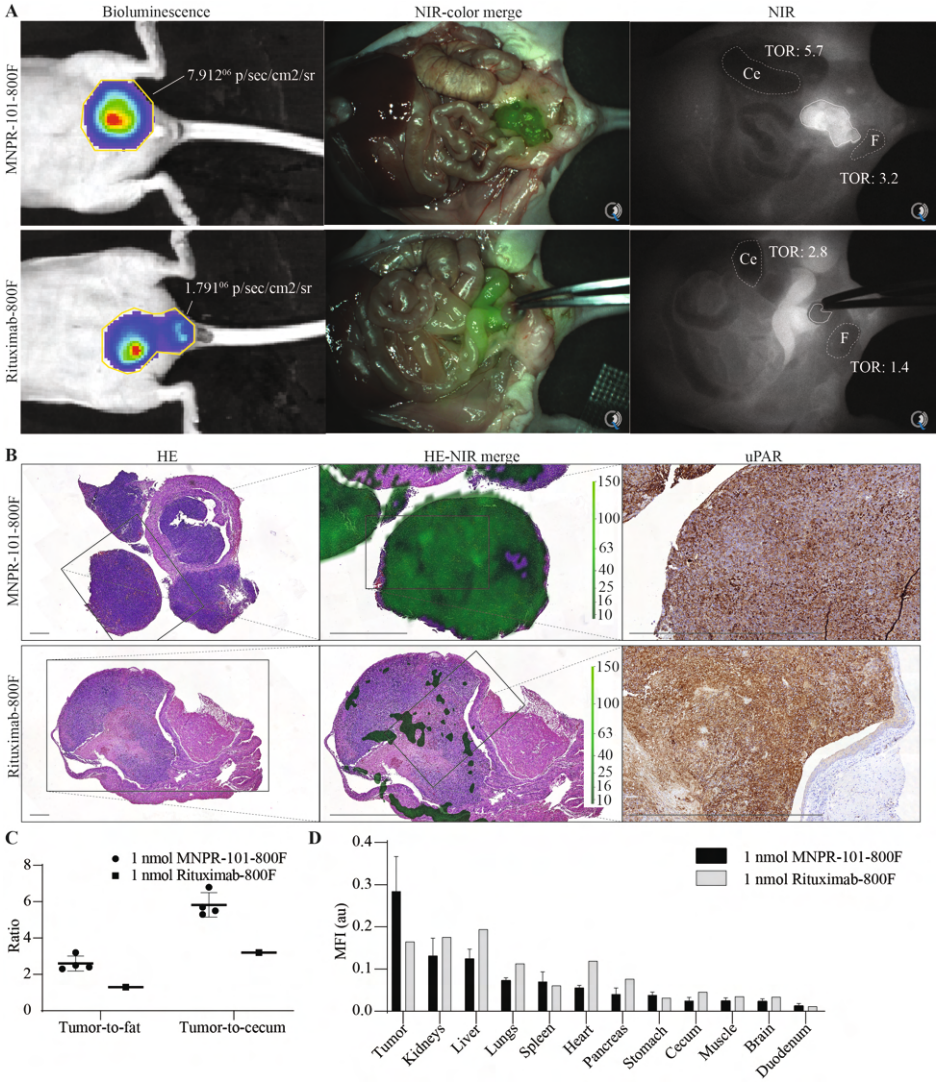

Figure 4. uPAR NIR-guided surgery in a preclinical orthotopic UCC xenograft model. (A) Bioluminescence imaging and NIR image-guided resection with the clinical Artemis NIR camera three days after 1 nmol injection of MNPR-101-800F or Rituximab-800F. (B) Post-mortem histological, fluorescence scanning (Odyssey) and uPAR immunolocalization of resected orthotopic tumors (C) In vivo signal-to-background ratios measured during image-guided resection with the clinical Artemis NIR camera and (D) post-mortem whole-body biodistribution determined using the Pearl. Ce, cecum; F, fat; HE, hematoxylin & eosin, NIR, near-infrared; nmol, nanomole; TOR, tumor-to-organ ratio; UCC, urothelial cell carcinoma; uPAR, urokinase plasminogen activator receptor.

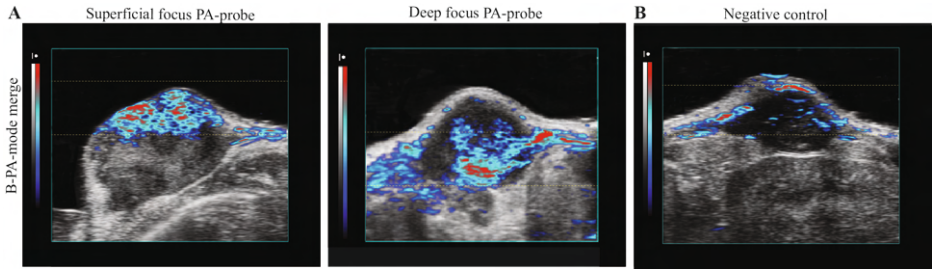

Figure 5. Photoacoustic imaging of subcutaneously implanted UM-UC-3luc2 tumours in vivo. (A) MNPR-101-800F. (B) Negative control. Area between the yellow dotted lines represent the focus area of the photoacoustic probe. B, brightness; PA, photo-acoustic.

Discussion

The recurring nature of UCCs and the tendency to progress are a significant burden for patients and health services [19, 20]. Consequently, every effort should be made to improve therapy. Here we implemented a novel approach that may facilitate and improve UCC detection and resection rates by intraoperative multi-modal guidance utilizing MNPR-101-800F.

The additional value of exogenous contrast agents during cystoscopy has already been demonstrated with 5-aminolevulinic acid (5-ALA) and its fluorescence metabolite protoporphyrin IX (PpIX) [21]. Using 5-ALA, 7-30% more UCCs were detected, residual tumor rate reduced by 20% and cancer-free survival increased. However, the fluorescence properties of PpIX (excitation 375-440 nm, emission 635, 704 nm) are poor regarding penetration depth, tissue absorption and scattering, and tissue autofluorescence and not adapted to most clinically used NIR imaging systems [22]. The favorable imaging characteristics of NIR-fluorophores pave the way for improved real-time NIR fluorescence guided resection of UCC.

To date, no single tracer is suitable for intraoperative guidance of all UCC specimens. As a result, a tracer library should be developed from which a surgeon can select the most suitable tracer [8]. Ideally, these tracers visualize unique characteristics of UCC which distinguishes the tumor from adjacent normal tissue. In case of uPAR and EpCAM, these membrane receptors have complementary expression patterns during the complex multistep process of switching from a sessile to an invasive cancer cell [23, 24]. In addition to uPAR targeting, we show our recently introduced EpCAM-targeting tracer, which is currently being evaluated on patients with gastrointestinal cancer, could also be used for UCC (NL7363) [25]. Other potential combinations encompass EGFR, HER2 and/or matrix-metalloproteases, some of which are currently being investigated in clinical studies with other tumor

types [8]. Release of these membrane proteins into the urine provide a possible surrogate biomarker for their respective tumor expression and provides a simple non-invasive method for tracer selection. While both uPAR and EpCAM are elevated in urine from UCC patients, the correlation with cellular expression has not yet been evaluated [26-29].

Although NIR-imaging has superior resolution, it is less suitable for imaging of lesions deeper than 1 cm [8]. PA, on the other hand, provides molecular contrast of up to 12 cm deep without compromising on the submillimeter spatial resolution. As a result, PA has been utilized for *in vivo* imaging of organelles to organs, and has been incorporated in imaging platforms for transvaginal imaging of ovarian cancer and transrectal imaging of prostate cancer [30-32]. In the case of UCC, improved imaging depth allows the visualization of deeper layers of the bladder, including the muscularis propria and per-vesical fat, informing urologists of possible advanced T-stage disease during cystoscopy and the need of the more aggressive (partial) cystectomy [33, 34].

We investigated whether NIR fluorescence-imaging could be performed in combination with PA, by utilizing a contrast agent with a reasonable extinction coefficient and relatively low quantum yield (for PA-imaging a large non-fluorescence relaxation is desired), such as 800F ($\mathcal{E} = 2.4x10^5$; $\Phi = 0.034$) [14]. In a proof-of-principle study, Tummers *et al.* imaged pancreatic cancer *ex vivo* using both fluorescence and PA-imaging modalities [35]. Similarly, the development of liver metastases *in vivo* was monitored bimodally using a single $\alpha_v\beta_3$ integrin targeting contrast agent, Angiostamp800 [36]. Our results show the feasibility of imaging through superficial structures such as the skin.

uPAR bimodal imaging is not limited to MNPR-101-800F. Its precursor, ATN-658 was previously dual labelled for SPECT and NIR imaging using the hybrid ^{111}In and ZW800-1 label for imaging of locoregional oral and colorectal cancer. While procuring TBRs of 5.0 ± 1.3 and being able to visualize 1-2 millimeter sized lesions, the tracer is less suitable for PA imaging due to ZW800-1 quantum yield ($\mathcal{E} = 2.5x10^5$; $\Phi = 0.150$) [12, 13, 37]. Another option is the uPAR targeting peptide AE105-Glu-Glu-ICG which has successfully identified multiple tumor types in various preclinical models with TBRs up to 3.5 ± 0.2 [38, 39]. Its fluorophore, indocyanine green (ICG) has a similar extinction coefficient and quantum yield as 800F ($\mathcal{E} = 2.7x10^5$; $\Phi = 0.027$) and has been used for previously for PA imaging [14]. Peptides generally clear rapidly from the circulation via the kidneys, which could be a limiting factor for bimodal imaging of UCC [40].

Conclusion

uPAR and EpCAM are complementary targets for NIR imaging of UCC that are indicative of separate tumor differentiation states. MNPR-101-800F targets uPAR and allows for simultaneous NIR and PA guidance. If confirmed in a clinical setting, such assistance can result in a paradigm shift, altering how urologists survey and treat UCC, thus potentially improving patient outcomes.

References

1. Bray F, Ferlay J, Soerjomataram I, Siegel RL, Torre LA, Jemal A. Global cancer statistics 2018: GLOBOCAN estimates of incidence and mortality worldwide for 36 cancers in 185 countries. CA Cancer J Clin. 2018;68:394-424. doi:10.3322/caac.21492.
2. Zehnder P, Studer UE, Skinner EC, Thalmann GN, Miranda G, Roth B, et al. Unaltered oncological outcomes of radical cystectomy with extended lymphadenectomy over three decades. BJU Int. 2013;112:E51-E8. doi:10.1111/bju.12215.
3. Mitra AP, Jordà M, Cote RJ. Pathological possibilities and pitfalls in detecting aggressive bladder cancer. Curr Opin Urol. 2012;22:397-404. doi:10.1097/MOU.0b013e328356ade6.
4. Simon M, Bosset P-O, Rouanne M, Benhamou S, Radulescu C, Molinié V, et al. Multiple recurrences and risk of disease progression in patients with primary low-grade (TaG1) non-muscle-invasive bladder cancer and with low and intermediate EORTC-risk score. PloS one. 2019;14:e0211721-e. doi:10.1371/journal.pone.0211721.
5. Kassouf W, Traboulsi SL, Schmitz-Dräger B, Palou J, Witjes JA, van Rhijn BWG, et al. Follow-up in non-muscle-invasive bladder cancer-International Bladder Cancer Network recommendations. Urol Oncol. 2016;34:460-8. doi:10.1016/j.urolonc.2016.05.028.
6. Novara G, Svatek RS, Karakiewicz PI, Skinner E, Ficarra V, Fradet Y, et al. Soft tissue surgical margin status is a powerful predictor of outcomes after radical cystectomy: a multicenter study of more than 4,400 patients. J Urol. 2010;183:2165-70. doi:10.1016/j.juro.2010.02.021.
7. Persson M, Skovgaard D, Brandt-Larsen M, Christensen C, Madsen J, Nielsen CH, et al. First-in-human uPAR PET: Imaging of Cancer Aggressiveness. Theranostics. 2015;5:1303-16. doi:10.7150/thno.12956.
8. Hernot S, van Manen L, Debie P, Mieog JSD, Vahrmeijer AL. Latest developments in molecular tracers for fluorescence image-guided cancer surgery. The Lancet Oncology. 2019;20:e354-e67. doi:10.1016/s1470-2045(19)30317-1.
9. Spizzo G, Fong D, Wurm M, Ensinger C, Obrist P, Hofer C, et al. EpCAM expression in primary tumour tissues and metastases: an immunohistochemical analysis. Journal of clinical pathology. 2011;64:415-20. doi:10.1136/jcp.2011.090274.
10. Dohn LH, Pappot H, Iversen BR, Illemann M, Hoyer-Hansen G, Christensen IJ, et al. uPAR Expression Pattern in Patients with Urothelial Carcinoma of the Bladder--Possible Clinical Implications. PloS one. 2015;10:e0135824. doi:10.1371/journal.pone.0135824.
11. Boonstra MC, Verspaget HW, Ganesh S, Kubben FJ, Vahrmeijer AL, van de Velde CJ, et al. Clinical applications of the urokinase receptor (uPAR) for cancer patients. Current pharmaceutical design. 2011;17:1890-910. doi:10.2174/138161211796718233.
12. Boonstra MC, van Driel PB, van Willigen DM, Stammes MA, Prevoo HA, Tummers QR, et al. uPAR-targeted multimodal tracer for pre- and intraoperative imaging in cancer surgery. Oncotarget. 2015;6:14260-73. doi:10.18632/oncotarget.3680.
13. Boonstra MC, Van Driel P, Keereweer S, Prevoo H, Stammes MA, Baart VM, et al. Preclinical uPAR-targeted multimodal imaging of locoregional oral cancer. Oral oncology. 2017;66:1-8. doi:10.1016/j.oraloncology.2016.12.026.
14. Weber J, Beard PC, Bohndiek SE. Contrast agents for molecular photoacoustic imaging. Nature methods. 2016;13:639-50. doi:10.1038/nmeth.3929.
15. Vahrmeijer AL, Hutteman M, van der Vorst JR, van de Velde CJ, Frangioni JV. Image-guided cancer surgery using near-infrared fluorescence. Nature reviews Clinical oncology. 2013;10:507-18. doi:10.1038/nrclinonc.2013.123.

16. Baart VM, van Duijn C, van Egmond SL, Dijckmeester WA, Jansen JC, Vahrmeijer AL, et al. EGFR and αvβ6 as Promising Targets for Molecular Imaging of Cutaneous and Mucosal Squamous Cell Carcinoma of the Head and Neck Region. Cancers. 2020;12. doi:10.3390/cancers12061474.
17. Xu X, Cai Y, Wei Y, Donate F, Juarez J, Parry G, et al. Identification of a new epitope in uPAR as a target for the cancer therapeutic monoclonal antibody ATN-658, a structural homolog of the uPAR binding integrin CD11b (alphaM). PloS one. 2014;9:e85349. doi:10.1371/journal.pone.0085349.
18. van der Horst G, van Asten JJ, Figdor A, van den Hoogen C, Cheung H, Bevers RF, et al. Real-time cancer cell tracking by bioluminescence in a preclinical model of human bladder cancer growth and metastasis. European urology. 2011;60:337-43. doi:10.1016/j.eururo.2011.05.005.
19. Leal J, Luengo-Fernandez R, Sullivan R, Witjes JA. Economic Burden of Bladder Cancer Across the European Union. European urology. 2016;69:438-47. doi:10.1016/j.eururo.2015.10.024.
20. Dy GW, Gore JL, Forouzanfar MH, Naghavi M, Fitzmaurice C. Global Burden of Urologic Cancers, 1990-2013. European urology. 2017;71:437-46. doi:10.1016/j.eururo.2016.10.008.
21. Burger M, Grossman HB, Droller M, Schmidbauer J, Hermann G, Drăgoescu O, et al. Photodynamic diagnosis of non-muscle-invasive bladder cancer with hexaminolevulinate cystoscopy: a meta-analysis of detection and recurrence based on raw data. European urology. 2013;64:846-54. doi:10.1016/j.eururo.2013.03.059.
22. Gioux S, Choi HS, Frangioni JV. Image-guided surgery using invisible near-infrared light: fundamentals of clinical translation. Molecular imaging. 2010;9:237-55.
23. Mahmood N, Mihalcioiu C, Rabbani SA. Multifaceted Role of the Urokinase-Type Plasminogen Activator (uPA) and Its Receptor (uPAR): Diagnostic, Prognostic, and Therapeutic Applications. Frontiers in oncology. 2018;8:24. doi:10.3389/fonc.2018.00024.
24. Nini A, Hoffmann MJ, Lampignano R, Grosse Siemer R, van Dalum G, Szarvas T, et al. Evaluation of HER2 expression in urothelial carcinoma cells as a biomarker for circulating tumor cells. Cytometry B Clin Cytom. 2020. doi:10.1002/cyto.b.21877.
25. Boogerd LSF, Boonstra MC, Prevoo H, Handgraaf HJM, Kuppen PJK, van de Velde CJH, et al. Fluorescence-guided tumor detection with a novel anti-EpCAM targeted antibody fragment: Preclinical validation. Surg Oncol. 2019;28:1-8. doi:10.1016/j.suronc.2018.10.004.
26. Bryan RT, Shimwell NJ, Wei W, Devall AJ, Pirrie SJ, James ND, et al. Urinary EpCAM in urothelial bladder cancer patients: characterisation and evaluation of biomarker potential. Br J Cancer. 2014;110:679-85. doi:10.1038/bjc.2013.744.
27. Snell KIE, Ward DG, Gordon NS, Goldsmith JC, Sutton AJ, Patel P, et al. Exploring the roles of urinary HAI-1, EpCAM & EGFR in bladder cancer prognosis & risk stratification. Oncotarget. 2018;9:25244-53. doi:10.18632/oncotarget.25397.
28. Casella R, Shariat SF, Monoski MA, Lerner SP. Urinary levels of urokinase-type plasminogen activator and its receptor in the detection of bladder carcinoma. Cancer. 2002;95:2494-9. doi:10.1002/cncr.10989.
29. Shariat SF, Casella R, Monoski MA, Sulser T, Gasser TC, Lerner SP. The addition of urinary urokinase-type plasminogen activator to urinary nuclear matrix protein 22 and cytology improves the detection of bladder cancer. J Urol. 2003;170:2244-7. doi:10.1097/01.ju.0000090965.71697.37.
30. Wang LV, Hu S. Photoacoustic tomography: in vivo imaging from organelles to organs. Science (New York, NY). 2012;335:1458-62. doi:10.1126/science.1216210.
31. Kumavor PD, Alqasemi U, Tavakoli B, Li H, Yang Y, Sun X, et al. Co-registered pulse-echo/photoacoustic transvaginal probe for real time imaging of ovarian tissue. J Biophotonics. 2013;6:475-84. doi:10.1002/jbio.201200163.

32. Kothapalli SR, Sonn GA, Choe JW, Nikoozadeh A, Bhuyan A, Park KK, et al. Simultaneous transrectal ultrasound and photoacoustic human prostate imaging. Sci Transl Med. 2019;11. doi:10.1126/scitranslmed.aav2169.
33. Kamaya A, Vaithilingam S, Chung BI, Oralkan O, Khuri-Yakub BT. Photoacoustic imaging of the bladder: a pilot study. J Ultrasound Med. 2013;32:1245-50. doi:10.7863/ultra.32.7.1245.
34. Liem EI, de Reijke TM. Can we improve transurethral resection of the bladder tumour for nonmuscle invasive bladder cancer? Curr Opin Urol. 2017;27:149-55. doi:10.1097/mou.0000000000000370.
35. Tummers WS, Miller SE, Teraphongphom NT, Gomez A, Steinberg I, Huland DM, et al. Intraoperative Pancreatic Cancer Detection using Tumor-Specific Multimodality Molecular Imaging. Annals of surgical oncology. 2018;25:1880-8. doi:10.1245/s10434-018-6453-2.
36. Lavaud J, Henry M, Gayet P, Fertin A, Vollaire J, Usson Y, et al. Noninvasive monitoring of liver metastasis development via combined multispectral photoacoustic imaging and fluorescence diffuse optical tomography. Int J Biol Sci. 2020;16:1616-28. doi:10.7150/ijbs.40896.
37. de Valk KS, Handgraaf HJ, Deken MM, Sibinga Mulder BG, Valentijn AR, Terwisscha van Scheltinga AG, et al. A zwitterionic near-infrared fluorophore for real-time ureter identification during laparoscopic abdominopelvic surgery. Nature communications. 2019;10:3118. doi:10.1038/s41467-019-11014-1.
38. Juhl K, Christensen A, Rubek N, Karnov KKS, von Buchwald C, Kjaer A. Improved surgical resection of metastatic pancreatic cancer using uPAR targeted in vivo fluorescent guidance: comparison with traditional white light surgery. Oncotarget. 2019;10:6308-16. doi:10.18632/oncotarget.27220.
39. Juhl K, Christensen A, Persson M, Ploug M, Kjaer A. Peptide-Based Optical uPAR Imaging for Surgery: In Vivo Testing of ICG-Glu-Glu-AE105. PloS one. 2016;11:e0147428. doi:10.1371/journal.pone.0147428.
40. Baart VM, Boonstra MC, Sier CFM. uPAR directed-imaging of head-and-neck cancer. Oncotarget. 2017;8:20519-20. doi:10.18632/oncotarget.16240.

Chapter 7

Side-by-side comparison of uPAR targeting optical imaging agents for image-guided surgery of solid tumors

---

Baart VM, van Manen L, Bhairosingh SS, Vuijk FA, Iamele L, de Jonge H, Scotti C, Resnati M, Cordfunke RA, Kuppen PJK, Mazar AP, Burggraaf J, Vahrmeijer AL, Sier CFM.

Mol Imaging Biol. 2023. 25(1):122-132.

Abstract

Radical resection is paramount for curative oncological surgery. Fluorescence guided surgery (FGS) aids in intraoperative identification of tumor-positive resection margins. This study aims to assess the feasibility of urokinase plasminogen activator receptor (uPAR) targeting antibody fragments for FGS in a direct comparison with their parent IgG in various relevant *in vivo* models.

Methods & Results: Humanized anti-uPAR monoclonal antibody MNPR-101 (uIgG) was proteolytically digested into F(ab')2 and Fab fragments named uFab2 and uFab. Unconjugated and IRDye800CW (F) conjugated uIgG, uFab2 and uFab specifically recognized uPAR in the nanomolar range as determined by surface plasmon resonance and cell assays. Subcutaneous HT-29 human colon tumors were clearly identifiable with tumor-to-background ratios (TBRs) > 2 after 72 hours for uIgG-800F and 24 hours for uFab2-800F and uFab-800F. For the latter two, mean fluorescence intensities (MFIs) dipped below predetermined threshold after 72 hours and 36 hours, respectively. Tumors were easily identified in the pancreatic ductal adenocarcinoma (BxPc-3-luc2), head-and-neck squamous cell carcinoma (OSC-19-luc2-GFP), and peritoneal carcinomatosis (HT29-luc2) orthotopic models with uIgG-800F consistently having the highest MFIs and uFab2-800F and uFab-800F having similar values. In biodistribution studies, kidney and liver fluorescence approached tumor fluorescence after uIgG-800F administration and surpassed tumor fluorescence after uFab2-800F or uFab-800F administration, resulting in interference in the abdominal orthotopic mouse models.

Conclusion: In a side-by-side comparison, FGS with uPAR targeting antibody fragments compared with the parent IgG resulted in earlier tumor visualization at the expense of peak fluorescence intensity.

Introduction

Cancer incidence is on the rise with one in five-to-six people awaiting a cancer diagnosis and one in eight-to-ten people eventually succumbing to the disease [1]. Despite recent advances in treatment, surgical resection remains the corner stone of curative therapy [1, 2]. The primary aim of oncological surgery is to achieve local control by radical resection (i.e. R0, tumor-negative margins), as tumor-positive margins negatively influence disease-free and overall survival [3-5]. As a result, correctly discerning malignant from benign tissue during surgery is fundamental for resection.

Surgeons can utilize intraoperative imaging techniques to aid in this differentiation. A relatively novel technology, fluorescence-guided surgery (FGS), uses advanced camera systems to capture near-infrared (NIR) fluorescence emitted by contrast agents, targeting for example ureters, nerves or tumors. FGS has the advantage that it is real-time, has a high contrast and sensitivity, does not utilize ionizing radiation, and is easy-to-use [6, 7]. For oncological FGS the crux lies in developing fluorescent tracers that specifically target proteins which are present in malignant cells and absent or quiet in surrounding tissue. A promising target for imaging of disease, including various types of cancer, is the urokinase plasminogen activator receptor (uPAR) [8, 9].

uPAR is a three-domain cell membrane bound receptor that plays a pivotal role in growth factor activation and extracellular matrix remodeling, stimulating proliferation, differentiation, and migration of cells. Its presence in cancer correlates with prognostic outcome variables such as metastatic disease and reduced overall- and disease-free survival. Furthermore, immunohistochemical studies have revealed absent to low levels of uPAR expression in healthy homeostatic tissue whereas at the interface between tumor and healthy tissue uPAR is highly overexpressed on both tumor and tumor-associated stromal cells [8-12]. Such a pattern is ideal for imaging and, not surprisingly, a PET tracer is currently undergoing extensive clinical trials in order to image 'cancer aggressiveness' and subsequently aid in tailoring treatment options to disease biology [13].

As uPAR expression is highest at the tumor borders, our group has primarily focused on developing uPAR targeted FGS tracers. We have successfully targeted uPAR for FGS in various *in vivo* human cancer models using a mouse monoclonal antibody and more recently with MNPR-101, a first-in-class humanized monoclonal antibody targeting domain three of uPAR [14-16]. This domain is ideal as recognition is independent of the often simultaneously upregulated uPAR-ligands urokinase and vitronectin, and remains membrane-bound when uPAR is cleaved [9].

The relatively large size of antibodies (≈ 150 kiloDalton (kDa)), however, might limit extravasation and the interaction of their crystallizable fragment (Fc) with the neonatal Fc receptor on endothelial cells results in an extended half-life, decreasing tissue penetration and delaying the optimal imaging window [17, 18]. As a consequence, there is often a delay of four to six days after administration before patients can be imaged with optimal results [19]. Reducing molecular size, the dominant variable in determining extravasation (distribution) and clearance, shortens imaging times and improves tumor penetration [20]. Clinically, these advantages should result in improved tumor fluorescence and contrast at earlier time points resulting in better visualization for surgeons and more rapid surgery, also allowing surgeons to utilize fluorescence in (semi-) acute settings [21]. As a result, shortening the imaging window is often presented as the holy grail of FGS when introducing novel small sized fluorescent tracers. Tumor specificity, tumor-to-background ratio (TBR) and tumor mean fluorescence intensity (MFI), however, are of equal importance. Positron emission tomography (PET) studies have for instance illustrated that antigen-binding fragments (Fab) and F(ab')$_2$ lead to much faster tumor targeting, but also a nearly two to three-fold lower peak uptake compared to the parent antibody [22, 23]. Whether this is also true for FGS remains to be elucidated. The current study aims to determine how uPAR targeting Fab and F(ab')$_2$ compare to their parent full-sized antibody (MNPR-101) in FGS of orthotopic PDAC, HNSSC and peritoneal carcinomatosis CRC models.

Materials and methods

Generation of Fab and F(ab')$_2$ from MNPR-101

MNPR-101, a humanized antibody targeting uPAR, was enzymatically fragmented into Fab and F(ab')$_2$ by respectively GingisKHAN and FabRICATOR kits, following the protocols of the manufacturer (Genovis AB, Lund, Sweden). The full-sized antibody and the generated fragments are further indicated as uIgG, uFab2 and uFab. Tracers (full-sized antibody and fragments) were conjugated with IRDye 800CW-NHS ester (from here on 800F; LI-COR biotechnology, Lincoln, USA) according to the manufacturer and as published before [16]. Digestion and conjugation results were evaluated using SDS-PAGE on pre-casted 4 - 20% gels (Criterion, Bio-Rad laboratories, Veenendaal, the Netherlands). Proteins on gels were stained with Coomassie brilliant blue G-250 (Bio-Rad laboratories, Veenendaal, the Netherlands) and fluorescence of 800F was determined using an Odyssey imager (LI-COR biotechnology, Lincoln, USA). Degrees of labeling were calculated and verified by MALDI-TOF mass spectrometry as described previously [24].

Surface plasmon resonance of antibody fragments

All surface plasmon resonance (SPR) experiments were performed on a Biacore T200 (GE Healthcare Life Sciences, Uppsala, Sweden) using a NiHC1500M sensor chip (Xantec Bioanalytics, Düsseldorf, Germany) as described previously (See ESM for details) [16].

Cells and culture conditions

Culture conditions of human embryonic kidney empty vector (HEK EV), HEK uPAR wildtype (HEK uPAR WT), HEK uPAR D2-D3 isoform (HEK uPAR D2-3), OSC-19-luc2-GFP, BxPC-3-luc2 and HT-29-luc2 cells are described in the ESM file.

Flow cytometry and cell-based plate assays

For flow cytometry cells were incubated in succession with primary antibody (-fragment), secondary anti-human IgG Fab fragment antibody (clone 4A11; ab771, Abcam, Cambridge, UK) and anti-mouse 488 antibody (A21121, Life Technologies, California, USA) using a standard flow cytometry protocol and measured on a LSRII flow cytometer (BD Biosciences, California, USA). Binding of serially diluted 800F labeled antibodies to cells cultured in 96-wells plates were determined using the Odyssey and fluorescence was corrected for cell density with a ToPro-3 iodide nuclear staining (T3605, Invitrogen, California, USA). The CD52-targeting humanized antibody Alemtuzumab coupled to 800F functioned as a conjugate control. For detailed methods see ESM.

In vivo *tumor models*

All *in vivo* experiments were approved by the Dutch Central Commission for Animal Experimentation (AVD1160020172925) and performed in accordance with the code of practice "*Dierproeven In Het Kankeronderzoek*". 6 – 10 week old female BALB/c-Nude mice (CAnN.Cg-*Foxn1nu*/Crl, Charles River Laboratories, Massachusetts, USA) were inoculated with tumor cells and randomized into experimental groups once tumors had reached predetermined sizes by digital caliper or bioluminescence using the IVIS® Spectrum Preclinical In Vivo Imaging System (Spectrum, PerkinElmer, Massachusetts, USA) (for details see ESM). Subcutaneous tumors were induced by subcutaneous injection of 500,000 HT-29 cells. Orthotopic OSC-19-luc2-GFP HNSCC, BxPC-3-luc2 PDAC, and HT-29-luc2 CRC peritoneal carcinomatosis models were induced as previously published [15, 25, 26].

Fluorescence imaging systems

Fluorescence images were acquired using the preclinical Pearl Trilogy Small Animal Imaging System (Pearl; LI-COR biotechnology, Lincoln, USA) and the Artemis clinical

system (Quest Medical Imaging, Middenmeer, the Netherlands). Pearl images were analyzed with Image Studio 5.2 (LI-COR biotechnology, Lincoln, USA). Frames from Artemis recordings, taken with standardized exposure times, were captured with Spectrum Capture Suite 1.4.3 (Quest Medical Imaging, Middenmeer, the Netherlands) and analyzed with Fiji Image-J [27].

Fluorescence imaging
100 μL of fluorescent tracer was administered intravenously at equal number of antigen binding sites, respectively 1 nmol for uIgG-800F and uFab2-800F, and 2 nmol for uFab-800F. Subcutaneous models were imaged at 1, 2, 4, 12, 24, 36, 48, 72, 96, and 120 hours while orthotopic models were imaged at the optimal imaging window after tumor exposure. Optimal time-points were selected based on TBR- and MFI- cut-offs, literature and visual interpretation. Outcome measures included TBR, MFI and Artemis exposure times (see ESM for details).

Post-mortem histological analysis
Tumors were resected with surrounding normal tissue, embedded in paraffin, sectioned, and scanned for 800 nm fluorescence using the Odyssey. After scanning, sections were stained for hematoxylin and eosin and digitalized with the Panoramic Digital slide Scanner and CaseViewer 2.3 (both 3D Histech, Budapest, Hungary). Overlays were created with Adobe Photoshop CC 2018 (Adobe Systems, California, USA).

Image analysis and statistics
TBRs were calculated by dividing the tumor MFI with background MFI measured using the Pearl. For subcutaneous models the background region-of-interest was the area next to the tumor equidistant

from metabolizing organs. For the SSC, PDAC, CRC peritoneal carcinomatosis models the background regions-of-interest were muscle, spleen and peritoneum, respectively. Means were reported with standard deviations and compared using two-way ANOVA with GraphPad Prism 8 (GraphPad Software, California, USA). A p-value < 0.05 was considered statistically significant.

Results

In vitro characterization of uIgG, uFab2 and uFab
MNPR-101 (150-155 kDa) was enzymatically digested and purified resulting in a 100 - 110 kDa uFab2-800F and 50 - 55 kDa uFab (Figure 1A). SPR determined the

K_D of uIgG, uFab2 and uFab for recombinant uPAR to be 2.19 x 10^{-10} ± 2.41 x10^{-11} M, 5.61 x 10^{-10} ± 1.61 x 10^{-11} M and 8.66 x 10^{-10} ± 4.17 x 10^{-10} M, respectively (Table 1, for sensograms see ESM file, suppl. fig. 1). Affinities did not differ significantly from each other (p = 0.59). K_a and K_d values of all tracers can be found in Suppl. Table 1 (see ESM). Flow cytometry confirmed specificity for uPAR by showing a right shift in signal when uIgG, uFab2 and uFab were incubated with HEK uPAR WT cells, HEK uPAR D2-3 cells but not with HEK EV cells (Figure 1B).

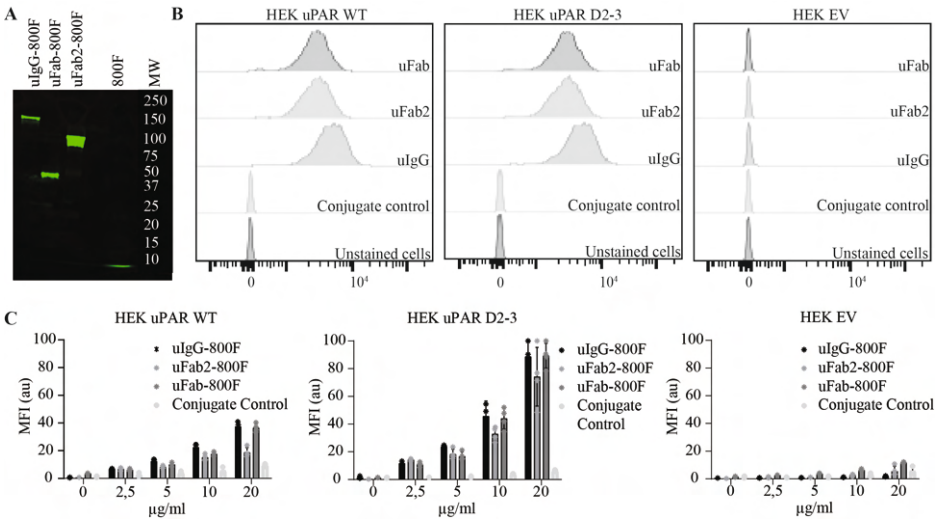

Figure 1. In vitro validation of proteolytic cleavage and fluorescent conjugation of uIgG, uFab2 and uFab. (A) Fluorescent signal on SDS-PAGE gel at respectively 150-155 kDa, 100-110 kDa, 50-55kDa and <10 kDa for uIgG-800F, uFab2-800F, uFab-800F and 800F. The latter represents free IRDye800CW dye, indicating the purity of the conjugations in the other lanes. (B) Flow cytometry histograms demonstrating retained binding of uFab2 and uFab to wildtype uPAR (left) and the D2-D3 isotype (middle) after proteolytic cleavage of uIgG into the antibody fragments. Specificity is furthermore confirmed using empty vector transfected HEK cells (right) and a conjugate control as controls. (C) Cell-based plate-assays showing dose-dependent binding of uIgG-800F, uFab2-800F, uFab-800F and conjugate control to uPAR positive HEK WT cells (left), uPAR D2-3 isotype positive HEK cells (middle) and uPAR negative EV cells (right). Au, arbitrary units; D2-3, domain 2-3; EV, empty vector; HEK, human embryonic kidney; MFI, mean fluorescent intensity; MW, molecular weight. uPAR, urokinase plasminogen activator receptor; WT, wild-type.

The calculated fluorescence labeling with 800F was comparable for uIgG, uFab2 and uFab, and the K_D did not differ significantly after labeling (uIgG vs. uIgG-800F p = 0.47; uFab2 vs. uFab2-800F p = 0.53; uFab vs. uFab-800F p = 0.32; Table 1). Cell-based plate assays showed a dose-dependent increase of the MFI on HEK uPAR WT cells and the HEK uPAR D2-3 cells, but not on HEK EV control cells (Figure 1C).

Table 1. Comparison of uIgG, uFab2 and uFab characteristics.

Tracer	Targeting Domain (Aa uPAR)	MW (kDa)	Valency	K_D (M)	Label	Degree of labelling	K_D after conjugation (M)	Pre/post labelling K_D difference (T-test; *p*)
uIgG	268-275	150 - 155	2	$2.19x10^{-10} \pm 2.41^{-11}$	800F	0.9	$2.56x10^{-10} \pm 4.71^{-11}$	0.47
uFab2	268-275	100 - 110	2	$5.61x10^{-10} \pm 1.61^{-10}$	800F	0.9	$3.84x10^{-10} \pm 1.51^{-10}$	0.53
uFab	268-275	50 - 55	1	$8.66x10^{-10} \pm 4.17^{-10}$	800F	1.2	$1.43x10^{-9} \pm 2.66^{-10}$	0.32

Aa, amino acids; M, molar; MW, molecular weight

Serial imaging of subcutaneous HT-29 tumors with uIgG-800F, uFab2-800F and uFab-800F

Imaging of subcutaneous HT-29 tumors in mice demonstrated tumor specificity and identified the imaging window of 1 nmol uIgG-800F, 1 nmol uFab2-800F and 2 nmol uFab-800F. Tumor accumulation of the full-sized antibody uIgG-800F could be seen as early as 1 hour after administration, but TBRs did not surpass two, an arbitrary cut-off point deemed suitable for NIR imaging, until 72 hours, due to relatively high background fluorescence at earlier time points [28]. The antibody

fragments uFab2-800F and uFab-800F accumulated more rapidly in tumors, with surpassing two after 24 hours (Figure 2A; for serial images see Suppl. Fig. 2, see ESM).

Tumor fluorescence consistently remained above 0.1 arbitrary units (a.u.) with uIgG-800F, but dipped below it after 72 hours with uFab2-800F and 36 hours with Fab-800F (MFI uIgG-800F 120 hours = 0.156 ± 0.016 au; MFI uFab2-800F 72 hours = 0.103 ± 0.017 au; MFI uFab-800F 36 hours = 0.213 ± 0.050 au; Figure 2A). During the imaging windows 72 – 120 hours, 24 – 72 hours, and 24 – 36 hours subcutaneous tumors were clearly identifiable with the clinical Artemis camera after uIgG-800F, uFab2-800F or uFab-800F administration, respectively (Figure 2B). Extra-tumoral uIgG-800F accumulation was not visible. At all time-points kidney fluorescence could be seen through the skin after uFAb2-800F and uFab-800F injection with kidney fluorescence surpassing tumor fluorescence (Figure 2B-C).

Fluorescence imaging of orthotopic tumor models with uIgG-800F, uFab2-800F, and uFab-800F

Using three orthotopic cancer models, BxPC-3 PDAC, OSC-19 tongue SCC and HT-29 CRC peritoneal carcinomatosis, FGS potential of uIgG-800F, uFab2-800F, and uFab-800F was compared. MFI of 1 nmol uIgG-800F, 1 nmol uFab2-800F and 2 nmol uFab-800F in 100 µL solution was 2.08 ± 0.38, 2.47 ± 0.44 and 4.1 ± 0.77 au, respectively. Tumor burdens, measured by bioluminescence, did not differ significantly between tracers at the time of injection ($p = 0.72$ for BxPC-3-luc2;

p = 0.72 for OSC-19-luc2-GFP; p = 0.31 for HT29-luc2; Suppl. Fig. 3, see ESM). Tumors were imaged at 96 hours for uIgG-800F, 48 hours for uFab2-800F and 36 hours for Fab-800F after tracer administration.

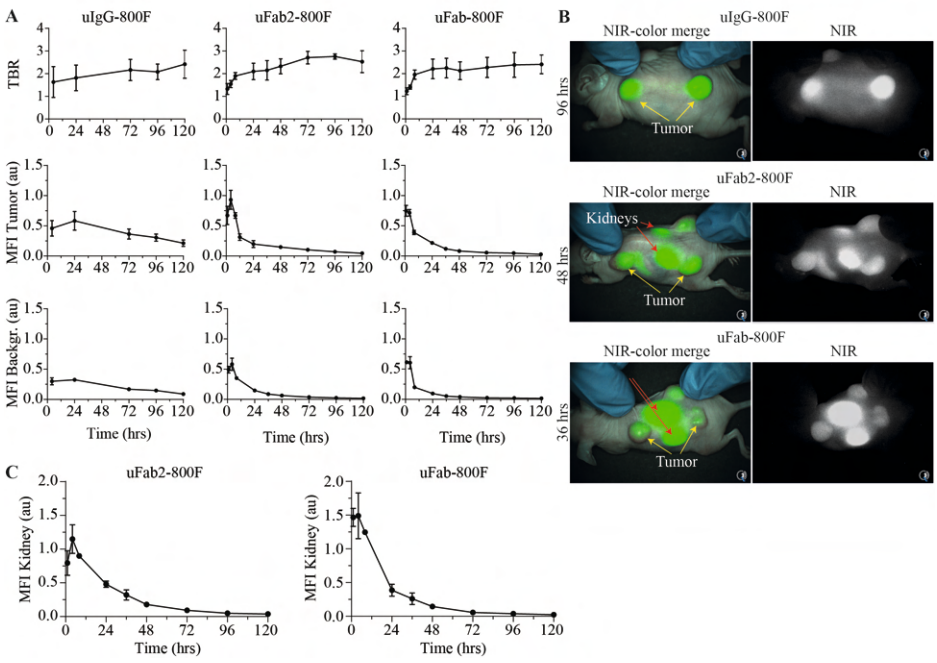

Figure 2. In vivo serial imaging of uIgG-800F, uFab2-800F and uFab-800F in subcutaneous HT-29 tumor bearing mice. (A) TBR and MFI measured using the Pearl over time after injection of 1 nmol uIgG-800F, 1 nmol uFab2-800F and 2 nmol uFab-800F. (B) Merge and 800 nm images taken with the Artemis clinical camera demonstrating real-time tumor imaging at 96 hrs for uIgG-800F, 48 hrs for uFab2-800F and 36 hrs for uFab-800F. These time-slots are shown as they fall within the optimal imaging window for each of the tracers. For images at other time periods see Supplementary Fig. 2 (ESM). Tumor and kidney fluorescence are identified with yellow and red arrows, respectively. (C) Transcutaneous kidney fluorescence over time after uFab2-800F and uFab-800F administration. Au, arbitrary units; hrs, hours MFI, mean fluorescence intensity; nm, nanometer; NIR, near-infrared; TBR, tumor-to-background ratio; T, time.

Fluorescence clearly accumulated in abdominal PDAC BxPC-3-luc2 tumors after intravenous injection of the various tracers. In particular with uFab-800F, transcutaneous kidney and liver fluorescence interfered with optimal tumor imaging (Figure 3A). TBRs were 2.5 ± 0.4 for uIgG-800F, 3.3 ± 1.2 for uFab2-800F and 2.3 ± 1.0 for uFab-800F. TBRs did not differ between all 3 tracers (p = 0.58; Figure 3B). Tumor MFI did not differ significantly but tumors could be visualized with shorter exposure times after uIgG-800F injection as opposed to uFab2-800F or uFab-800F (p = 0.32; Multiple comparisons, uIgG-800F vs. uFab2-800F p = 0.32, uIgG-800F vs. uFab-800F p = 0.46, uFab2-800F vs. uFab-800F p = 0.95; Figure 3C).

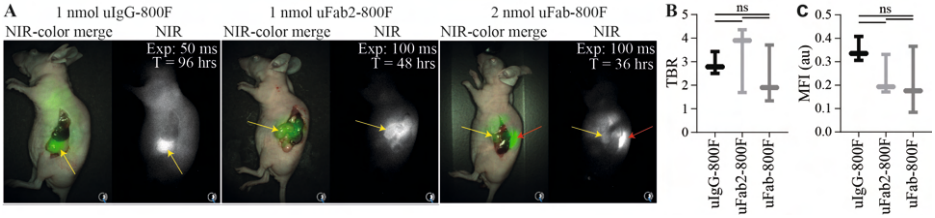

Figure 3. In vivo fluorescence imaging of orthotopic BxPC-3 pancreas adenocarcinomas with uIgG-800F, uFab2-800F and uFab-800F during the optimal time period. (A) NIR-images of orthotopic BxPC-3 pancreas adenocarcinomas taken with the Artemis clinical camera 96 hrs are uIgG-800F (left panel), 48 hrs are uFab2-800F (middle panel) and 36 hrs after uFab-800F (left panel) administration. Tumors are identified with a yellow arrow and kidney fluorescence, when present, with a red arrow. Note the lower exposure time needed after uIgG-800F administration reflecting a higher MFI. (B) TBRs and (C) tumor MFIs measured using the Pearl do not differ significantly between uIgG-800F, uFab2-800F and uFab-800F at respectively 96 hrs, 48 hrs and 36 hrs after injection. Au, arbitrary units; exp, exposure; hrs, hours; MFI, mean fluorescence intensity; NIR, near-infrared; nmol, nanomole; ns, not significant; T, time; TBR, tumor-to-background ratio.

After intravenous injection of uIgG-800F, uFab2-800F, or uFab-800F OSC-19-luc2-GFP superficial squamous tongue tumors were easily identified with the Artemis clinical system. Shorter exposure times were needed after injection of uIgG-800F as opposed to uFab2-800F or uFab-800F (Figure 4A). TBRs of 2.8 ± 0.5, 3.6 ± 0.6 and 3.2 ± 0.4 were achieved for uIgG-800F, uFab2-800F and uFab-800F, respectively. TBRs did not differ significantly between tracers (p = 0.33; Figure 4B). MFI, however, did differ significantly with uIgG-800F having superior absolute fluorescence (p = 0.01; Multiple comparisons, uIgG-800F vs. uFab2-800F p = 0.02, uIgG-800F vs. uFab-800F p = 0.03, uFab2-800F vs. uFab-800F p = 0.88; Figure 4C).

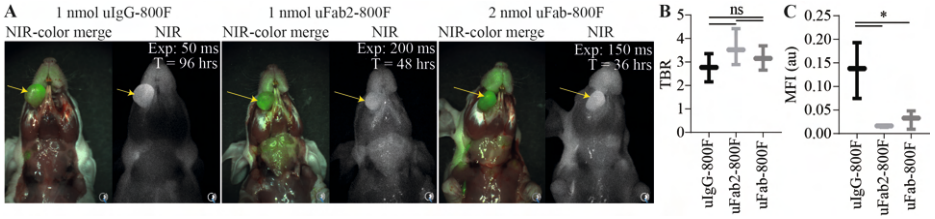

Figure 4. In vivo fluorescence imaging of uIgG-800F, uFab2-800F and uFab-800Fduring the optimal imaging window in orthotopic squamous cell OSC-19 tongue tumors. (A) NIR-images taken with the Artemis clinical camera of orthotopic OSC-19 tongue tumors 96 hrs after uIgG-800F, 48 hrs after uFab2-800F and 36 hrs after uFab-800F administration. Tumors are identified with a yellow arrow. Note the lower exposure time needed to visualize the tumor after uIgG-800F administration compared to uFab2-800F and uFab-800F. (B) TBRs and (C) tumor MFIs measured using the Pearl for uIgG-800F, uFab2-800F and uFab-800F at respectively 96, 48 and 36 hrs after administration demonstrating similar TBRs between the groups but a higher MFI for uIgG-800F. Au, arbitrary units; exp, exposure; hrs, hours; MFI, mean fluorescence intensity; NIR, near-infrared; nmol, nanomole; ns, not significant; T, time; TBR, tumor-to-background ratio.

Fluorescence detection of small lesions was studied using a HT-29 CRC peritoneal carcinomatosis model. Average lesion diameters were 3.2 ± 0.8 mm, 3.7 ± 1.2 mm and 4.7 ± 0.6 mm for uIgG-800F, uFab2-800F or uFab-800F (p = 0.18). Similarly to the OSC-19-luc2-GFP tongue tumors and the BxPc-3-luc2 PDAC tumors, FGS with the Artemis clinical system was performed with lower exposure times in the uIgG-800F groups compared to the other two groups (Figure 5A). TBRs, after uIgG-800F, uFab2-800F or uFab-800F administration were 5.8 ± 2.5, 4.9 ± 1.1 and 5.4 ± 0.8, respectively, and did not differ significantly between tracer groups (p = 0.81; Figure 5B). Lesion MFI approached statistically significant difference with IgG-800F being superior (p = 0.07; Multiple comparisons, uIgG-800F vs. uFab2-800F p = 0.09, uIgG-800F vs. uFab-800F p = 0.14, uFab2-800F vs. uFab-800F p = 0.99; Figure 5C).

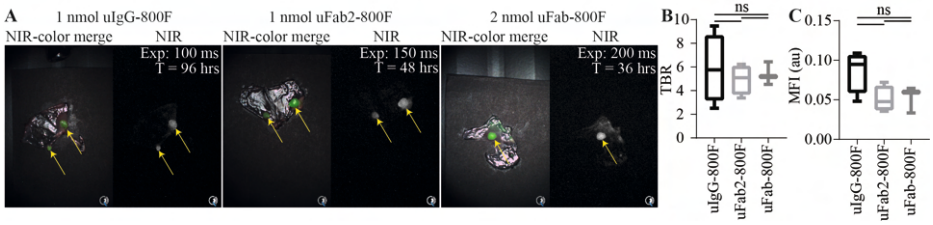

Figure 5. In vivo fluorescence imaging of small lesions with uIgG-800F, uFab2-800F and uFab-800F at the optimal imaging window using an orthotopic HT-29 colorectal cancer peritoneal carcinomatosis model. (A) NIR-images taken with the Artemis clinical camera of the peritoneum containing HT-29 lesions 96 hrs are uIgG-800F, 48 hrs after uFab2-800F and 36 hrs after uFab-800F administration. Tumors are identified with the yellow arrow. Note the differing exposure times needed to create similar images reflecting the differing MFI achieved with each of the tracers. (B) average TBR and (C) lesion MFI measured using the Pearl achieved 96 hrs after uIgG-800F, 48 hrs after uFab2-800F and 36 hrs after uFab-800F injection. Au, arbitrary units; exp, exposure; hrs, hours; MFI, mean fluorescence intensity; NIR, near-infrared; nmol, nanomole; ns, not significant; T, time; TBR, tumor-to-background ratio.

Ex vivo characterization of normal and tumor tissue

E*x vivo* macroscopic analysis of normal tissue, showed that most of the fluorescence was located in the metabolizing organs (Figure 6A-B). Liver MFI differed significantly between tracers with uFab-800F having the highest, and uIgG-800F and uFab2-800F having similar MFI's (p < 0.01; Multiple comparisons, uIgG-800F vs. uFab2-800F p = 0.28, uIgG-800F vs. uFab-800F p < 0.01, uFab2-800F vs. uFab-800F p < 0.01). Kidney MFI differed significantly between all tracer types with uIgG-800F having the lowest MFI (p < 0.01; Multiple comparisons, uIgG-800F vs. uFab2-800F p < 0.01, uIgG-800F vs. uFab-800F p < 0.01, uFab2-800F vs. uFab-800F p < 0.01). MFI of the other organs did not approach or pass that of tumor MFI's and did not significantly impact background fluorescence. *Ex vivo* macroscopic tumor fluorescence could be clearly visualized with all three tracers. uIgG-800F tumor MFI, however, was consistently

higher than uFab2-800F or uFab-800F in all three orthotopic tumor models (Figure 6B). *Post-mortem* overlay of histology with fluorescent signal confirmed tumor specific accumulation at the tumor cells using all three tracers (Figure 6C).

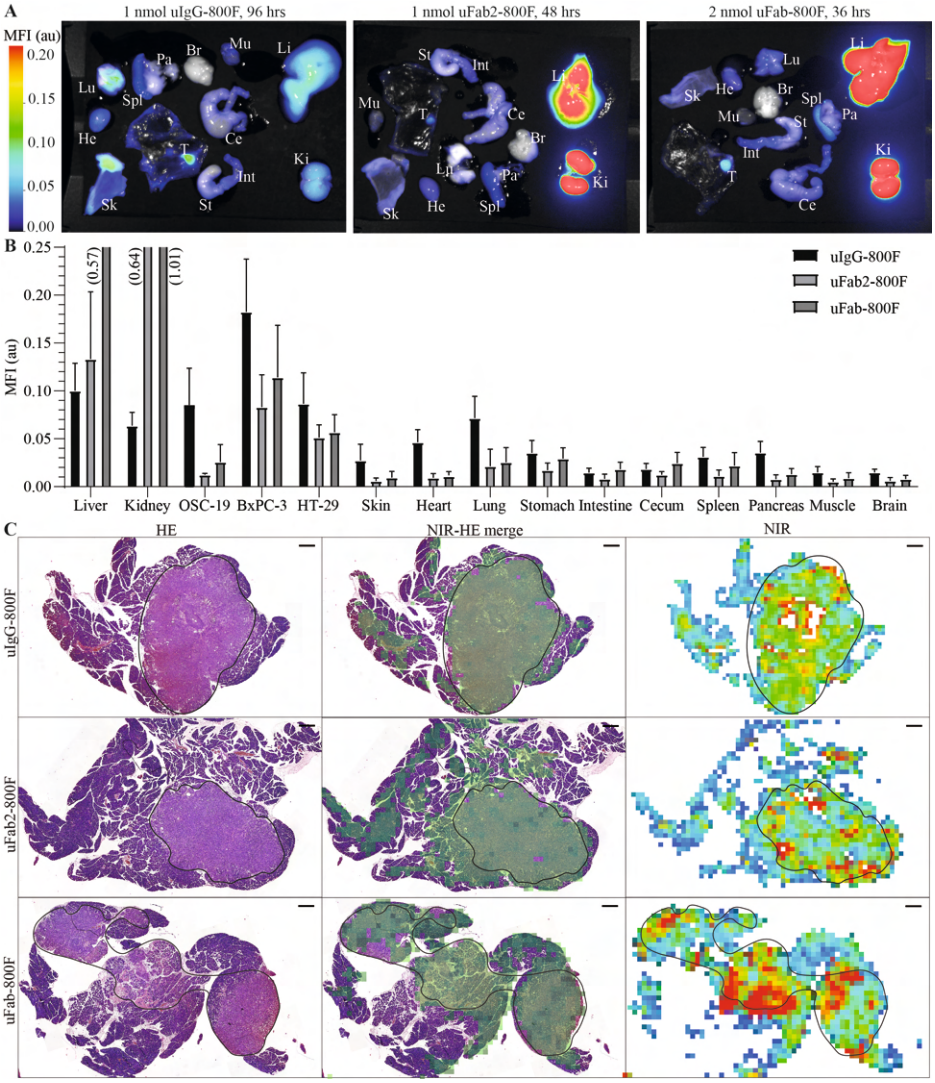

Figure 6. Ex vivo macroscopic and microscopic fluorescence biodistribution of uIgG-800F, uFab2-800F and uFab-800F at optimal imaging window. (A) Ex vivo biodistribution visualized with the Pearl and (B) quantified in a bar graph of uIgG-800F, uFab2-800F and Fab-800F at respectively 96, 48 and 36 hrs after administration. Fluorescence intensity across the images are matched. (C) Overlay of HE-staining and 800 nm fluorescence showing fluorescence accumulation in tumor area compared to surrounding normal tissue. Tumor tissue is delineated by the black line. The black line represents 500 µm. au, arbitrary units; Br, brain; Ce, cecum; He, heart; HE, hematoxylin & eosin; Hrs, hours; Int, intestine; Ki, kidneys; Li, liver; Lu, lung; MFI, mean fluorescence intensity; Mu, muscle; nm, nanometer; nmol, nanomole; NIR, near-infrared; Pa, pancreas; Sk, skin; Spl, spleen; St, stomach.

Discussion

Optimizing NIR contrast agents for molecular imaging is a challenge, as tumor visualization is dependent on a multitude of factors including, but not limited to, tracer size, valency, affinity, and labeling ratio [29-31]. By decreasing size, the current study evaluated whether tumor specific imaging could be retained and concurrently pharmacokinetics improved for the validated humanized anti-uPAR monoclonal antibody MNPR-101. Although the 100 kDa $F(ab')_2$ and 50 kDa Fab performed similarly *in vitro* to the 150 kDa IgG, *in vivo* imaging resulted in more rapid FGS with the two smaller fragments at the cost of peak tumor fluorescence.

Only few reports have directly compared antibodies with their fragments for FGS. Fluorescent anti-HER3 IgG and single chain variable fragment (scFv)-Fc had higher tumor MFIs compared to scFv, Fab, diabody and scFv-C_H3 in HNSCC xenografts [32]. In another study, EphB4-targeting IgG showed maximum tumor uptake while $F(ab')_2$ and Fab resulted in step-wise lower tumor signal [33]. A third study, using ICAM-1 Fabs, tumor MFI decreased to such an extent compared to the full-sized antibody that it matched that of non-specific controls [34]. These results, although differing in constructs and/or targets, match ours and are comparable to previous PET studies where CD105 targeting $F(ab')_2$ and Fab lead to earlier imaging but lower peak signal [22, 23].

Previously, however, we achieved high peak tumor signal with the epithelial cell adhesion molecule (EpCAM) targeting Fab VB6-845-IRDye800CW resulting in clinical translation (NTR7570) [35]. Expression characteristics of the targeted receptor could explain this difference in peak MFI attained by the Fabs. The colorectal HT-29 and breast MCF-7 cell lines used by Boogerd et al. express respectively 195,000 and 260,000 copies of EpCAM while BxPc-3, OSC-19 and HT-29 have 10,000 – 30,000 copies of uPAR [14, 35]. For receptors with lower cell expression, like uPAR, HER3, and EphB4, longer circulation times could be required to establish sufficient accumulation of tracer in tumors and clearance from background tissue [32, 36, 37].

In addition to receptor-expression, tracer extravasation and clearance can clarify differences in tumor uptake. IgGs compensate their unfavorable slow extravasation characteristics with extended circulation times, in part due to their Fc-receptor mediated recycling and minimal renal clearance, providing a tracer multiple chances for extravasation [17, 38]. In contrast, the improved extravasation of molecules ranging in size between 20 – 50 kDa is not in proportion to the rapid renal clearance resulting in worsened tumor accumulation compared to IgGs [39, 40]. At and below 20 kDa, like for nanobodies and peptides, renal clearance is practically at first-pass and as such cannot improve, while extravasation increases rapidly with

decreasing size resulting in favorable tumor accumulation again [40]. Once in the tumor compartment, the superior diffusion of smaller molecules will result in a more homogenous tumor distribution compared to their larger counterparts [31].

Nonetheless, these disadvantages can be compensated by improving target affinity as there is an inverse relation between size and affinity (K_D) required to reach similar tumor uptakes. K_Ds of 10^{-8} to 10^{-6} M for antibodies result in similar degrees of tumor retention as Fabs or scFvs with a K_D of 10^{-10} to 10^{-8} M [41-43]. Our anti-uPAR Fab has a nanomolar affinity, approximately ten-fold higher than the ICAM-1 Fab, and similar to the HER-3 Fab while VB6-845-IRDye800CW has a picomolar affinity[35]. In conclusion, the combination of receptor density and tracer affinity in combination with size play a pivotal role in achieving high peak intensity, possibly explaining why VB6-845-IRDye800CW achieved superior imaging conditions and why, for the other targets, the larger agents resulted in superior MFIs.

The currently described uPAR targeting antibody fragments are not the only uPAR-targeting contrast agents under development. The growth factor domain of urokinase (ATF), the natural ligand of uPAR with a K_D of 2.5×10^{-10} M, has been coupled with various dyes like Cy5.5 and NIR830 for FGS as approximately 18 kDa peptides and much larger nanoparticle probes [44-46]. The 9-mer peptide ICG-Glu-Glu-AE105 also targets the uPAR-ATF interaction with a K_D of 134×10^{-9} M and results in rapid (6 - 24 hours) tumor localization in various *in vivo* xenograft models [47-49]. While the delayed imaging window of uIgG-800F and rapid imaging window of ATF peptides and ICG-Glu-Glu-AE105 is evident, peak fluorescence is much harder to compare as these constructs not only differ in size and affinity but also in fluorophore. In this case, IRDye800CW has a higher extinction coefficient and quantum yield than ICG and can be expected to be brighter [50]. Lastly, the targeting epitope is a crucial difference between ATF peptides, ICG-Glu-Glu-AE105 and huIgG-800CW where the former two, as uPA competitors, are dependent on low endogenous uPA expression and the latter is not [51]. Co-injection experiments of uPA and ICG-Glu-Glu-AE105 have resulted in an almost 50 % decrease in fluorescence signal [47]. huIgG-800CW specifically targets the D2-D3 uPAR isotype, often found to be overexpressed in cancer [9, 16].

While the conclusions drawn in this study reflect the literature, the current study contains a couple limitations. Although the limited group sizes were sufficient according to previous sample size calculations to identify the most relevant differences in TBRs (increase in 50%, see ESM) more subtle differences could have been missed. Ethical constraints, however, limited researching this avenue. In addition, using orthotopic models minimalized the time-points tumors could be visualized *in vivo*, potentially missing better imaging moments. This was negated by first imaging the tracers serially in a subcutaneous tumor model and carefully defining what

determined a suitable time window (see ESM). Lastly, administrating tracers based on fluorescence as opposed to antigen binding sites could potentially have allowed for a more accurate comparison of fluorescence intensity, however, the results, if different at all when injecting a surplus amount of tracer, would have skewed the conclusion even more towards full-sized antibodies.

Conclusion

To conclude, this study successfully introduces two novel uPAR antibody-fragment tracers based on the extensively validated MNPR-101 humanized parental antibody. $F(ab')_2$ and Fab greatly improved time-to-imaging while the whole antibody demonstrated superior peak fluorescence. In the clinic, the various pharmacokinetic profiles of the tracers should be considered as Fab utilization is better in (semi-) acute settings (same-day or next-day surgery), but should not be used when absolute receptor expression is expected to be relatively low. In these cases, surgeons should veer towards full-sized antibodies or constructs smaller than 20kDa, such as nanobodies or peptides.

References

1. Allemani C, Matsuda T, Di Carlo V, Harewood R, Matz M, Nikšić M, et al. Global surveillance of trends in cancer survival 2000-14 (CONCORD-3): analysis of individual records for 37 513 025 patients diagnosed with one of 18 cancers from 322 population-based registries in 71 countries. Lancet (London, England). 2018;391:1023-75. doi:10.1016/s0140-6736(17)33326-3.
2. Miller KD, Nogueira L, Mariotto AB, Rowland JH, Yabroff KR, Alfano CM, et al. Cancer treatment and survivorship statistics, 2019. CA Cancer J Clin. 2019;69:363-85. doi:10.3322/caac.21565.
3. Khan MA, Hakeem AR, Scott N, Saunders RN. Significance of R1 resection margin in colon cancer resections in the modern era. Colorectal disease : the official journal of the Association of Coloproctology of Great Britain and Ireland. 2015;17:943-53. doi:10.1111/codi.12960.
4. Ghaneh P, Kleeff J, Halloran CM, Raraty M, Jackson R, Melling J, et al. The Impact of Positive Resection Margins on Survival and Recurrence Following Resection and Adjuvant Chemotherapy for Pancreatic Ductal Adenocarcinoma. Annals of surgery. 2019;269:520-9. doi:10.1097/sla.0000000000002557.
5. Wolf AS, Swanson SJ, Yip R, Liu B, Tarras ES, Yankelevitz DF, et al. The Impact of Margins on Outcomes After Wedge Resection for Stage I Non-Small Cell Lung Cancer. The Annals of thoracic surgery. 2017;104:1171-8. doi:10.1016/j.athoracsur.2017.04.024.
6. Hernot S, van Manen L, Debie P, Mieog JSD, Vahrmeijer AL. Latest developments in molecular tracers for fluorescence image-guided cancer surgery. The Lancet Oncology. 2019;20:e354-e67. doi:10.1016/s1470-2045(19)30317-1.
7. van Manen L, Handgraaf HJM, Diana M, Dijkstra J, Ishizawa T, Vahrmeijer AL, et al. A practical guide for the use of indocyanine green and methylene blue in fluorescence-guided abdominal surgery. Journal of surgical oncology. 2018;118:283-300. doi:10.1002/jso.25105.
8. Boonstra MC, Verspaget HW, Ganesh S, Kubben FJ, Vahrmeijer AL, van de Velde CJ, et al. Clinical applications of the urokinase receptor (uPAR) for cancer patients. Current pharmaceutical design. 2011;17:1890-910. doi:10.2174/138161211796718233.
9. Baart VM, Houvast RD, de Geus-Oei LF, Quax PHA, Kuppen PJK, Vahrmeijer AL, et al. Molecular imaging of the urokinase plasminogen activator receptor: opportunities beyond cancer. EJNMMI Res. 2020;10:87. doi:10.1186/s13550-020-00673-7.
10. Baart VM, van Duijn C, van Egmond SL, Dijckmeester WA, Jansen JC, Vahrmeijer AL, et al. EGFR and αvβ6 as Promising Targets for Molecular Imaging of Cutaneous and Mucosal Squamous Cell Carcinoma of the Head and Neck Region. Cancers. 2020;12. doi:10.3390/cancers12061474.
11. de Geus SW, Baart VM, Boonstra MC, Kuppen PJ, Prevoo HA, Mazar AP, et al. Prognostic Impact of Urokinase Plasminogen Activator Receptor Expression in Pancreatic Cancer: Malignant Versus Stromal Cells. Biomarker insights. 2017;12:1177271917715443. doi:10.1177/1177271917715443.
12. Boonstra MC, Verbeek FP, Mazar AP, Prevoo HA, Kuppen PJ, van de Velde CJ, et al. Expression of uPAR in tumor-associated stromal cells is associated with colorectal cancer patient prognosis: a TMA study. BMC cancer. 2014;14:269. doi:10.1186/1471-2407-14-269.
13. Fosbøl M, Kurbegovic S, Johannesen HH, Røder MA, Hansen AE, Mortensen J, et al. Urokinase-Type Plasminogen Activator Receptor (uPAR) PET/MRI of Prostate Cancer for Noninvasive Evaluation of Aggressiveness: Comparison with Gleason Score in a Prospective Phase 2 Clinical Trial. Journal of nuclear medicine : official publication, Society of Nuclear Medicine. 2021;62:354-9. doi:10.2967/jnumed.120.248120.

14. Boonstra MC, van Driel PB, van Willigen DM, Stammes MA, Prevoo HA, Tummers QR, et al. uPAR-targeted multimodal tracer for pre- and intraoperative imaging in cancer surgery. Oncotarget. 2015;6:14260-73. doi:10.18632/oncotarget.3680.
15. Boonstra MC, Van Driel P, Keereweer S, Prevoo H, Stammes MA, Baart VM, et al. Preclinical uPAR-targeted multimodal imaging of locoregional oral cancer. Oral oncology. 2017;66:1-8. doi:10.1016/j.oraloncology.2016.12.026.
16. Baart VM, van der Horst G, Deken MM, Bhairosingh SS, Schomann T, Sier VQ, et al. A multimodal molecular imaging approach targeting urokinase plasminogen activator receptor for the diagnosis, resection and surveillance of urothelial cell carcinoma. European journal of cancer (Oxford, England : 1990). 2021;146:11-20. doi:10.1016/j.ejca.2021.01.001.
17. Zalevsky J, Chamberlain AK, Horton HM, Karki S, Leung IW, Sproule TJ, et al. Enhanced antibody half-life improves in vivo activity. Nat Biotechnol. 2010;28:157-9. doi:10.1038/nbt.1601.
18. Holliger P, Hudson PJ. Engineered antibody fragments and the rise of single domains. Nat Biotechnol. 2005;23:1126-36. doi:10.1038/nbt1142.
19. de Valk KS, Deken MM, Schaap DP, Meijer RP, Boogerd LS, Hoogstins CE, et al. Dose-Finding Study of a CEA-Targeting Agent, SGM-101, for Intraoperative Fluorescence Imaging of Colorectal Cancer. Annals of surgical oncology. 2021;28:1832-44. doi:10.1245/s10434-020-09069-2.
20. Williams LE, Wu AM, Yazaki PJ, Liu A, Raubitschek AA, Shively JE, et al. Numerical selection of optimal tumor imaging agents with application to engineered antibodies. Cancer Biother Radiopharm. 2001;16:25-35. doi:10.1089/108497801750095989.
21. Debie P, Devoogdt N, Hernot S. Targeted Nanobody-Based Molecular Tracers for Nuclear Imaging and Image-Guided Surgery. Antibodies (Basel). 2019;8. doi:10.3390/antib8010012.
22. Hong H, Zhang Y, Orbay H, Valdovinos HF, Nayak TR, Bean J, et al. Positron emission tomography imaging of tumor angiogenesis with a (61/64)Cu-labeled F(ab')(2) antibody fragment. Mol Pharm. 2013;10:709-16. doi:10.1021/mp300507r.
23. Zhang Y, Hong H, Orbay H, Valdovinos HF, Nayak TR, Theuer CP, et al. PET imaging of CD105/endoglin expression with a ^{61}/^{64}Cu-labeled Fab antibody fragment. Eur J Nucl Med Mol Imaging. 2013;40:759-67. doi:10.1007/s00259-012-2334-2.
24. van Driel PB, Boonstra MC, Prevoo HA, van de Giessen M, Snoeks TJ, Tummers QR, et al. EpCAM as multi-tumour target for near-infrared fluorescence guided surgery. BMC cancer. 2016;16:884. doi:10.1186/s12885-016-2932-7.
25. Tseng W, Leong X, Engleman E. Orthotopic mouse model of colorectal cancer. J Vis Exp. 2007:484. doi:10.3791/484.
26. Kim MP, Evans DB, Wang H, Abbruzzese JL, Fleming JB, Gallick GE. Generation of orthotopic and heterotopic human pancreatic cancer xenografts in immunodeficient mice. Nat Protoc. 2009;4:1670-80. doi:10.1038/nprot.2009.171.
27. Schindelin J, Arganda-Carreras I, Frise E, Kaynig V, Longair M, Pietzsch T, et al. Fiji: an open-source platform for biological-image analysis. Nature methods. 2012;9:676-82. doi:10.1038/nmeth.2019.
28. Hoogstins CE, Weixler B, Boogerd LS, Hoppener DJ, Prevoo HA, Sier CF, et al. In Search for Optimal Targets for Intraoperative Fluorescence Imaging of Peritoneal Metastasis From Colorectal Cancer. Biomarkers in cancer. 2017;9:1179299x17728254. doi:10.1177/1179299x17728254.
29. Muchekehu R, Liu D, Horn M, Campbell L, Del Rosario J, Bacica M, et al. The Effect of Molecular Weight, PK, and Valency on Tumor Biodistribution and Efficacy of Antibody-Based Drugs. Transl Oncol. 2013;6:562-72. doi:10.1593/tlo.13409.

30. Vira S, Mekhedov E, Humphrey G, Blank PS. Fluorescent-labeled antibodies: Balancing functionality and degree of labeling. Anal Biochem. 2010;402:146-50. doi:10.1016/j.ab.2010.03.036.
31. Xenaki KT, Oliveira S, van Bergen En Henegouwen PMP. Antibody or Antibody Fragments: Implications for Molecular Imaging and Targeted Therapy of Solid Tumors. Front Immunol. 2017;8:1287. doi:10.3389/fimmu.2017.01287.
32. El-Sayed A, Bernhard W, Barreto K, Gonzalez C, Hill W, Pastushok L, et al. Evaluation of antibody fragment properties for near-infrared fluorescence imaging of HER3-positive cancer xenografts. Theranostics. 2018;8:4856-69. doi:10.7150/thno.24252.
33. Li D, Liu S, Liu R, Zhou Y, Park R, Naga K, et al. EphB4-targeted imaging with antibody h131, h131-F(ab')2 and h131-Fab. Mol Pharm. 2013;10:4527-33. doi:10.1021/mp400354y.
34. Leelawattanachai J, Kwon KW, Michael P, Ting R, Kim JY, Jin MM. Side-by-Side Comparison of Commonly Used Biomolecules That Differ in Size and Affinity on Tumor Uptake and Internalization. PloS one. 2015;10:e0124440. doi:10.1371/journal.pone.0124440.
35. Boogerd LSF, Boonstra MC, Prevoo H, Handgraaf HJM, Kuppen PJK, van de Velde CJH, et al. Fluorescence-guided tumor detection with a novel anti-EpCAM targeted antibody fragment: Preclinical validation. Surg Oncol. 2019;28:1-8. doi:10.1016/j.suronc.2018.10.004.
36. Rosestedt M, Andersson KG, Mitran B, Tolmachev V, Löfblom J, Orlova A, et al. Affibody-mediated PET imaging of HER3 expression in malignant tumours. Sci Rep. 2015;5:15226. doi:10.1038/srep15226.
37. Stammes MA, Prevoo HA, Ter Horst MC, Groot SA, Van de Velde CJ, Chan AB, et al. Evaluation of EphA2 and EphB4 as Targets for Image-Guided Colorectal Cancer Surgery. Int J Mol Sci. 2017;18. doi:10.3390/ijms18020307.
38. Dreher MR, Liu W, Michelich CR, Dewhirst MW, Yuan F, Chilkoti A. Tumor vascular permeability, accumulation, and penetration of macromolecular drug carriers. J Natl Cancer Inst. 2006;98:335-44. doi:10.1093/jnci/djj070.
39. Thurber GM, Zajic SC, Wittrup KD. Theoretic criteria for antibody penetration into solid tumors and micrometastases. Journal of nuclear medicine : official publication, Society of Nuclear Medicine. 2007;48:995-9. doi:10.2967/jnumed.106.037069.
40. Wittrup KD, Thurber GM, Schmidt MM, Rhoden JJ. Practical theoretic guidance for the design of tumor-targeting agents. Methods Enzymol. 2012;503:255-68. doi:10.1016/b978-0-12-396962-0.00010-0.
41. Schmidt MM, Wittrup KD. A modeling analysis of the effects of molecular size and binding affinity on tumor targeting. Mol Cancer Ther. 2009;8:2861-71. doi:10.1158/1535-7163.Mct-09-0195.
42. Fouliard S, Chenel M, Marcucci F. Influence of the duration of intravenous drug administration on tumor uptake. Frontiers in oncology. 2013;3:192. doi:10.3389/fonc.2013.00192.
43. Adams GP, Schier R, Marshall K, Wolf EJ, McCall AM, Marks JD, et al. Increased affinity leads to improved selective tumor delivery of single-chain Fv antibodies. Cancer Res. 1998;58:485-90.
44. Yang L, Sajja HK, Cao Z, Qian W, Bender L, Marcus AI, et al. uPAR-targeted optical imaging contrasts as theranostic agents for tumor margin detection. Theranostics. 2013;4:106-18. doi:10.7150/thno.7409.
45. Abdalla MO, Karna P, Sajja HK, Mao H, Yates C, Turner T, et al. Enhanced noscapine delivery using uPAR-targeted optical-MR imaging trackable nanoparticles for prostate cancer therapy. Journal of controlled release : official journal of the Controlled Release Society. 2011;149:314-22. doi:10.1016/j.jconrel.2010.10.030.

46. Lin L, Gårdsvoll H, Huai Q, Huang M, Ploug M. Structure-based engineering of species selectivity in the interaction between urokinase and its receptor: implication for preclinical cancer therapy. The Journal of biological chemistry. 2010;285:10982-92. doi:10.1074/jbc.M109.093492.
47. Juhl K, Christensen A, Persson M, Ploug M, Kjaer A. Peptide-Based Optical uPAR Imaging for Surgery: In Vivo Testing of ICG-Glu-Glu-AE105. PloS one. 2016;11:e0147428. doi:10.1371/journal.pone.0147428.
48. Christensen A, Juhl K, Persson M, Charabi BW, Mortensen J, Kiss K, et al. uPAR-targeted optical near-infrared (NIR) fluorescence imaging and PET for image-guided surgery in head and neck cancer: proof-of-concept in orthotopic xenograft model. Oncotarget. 2017;8:15407-19. doi:10.18632/oncotarget.14282.
49. Juhl K, Christensen A, Rubek N, Karnov KKS, von Buchwald C, Kjaer A. Improved surgical resection of metastatic pancreatic cancer using uPAR targeted in vivo fluorescent guidance: comparison with traditional white light surgery. Oncotarget. 2019;10:6308-16. doi:10.18632/oncotarget.27220.
50. Gioux S, Choi HS, Frangioni JV. Image-guided surgery using invisible near-infrared light: fundamentals of clinical translation. Molecular imaging. 2010;9:237-55.
51. Baart VM, Boonstra MC, Sier CFM. uPAR directed-imaging of head-and-neck cancer. Oncotarget. 2017;8:20519-20. doi:10.18632/oncotarget.16240.

Part V
Summary and general discussion

Chapter 8

Summary

Summary

Part I. Introduction
Cancers accounts for approximately one-in-six deaths worldwide. Despite the advances in treatment options over the past couple decades surgery remains the cornerstone for almost all solid tumors. Radical excision is crucial for curative treatment, however, intraoperative tumor identification is hampered by (1) fibrosis, inflammation and necrosis due to neoadjuvant therapy, and (2) an altered surgical field due to the adoption of laparoscopic and robotic procedures. In response, various imaging techniques have been introduced to the operating theater to aid surgeons in tumor discrimination of which fluorescence guided surgery (FGS) is one. FGS utilizes near-infrared light to visualize, an often intravenously administered, tumor-targeting tracer in real-time. In order to create an optimal contrast between malignant and non-malignant tissue such a tracer needs to target a tumor-specific protein that is highly expressed on tumor tissue but absent on the surrounding tissue.

Part II. uPAR as a tumor target in various tumor types
The urokinase plasminogen activator receptor (uPAR) is such a tracer that is highly expressed on malignant tumor cells and tumor-associated stromal cells, while being practically absent on non-malignant (normal, benign or reactive) cells. In addition, in various malignancies uPAR expression is a prognostic factor. In **Chapter 2** the prognostic value of uPAR expression for patients with pancreatic adenocarcinoma was studied. 66% of cases expressed uPAR on malignant cells while 82% expressed uPAR on stromal cells. uPAR expression on malignant and stromal cells is inversely related with overall survival and disease-free survival. These results further strengthen the case that uPAR is strong prognostic marker for aggressive diseases and could potentially be used for treatment stratification. Furthermore, the expression of uPAR on malignant and tumor-associated stromal cells render it as a possible target for FGS.

Another case where FGS could revolutionize treatment as tumor borders are difficult if not impossible to determine is high-risk squamous cell carcinoma of the head-and-neck region. Using a practical approach, **Chapter 3** determined to identify possible tumor targets for FGS of these challenging cases. The expression patterns of seven targets with fluorescent tracers undergoing development were evaluated on tumor cells, tumor-associated stromal cells and normal epithelium. The epidermal growth factor receptor, integrin $\alpha_v ß_6$ and uPAR were identified as possible targets with the former two having high expression on tumor cells, no expression on stromal cells, and moderate to high expression on normal epithelium.

In contrast normal epithelium was consistently negative for uPAR while tumor and tumor-associated stromal cells were moderately positive.

Part III. uPAR as target: beyond cancer imaging

uPAR overexpression is not exclusive to cancer but also occurs in a range of other diseases where extracellular matrix remodeling plays an important role. Therefore, **Chapter 4** takes a closer look at the role of uPAR in atherosclerosis, rheumatoid arthritis (RA), Alzheimer's disease (AD), multiple sclerosis (MS) and inflammatory bowel disease (IBD). In addition, avenues are identified where uPAR targeted molecular imaging could offer insights for new directions in diagnosis, surveillance or treatment options. These range from utilizing molecular imaging to increase our understanding of MS or AD to identification atherosclerotic plaques that are at risk for rupture to predicting disease aggravation in RA or IBD.

Part IV. Development of uPAR targeted tracers

After identifying a possible target, a fluorescent tracer that specifically targets this receptor needs to be developed. There are various pharmacological and practical that need to be considered when designing a fluorescent tracer. This discussion is introduced in **Chapter 5** where the results of a fluorescent uPAR targeting monoclonal antibody and peptide are compared in light of two recently published articles where both tracers were evaluated in preclinical head-and-neck cancer models. The long half-life of the antibody results in delayed but prolonged imaging. More rapid imaging can be achieved with the peptide, however, it suffers from urokinase competition for uPAR binding.

In **Chapter 6** a novel humanized fluorescent antibody, based on the mouse monoclonal antibody targeting domain 2-3 of uPAR of the previous chapter, is introduced and evaluated preclinically. In preclinical subcutaneous and orthotopic human urothelial cell carcinoma models tumors can be specifically delineated from background tissues with significantly higher tumor-to-background ratios than multiple isotype controls. In addition, the multimodal functionality of the tracer is demonstrated by photoacoustic 3D in depth imaging.

As mentioned earlier, antibodies have a prolonged half-life which delays the optimal imaging window. Decreasing the molecular weight of the antibody alters the biodistribution of the tracer, resulting in earlier tumor penetration and background clearance and ultimately allowing for earlier imaging. In **Chapter 7** $F(ab')_2$ and Fab fragments are created from the humanized monoclonal antibody introduced in the previous chapter and extensively compared in multiple preclinical mouse models. The ultimate imaging window is reduced from 72 hours to 24 hours post administration with the fragments. While the tumor-to-background ratios do not differ

between the full-sized antibody and the two smaller fragments, the peak tumor signal decreases with size of the tracer. The earlier tumor visualization achieved by antibody fragments comes at the expense of peak fluorescence intensity which could potential influence sensitivity of the tracer.

Chapter 9

General discussion and future perspectives

Baart VM

General discussion and future perspectives

In merely a decade the targeted-fluorescence guided surgery (FGS) field has made significant strides forward, from the initial proof-of-concept trial by van Dam et al. in 2011 to the in 2021 United States Food and Drug Administration approval of the first targeted near-infrared (NIR) fluorescence contrast agent pafolacianine (Cytalux; i.e. OTL38) [1]. FGS has matured from promises of clinical benefit to demonstrating the applicability in a randomized phase III-trial; pafolacianine identified 33% additional lesions in ovarian cancer patients that otherwise would have been missed by the operating surgeon [2]. As more phase-III trials with other agents are expected to report their outcomes in the upcoming years, the surgical scientific community stands at the footsteps of an era of precision surgery, where tumors can be color-coded to aid intraoperative decision making and resection [3].

Fundamental for a fluorescent tracer is the framework of clinical application applied and whether the desired contrast is achieved. For example, 40% of ovarian cancer patients show residual lesions larger than 1 cm by postoperative computed tomography after cytoreductive complete resection. Subsequently this group had inferior outcomes compared to patients where intraoperative assessment was in accordance with postoperative imaging [4]. The NIR contrast agent pafolacianine can play a role into this clinical framework, by offering an innovative approach to identify and resect these missed lesions intraoperatively. For this purpose pafolacianine has been improved upon its predecessor EC17 by utilizing the NIR window as opposed to blue light. This exchange of fluorophore enhances the contrast by decreasing background autofluorescence and improving penetration depth of the signal [1, 5]. While the steps being made are exciting, the pafolacianine FDA approval also obliges us to ask what the next-generation of FGS contrast agents will look like and particularly whether there is room for urokinase plasminogen activator receptor (uPAR)-targeted FGS in this landscape.

The following section will therefore discuss (I) the clinical frameworks where FGS could be of clinical value, (II) where uPAR fits in these clinical frameworks, (III) how tumor contrast can be enhanced by smart tracer design.

Part I. Clinical frameworks for FGS

As the possibilities with FGS broaden, it becomes paramount to focus on the clinical frameworks where FGS can potentially enhance patient survival by improving surgical outcomes [6]. Based on the current literature, Table 1 identifies fourteen clinical questions for eleven solid tumor types where FGS offers a potential application. While one question addresses staging by identifying radiographically occult lesions and two focus on identifying additional lesions during debulking procedures, the majority (11) focus on improving locoregional tumor control by improving R0 resection margin rates. Especially in (potentially) locally advanced tumors, such as those in the head & neck, brain or rectum, margin positivity rates are high and the potential of additional intraoperative guidance via FGS is obvious [7-9].

After defining the clinical framework potential targets need to be assessed. Identifying a target expressed across all tumors and absent in non-malignant tissue, comprising normal, benign and reactive tissue like inflamed or fibrotic, is the holy grail of molecular imaging modalities including FGS. Finding such a target, however, is nearly impossible as cancer is an umbrella term for more than 100 diseases that fails to highlight the inter-tumoral heterogeneity that exists, even between tumors from similar anatomical origins[1] [10, 11]. Not surprisingly, the twenty FGS-tracers that are undergoing clinical translation target fifteen different proteins or processes [3]. In Table 1 potential targets are identified for the FGS clinical frameworks mentioned above, based on (pre-) clinical data and stage of development[2]. While the folate receptor is specific for ovarian cancer, carcinoembryonic antigen (CEA) for gastro-intestinal tumors, and epidermal growth factor receptor (EGFR) for head & neck cancer, uPAR's versatility as potential target for head & neck, pancreatic, ovarian, prostate, and bladder cancer suggests merits as a next-generation target.

1 Intra-tumoral heterogeneity complicates matters even further when subclones in the tumor decrease or eliminate the expression of the target.

2 The list of potential targets is meant to be exemplary and is not an exhaustive list.

Table 1. Possible clinical frameworks where FGS is a potential solution to improve surgical outcomes and relevant targets.

Tumor Type	Clinical Framework	Framework type	Potential targets[#]
Glioma	Increasing percentage of patients with maximal cytoreductive surgery by improving visualization of the infiltrative zone (≈65% [8])	Locoregional control	Protoporphyrin IX precursors; **uPAR**
Head & neck cancer	Reducing tumor-positive margins of head & neck squamous cell carcinoma patients treated by resection (≈ 23.3% [7])	Locoregional control	Integrin αvß6; EGFR; **uPAR**
Breast cancer	Improving re-excision rates of breast cancer patients treated by lumpectomy (≈ 21.6% [12])	Locoregional control	Cathepsin/ proteolytic activity
Lung	Reducing positive resection margins (5-15% [13])	Locoregional control	Non-targeted; folate receptor; CAIX; Collagen XVII
Esophageal cancer	Reducing margin positivity rate in patients with esophageal cancer undergoing an esophagectomy (≈ 9.4% [14])	Locoregional control	EpCAM; CEA
Primary and secondary liver cancer	Reducing tumor-positive margins of primary and secondary hepatic lesions (≈ 28% tumor-positive margins for colorectal liver metastases [15])	Locoregional control	Non-targeted; CEA
Pancreatic cancer	Preventing unnecessary laparotomies in patients with pancreatic ductal adenocarcinoma by detecting radiographically occult disease during the staging laparoscopy (≈ 20% have unresectable disease during laparotomy [16])	Staging	Integrin αvß6; CEA; **uPAR**
	Reducing R1 positive margins in patients with pancreatic ductal adenocarcinoma undergoing laparotomy with curative intent (≈ 50-70% [17])	Locoregional control	
Colorectal	Improving cytoreductive resections in patients with peritoneal carcinomatosis of colorectal origin [18]	Identifying additional lesions	CEA; EpCAM
	Reducing R1 resection margins in patients with locally advanced rectal cancer (≈ 16% [9])	Locoregional control	
Ovarian	Improving detection of subclinical peritoneal nodules in staging and debulking procedures for patients with epithelial ovarian carcinoma [6]	Identifying additional lesions	Folate receptor; **uPAR**; EpCAM
Prostate	Reducing positive margins during in patients undergoing radical prostatectomy (≈ 15% [19])	Locoregional control	PSMA; **uPAR**
Bladder	Reducing recurrence rates in patients with non-muscle invasive bladder cancer (30-80% [20])	Locoregional control	Protoporphyrin IX precursors; **uPAR**
	Reducing positive soft tissue surgical margins in patients undergoing radical cystectomy for primary urothelial cancer (≈ 4.2% [21])	Locoregional control	

targets are identified based on available (pre-)clinical data and stage of development. The list is not meant to be exhaustive. See Table 2 and 3 for in-depth evidence supporting the targets relevance. CAIX, carbonic anhydrase IX; CEA, carcinoembryonic antigen; EGFR, epidermal growth factor receptor; EpCAM, epithelial cell adhesion molecule; PSMA, prostate-specific membrane antigen; uPAR, urokinase plasminogen activator receptor.

Part II. Clinical framework of uPAR-based FGS

Biology of uPAR

Understanding the complex biology of uPAR helps to explain its versatility as a target. Mechanistically, uPAR can be considered a lynchpin protein or central orchestrator in many of the pathways fundamental to cancer. Proteomic studies, for instance, show that a moderate downregulation of uPAR (approx. 43%) reverses signaling pathways associated with eight of the ten defined 'Hallmarks of Cancer', most importantly those involving the evasion of cancer cell death, promoting cancer cell proliferation, activating invasion and metastases, and promoting immune evasion [22-26]. *In vitro* and *in vivo* studies confirm many of these associations and show uPAR to be closely related to tumor-aggressiveness [27]. Because of the universal characteristics uPAR seems a marker for cancer biology rather than a marker for specific cancer types.

Not surprisingly, uPAR (over-)expression has been described in almost every solid malignancy and expression is often correlated with poor prognosis [27-29]. We confirm this pattern for pancreatic ductal adenocarcinoma in **Chapter 2**,where uPAR expression in both neoplastic and stromal cells is inversely associated with overall survival (OS) and disease-free survival (DFS) of the patients. Similarly, we show in **Chapter 3,** that uPAR is overexpressed in the majority of squamous cell carcinoma's of the head and neck, again on both neoplastic and tumor-associated stromal cells, whereas adjacent normal tissue contained no uPAR expression. The results from this study are especially relevant for FGS as tissue samples were specifically selected and evaluated based on the presence of tumor margins. As such, this studies builds on the evidence that uPAR expression particularly localizes towards the invasive edge, often the margin at risk during surgical resection [30].

Clinical experience with uPAR

uPAR's pathophysiological role in tumor progression and the association with DFS and OS in numerous solid tumor types make it an established prognostic target and potential aid in treatment stratification. Not surprisingly, the first phase II clinical trial demonstrating molecular imaging of uPAR was focused down this avenue: Fosbøl et al. have been able to discriminate prostate cancer patients in low-risk and intermediate-risk Gleason score based on standardized uptake values (SUV) of the uPAR targeting positron emission tomography (PET) ligand ^{68}Ga-NOTA-AE105 [31]. Similarly, in two different phase II clinical trials relapse-free survival has been predicted in patients with head and neck squamous cell carcinoma, and prognosis has been associated with uPAR in patients with neuroendocrine neoplasms using the same tracer [32, 33]. A fourth phase II clinical trial in patients with metastatic

castration-resistant prostate cancer undergoing radium-223 therapy had to be prematurely terminated because of inclusion challenges due to changes in treatment guidelines. However the acquired data showed an association between SUV_{max} of the index lesion and OS [34]. As the road has been paved for uPAR-based PET, it might be time for uPAR-based FGS to follow.

uPAR-based FGS

The clinical framework within which uPAR FGS has the most potential focusses on patient-groups where tumor margins are narrow and most at risk as uPAR's upregulation is often most prominent at the (invasive) tumor-stromal interface [30, 35]. For instance, irradical resection rates can be up to 60% for high risk squamous cell carcinomas of the head & neck (HNSSC) and are directly associated with poor patient outcomes. As uPAR is (over-) expressed in the majority of HNSSC patients (up to 100% of patients), uPAR FGS in the complicated head & neck surgical landscape is a promising avenue to lower irradical resection rates [29, 36, 37]. A similar case could be made for malignant gliomas, where maximal cytoreductive surgery is an essential part in the treatment process, but where it is achieved in less than 35% of cases without additional imaging and in 65% of patients with 5-aminolevulinic acid based intraoperative imaging [8, 38]. As uPAR is (over-)expressed in the majority of glioma's, targeting uPAR for FGS could potentially improve the negative margin rates [39-41].

Recently, FluoGuide, a clinical stage biotechnology company focused on FGS that is translating a uPAR targeting fluorescent peptide towards the clinic, confirmed the uPAR approach by reporting a first-in-human study using the uPAR targeting peptide FG001 (AE105-Glu-Glu-ICG) for the visualization of malignant gliomas. In this open-label, non-randomized, dose-escalation phase I/IIa study FG001 was deemed safe and resulted in TBRs of approximately 2.3 (1.8-2.6) with the Orbeye camera system and 3.5 (2.8-4.6) with the Zeiss Pentero C camera system. The specificity, sensitivity, positive-predictive value and negative-predictive value were 100% (59-100%), 79% (58-93%), 100% (82-100%) and 58% (28-85%), respectively [42]. Based on these results, FluoGuide has commenced with phase IIb studies in high grade glioma patients and initiated phase IIa trials in patients with lung cancer and head & neck cancer (EudraCT number 2022-0013612-12, 2021-004389-37).

uPAR FGS compared to other targets

uPAR is a versatile target that has, as outlined above, potential as FGS target for various tumor types where local tumor margins are at risk. Obviously, uPAR is not the only target that is being studied. The key question is how uPAR performs compared to other targets for the clinical frameworks previously identified?

Although alternative targets exists, adequately comparing targets is challenging. The literature that exists is mostly based on immunohistochemical (IHC) methods, and studies comparing targets in *in vivo* or clinical settings are practically non-existent[43-48]. Therefore, it is important to be aware of the biases and/or limitations of IHC studies. First-of-all, as Ahn et al. so eloquently demonstrated using different monoclonal antibodies targeting the same receptor can result in two very contrasting expression patterns [49]. Secondly, the tissue origin is of utmost important as Serpa et al. show that expression patterns differs significantly between location: 76.7% of cases were positive at the invasion front but only 48.4% at the tumor core [50]. Lastly, studies differ in scoring systems and what accounts a positive score. A close look needs to be taken whether only epithelial cells are scored or also the stromal compartment, and what percentage of cells should show expression for a positive expression score.

Despite the limitations, Table 2 compares the expression pattern of uPAR with other promising targets for the uPAR clinical frameworks identified earlier. For most indications alternative targets can be found with similar expression rates on tumor tissue. However, unlike uPAR[3], these alternatives often have significant expression in normal tissue, potentially increasing background fluorescence [30]. For example, as identified in **Chapter 3,** both integrin $\alpha_v ß_6$ and EGFR are weakly to highly expressed on normal squamous epithelium, whereas uPAR is absent. Furthermore, another advantage of uPAR is that it is also expressed on the tumor-associated stromal compartment whereas integrin $\alpha_v ß_6$, EGFR, CEA, EpCAM, and prostate-specific membrane antigen (PSMA) are solely expressed on the tumor compartment [49-51]. The challenge, however, with targeting uPAR is its heterogenous pattern of expression. Whether this heterogeneity is relevant, as high uPAR is often expressed at FGS sites like tumor border, or impairing like less prominent presence in tumor cores, remains to be evaluated [50]. Table 3 compares targets for the clinical frameworks where uPAR has less potential.

3 In normal tissue, uPAR expression is mostly limited to bone-marrow derived white blood cells, pulmonary alveoli, glomeruli and a sporadic endothelial cell. In healthy individuals, uPAR is not critical for normal physiology. uPAR becomes upregulated in tissues undergoing active remodeling such as during wound-healing, embryo implantation or mammary gland involution [29].

Table 2. Comparison of uPAR to other potential targets for the clinical frameworks where uPAR has been identified as being promising.

Target	Potential Tracer	Remarks
Glioma		
uPAR	FG001 *FG002* *huATN658-IRDye800CW** *huNb2-IRDye800CW*	⊕ 95% elevated uPAR expression [41] ⊕ Specificity 79%, Sensitivity 100%, PPV 100%, NPV 58% [42] ⊕ Average TBR 2.3-3.5 [42] ⊕/⊖ Heterogenous staining pattern [40]
Chlorotoxin derived peptide	BLZ-100	⊕ 6/6 (100%) high-grade tumors fluorescence [52] ⊕/⊖ Unclear binding mechanism [52]
EGFR	Cetuximab-IRDye800CW Panitumumab-IRDye800CW ABY-029	⊕ Overexpressed in 54-80% of patients [53-55] ⊕ Expression decreased in normal brain tissue [56] ⊕ TBR 4.0 ± 0.5 [56]
Head & neck cancer		
uPAR	See above	⊕ Expressed in 64-100% of primary tumors [36, 37, 57] ⊕ Expressed on both tumor and tumor-surrounding stromal cells [36, 37, 57] ⊕ Absent on normal squamous epithelium and adnexa [36, 37, 57] ⊕/⊖ Expression can be heterogenous [36, 37]
Integrin $\alpha_v ß_6$	*R01-MG-IRDye800CW**	⊕ Expressed in 87-95% of primary tumors [36, 58] ⊕/⊖ Low to moderate expression on normal squamous epithelium and adnexa [36, 58]
EGFR	See above	⊕ Expressed in 100% of primary tumors [36, 37] ⊖ High expression on normal squamous epithelium and adnexa [36, 37]
Pancreatic cancer		
uPAR	See above	⊕ Expressed in 67-82% of patients [43, 59] ⊕ Significantly overexpressed compared to chronic pancreatitis [44] ⊕ Expressed on both tumor and tumor-surrounding stromal cells [44, 59] ⊕ Complete absence of staining in normal pancreatic tissue [44] ⊖ High uPAR expression in negative lymph nodes [44]
Integrin $\alpha_v ß_6$	See above	⊕ Highly expressed in 88% patients [43] ⊕ Sensitivity of 84% and specificity of 100% for tumor lymph nodes [44] ⊕ Significantly overexpressed compared to chronic pancreatitis ⊖ Moderate staining in normal ductal structures [44]
CEA	SGM-101	⊕ Highly expressed in 71% of patients [43] ⊕ Completely absent in normal pancreatic parenchyma [44] ⊕ Significantly overexpressed compared to chronic pancreatitis ⊕ Sensitivity of 68% and specificity of 100% for tumor lymph nodes [44] ⊖ Heterogenous expression and loss of expression after neoadjuvant treatment [44]

Table 2. Continued.

Target	Potential Tracer	Remarks
Ovarian cancer		
uPAR	See above	⊕ Expressed in >80% of patients in 7/9 studies [60] ⊕ Expression independent of histology [60] ⊕ Expressed predominantly on tumor cells but also on tumor-surrounding stromal cells [60] ⊕ Expression low to absent on benign tissue [60] ⊕ No difference in expression between primary and metastatic lesions [60]
Folate-receptor	OTL38	⊕ Overexpressed in 72-97% of patients [61, 62] ⊕Additional lesions not detected by white light in 33% of patients [63] ⊕ Sensitivity 83% (0.74-0.89) [63] ⊖ Lesion false-positive 32.7% [63]
EpCAM	*R01-MG-IRDye800CW*	⊕ Overexpressed in 78-88% of lesions [64, 65] ⊕ Sensitivity 88%, specificity 100%, PPV 100%, NPV 94% for tumor-positive lymph nodes [65] ⊕/⊖ Overexpression rate dependent of histology [64] ⊖ Low to high expression on normal epithelium of the digestive tract [66]
Prostate		
uPAR	See above	⊕ Overexpressed in 64% of primary tissue and in >90% of lymph node metastases [67] ⊕ Not expressed in normal prostate or benign tissue [67, 68] ⊕ Expressed on tumor associated stromal cells [67, 68] ⊖ Expression can be heterogenous [67, 68]
PSMA	*OTL78*	⊕ Expressed in 80-96% of primary tumors and 84% of metastases [69, 70] ⊕/⊖ Expressed in the small intestine, proximal renal tubules, and salivary and lacrimal glands [71] ⊖ Expressed in normal prostate epithelium [71]
Bladder		
uPAR	See above	⊕ Expressed on 96% of tumors [72] ⊕ Expressed particularly at the invasive front [72] ⊕ Expression independent of grade and stage [72] ⊕ Expressed on tumor associated stromal cells [72] ⊕ Absent in normal bladder epithelium [72, 73] ⊕/⊖ Expression can be heterogenous [73]
Protoporphyrin IX precursors	HAL 5-ALA	⊕ Relative reduction of 16-20% (56 vs. 47%; $p<0.026$) in recurrence after transurethral resection [73, 74] ⊕ 7-32% additional patients identified ($p<0.0001$) [73, 74] ⊕ Intravesical application [74] ⊖ Not suitable for radical cystectomy

* tracers in italics are in preclinical development stage

Table 3. Comparison of potential FGS targets and their tracers, where uPAR has less potential

Target	Potential Tracer	Remarks
Lung		
Non-targeted	ICG	⊕ Sensitivity 86.4-89.3%, 11.8-18.2 false-positive [77] ⊕ Detects additional lesions (9/14 malignant) [77] ⊖ 9.1-13% false negative [77]
Folate receptor	OTL38	⊕ 72-87% of lung adenocarcinomas [77] ⊖ 13-57% of lung squamous cell carcinomas [77] ⊕ Sensitivity 84% in adenocarcinomas and 58% in squamous cell carcinomas [78, 79] ⊕ 56.3-100% of fluorescent margins true positives [80-82] ⊖ No difference in TBR between malignant and benign lesions [83]
Breast cancer		
Cathepsin activity	LUM015	⊕ Adequate fluorescence for tumor detection in 87-100% of patients [84, 85] ⊕ Signal not dependent on tumor subtype ⊕ Specificity 73% [84, 85] ⊕ Sensitivity for residual tumor detection 100% [84, 85]
Proteolytic activity	AVB-620	⊕ Signal not dependent on tumor subtype [86] ⊕ Specificity 78% [86] ⊕ Lumpectomy re-excision rate 6% as opposed to 20-40% [86] ⊕ 75% additional positive margins detected [86]
Esophagus		
EpCAM	*VB5-845D-800CW**	⊕ Expressed in 98% - 100% of primary tumors [87, 88] ⊕ Expressed in 100% of residual tumor tissue after neoadjuvant chemoradiotherapy [87] ⊕ Tumor-to-normal ratio >10 [87] ⊕/⊖ Low to moderate expression in normal epithelial tissue [87, 88]
CEA	SGM-101	⊕ Tumor-to-normal ratio 3.62 [87] ⊕/⊖ Expressed in 54% of primary tumors [87] ⊕/⊖ Low to moderate expression in normal epithelial tissue [87]
Primary and secondary liver cancer		
Non-targeted	ICG	⊕ Suitable for all primary and secondary liver lesions [89, 90] ⊕ Tumor negative margins in 88% of lesions with no fluorescence in wound bed vs. 0% of lesions with fluorescence in wound bed [91]
CEA	SGM-101	⊕/⊖ Suitable for secondary liver lesions where the primary is known to express CEA (i.e. colorectal and pancreatic metastases → 89% true positive) [92]
Colorectal		
CEA	SGM-101	⊕ Overexpressed in 98.8% of tumors compared to matched normal tissue [93] ⊕ Expression on healthy tissue is on average 60 times lower [11] ⊕ CEA expression is not altered after chemoradiotherapy [94]
EpCAM	*VB5-845D-800CW*	⊕ Overexpressed in 94-97.7% of tumors [64, 94, 95] ⊕ EpCAM expression is not altered after chemoradiotherapy [94] ⊕/⊖ EpCAM is also expressed in normal tissue [96]

* tracers in italics are in preclinical development stage

uPAR FGS indications beyond oncology

uPAR expression is not unique to cancer and, as elaborated on in **Chapter 4**, uPAR plays a relevant pathophysiological role in a multitude of other diseases, including atherosclerosis, rheumatoid arthritis (RA), Alzheimer's disease, multiple sclerosis, and inflammatory bowel disease. There are currently no clear indications

for uPAR FGS beyond oncology. However, there are a couple avenues to explore where uPAR non-invasive molecular imaging deserves further exploration. Just recently, in a proof-of-concept retrospective analysis study, Khare et al. were able to clinically visualize heterogenous uptake of [^{64}Cu]Cu-DOTA-AE105 on PET/CT in atherosclerotic lesions of the large conductive arteries of ten cancer patients enrolled in the phase I clinical trial of the respective tracer [75]. While this study suggests the feasibility of atherosclerotic imaging via uPAR, further properly powered studies will need to demonstrate the clinically utility. Another potential avenue worth exploring is that of therapy (de-) escalation of RA. uPAR plays an essential role in disease pathophysiology and RA activity is correlated with plasma levels of soluble uPAR, derived from uPAR expressing cells [76]. A rather simple urine or plasma ELISA for uPAR could aid clinicians in proper managing of RA. Compared to cancer, our understanding of uPAR in these various diseases is limited[4] and as our understanding expands, additional diagnostic, prognostic, and therapeutic opportunities will present themselves.

Part III. Enhancing tumor contrast by smart tracer design

The primary aim of a molecular imaging tracer is delivering the NIR fluorescent agent to the target site. Rapid clearance from irrelevant sites is therefor of key importance to achieve high contrasts between the target site and the adjacent tissue. Characteristics, such as molecular weight, affinity, 3D confirmation, charge, and conjugation method of the tracer play a pivotal role in creating this contrast as these characteristics play a determining factor in tracer distribution and kinetics. Therefore, in **Chapters 5-8** exceedingly smaller antibody-based uPAR targeting tracers have been developed in order to identify the most appropriate construct for FGS to apply into the clinic. This intermezzo is not specific for uPAR but explains basic characteristics of tracer design which are employed in **Chapters 6-8**.

4 A PubMed search on "uPAR" and "Cancer" yields more than 1700 entries while searches on "uPAR" and "atherosclerosis", "uPAR" and "rheumatoid arthritis", "uPAR" and "Alzheimer", "uPAR" and "multiple sclerosis", and "uPAR" and "inflammatory bowel disease" result in 68, 27, 13, 10 and 7 results respectively. Date of search: July 2022.

The influence of molecular weight on tumor signal

There exists an inverted bell-shaped trade-off between molecular weight and tumor accumulation when comparing molecular imaging tracers with similar target affinities [97]. Underlying variables, amongst others, of this relationship are tracer diffusion/extravasation (i.e. tumor uptake) and clearance (i.e. tracer removal). Diffusion is the net movement of molecules from regions of high concentration to regions of low concentration and the speed of this is inversely proportional to the molecular radius [98]. Therefore, smaller tracers such as $F(ab')_2$s (≈110 kDa), Fabs (≈55kDa) and VHHs (≈15kDa) are expected to diffuse more rapidly into tissue than full-sized antibodies (≈150kDa). Where improving diffusion stimulates tumor uptake, improving clearance reduces this. Clearance can be modulated by decreasing molecular weight, so that tracers fall below the size cut-off for glomerular filtration by the kidneys, estimated between 30-50 kDa, and by removing Fc-domains so that Fc receptor-mediated recycling is bypassed [99]. Importantly, in modeling and *in vivo* studies there exists an impasse around 25-50 kDa, where the improved diffusion offered by decrease in tracer radius is not compensated in proportion for the rapid renal clearance that starts occurring at this molecular weight, resulting in lower signal intensities than tracers with larger or smaller molecular weights [100-107].

The influence of affinity on tumor signal

Where molecular weight influences tumor uptake and clearance from the circulation, affinity keeps a tracer in the tumor. Improving affinity, up to a plateau level (for antibodies around 10n*M* K_d), improves signal intensity linearly[5]. This plateau level increases with decreasing molecular size [108-112]. High affinities are especially relevant for small compounds, such as peptides, as their rapid diffusion into the tumor also means they rapidly diffuse out of the tumor. Therefore relatively small peptides are dependent on high affinities to be retained. Modelling studies show that peptides need approximately a hundred-fold higher affinity to keep them anchored to the tumor and achieve similar signal intensities than the much larger monoclonal antibodies [97].

The influence of conjugation method on tumor signal

Next to molecular weight and affinity, the method of conjugating the contrast agent with the tracer is a third component that can influence imaging results dramatically.

5 It is relevant to realize that while improving affinity above the threshold might not improve tracer accumulation there can be other effects achieved with higher affinities. For instance, in the case of antibody-directed cellular cytotoxicity higher affinities do result in more effective treatment [35].

Conjugation can be either non-specific (free amine-groups) or site-specific. While the former is both rapid and easy, it results in heterogenous products with potential modifications on or near complementarity-determining regions potentially altering binding affinity and specificity [113]. This random effect increases with the degree-of-labelling (DoL) and defining a DoL that balances fluorescence intensity and potential pharmacokinetic effects (increased clearance, increased liver uptake) is crucial. Current studies set the optimal DoL around 0.3 - 2.0 for antibodies[6] [114-116]. The alternative, site-specific labelling, ensures a more homogenous end-product with superior plasma stability, binding efficiency, and tumor uptake [113]. This effect is more pronounced for smaller antibody-based compounds where, for example, non-site-specific labelled nanobodies resulted in a lack of specific tumor signal at a DoL of 1.1 – 1.4 compared to site-specific labelled nanobodies with a DoL of 1.0 [117]. Disadvantages for site-specific conjugation are the more challenging purification methods needed and potential of 3D-damage to the tracer. Peptides are in principle always site specifically labelled.

The influence of tracer design on logistics

An important last argument, especially for advocates of smaller tracers such as peptides and nanobodies, is the clinical logistics, as their rapid clearance allows same-day imaging [118, 119]. In FGS clinical trials, antibodies and even tracers as small as Fabs have to be administered 3-5 days prior to surgery in order to achieve adequate fluorescence contrast between target sites and the background, while the much smaller peptides can be administered the same day, minutes to hours before surgery [5, 120, 121]. Practically this difference translates to patients being burdened with an additional hospital visit when receiving tracers that are not amendable to same-day imaging [118]. The production also differs between antibody-based productions and peptides. The latter are made in non-biological systems resulting in possible favorable safety profiles and lower production costs [122]. It should be clear that while optimizing patient experience and keeping costs low is important, logistics should not be the deciding factor, unless two tracers clinically give similar results.

6 Non-site specific labelling follows a Poisson distribution. *In vivo*, fluorescence, however, is skewed towards antibodies with several dyes as antibodies with no dyes are not fluorescent and antibodies with two or more dyes are approximately twice as fluorescent (or more). At an DoL of 1.2 70% of the fluorescence comes from antibodies with 2 or more dyes [47]. Therefore, over-labelling is a serious issue that influences signal specificity. Our group aims for a DoL of 0.9 – 1.5.

Identifying optimal tracer characteristics

In conclusion, selecting optimal tracer characteristics for FGS requires, amongst others, balancing molecular weight, affinity and conjugation methods. First-of-all, site-specific conjugation is preferred for all tracers and essential for smaller tracers. Secondly, higher affinities are more crucial for smaller tracers than larger ones. Thirdly, a molecular weight between 20-50kDa should be avoided as this range leads to inferior signal intensities compared to tracers that are larger or smaller. Logistics and production costs can play a further role in identifying the optimal tracer by categorizing tracers into two groups: same-day vs. different-day imaging. Tracers larger than 20-50kDa fall into the different-day imaging. Here, in vivo comparative studies show higher peak tumor fluorescence for antibodies than their constructs, a quality that is imperative in identifying smaller tumor lesions, and therefore have an advantage. There is practically no data comparing different tracers < 20kDa and therefore an ideal construct in the same-day imaging category is hard to identify.

In **Chapters 6-7** an uPAR targeting monoclonal antibody, F(ab')2, and Fab, were introduced *in vivo* (Figure 1A). The major difference between these structures was their molecular weight, as their affinities for uPAR were equal or similar and labelling methods were the same. The difference in molecular weight (molecular weights: IgG, 150kDa; F(ab')2, 110kDa; Fab, 55kDa) lead to differing absolute tumor signal (Figure 1B). It was highest for the monoclonal antibody and it was significantly lower for the F(ab')2 and Fab. While a high absolute signal improves sensitivity, ultimately, a clear contrast between tumor and background tissue is needed for accurate intraoperative visualization. This is contrast is generally reported as the tumor-to-background ratio (TBR), where a ratio higher than 1.5 is deemed permissible and above 2.0 preferred [123]. TBRs did not differ between the tracers. Furthermore, the ideal imaging window differed between the tracers where tumors could be imaged within 24hrs for the Fab, 36hrs for the F(ab')2 and 72hrs for the full-sized antibody. In this comparison, the monoclonal antibody is the most ideal candidates to develop into clinical constructs as it results in the best imaging at the expense of larger imaging window.

How do the uPAR targeting tracers developed in this thesis compare to the uPAR targeting peptide AE105-Glu-Glu-ICG currently in clinical trials? In terms of imaging characteristics AE105-Glu-Glu-ICG has a rapid imaging window allowing same-day imaging and reported TBRs of 2.3 [42]. However, the superior binding characteristics of an antibody-based construct and the use of a brighter fluorophore (IRDye800CW vs. ICG) could potentially lead to higher absolute tumor signals for the monoclonal antibody compared to the peptide[7] [118, 122, 124]. Whether this is true can only be determined in a direct comparison between the various uPAR targeting tracers.

7 FluoGuide has recently started developing a variant of AE105 conjugated with IRDye800CW with the aim of improving the peptides TBR [124].

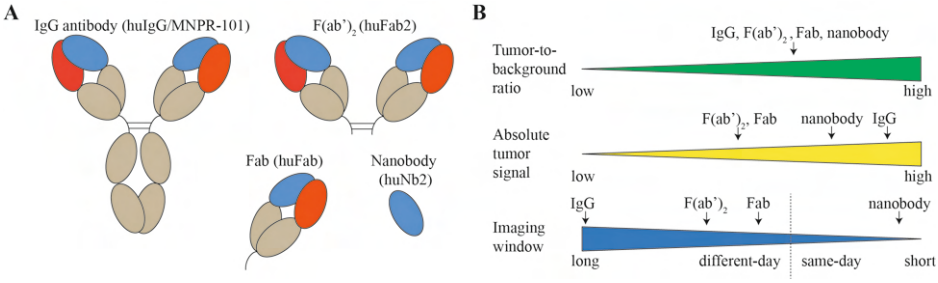

Figure 1. Comparison of various targeting FGS tracers. (A) Schematic representation of a IgG, F(ab')2, and Fab (B) Schematic representing differences in the outcomes tumor-to-background ratio, absolute tumor signal and imaging window between the different uPAR targeting tracers mentioned in this thesis. Peptide was not included on the absolute tumor signal scale as this cannot be reliably compared between different NIR-camera systems.

Conclusion

The field of uPAR research has come a long way since its initial discovery as a cell-based binding site for urokinase. Its role has greatly expanded from mere urokinase receptor to a central orchestrator of a multitude of pathways covering, amongst other things, cell proliferation, differentiation, and migration. While its intricacies are still being unraveled as we speak, its association with disease is undeniable. The immunohistochemical, in vivo and phase I/II clinical evidence gathered over the last two decades supports uPAR as a promising next generational target for FGS; in conclusion, the time is ripe for translating our preclinical knowledge of uPAR FGS to the clinic.

References

1. van Dam GM, Themelis G, Crane LM, Harlaar NJ, Pleijhuis RG, Kelder W, et al. Intraoperative tumor-specific fluorescence imaging in ovarian cancer by folate receptor-α targeting: first in-human results. Nat Med. 2011;17:1315-9. doi:10.1038/nm.2472.
2. Tanyi JL, Randall LM, Chambers SK, Butler KA, Winer IS, Langstraat CL, et al. A Phase III Study of Pafolacianine Injection (OTL38) for Intraoperative Imaging of Folate Receptor-Positive Ovarian Cancer (Study 006). Journal of clinical oncology : official journal of the American Society of Clinical Oncology. 2022:Jco2200291. doi:10.1200/jco.22.00291.
3. Hernot S, van Manen L, Debie P, Mieog JSD, Vahrmeijer AL. Latest developments in molecular tracers for fluorescence image-guided cancer surgery. The Lancet Oncology. 2019;20:e354-e67. doi:10.1016/s1470-2045(19)30317-1.
4. Eskander RN, Kauderer J, Tewari KS, Mannel RS, Bristow RE, O'Malley DM, et al. Correlation between Surgeon's assessment and radiographic evaluation of residual disease in women with advanced stage ovarian cancer reported to have undergone optimal surgical cytoreduction: An NRG Oncology/Gynecologic Oncology Group study. Gynecologic oncology. 2018;149:525-30. doi:10.1016/j.ygyno.2018.03.043.
5. Hoogstins CE, Tummers QR, Gaarenstroom KN, de Kroon CD, Trimbos JB, Bosse T, et al. A Novel Tumor-Specific Agent for Intraoperative Near-Infrared Fluorescence Imaging: A Translational Study in Healthy Volunteers and Patients with Ovarian Cancer. Clinical cancer research : an official journal of the American Association for Cancer Research. 2016;22:2929-38. doi:10.1158/1078-0432.Ccr-15-2640.
6. Tipirneni KE, Warram JM, Moore LS, Prince AC, de Boer E, Jani AH, et al. Oncologic Procedures Amenable to Fluorescence-guided Surgery. Annals of surgery. 2017;266:36-47. doi:10.1097/sla.0000000000002127.
7. Li MM, Puram SV, Silverman DA, Old MO, Rocco JW, Kang SY. Margin Analysis in Head and Neck Cancer: State of the Art and Future Directions. Annals of surgical oncology. 2019;26:4070-80. doi:10.1245/s10434-019-07645-9.
8. Stummer W, Pichlmeier U, Meinel T, Wiestler OD, Zanella F, Reulen HJ. Fluorescence-guided surgery with 5-aminolevulinic acid for resection of malignant glioma: a randomised controlled multicentre phase III trial. The Lancet Oncology. 2006;7:392-401. doi:10.1016/s1470-2045(06)70665-9.
9. van Gijn W, Marijnen CA, Nagtegaal ID, Kranenbarg EM, Putter H, Wiggers T, et al. Preoperative radiotherapy combined with total mesorectal excision for resectable rectal cancer: 12-year follow-up of the multicentre, randomised controlled TME trial. The Lancet Oncology. 2011;12:575-82. doi:10.1016/s1470-2045(11)70097-3.
10. Hoadley KA, Yau C, Hinoue T, Wolf DM, Lazar AJ, Drill E, et al. Cell-of-Origin Patterns Dominate the Molecular Classification of 10,000 Tumors from 33 Types of Cancer. Cell. 2018;173:291-304.e6. doi:10.1016/j.cell.2018.03.022.
11. Boonstra MC, de Geus SW, Prevoo HA, Hawinkels LJ, van de Velde CJ, Kuppen PJ, et al. Selecting Targets for Tumor Imaging: An Overview of Cancer-Associated Membrane Proteins. Biomarkers in cancer. 2016;8:119-33. doi:10.4137/bic.S38542.
12. Landercasper J, Whitacre E, Degnim AC, Al-Hamadani M. Reasons for re-excision after lumpectomy for breast cancer: insight from the American Society of Breast Surgeons Mastery(SM) database. Annals of surgical oncology. 2014;21:3185-91. doi:10.1245/s10434-014-3905-1.
13. Predina JD, Keating J, Patel N, Nims S, Singhal S. Clinical implications of positive margins following non-small cell lung cancer surgery. Journal of surgical oncology. 2016;113:264-9. doi:10.1002/jso.24130.

14. Schlick CJR, Khorfan R, Odell DD, Merkow RP, Bentrem DJ. Margin Positivity in Resectable Esophageal Cancer: Are there Modifiable Risk Factors? Annals of surgical oncology. 2020;27:1496-507. doi:10.1245/s10434-019-08176-z.
15. Fretland Å A, Dagenborg VJ, Bjørnelv GMW, Kazaryan AM, Kristiansen R, Fagerland MW, et al. Laparoscopic Versus Open Resection for Colorectal Liver Metastases: The OSLO-COMET Randomized Controlled Trial. Annals of surgery. 2018;267:199-207. doi:10.1097/sla.0000000000002353.
16. Allen VB, Gurusamy KS, Takwoingi Y, Kalia A, Davidson BR. Diagnostic accuracy of laparoscopy following computed tomography (CT) scanning for assessing the resectability with curative intent in pancreatic and periampullary cancer. The Cochrane database of systematic reviews. 2016;7:Cd009323. doi:10.1002/14651858.CD009323.pub3.
17. Lwin TM, Hoffman RM, Bouvet M. The development of fluorescence guided surgery for pancreatic cancer: from bench to clinic. Expert review of anticancer therapy. 2018;18:651-62. doi:10.1080/14737140.2018.1477593.
18. de Gooyer JM, Elekonawo FMK, Bremers AJA, Boerman OC, Aarntzen E, de Reuver PR, et al. Multimodal CEA-targeted fluorescence and radioguided cytoreductive surgery for peritoneal metastases of colorectal origin. Nature communications. 2022;13:2621. doi:10.1038/s41467-022-29630-9.
19. Yossepowitch O, Briganti A, Eastham JA, Epstein J, Graefen M, Montironi R, et al. Positive surgical margins after radical prostatectomy: a systematic review and contemporary update. European urology. 2014;65:303-13. doi:10.1016/j.eururo.2013.07.039.
20. van Rhijn BW, Burger M, Lotan Y, Solsona E, Stief CG, Sylvester RJ, et al. Recurrence and progression of disease in non-muscle-invasive bladder cancer: from epidemiology to treatment strategy. European urology. 2009;56:430-42. doi:10.1016/j.eururo.2009.06.028.
21. Dotan ZA, Kavanagh K, Yossepowitch O, Kaag M, Olgac S, Donat M, et al. Positive surgical margins in soft tissue following radical cystectomy for bladder cancer and cancer specific survival. J Urol. 2007;178:2308-12; discussion 13. doi:10.1016/j.juro.2007.08.023.
22. Ahn SB, Mohamedali A, Pascovici D, Adhikari S, Sharma S, Nice EC, et al. Proteomics Reveals Cell-Surface Urokinase Plasminogen Activator Receptor Expression Impacts Most Hallmarks of Cancer. Proteomics. 2019;19:e1900026. doi:10.1002/pmic.201900026.
23. Hanahan D. Hallmarks of Cancer: New Dimensions. Cancer Discov. 2022;12:31-46. doi:10.1158/2159-8290.Cd-21-1059.
24. Hanahan D, Weinberg RA. Hallmarks of cancer: the next generation. Cell. 2011;144:646-74. doi:10.1016/j.cell.2011.02.013.
25. Hanahan D, Weinberg RA. The hallmarks of cancer. Cell. 2000;100:57-70. doi:10.1016/s0092-8674(00)81683-9.
26. Saldanha RG, Xu N, Molloy MP, Veal DA, Baker MS. Differential proteome expression associated with urokinase plasminogen activator receptor (uPAR) suppression in malignant epithelial cancer. Journal of proteome research. 2008;7:4792-806. doi:10.1021/pr800357h.
27. Mahmood N, Mihalcioiu C, Rabbani SA. Multifaceted Role of the Urokinase-Type Plasminogen Activator (uPA) and Its Receptor (uPAR): Diagnostic, Prognostic, and Therapeutic Applications. Frontiers in oncology. 2018;8:24. doi:10.3389/fonc.2018.00024.
28. Smith HW, Marshall CJ. Regulation of cell signalling by uPAR. Nature reviews Molecular cell biology. 2010;11:23-36. doi:10.1038/nrm2821.
29. Boonstra MC, Verspaget HW, Ganesh S, Kubben FJ, Vahrmeijer AL, van de Velde CJ, et al. Clinical applications of the urokinase receptor (uPAR) for cancer patients. Current pharmaceutical design. 2011;17:1890-910. doi:10.2174/138161211796718233.

30. Leth JM, Ploug M. Targeting the Urokinase-Type Plasminogen Activator Receptor (uPAR) in Human Diseases With a View to Non-invasive Imaging and Therapeutic Intervention. Frontiers in cell and developmental biology. 2021;9:732015. doi:10.3389/fcell.2021.732015.
31. Fosbøl M, Kurbegovic S, Johannesen HH, Røder MA, Hansen AE, Mortensen J, et al. Urokinase-Type Plasminogen Activator Receptor (uPAR) PET/MRI of Prostate Cancer for Noninvasive Evaluation of Aggressiveness: Comparison with Gleason Score in a Prospective Phase 2 Clinical Trial. Journal of nuclear medicine : official publication, Society of Nuclear Medicine. 2021;62:354-9. doi:10.2967/jnumed.120.248120.
32. Carlsen EA, Loft M, Loft A, Berthelsen AK, Langer SW, Knigge U, et al. Prospective phase II trial of prognostication by (68)Ga-NOTA-AE105 uPAR PET in patients with neuroendocrine neoplasms: Implications for uPAR targeted therapy. Journal of nuclear medicine : official publication, Society of Nuclear Medicine. 2022. doi:10.2967/jnumed.121.263177.
33. Risør LM, Clausen MM, Ujmajuridze Z, Farhadi M, Andersen KF, Loft A, et al. Prognostic value of Urokinase-type Plasminogen Activator Receptor (uPAR)-PET/CT in Head and Neck Squamous Cell Carcinomas and Comparison with (18)F-FDG-PET/CT: A single-center prospective study. Journal of nuclear medicine : official publication, Society of Nuclear Medicine. 2021. doi:10.2967/jnumed.121.262866.
34. Fosbøl M, Mortensen J, Petersen PM, Loft A, Madsen J, Kjaer A. uPAR PET/CT for Prognostication and Response Assessment in Patients with Metastatic Castration-Resistant Prostate Cancer Undergoing Radium-223 Therapy: A Prospective Phase II Study. Diagnostics (Basel). 2021;11. doi:10.3390/diagnostics11061087.
35. Baart VM, Houvast RD, de Geus-Oei LF, Quax PHA, Kuppen PJK, Vahrmeijer AL, et al. Molecular imaging of the urokinase plasminogen activator receptor: opportunities beyond cancer. EJNMMI Res. 2020;10:87. doi:10.1186/s13550-020-00673-7.
36. Baart VM, van Duijn C, van Egmond SL, Dijckmeester WA, Jansen JC, Vahrmeijer AL, et al. EGFR and αvβ6 as Promising Targets for Molecular Imaging of Cutaneous and Mucosal Squamous Cell Carcinoma of the Head and Neck Region. Cancers (Basel). 2020;12. doi:10.3390/cancers12061474.
37. Christensen A, Grønhøj C, Jensen JS, Lelkaitis G, Kiss K, Juhl K, et al. Expression patterns of uPAR, TF and EGFR and their potential as targets for molecular imaging in oropharyngeal squamous cell carcinoma. Oncol Rep. 2022;48. doi:10.3892/or.2022.8359.
38. Hadjipanayis CG, Widhalm G, Stummer W. What is the Surgical Benefit of Utilizing 5-Aminolevulinic Acid for Fluorescence-Guided Surgery of Malignant Gliomas? Neurosurgery. 2015;77:663-73. doi:10.1227/neu.0000000000000929.
39. Gilder AS, Natali L, Van Dyk DM, Zalfa C, Banki MA, Pizzo DP, et al. The Urokinase Receptor Induces a Mesenchymal Gene Expression Signature in Glioblastoma Cells and Promotes Tumor Cell Survival in Neurospheres. Sci Rep. 2018;8:2982. doi:10.1038/s41598-018-21358-1.
40. Salajegheh M, Rudnicki A, Smith TW. Expression of urokinase-type plasminogen activator receptor (uPAR) in primary central nervous system neoplasms. Appl Immunohistochem Mol Morphol. 2005;13:184-9. doi:10.1097/01.pai.0000138448.85231.da.
41. Persson M, Nedergaard MK, Brandt-Larsen M, Skovgaard D, Jørgensen JT, Michaelsen SR, et al. Urokinase-Type Plasminogen Activator Receptor as a Potential PET Biomarker in Glioblastoma. Journal of nuclear medicine : official publication, Society of Nuclear Medicine. 2016;57:272-8. doi:10.2967/jnumed.115.161703.
42. FluoGuide. Presentation of FG001 results from the first clinical trial in aggressive brain cancer. youtube; 2022.

43. de Geus SW, Boogerd LS, Swijnenburg RJ, Mieog JS, Tummers WS, Prevoo HA, et al. Selecting Tumor-Specific Molecular Targets in Pancreatic Adenocarcinoma: Paving the Way for Image-Guided Pancreatic Surgery. Mol Imaging Biol. 2016;18:807-19. doi:10.1007/s11307-016-0959-4.
44. Tummers WS, Farina-Sarasqueta A, Boonstra MC, Prevoo HA, Sier CF, Mieog JS, et al. Selection of optimal molecular targets for tumor-specific imaging in pancreatic ductal adenocarcinoma. Oncotarget. 2017;8:56816-28. doi:10.18632/oncotarget.18232.
45. Rijs Z, Shifai AN, Bosma SE, Kuppen PJK, Vahrmeijer AL, Keereweer S, et al. Candidate Biomarkers for Specific Intraoperative Near-Infrared Imaging of Soft Tissue Sarcomas: A Systematic Review. Cancers (Basel). 2021;13. doi:10.3390/cancers13030557.
46. Linders D, Deken M, van der Valk M, Tummers W, Bhairosingh S, Schaap D, et al. CEA, EpCAM, αvβ6 and uPAR Expression in Rectal Cancer Patients with a Pathological Complete Response after Neoadjuvant Therapy. Diagnostics (Basel). 2021;11. doi:10.3390/diagnostics11030516.
47. Linders DGJ, Bijlstra OD, Fallert LC, Hilling DE, Walker E, Straight B, et al. Cysteine Cathepsins in Breast Cancer: Promising Targets for Fluorescence-Guided Surgery. Mol Imaging Biol. 2022. doi:10.1007/s11307-022-01768-4.
48. Houvast RD, Thijse K, Groen JV, Chua J, Vankemmelbeke M, Durrant LG, et al. An Immunohistochemical Evaluation of Tumor-Associated Glycans and Mucins as Targets for Molecular Imaging of Pancreatic Ductal Adenocarcinoma. Cancers (Basel). 2021;13. doi:10.3390/cancers13225777.
49. Ahn SB, Chan C, Dent OF, Mohamedali A, Kwun SY, Clarke C, et al. Epithelial and stromal cell urokinase plasminogen activator receptor expression differentially correlates with survival in rectal cancer stages B and C patients. PloS one. 2015;10:e0117786. doi:10.1371/journal.pone.0117786.
50. Serpa MS, Mafra RP, Queiroz S, Silva LPD, Souza LB, Pinto LP. Expression of urokinase-type plasminogen activator and its receptor in squamous cell carcinoma of the oral tongue. Braz Oral Res. 2018;32:e93. doi:10.1590/1807-3107bor-2018.vol32.0093.
51. Oh F, Modiano JF, Bachanova V, Vallera DA. Bispecific Targeting of EGFR and Urokinase Receptor (uPAR) Using Ligand-Targeted Toxins in Solid Tumors. Biomolecules. 2020;10. doi:10.3390/biom10060956.
52. Patil CG, Walker DG, Miller DM, Butte P, Morrison B, Kittle DS, et al. Phase 1 Safety, Pharmacokinetics, and Fluorescence Imaging Study of Tozuleristide (BLZ-100) in Adults With Newly Diagnosed or Recurrent Gliomas. Neurosurgery. 2019;85:E641-e9. doi:10.1093/neuros/nyz125.
53. Hatanpaa KJ, Burma S, Zhao D, Habib AA. Epidermal growth factor receptor in glioma: signal transduction, neuropathology, imaging, and radioresistance. Neoplasia. 2010;12:675-84. doi:10.1593/neo.10688.
54. Heimberger AB, Hlatky R, Suki D, Yang D, Weinberg J, Gilbert M, et al. Prognostic effect of epidermal growth factor receptor and EGFRvIII in glioblastoma multiforme patients. Clinical cancer research : an official journal of the American Association for Cancer Research. 2005;11:1462-6. doi:10.1158/1078-0432.Ccr-04-1737.
55. Bredel M, Pollack IF, Hamilton RL, James CD. Epidermal growth factor receptor expression and gene amplification in high-grade non-brainstem gliomas of childhood. Clinical cancer research : an official journal of the American Association for Cancer Research. 1999;5:1786-92.
56. Miller SE, Tummers WS, Teraphongphom N, van den Berg NS, Hasan A, Ertsey RD, et al. First-in-human intraoperative near-infrared fluorescence imaging of glioblastoma using cetuximab-IRDye800. J Neurooncol. 2018;139:135-43. doi:10.1007/s11060-018-2854-0.

57. Boonstra MC, Van Driel P, Keereweer S, Prevoo H, Stammes MA, Baart VM, et al. Preclinical uPAR-targeted multimodal imaging of locoregional oral cancer. Oral oncology. 2017;66:1-8. doi:10.1016/j.oraloncology.2016.12.026.
58. Ahmedah HT, Patterson LH, Shnyder SD, Sheldrake HM. RGD-Binding Integrins in Head and Neck Cancers. Cancers (Basel). 2017;9. doi:10.3390/cancers9060056.
59. de Geus SW, Baart VM, Boonstra MC, Kuppen PJ, Prevoo HA, Mazar AP, et al. Prognostic Impact of Urokinase Plasminogen Activator Receptor Expression in Pancreatic Cancer: Malignant Versus Stromal Cells. Biomark Insights. 2017;12:1177271917715443. doi:10.1177/1177271917715443.
60. Kenny HA, Leonhardt P, Ladanyi A, Yamada SD, Montag A, Im HK, et al. Targeting the urokinase plasminogen activator receptor inhibits ovarian cancer metastasis. Clinical cancer research : an official journal of the American Association for Cancer Research. 2011;17:459-71. doi:10.1158/1078-0432.Ccr-10-2258.
61. Markert S, Lassmann S, Gabriel B, Klar M, Werner M, Gitsch G, et al. Alpha-folate receptor expression in epithelial ovarian carcinoma and non-neoplastic ovarian tissue. Anticancer Res. 2008;28:3567-72.
62. Kalli KR, Oberg AL, Keeney GL, Christianson TJ, Low PS, Knutson KL, et al. Folate receptor alpha as a tumor target in epithelial ovarian cancer. Gynecologic oncology. 2008;108:619-26. doi:10.1016/j.ygyno.2007.11.020.
63. Tanyi JL, Chon HS, Morgan MA, Chambers SK, Han ES, Butler KA, et al. Phase 3, randomized, single-dose, open-label study to investigate the safety and efficacy of pafolacianine sodium injection (OTL38) for intraoperative imaging of folate receptor positive ovarian cancer. Journal of Clinical Oncology. 2021;39:5503-. doi:10.1200/JCO.2021.39.15_suppl.5503.
64. Spizzo G, Fong D, Wurm M, Ensinger C, Obrist P, Hofer C, et al. EpCAM expression in primary tumour tissues and metastases: an immunohistochemical analysis. Journal of clinical pathology. 2011;64:415-20. doi:10.1136/jcp.2011.090274.
65. Muynck L, Gaarenstroom KN, Sier CFM, Duijvenvoorde MV, Bosse T, Mieog JSD, et al. Novel Molecular Targets for Tumor-Specific Imaging of Epithelial Ovarian Cancer Metastases. Cancers (Basel). 2020;12. doi:10.3390/cancers12061562.
66. De Vos J, Devoogdt N, Lahoutte T, Muyldermans S. Camelid single-domain antibody-fragment engineering for (pre)clinical in vivo molecular imaging applications: adjusting the bullet to its target. Expert Opin Biol Ther. 2013;13:1149-60. doi:10.1517/14712598.2013.800478.
67. Cozzi PJ, Wang J, Delprado W, Madigan MC, Fairy S, Russell PJ, et al. Evaluation of urokinase plasminogen activator and its receptor in different grades of human prostate cancer. Hum Pathol. 2006;37:1442-51. doi:10.1016/j.humpath.2006.05.002.
68. Kumano M, Miyake H, Muramaki M, Furukawa J, Takenaka A, Fujisawa M. Expression of urokinase-type plasminogen activator system in prostate cancer: correlation with clinicopathological outcomes in patients undergoing radical prostatectomy. Urol Oncol. 2009;27:180-6. doi:10.1016/j.urolonc.2008.01.012.
69. Mannweiler S, Amersdorfer P, Trajanoski S, Terrett JA, King D, Mehes G. Heterogeneity of prostate-specific membrane antigen (PSMA) expression in prostate carcinoma with distant metastasis. Pathol Oncol Res. 2009;15:167-72. doi:10.1007/s12253-008-9104-2.
70. Bostwick DG, Pacelli A, Blute M, Roche P, Murphy GP. Prostate specific membrane antigen expression in prostatic intraepithelial neoplasia and adenocarcinoma: a study of 184 cases. Cancer. 1998;82:2256-61. doi:10.1002/(sici)1097-0142(19980601)82:11<2256::aid-cncr22>3.0.co;2-s.
71. Fendler WP, Eiber M, Beheshti M, Bomanji J, Ceci F, Cho S, et al. (68)Ga-PSMA PET/CT: Joint EANM and SNMMI procedure guideline for prostate cancer imaging: version 1.0. Eur J Nucl Med Mol Imaging. 2017;44:1014-24. doi:10.1007/s00259-017-3670-z.

72. Dohn LH, Pappot H, Iversen BR, Illemann M, Høyer-Hansen G, Christensen IJ, et al. uPAR Expression Pattern in Patients with Urothelial Carcinoma of the Bladder--Possible Clinical Implications. PloS one. 2015;10:e0135824. doi:10.1371/journal.pone.0135824.
73. Baart VM, van der Horst G, Deken MM, Bhairosingh SS, Schomann T, Sier VQ, et al. A multimodal molecular imaging approach targeting urokinase plasminogen activator receptor for the diagnosis, resection and surveillance of urothelial cell carcinoma. European journal of cancer (Oxford, England : 1990). 2021;146:11-20. doi:10.1016/j.ejca.2021.01.001.
74. Stenzl A, Burger M, Fradet Y, Mynderse LA, Soloway MS, Witjes JA, et al. Hexaminolevulinate guided fluorescence cystoscopy reduces recurrence in patients with nonmuscle invasive bladder cancer. J Urol. 2010;184:1907-13. doi:10.1016/j.juro.2010.06.148.
75. Khare HA, Døssing KBV, Ringgaard L, Christensen E, Urbak L, Sillesen H, et al. In vivo detection of urokinase-type plasminogen activator receptor (uPAR) expression in arterial atherogenesis using [(64)Cu]Cu-DOTA-AE105 positron emission tomography (PET). Atherosclerosis. 2022;352:103-11. doi:10.1016/j.atherosclerosis.2022.03.026.
76. Enocsson H, Lukic T, Ziegelasch M, Kastbom A. Serum levels of the soluble urokinase plasminogen activator receptor (suPAR) correlates with disease activity in early rheumatoid arthritis and reflects joint damage over time. Transl Res. 2021;232:142-9. doi:10.1016/j.trsl.2021.02.007.
77. Neijenhuis LKA, de Myunck L, Bijlstra OD, Kuppen PJK, Hilling DE, Borm FJ, et al. Near-Infrared Fluorescence Tumor-Targeted Imaging in Lung Cancer: A Systematic Review. Life (Basel). 2022;12. doi:10.3390/life12030446.
78. Predina JD, Newton AD, Connolly C, Dunbar A, Baldassari M, Deshpande C, et al. Identification of a Folate Receptor-Targeted Near-Infrared Molecular Contrast Agent to Localize Pulmonary Adenocarcinomas. Mol Ther. 2018;26:390-403. doi:10.1016/j.ymthe.2017.10.016.
79. Predina JD, Newton AD, Xia L, Corbett C, Connolly C, Shin M, et al. An open label trial of folate receptor-targeted intraoperative molecular imaging to localize pulmonary squamous cell carcinomas. Oncotarget. 2018;9:13517-29. doi:10.18632/oncotarget.24399.
80. Predina JD, Newton A, Corbett C, Xia L, Sulyok LF, Shin M, et al. Localization of Pulmonary Ground-Glass Opacities with Folate Receptor-Targeted Intraoperative Molecular Imaging. J Thorac Oncol. 2018;13:1028-36. doi:10.1016/j.jtho.2018.03.023.
81. Gangadharan S, Sarkaria IN, Rice D, Murthy S, Braun J, Kucharczuk J, et al. Multiinstitutional Phase 2 Clinical Trial of Intraoperative Molecular Imaging of Lung Cancer. Ann Thorac Surg. 2021;112:1150-9. doi:10.1016/j.athoracsur.2020.09.037.
82. Keating JJ, Runge JJ, Singhal S, Nims S, Venegas O, Durham AC, et al. Intraoperative near-infrared fluorescence imaging targeting folate receptors identifies lung cancer in a large-animal model. Cancer. 2017;123:1051-60. doi:10.1002/cncr.30419.
83. Azari F, Kennedy G, Bernstein E, Delikatny J, Lee JYK, Kucharczuk J, et al. Evaluation of OTL38-Generated Tumor-to-Background Ratio in Intraoperative Molecular Imaging-Guided Lung Cancer Resections. Mol Imaging Biol. 2021. doi:10.1007/s11307-021-01618-9.
84. Lanahan CR, Kelly BN, Gadd MA, Specht MC, Brown CL, Hughes KS, et al. Performance of a novel protease-activated fluorescent imaging system for intraoperative detection of residual breast cancer during breast conserving surgery. Breast cancer research and treatment. 2021;187:145-53. doi:10.1007/s10549-021-06106-w.
85. Smith BL, Lanahan CR, Specht MC, Kelly BN, Brown C, Strasfeld DB, et al. Feasibility Study of a Novel Protease-Activated Fluorescent Imaging System for Real-Time, Intraoperative Detection of Residual Breast Cancer in Breast Conserving Surgery. Annals of surgical oncology. 2020;27:1854-61. doi:10.1245/s10434-019-08158-1.

86. The American Society of Breast Surgeons Official Proceedings, Volume XXII 2021 Annual Meeting Scientific Session Abstracts. Annals of surgical oncology. 2021;28:163-400. doi:10.1245/s10434-021-10068-0.
87. de Gouw D, Rijpkema M, de Bitter TJJ, Baart VM, Sier CFM, Hernot S, et al. Identifying Biomarkers in Lymph Node Metastases of Esophageal Adenocarcinoma for Tumor-Targeted Imaging. Mol Diagn Ther. 2020;24:191-200. doi:10.1007/s40291-020-00448-9.
88. Went PT, Lugli A, Meier S, Bundi M, Mirlacher M, Sauter G, et al. Frequent EpCam protein expression in human carcinomas. Hum Pathol. 2004;35:122-8. doi:10.1016/j.humpath.2003.08.026.
89. van Manen L, Handgraaf HJM, Diana M, Dijkstra J, Ishizawa T, Vahrmeijer AL, et al. A practical guide for the use of indocyanine green and methylene blue in fluorescence-guided abdominal surgery. Journal of surgical oncology. 2018;118:283-300. doi:10.1002/jso.25105.
90. Boogerd LS, Handgraaf HJ, Lam HD, Huurman VA, Farina-Sarasqueta A, Frangioni JV, et al. Laparoscopic detection and resection of occult liver tumors of multiple cancer types using real-time near-infrared fluorescence guidance. Surg Endosc. 2017;31:952-61. doi:10.1007/s00464-016-5007-6.
91. Achterberg FB, Sibinga Mulder BG, Meijer RPJ, Bonsing BA, Hartgrink HH, Mieog JSD, et al. Real-time surgical margin assessment using ICG-fluorescence during laparoscopic and robot-assisted resections of colorectal liver metastases. Ann Transl Med. 2020;8:1448. doi:10.21037/atm-20-1999.
92. Meijer RPJ, de Valk KS, Deken MM, Boogerd LSF, Hoogstins CES, Bhairosingh SS, et al. Intraoperative detection of colorectal and pancreatic liver metastases using SGM-101, a fluorescent antibody targeting CEA. Eur J Surg Oncol. 2021;47:667-73. doi:10.1016/j.ejso.2020.10.034.
93. Tiernan JP, Perry SL, Verghese ET, West NP, Yeluri S, Jayne DG, et al. Carcinoembryonic antigen is the preferred biomarker for in vivo colorectal cancer targeting. Br J Cancer. 2013;108:662-7. doi:10.1038/bjc.2012.605.
94. Boogerd LS, van der Valk MJ, Boonstra MC, Prevoo HA, Hilling DE, van de Velde CJ, et al. Biomarker expression in rectal cancer tissue before and after neoadjuvant therapy. Onco Targets Ther. 2018;11:1655-64. doi:10.2147/ott.S145473.
95. Went P, Vasei M, Bubendorf L, Terracciano L, Tornillo L, Riede U, et al. Frequent high-level expression of the immunotherapeutic target Ep-CAM in colon, stomach, prostate and lung cancers. Br J Cancer. 2006;94:128-35. doi:10.1038/sj.bjc.6602924.
96. Schmelzer E, Reid LM. EpCAM expression in normal, non-pathological tissues. Front Biosci. 2008;13:3096-100. doi:10.2741/2911.
97. Schmidt MM, Wittrup KD. A modeling analysis of the effects of molecular size and binding affinity on tumor targeting. Mol Cancer Ther. 2009;8:2861-71. doi:10.1158/1535-7163.Mct-09-0195.
98. Thurber GM, Schmidt MM, Wittrup KD. Antibody tumor penetration: transport opposed by systemic and antigen-mediated clearance. Adv Drug Deliv Rev. 2008;60:1421-34. doi:10.1016/j.addr.2008.04.012.
99. Xenaki KT, Oliveira S, van Bergen En Henegouwen PMP. Antibody or Antibody Fragments: Implications for Molecular Imaging and Targeted Therapy of Solid Tumors. Front Immunol. 2017;8:1287. doi:10.3389/fimmu.2017.01287.
100. Baart VM, van Manen L, Bhairosingh SS, Vuijk FA, Iamele L, de Jonge H, et al. Side-by-Side Comparison of uPAR-Targeting Optical Imaging Antibodies and Antibody Fragments for Fluorescence-Guided Surgery of Solid Tumors. Mol Imaging Biol. 2021. doi:10.1007/s11307-021-01657-2.

101. Hong H, Zhang Y, Orbay H, Valdovinos HF, Nayak TR, Bean J, et al. Positron emission tomography imaging of tumor angiogenesis with a (61/64)Cu-labeled F(ab')(2) antibody fragment. Mol Pharm. 2013;10:709-16. doi:10.1021/mp300507r.
102. Zhang Y, Hong H, Orbay H, Valdovinos HF, Nayak TR, Theuer CP, et al. PET imaging of CD105/endoglin expression with a ^{61}/^{64}Cu-labeled Fab antibody fragment. Eur J Nucl Med Mol Imaging. 2013;40:759-67. doi:10.1007/s00259-012-2334-2.
103. El-Sayed A, Bernhard W, Barreto K, Gonzalez C, Hill W, Pastushok L, et al. Evaluation of antibody fragment properties for near-infrared fluorescence imaging of HER3-positive cancer xenografts. Theranostics. 2018;8:4856-69. doi:10.7150/thno.24252.
104. Li D, Liu S, Liu R, Zhou Y, Park R, Naga K, et al. EphB4-targeted imaging with antibody h131, h131-F(ab')2 and h131-Fab. Mol Pharm. 2013;10:4527-33. doi:10.1021/mp400354y.
105. Leelawattanachai J, Kwon KW, Michael P, Ting R, Kim JY, Jin MM. Side-by-Side Comparison of Commonly Used Biomolecules That Differ in Size and Affinity on Tumor Uptake and Internalization. PloS one. 2015;10:e0124440. doi:10.1371/journal.pone.0124440.
106. Thurber GM, Zajic SC, Wittrup KD. Theoretic criteria for antibody penetration into solid tumors and micrometastases. Journal of nuclear medicine : official publication, Society of Nuclear Medicine. 2007;48:995-9. doi:10.2967/jnumed.106.037069.
107. Wittrup KD, Thurber GM, Schmidt MM, Rhoden JJ. Practical theoretic guidance for the design of tumor-targeting agents. Methods Enzymol. 2012;503:255-68. doi:10.1016/b978-0-12-396962-0.00010-0.
108. Tang Y, Lou J, Alpaugh RK, Robinson MK, Marks JD, Weiner LM. Regulation of antibody-dependent cellular cytotoxicity by IgG intrinsic and apparent affinity for target antigen. Journal of immunology (Baltimore, Md : 1950). 2007;179:2815-23. doi:10.4049/jimmunol.179.5.2815.
109. Graff CP, Wittrup KD. Theoretical analysis of antibody targeting of tumor spheroids: importance of dosage for penetration, and affinity for retention. Cancer Res. 2003;63:1288-96.
110. Adams GP, Schier R, Marshall K, Wolf EJ, McCall AM, Marks JD, et al. Increased affinity leads to improved selective tumor delivery of single-chain Fv antibodies. Cancer Res. 1998;58:485-90.
111. Zahnd C, Kawe M, Stumpp MT, de Pasquale C, Tamaskovic R, Nagy-Davidescu G, et al. Efficient tumor targeting with high-affinity designed ankyrin repeat proteins: effects of affinity and molecular size. Cancer Res. 2010;70:1595-605. doi:10.1158/0008-5472.Can-09-2724.
112. Rudnick SI, Lou J, Shaller CC, Tang Y, Klein-Szanto AJ, Weiner LM, et al. Influence of affinity and antigen internalization on the uptake and penetration of Anti-HER2 antibodies in solid tumors. Cancer Res. 2011;71:2250-9. doi:10.1158/0008-5472.Can-10-2277.
113. Sadiki A, Vaidya SR, Abdollahi M, Bhardwaj G, Dolan ME, Turna H, et al. Site-specific conjugation of native antibody. Antib Ther. 2020;3:271-84. doi:10.1093/abt/tbaa027.
114. Cohen R, Stammes MA, de Roos IH, Stigter-van Walsum M, Visser GW, van Dongen GA. Inert coupling of IRDye800CW to monoclonal antibodies for clinical optical imaging of tumor targets. EJNMMI Res. 2011;1:31. doi:10.1186/2191-219x-1-31.
115. Conner KP, Rock BM, Kwon GK, Balthasar JP, Abuqayyas L, Wienkers LC, et al. Evaluation of near infrared fluorescent labeling of monoclonal antibodies as a tool for tissue distribution. Drug Metab Dispos. 2014;42:1906-13. doi:10.1124/dmd.114.060319.
116. Cilliers C, Nessler I, Christodolu N, Thurber GM. Tracking Antibody Distribution with Near-Infrared Fluorescent Dyes: Impact of Dye Structure and Degree of Labeling on Plasma Clearance. Mol Pharm. 2017;14:1623-33. doi:10.1021/acs.molpharmaceut.6b01091.

117. Debie P, Van Quathem J, Hansen I, Bala G, Massa S, Devoogdt N, et al. Effect of Dye and Conjugation Chemistry on the Biodistribution Profile of Near-Infrared-Labeled Nanobodies as Tracers for Image-Guided Surgery. Mol Pharm. 2017;14:1145-53. doi:10.1021/acs.molpharmaceut.6b01053.
118. Kurbegovic S, Juhl K, Chen H, Qu C, Ding B, Leth JM, et al. Molecular Targeted NIR-II Probe for Image-Guided Brain Tumor Surgery. Bioconjugate chemistry. 2018;29:3833-40. doi:10.1021/acs.bioconjchem.8b00669.
119. Keyaerts M, Xavier C, Heemskerk J, Devoogdt N, Everaert H, Ackaert C, et al. Phase I Study of 68Ga-HER2-Nanobody for PET/CT Assessment of HER2 Expression in Breast Carcinoma. Journal of nuclear medicine : official publication, Society of Nuclear Medicine. 2016;57:27-33. doi:10.2967/jnumed.115.162024.
120. Boogerd LSF, Hoogstins CES, Schaap DP, Kusters M, Handgraaf HJM, van der Valk MJM, et al. Safety and effectiveness of SGM-101, a fluorescent antibody targeting carcinoembryonic antigen, for intraoperative detection of colorectal cancer: a dose-escalation pilot study. The lancet Gastroenterology & hepatology. 2018;3:181-91. doi:10.1016/s2468-1253(17)30395-3.
121. de Valk KS, Deken MM, Schaap DP, Meijer RP, Boogerd LS, Hoogstins CE, et al. Dose-Finding Study of a CEA-Targeting Agent, SGM-101, for Intraoperative Fluorescence Imaging of Colorectal Cancer. Annals of surgical oncology. 2021;28:1832-44. doi:10.1245/s10434-020-09069-2.
122. Baart VM, Boonstra MC, Sier CFM. uPAR directed-imaging of head-and-neck cancer. Oncotarget. 2017;8:20519-20. doi:10.18632/oncotarget.16240.
123. Galema HA, Meijer RPJ, Lauwerends LJ, Verhoef C, Burggraaf J, Vahrmeijer AL, et al. Fluorescence-guided surgery in colorectal cancer; A review on clinical results and future perspectives. Eur J Surg Oncol. 2022;48:810-21. doi:10.1016/j.ejso.2021.10.005.
124. Gioux S, Choi HS, Frangioni JV. Image-guided surgery using invisible near-infrared light: fundamentals of clinical translation. Molecular imaging. 2010;9:237-55.

Appendices

Appendix A

Dutch summary – Nederlandse samenvatting

Samenvatting

Deel I. Inleiding

Wereldwijd is kanker verantwoordelijk voor ongeveer één op de zes sterfgevallen. Ondanks de vooruitgang in behandelingsmogelijkheden in de afgelopen decennia blijft chirurgie de hoeksteen voor behandeling van bijna alle solide tumoren. Radicale excisie is cruciaal voor een curatieve behandeling, maar intra-operatieve tumoridentificatie wordt bemoeilijkt door (1) fibrose, ontsteking en necrose als gevolg van neo-adjuvante therapie en (2) een veranderd operatiegebied als gevolg van de toepassing van laparoscopische en robotprocedures. Om chirurgen te helpen bij het onderscheiden van tumoren zijn er verschillende beeldvormingstechnieken geïntroduceerd in de operatiekamer, waarvan fluorescentie geleide chirurgie (FGS) er één is. FGS maakt gebruik van nabij-infrarood licht om een, vaak intraveneus toegediende, tumor-gerichte tracer in real-time te visualiseren. Om een optimaal contrast te creëren tussen kwaadaardig en niet-kwaadaardig weefsel moet zo'n tracer gericht zijn op een tumor-specifiek eiwit dat sterk tot expressie komt in tumorweefsel, maar afwezig is in het omringende weefsel.

Deel II. uPAR als tumordoelwit in verschillende tumortypes

De urokinase plasminogeen activator receptor (uPAR) is zo'n tracer die sterk tot expressie komt op kwaadaardige tumorcellen en tumor-geassocieerde stromale cellen, terwijl hij vrijwel afwezig is op niet-maligne (normale, goedaardige of reactieve) cellen. Bovendien is uPAR-expressie in verschillende maligniteiten een prognostische factor. In **Hoofdstuk 2** werd de prognostische waarde van uPAR-expressie voor patiënten met pancreasadenocarcinoom onderzocht. In 66% van de gevallen kwam uPAR tot expressie op kwaadaardige cellen, terwijl uPAR in 82% van de gevallen tot expressie kwam op tumor-geassocieerde stromale cellen. uPAR-expressie op kwaadaardige en stromale cellen is omgekeerd gerelateerd aan algehele overleving en ziektevrije overleving. Deze resultaten versterken de hypothese dat uPAR een sterke prognostische marker is voor agressieve ziekten en mogelijk kan worden gebruikt voor stratificatie van de behandeling. Bovendien maakt de expressie van uPAR op kwaadaardige en tumorgeassocieerde stromale cellen deze receptor tot een mogelijk doelwit voor FGS.

Een ander geval waarbij FGS veel impact zou kunnen hebben omdat de tumorgrenzen moeilijk, zo niet onmogelijk, te bepalen zijn, is hoog risico plaveiselcelcarcinoom van het hoofd-halsgebied. Met behulp van een praktische benadering werden in **Hoofdstuk 3** mogelijke tumortargets geïdentificeerd voor FGS. De expressiepatronen van zeven targets, waarvoor fluorescerende tracers in ontwikkeling zijn, werden geëvalueerd op tumorcellen, tumorgeassocieerde stromale cellen

en normaal epitheel. De epidermale groeifactorreceptor, integrine $\alpha_v ß_6$ en uPAR werden geïdentificeerd als mogelijke targets, waarbij de eerste twee een hoge expressie hadden op tumorcellen, geen expressie op stromale cellen en een matige tot hoge expressie op normaal epitheel. Normaal epitheel was daarentegen consistent negatief voor uPAR, terwijl tumor- en tumorgeassocieerde stromale cellen matig positief waren.

Deel III. uPAR als doelwit: andere ziektes dan kanker
Over-expressie van uPAR komt niet alleen voor bij kanker, maar ook bij allerlei andere ziekten waarbij extracellulaire matrix re-modellering een belangrijke rol speelt. Daarom werd in **Hoofdstuk 4** nader ingegaan op de rol van uPAR in atherosclerose, reumatoïde artritis (RA), de ziekte van Alzheimer (AD), multiple sclerose (MS) en inflammatoire darmziekten (IBD). Daarnaast werden mogelijkheden geïdentificeerd waar uPAR inzichten zou kunnen bieden op het gebied van gerichte moleculaire beeldvorming voor nieuwe richtingen in diagnose, monitoring of behandelingsopties. Deze variëren van het gebruik van moleculaire beeldvorming om meer inzicht te krijgen in MS of AD, tot de identificatie van atherosclerotische plaques die risico lopen op scheuren en het voorspellen van ziekteverergering bij RA of IBD.

Deel IV. Ontwikkeling van uPAR-gerichte tracers
Na het identificeren van een mogelijk doelwit moet een fluorescente tracer worden ontwikkeld die specifiek gericht is op deze receptor. Er zijn verschillende farmacologische en praktische aspecten waarmee rekening moet worden gehouden bij het ontwerpen van een fluorescente tracer. Deze discussie werd geïntroduceerd in **Hoofdstuk 5**, waar de werking van een fluorescerend uPAR-gericht monoklonaal antilichaam en een peptide werden vergeleken naar aanleiding van twee wetenschappelijke publicaties, waarin beide tracers werden geëvalueerd in preklinische hoofd-hals kankermodellen. De lange halfwaardetijd van het antilichaam resulteerde in vertraagde maar langdurige beeldvorming. Met het peptide kon een snellere beeldvorming worden bereikt, maar het nadeel was dat het concurreert met urokinase voor binding aan uPAR waardoor er potentieel minder signaal in de tumor terecht komt.

In **Hoofdstuk 6** werd een nieuw gehumaniseerd fluorescerend antilichaam geïntroduceerd, dat is gebaseerd op het muis-monoklonale antilichaam uit het vorige hoofdstuk, gericht tegen domein 2-3 van uPAR. Dit antilichaam werd preklinisch geëvalueerd. In preklinische subcutane en orthotope blaaskanker modellen konden tumoren specifiek worden onderscheiden van achtergrondweefsels. Hierbij waren tumor-achtergrondratio's significant hoger dan bij de controles. Daarnaast werd

de multimodale functionaliteit van de tracer aangetoond door foto-akoestische 3D beeldvorming.

Zoals eerder vermeld, hebben antilichamen een langere halfwaardetijd waardoor het optimale beeldvormingsvenster wordt uitgesteld. Door het molecuulgewicht van het antilichaam te verlagen verandert de bio-distributie van de tracer, wat resulteert in snellere penetratie in de tumor, snellere achtergrondklaring en uiteindelijk snellere beeldvorming. In **Hoofdstuk 7** werden F(ab')2 en Fab-fragmenten gemaakt van het gehumaniseerde monoklonale antilichaam dat in het vorige hoofdstuk werd geïntroduceerd en uitgebreid vergeleken in meerdere preklinische muismodellen. Het uiteindelijke beeldvormingsvenster was teruggebracht van 72 uur tot 24 uur na toediening van de fragmenten. Hoewel de verhouding tumor-achtergrond niet verschilde tussen het antilichaam met volledige grootte en de twee kleinere fragmenten, nam het pieksignaal van de tumor af met de grootte van de tracer. De eerdere tumorvisualisatie die wordt bereikt door antilichaamfragmenten gaat ten koste van de piekfluorescentie-intensiteit die de gevoeligheid van de tracer mogelijk beïnvloedt.

Appendix B

List of publications

List of publications

Houvast RD, Badr N, March T, de Muynck LDAN, Sier VQ, Schomann T, Bhairosingh S, **Baart VM**, Peeters JAHM, van Westen GJP, Pluckthun A, Burggraaf J, Kuppen PJK, Varhmeijer AL, Sier CFM. Prelinical evaluation of EpCAM-binding designed ankyrin repeat proteins (DARPins) as targeting moieties for bimodal near-infrared fluorescence and photoacoustic imaging of cancer. *Eur J Nucl Med Mol Imaging. 2023 Aug 29*; Online ahead of print. PMID 37642704.

Van Manen L, de Muynck LDAN, **Baart VM**, Bhairosingh S, Debie P, Vahrmeijer AL, Hernot S, Mieog JSD. Near-infrared fluorescence imaging of pancreatic cancer using a fluorescently labelled anti-CEA nanobody probe: preclinical study. *Biomolecules 2023 Mar 30*; 13(4):618. PMID 37189366.

Peng L, Li Y, Yao S, Gaedcke J, **Baart VM**, Sier CFM, Neesse A, Ellenrieder V, Bohnenberger H, Fuchs F, Kitz J, Strobel P, Kuffer S. Urokianse-type plasminogen activator receptor (uPAR) cooperates with mutated KRAS in regulating cellular plasticity and gemcitabine response in pancreatic adenocarcinomas. *Cancers (Basel) 2023 Mar 3*; 15(5):1587. PMID 36900379.

Vuijk FA, Kleiburg F, Noortman WA, Heijmen L, Feshtali Shahbazi S, van Velden FHP, **Baart VM**, Bhairosingh SS, Windhorst BD, Hawinkels LJAC, Dibbets-Schneider P, Bouwman N, Crobach SALP, Farina-Sarasqueta A, Marinelli AWKS, Oprea-Lager DE, Swijnenburg RJ, Smit F, Vahrmeijer AL, de Geus-Oei LF, Hilling SE, Slingerland M. Prostate-specific membrane antigen targeted PET/CT imaging in patients with colon, gastric and pancreatic cancer. *Cancers (Basel) 2022 Dec 15;*14(24):6209. PMID: 36551695.

Harryvan TJ, Hawinkels LJAC, **mini-tumor workgroup***, Östman A, ten Dijke P, Strell C, Hornsveld M. A novel pancreatic cancer mini-tumor model to study desmoplasia and myofibroblastic cancer-associated fibroblast differentiation. *Gastro Hep Advances 2022; 1:*678-681. PMID: 35937541.

Baart VM, van Manen L, Bhairosingh SS, Vuijk FA, Iamele L, de Jonge H, Scotti C, Resnati M, Cordfunke RA, Kuppen PJK, Mazar AP, Burggraaf J, Vahrmeijer AL, Sier CFM. Side-by-side comparison of uPAR-targeting optical imaging antibodies and antibody fragments for fluorescence-guided surgery of solid tumors. *Mol Imaging Biol. 2023 Feb*; 25(1):122-132. PMID: 34642899.

Baart VM, van der Horst G, Deken MM, Bhairosingh SS, Schomann T, Vincent VQ, van der Mark MH, Iamele L, de Jonge H, Resnati M, Mazar AP, Pelger RCM, van der Pluijm G, Kuppen PJK, Vahrmeijer AL, Sier CFM. A multimodal molecular imaging approach targeting urokinase plasminogen activator receptor for the diagnosis, resection and surveillance of urothelial cell carcinoma. *Eur J Cancer. 2021 Mar;146:11-20.* PMID: 33561783.

Baart VM, Deken MM, Bordo MW, Bhairosingh SS, Salvatori DCF, Hyun H, Choi HS, Sier CFM, Kuppen PJK, Terwisscha van Scheltinga AGT, March TL, Valentijn ARPM, Frangioni JV, Vahrmeijer AL. Small molecules for multi-wavelength near-infrared fluorescent mapping of regional and sentinel lymph nodes in colorectal cancer staging. *Front Oncol. 2020 Dec 17;10:586112.* PMID: 33392081.

Houvast RD, Vankemmelbeke M, Durrant LG, Wuhrer M, **Baart VM**, Kuppen PJK, de Geus-Oei LF, Vahrmeijer AL, Cornelis FM Sier. Targeting glycans and heavily glycosylated proteins for tumor imaging. *Cancers (Basel). 2020 Dec 21;12(12):3870.* PMID: 33371487.

Wellens LM, Deken MM, Sier CFM, Jonhson HR, de la Jara Ortiz F, Bhairosingh SS, Houvast RD, Kholosy WM, **Baart VM**, Pieters AMMJ, de Krijger RR, Molenaar JJ, Wehrens EJ, Dekkers JF, Wijnen MHWA, Vahrmeijers AL, Rios AC. Anti-GD2-IRDye800CW as a targeted probe for fluorescence-guided surgery in neuroblastoma. *Sci Rep. 2020 Oct 19;10(1):17667.* PMID: 33077751.

Houvast RD, **Baart VM**, Bhairosingh SS, Cordfunke RA, Chua JX, Vankemmelbeke M, Parsons T, Kuppen PJK, Durrant LG, Vahrmeijer AL, Sier CFM. Glycan-based near-infrared fluorescent (NIRF) imaging of gastrointestinal tumors: a preclinical proof-of-concept in vivo study. *Mol Imaging Biol. 2020 Dec;22(6):1511-1522.* PMID: 32780212.

Baart VM, Houvast RD, de Geus-Oei LF, Quax PHA, Kuppen PJK, Vahrmeijer AL, Sier CFM. Molecular imaging of the urokinase plasminogen activator receptor: opportunities beyond cancer. *EJNMMI Res. 2020 Jul 29;10(1):87.* PMID: 32725278.

Baart VM, van Duijn C, van Egmond SL, Dijckmeester WA, Jansen JC, Vahrmeijer AL, Sier CFM, Cohen D. EGFR and αvß6 as promising targets for molecular imaging of cutaneous and mucosal squamous cell carcinoma of the head and neck region. *Cancers (Basel). 2020 Jun 5;12(6):1474.* PMID: 32516897.

de Gouw DJJM, Rijpkema M, de Bitter TJJ, **Baart VM**, Sier CFM, Hernot S, van Dam GM, Nagtegaal ID, Klarenbeek BR, Rosman C, van der Post RS. Identifying biomarkers in lymph node metastases of esophageal adenocarcinoma for tumor-targeted imaging. *Mol Diagn Ther. 2020 Apr;24(2):191-200.* PMID: 32048177.

Voeten SC, **Baart VM**, Krijnen P, Schipper IB. Optimal timing of a hip fracture operation. *Ned Tijdschr Geneeskd. 2019 Jan 29;163:D2911.* PMID: 3719881.

de Geus SWL, **Baart VM**, Boonstra MC, Kuppen PJK, Prevoo HAJM, Mazar AP, Bonsing BA, Morreau H, van de Velde CJH, Vahrmeijer AL, Sier CFM. Prognostic impact of urokinase plasminogen activator receptor expression in pancreatic cancer: malignant versus stromal cells. *Biomark Insights. 2017 Jun 22;12:117727197715443.* PMID: 28690396.

Baart VM, Boonstra MC, Sier CFM. uPAR directed-imaging of head-and-neck cancer. *Oncotarget. 2017 Mar 28;8(13):20519-20520.* PMID: 28423554.

Boonstra MC, van Driel PBAA, Keereweer S, Prevoo HAJM, Stammes MA, **Baart VM**, Löwik CWGM, Mazar AP, van de Velde CJH, Vahrmeijer AL, Sier CFM. Preclinical uPAR-targeted multimodal imaging of locoregional oral cancer. *Oral Oncol. 2017 Mar;66:1-8.* PMID: 28249642.

Appendix C

Curriculum vitae

Curriculum vitae

Victor Michiel Baart was born 10 October 1994 in Islamabad, Pakistan as the youngest of four to Joan and Esther Baart. After moving to Germany in his youth he received his High School diploma Summa Cum Laude in 2013.

This same year he left for Middelburg, the Netherlands, to study at the University College Roosevelt where he discovered a passion for medicine. In 2014 Victor started studying Medicine at the Leiden University Medical Center (LUMC).

In Leiden Victor's interest was drawn to the various research groups hosted by the LUMC and via the "Excellente Student MD/PhD" track he came into contact with the "Vahrmeijer Lab For Molecular-Targeted Precision Surgery". Vahrmeijer's lab was especially interesting as their research on fluorescence-guided surgery combined a technical and intellectual challenge with a hands-on approach and a high potential for positive clinical impact. Victor started as a student-researcher at the Vahrmeijer lab but after receiving the MD/PhD scholarship he continued as a PhD-candidate in September 2017. The scholarship enabled him to work full-time on the PhD for two years. After these two years he continued his research in part-time. Victor co-authored more than eighteen peer-reviewed papers and one book chapter during his PhD. Additionally, he participated through posters and presentations at five international conferences.

In 2019 Victor was selected to participate in the Leiden Leadership Programme offered by the Honours Academy of the University Leiden. He combined this with his PhD, now in part-time, and his clinical rotations (Master) which he started in November 2019 . Upon completing his medical studies in August 2022 Victor joined the Ministry of Health, Welfare and Sport for a short traineeship focused on oncological care policy in the Netherlands. Simultaneously he worked as a doctor at the emergency general practitioner post. After finishing his traineeship Victor continued his career as resident(-not-in-training) at Groene Hart Ziekenhuis in Gouda.

Outside of his professional career Victor is an avid football player and runner and has volunteered extensively at various sports-, student- and medically-focused organizations. During his student years he was also an active member of Navigators Studentenvereniging Leiden (NSL).

Appendix D

Acknowledgements – Dankwoord

Baart VM

Acknowledgements - Dankwoord

Attaining a PhD takes teamwork. I, therefore, cannot stand here without recognizing the many people who contributed to my journey.

Mijn reis begon bij prof. H.J. Tanke die mij als bachelor student opving en de weg wees naar de fluorescentie chirurgie. Eenmaal daar hebben uw woorden van aanbeveling een grote rol gespeeld in het binnenhalen van de MD-PhD beurs bij de Raad van Bestuur. Zonder uw bijdrage had ik hier nooit aan kunnen beginnen. Dank!

Prof. Burggraaf, vanaf onze eerste kennismaking in 2018 bij het KNAW Colloquium over fluorescentie chirurgie was ik onder de indruk van uw expertise en heldere manier van communiceren. Dank dat u mij als promotor wilde begeleiden, want deze combinatie van eigenschappen maken het promoveren onder u een genot.

Beste dr. Vahrmeijer, Alex, jouw open uitstraling, gezelligheid en expertise zorgen ervoor dat je een verbinder bent waardoor je in staat bent de mooiste samenwerkingen aan te gaan. Dank dat ik onder jouw begeleiding bij de Image-Guided groep mocht komen, dank voor jouw enthousiasme en dank voor het meedenken met mijn ideeën.

Beste Kees, ik zou wel een museum kunnen vullen met de tekeningen die jij hebt gemaakt om mij de theorieën achter ons onderzoek uit te leggen. Door in mij te investeren heb je een groot aandeel gehad in het vormen van de onderzoeker die ik vandaag ben.

Beste Shadhvi en Marieke, de twee top-analisten van de Image-Guided. Bedankt dat ik altijd bij jullie terecht kon met mijn vragen over het lab. Shadhvi, bijzonder bedankt voor de extra ondersteuning tijdens mijn coschappen.

Beste collega's van de Image-Guided, wat gaaf dat wij samen dit onderzoek mogen doen. Ook al zijn we allemaal op ons eigen domein bezig, heb ik veel van jullie kunnen leren. Marion, wat hebben wij ongelofelijk veel uren samen gespendeerd op de E-0 en wat heb ik veel geleerd van jou wat betreft dierexperimenteel onderzoek. Ruben en Labrinus, bedankt dat jullie mij te hulp schoten om de laatste experimenten van mijn proefschrift af te ronden.

Beste C7-138, Opperbazen, Stephanie, Kiki, Randa, Floris, Daniel, Labrinus, Ruben, Sophie, Meaghan, Annelieke, Nada, hoewel de samenstelling van onze mooie vissenkom door de jaren heen is veranderd, ben ik blij dat ik met jullie hier heb mogen zitten. De herinneringen, zoals de rekening bij Aloha en rotswanden beklimmen in Saguenay, Canada, zal ik blijven koesteren.

Beste Heelkunde Research Lab, beste Peter, Wilma, Geeske, Ronald, Erna, en Connie, bedankt dat ik gebruik mocht maken van jullie lab en expertise.

Beste collega-onderzoekers verspreid door het LUMC, van de MDL tot de urologie tot het PDC, bedankt dat ik bij jullie mocht binnenstappen om iets van jullie kennis en kunde op te pakken en mee te nemen naar mijn eigen onderzoeksgroep.

Tabitha, super bedankt dat je je creativiteit, tijd en talent wilde inzetten op te helpen met het opmaak van deze thesis.

Beste Presley, Infinitas, Uitfinitas, Infinihunks, Himfinity, NSL-vrienden, Tapirs en losse vrienden, met jullie was er altijd wel iets niet onderzoeks-achtig te doen. Bedankt voor de vele waardevolle momenten, van serieuze gesprekken aan de eettafel tot dansen in de nacht en van taking-it-easy tot je longen uit het lijf rennen op het voetbalveld.

Dear Flore, since stepping foot in the LUMC we have been hanging out. Thanks for being my friend and believer during the PhD. Thanks for enriching my life by sharing the people, music, books and movies you are currently obsessing over.

Dear Christine, through the ups and downs you have been a valuable friend throughout my PhD. Thanks for hanging out with me, being interested and excited for my life and research, and igniting my competitive-side. Although you might not agree, I'm confidant I'm still the first.

Beste sibs en aanhang, jullie hebben mij zien opgroeien tot de persoon die ik nu ben. Wat ben ik dankbaar voor de relatie die wij hebben waardoor ik weet dat jullie deur altijd open staat voor een gezellige maaltijd of spelletje.

Beste pap en mam, jullie hebben ons aangemoedigd om zowel onze professionele interesses achter na te gaan als ook om op de rem te trappen en te realiseren dat er meer is dan werk. Daarnaast konden jullie uit eigen ervaring mee praten over het promoveren en de offers die het kan kosten. Dank dat jullie achter mij stonden en de wijze lessen.

Beste Elise, wat een zegen dat jij in mijn leven bent. Ik weet nog goed dat ik juist aan jou wilde laten zien dat ik de promotiebeurs had gekregen. Wat was je lyrisch om dat nieuws te horen. Die herinnering doet mij nog steeds goed. Ik ben blij dat wij samen zijn. Jouw empathische en inlevende houding is second-to-none en waren een constante steun in de rug. Je bent een constante aanmoediging geweest gedurende het promotie-traject. De vele terrassen die wij samen hebben bezocht ook. Thanks for being there. Jag älskar dig.